AN INVESTIGATION OF THE FAILURE MECHANISMS OF A CARBON FIBRE REINFORCED COMPOSITE MATERIAL IN BENDING.

By

Alan Maybury, B.Sc., Dip.W.P.

A THESIS SUBMITTED TO THE
UNIVERSITY OF ASTON IN BIRMINGHAM
FOR THE DEGREE OF DOCTOR OF PHILOSOPHY

APRIL 1973.

Summary

The mode of failure of a carbon fibre reinforced composite beam has been studied. Early investigations showed that there were two distinct types of failure, tensile and compressive, depending which of these properties was the weaker.

Composite specimens were prepared under controlled conditions and their tensile and compressive strengths investigated using optimum test procedures. A large scatter exists on the tensile strengths of the composite such that the 'law of mixtures' gives as reliable a prediction of the strength as the more sophisticated analysis. However this simple analysis does not predict the gauge length effect or the loss in efficiency in transferring the load from fibre to fibre at the high fibre volume fractions shown by the test results.

As indicated by the macro and micro-stability analysis the compressive strength is directly dependent upon the shear modulus of the matrix. As the shear modulus is increased there is a similar improvement in the compressive strength. The test results also indicate a dependence of the compressive strength upon voidage. Both the micro and macro-analysis predict a compressive strength approximately three times the measured strength. A tentative sequence of failure is suggested to explain this disparity which combines the macro-analysis and the effect of voidage, where the compressive buckle initiates at a stress concentrating flaw.

The test results show that the mode of failure when a beam fails in tension is gradual, whereas when it fails in compression it exhibits brittle behaviour. Possible ways of improving the compressive strength over the tensile strength of the composite by increasing the shear modulus of the matri have been suggested, thus giving the more controlled tensile mode of bending

Index

Chapter 1

Introduction

As the demand for even larger and faster aircraft increases new aircraft design concepts are urgently needed. To help to meet this demand Rolls-Royce have developed the RB211 advanced technology engine which has been sold to power the Lockheed Tristar air bus. The RB211 is a high by-pass, three shaft engine designed to give high thrusts for large subsonic aircraft, with a much lower specific fuel consumption and noise level than in previous types of engine. The low pressure compressor consists of a single stage, normally referred to as the fan. This stage has to pass the complete mass flow of the engine, and to do this a very large compressor fan is required. The outside diameter of the fan casing is over 2.3 metres and each blade is nearly one metre in length. The fan is liable to be a very heavy piece of machinery, and the overall efficiency of the engine is very sensitive to the efficiency of the fan. Thus, the weight and efficiency both have direct effects on the overall operating costs of the aircraft.

When the engine is at full power high centrifugal stresses are imposed on the fan blade, as a result of its high tip speed. Titanium and carbon fibre composites, because of their high strength to weight ratio, appear to be the most attractive materials to produce a solid fan blade. Another possible contender is a hollow titanium construction; however such a construction requires very expensive machining and fabrication operations, which with titanium is technically very complex.

Because of the density difference, a component made of solid titanium will weigh almost three times as much as the carbon fibre composite fan blade. To carry this increased weight, the supporting shafts and bearings would all

have to be increased in size, making the final weight of the engine far greater if titanium fan blades are used rather than carbon fibre composites. Therefore, on the basis of weight, titanium is not at all competitive, however carbon fibre composites have serious operating problems.

The jet engine, which works by drawing in air at one end and pushing it from the other end acts as a very efficient vacuum cleaner, effectively 'sucking-in' dust, stones, birds and any other object which happens to be near its flight path. Hence, as well as resisting high centrifugal loads, the fan blades must resist impact by solid bodies.

If the blades have a low specific stiffness then they may not be able to withstand the buffeting of the air, as it passes through the engine, without vibrational instability. This together with fluctuating centrifugal stresses gives rise to a complicated fatigue loading on the fan blade. Therefore any material used to produce a fan blade, must also have a high specific stiffness as well as a high specific strength, to withstand impact conditions.

The fan blades must be capable of withstanding the effects of all types of environmental conditions, and all known types of contaminants associated with an aircraft engine. There are a number of environmental hazards to a compressor blade, such as, the effects of operating temperature, contamination, erosion and impact. The range of temperatures experienced during flight, are of great importance, because the matrix properties of a fibre reinforced plasti fan blade are greatly affected by slight changes in temperature. Hence the working temperatures place a limit upon the material selection for the matrix. Contamination and erosion (i.e. low mass impact such as rain, dust, etc.) can be minimised by the choice of a suitable coating on the outside of the fan blade. Impact is a far more complex problem and if it can be fully solved

then carbon fibre composites appear to have a bright future.

A series of simulated bird impact tests have been completed on carbon fibre composite fan blades and the modes of failure observed by a high speed ciné camera. The model bird is fired at the blade striking it, at a specified velocity, approximately 0.2 m from the blade tip. As the bird strikes it deforms the blade as a cantilever and imparts a slight twisting motion (Fig. 1). The tip deflections of the blades, under impact conditions, are very large. The final catastrophic failure is a bending failure, the bending failure being a mixture of tensile compressive and shear failures.

Many other structures are subjected to bending stresses during normal working conditions, in particular air frame and motor vehicle structures. As these are possible future applications for composite materials, a study of the flexural properties is of immense importance.

Flexural failure in composite materials appears to be a combination of compression, tensile and shear failure. As an aid to understanding how the fan blade behaves under bending stresses, and to separate the important parameters, an investigation into the behaviour of carbon fibre composites in tension and compression, and how they combine in the bending of a beam, has been made.

There are various types of carbon fibres from the high modulus - low strength fibres ($E = 370\ GNm^{-2}$, $UTS = 1.6\ GNm^{-2}$), to the high strength - l modulus fibres ($E = 190\ GNm^{-2}$, $UTS = 2.4\ GNm^{-2}$) used in this investigation The properties of the fibres are controlled by the heat treatment they receive (see section 4). At the time that this project was conducted the low modulus - high strength fibre was being produced on a large scale by

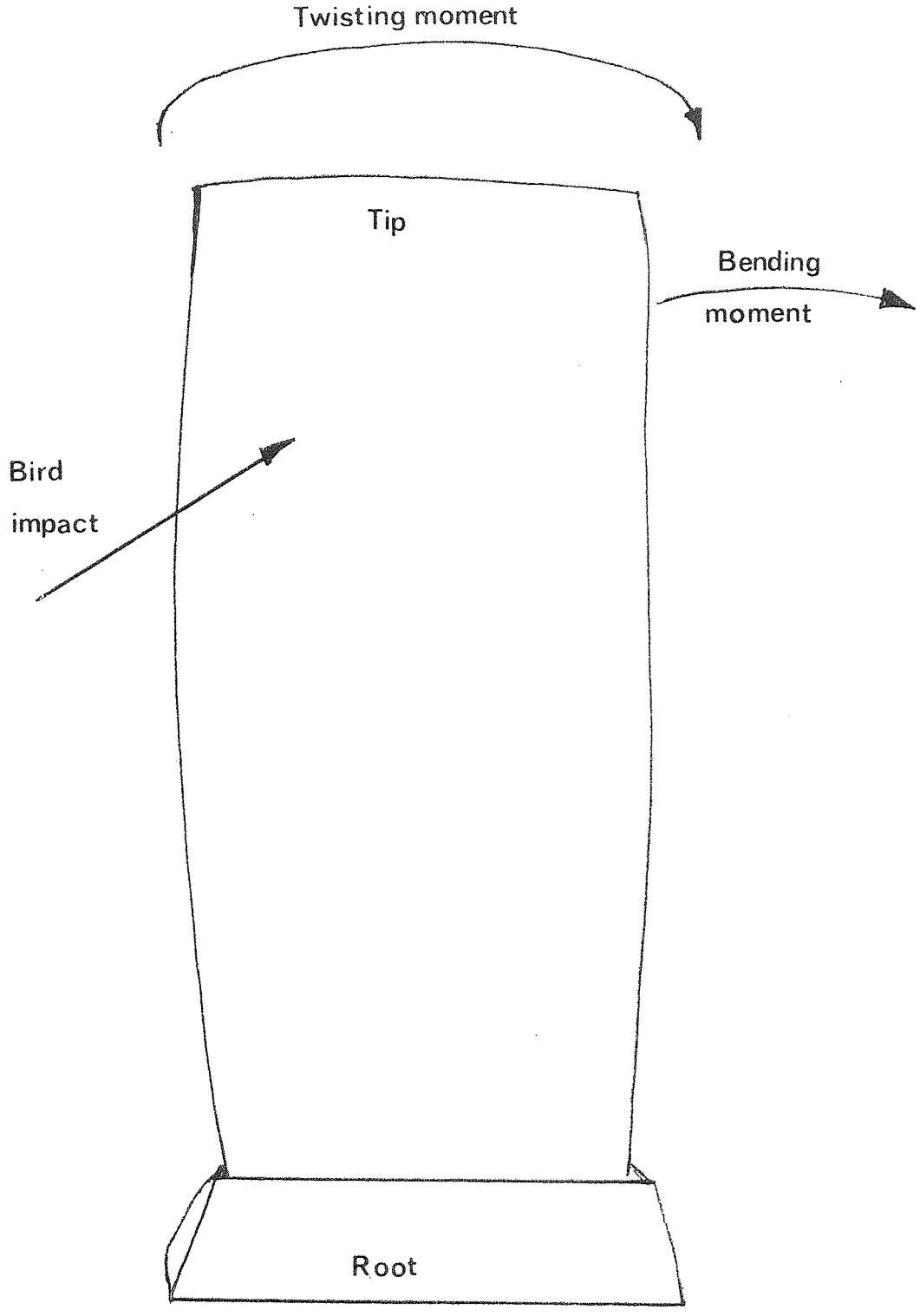

Fig.1 Fan blade loading under bird impact

Rolls Royce. This fibre was chosen by Rolls Royce because of its availability and therefore the research laboratory was required to do most of its work on this particular material.

Chapter 2

Theoretical Aspects of Fibre Reinforcement

2.1. Tensile Behaviour

2.1.1 Law of mixtures

The simplest concept of a composite material is one which contains continuous fibres which are uniformly distributed throughout the matrix. The fibres are uniform, all lying in one direction and firmly gripped by the matrix so that no slippage can occur at the interface between the reinforcement and the matrix. (Fig. 2)

The total load in the composite (P_c) is shared between the fibre load (P_f) and the matrix load (P_m).

$$P_c = P_f + P_m$$

in terms of stress $\sigma_c A_c = \sigma_f A_f + \sigma_m A_m$

$$\therefore \quad \underline{\sigma_c = \sigma_f V_f + \sigma_m V_m} \qquad - \ 2.1$$

Since a perfect bond has been assumed between the fibre and the matrix, the strain experienced by the composite is equal to the strain in the fibre and matrix.

$$\text{i.e.} \quad \epsilon_c = \epsilon_f = \epsilon_m$$

Hence dividing 2.1 by $\epsilon_c = \epsilon_f = \epsilon_m$

$$\underline{E_c = E_m V_m + E_f V_f} \qquad - \ 2.2$$

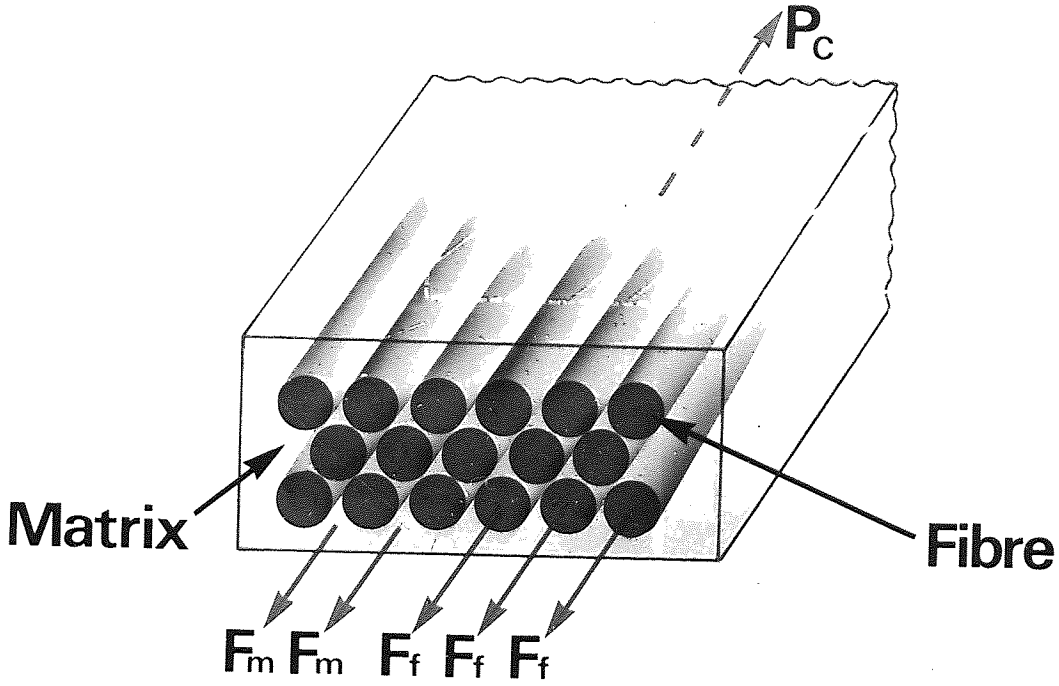

$$\Sigma F_m = P_m = \sigma_m A_m \qquad \Sigma F_f = P_f = \sigma_f A_f$$

$$P_c = P_f + P_m$$

Fig. 2. UNIDIRECTIONAL COMPOSITE LOADED IN THE FIBRE DIRECTION.

Equations 2.1 and 2.2 are applicable only when the fibres and matrix obey Hooke's Law.

E	= Young's modulus	P	= load	f	= fibre
σ	= stress	A	= area	m	= matrix
ϵ	= strain	V	= Volume fraction	c	= composite

2.1.2 A composite containing discontinuous fibres

When a composite, containing uniaxially aligned discontinuous fibres, is stressed parallel to the fibres, the axial displacements in the fibre and matrix are different because of the difference in the elastic moduli. The concept is of each fibre embedded in a continuous matrix with the state of stress and strain perturbed locally by the presence of the fibres. In this study it is assumed that macroscopically the composite as a whole is strained homogeneously. (Fig. 3)

The difference between the axial displacements of the fibre and the matrix means that shear strains are produced in the matrix on all planes parallel to the axis of the fibres and in the direction of this axis. These shear strains, with the accompanying shear stresses, are the mechanism by which the fibres are loaded and this load transmitted from fibre to fibre. As a result of these matrix shear strains around the fibre, the tensile stress within the fibre increases from a low value at the fibre ends, which are unable to sustain any load, to a maximum somewhere along the length of the fibre. Conversely, the shear stress in the matrix is a maximum at the fibre ends but decreases along the length of the fibre. Hence a portion of the end of each fibre is stressed at less than the maximum stress σ_f in a continuous fibre. The maximum ineffective length, that is the distance over which the fibre is loaded ~~to a~~ below the maximum fibre stress, is denoted by $l_c/2$, where l_c is defined as the critical length of the specimen.

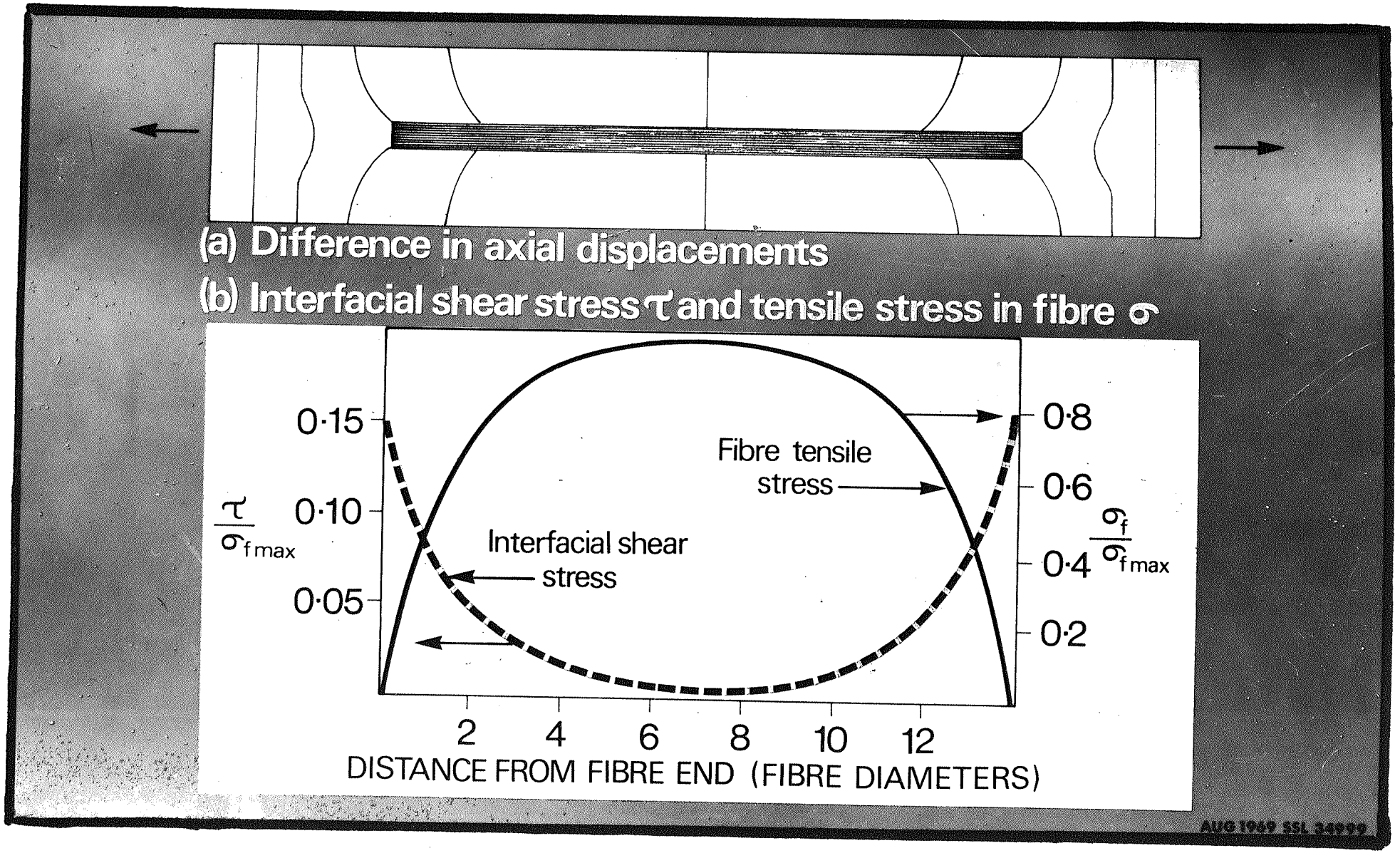

Fig.3 . FIBRE EMBEDDED IN MATRIX UNDER STRESS.

Kelly and Davies (1) have shown that the ratio of the strength of a discontinuous, uniaxial composite, of fibre length ℓ, to the strength of a continuous fibre composite, with the same fibre properties, must lie within the shaded portion of Fig. 4. From Fig. 4, if the ratio of the length of the fibres to their critical length is greater than 20 : 1 then the strength of the composite is not significantly different from what it would have been if it had contained continuous fibres.

2.1.3 Statistical Concepts

So far we have only considered materials which obey Hooke's law, are perfectly bonded to the matrix, and all have an intrinsic strength of σ^*_f. But unfortunately with carbon fibres in an epoxy resin matrix, these assumptions do not apply. Carbon fibres have brittle failure characteristics and are therefore susceptible to the presence of stress concentrating defects which cause a considerable variation in strength about some mean value. (2)

The strength of a brittle fibre composite cannot be found by simply inserting the mean fibre strength into the law of mixtures. A good illustration of this is what happens when a bundle of fibres with a mean strength σ^*_f, and standard deviation S is pulled. Initially all the fibres bear their share of the load until the first fibre breaks. This fibre can no longer bear any load and its load must then be carried by the remaining fibres. Thus, because fibres are breaking, the stress on the remaining fibres must increase, so that the total load on the bundle is maintained. As more fibres break, the stress builds up on the remaining fibres until the bundle fails at a strength below the mean strength of fibres. The wider the scatter on the fibre strength, the lower the total bundle strength will be, compared with the mean fibre strength. Fig. 5 shows a theoretical plot

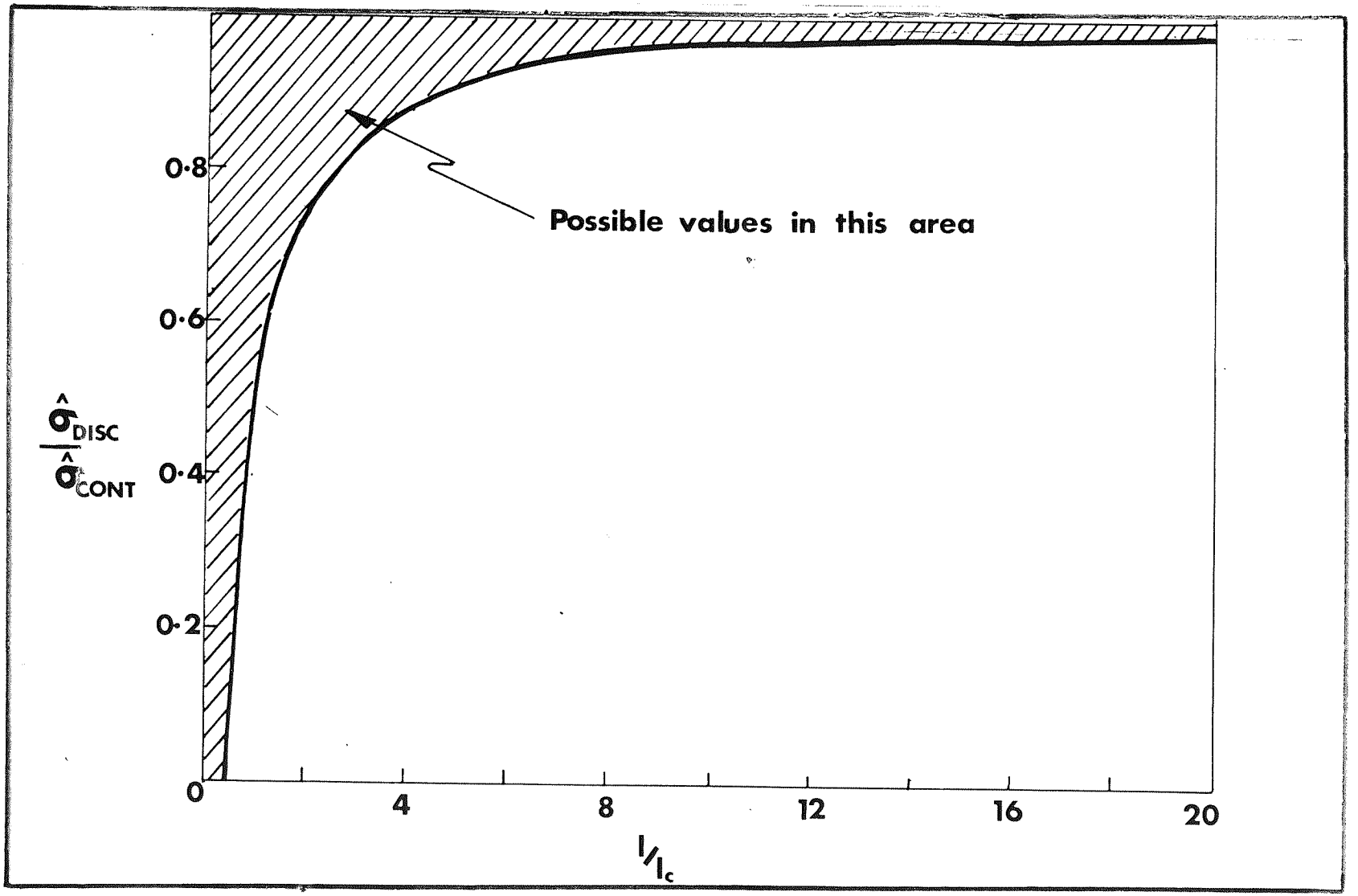

Fig. 4 . **THE RATIO OF THE STRENGTHS OF COMPOSITES CONTAINING DISCONTINUOUS AND CONTINUOUS FIBRES AS A FUNCTION OF l/l_c (Kelly and Davies)**

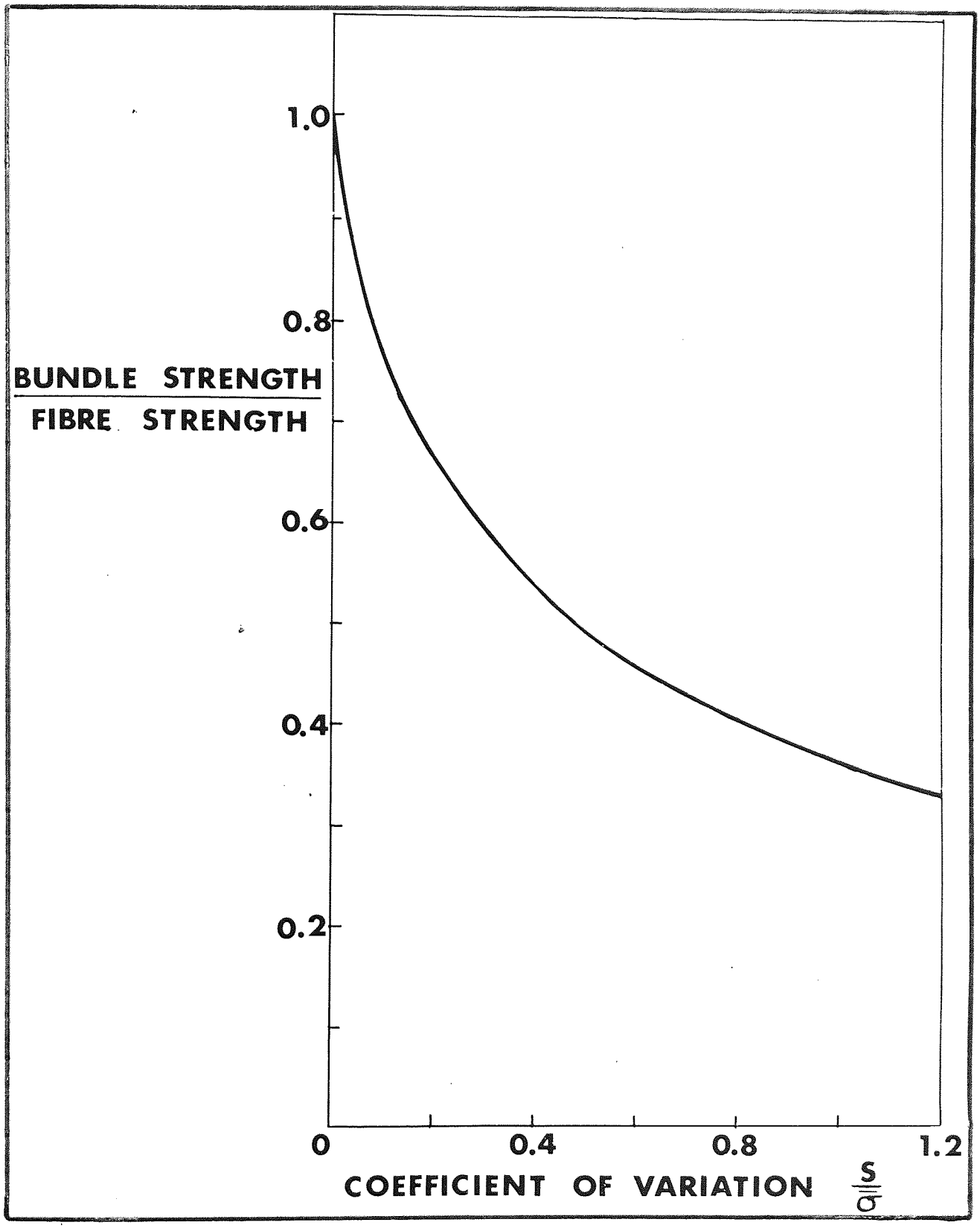

Fig. 5. RATIO OF BUNDLE STRENGTH TO MEAN FIBRE STRENGTH v COEFFICIENT OF VARIATION OF FIBRE STRENGTH (Coleman)

of bundle strength for glass fibres against increasing coefficient of variation (3), where the coefficient of variation (υ) is defined as:-

$$\upsilon = \frac{100s}{\sigma_f}$$

However when the fibres are embedded in a matrix, their behaviour changes. When a fibre fails it can still bear a load. As we have seen earlier, it is reloaded by shear stresses in the matrix and at a distance $l_c/2$ from the broken end it is again fully loaded. The fibre is therefore ineffective over a length l_c centred on the fracture (Fig. 6) and provided that the neighbouring fibres are still able to bear load within this ineffective region, and that the crack is not propagated through the matrix, then the composite will not fail. The purpose of the matrix is to isolate one fibre failure from another. Hence some way of coupling the statistical nature of the fibre strength, and the ineffective fibre length, to the composite strength is desirable.

Various statistical theories have been developed for the strength of composites. The source of a number of such theories is the work of Rosen (4). The model that he used was one of parallel fibres in a homogeneous matrix. The fibres are treated as having a statistical distribution of flaws or imperfections that result in fibre failure under an applied stress. As mentioned previously a portion of the fibre, about the fracture, is ineffective for bearing the full applied stress. As the fibres are loaded, failure occurs at points of imperfections along the fibres. Increasing load produces an increasing accumulation of fibre fractures until a sufficient number of ineffective fibre lengths combine, in any single cross sectional plane, to cause failure of the remaining fibres, thus producing composite failure.

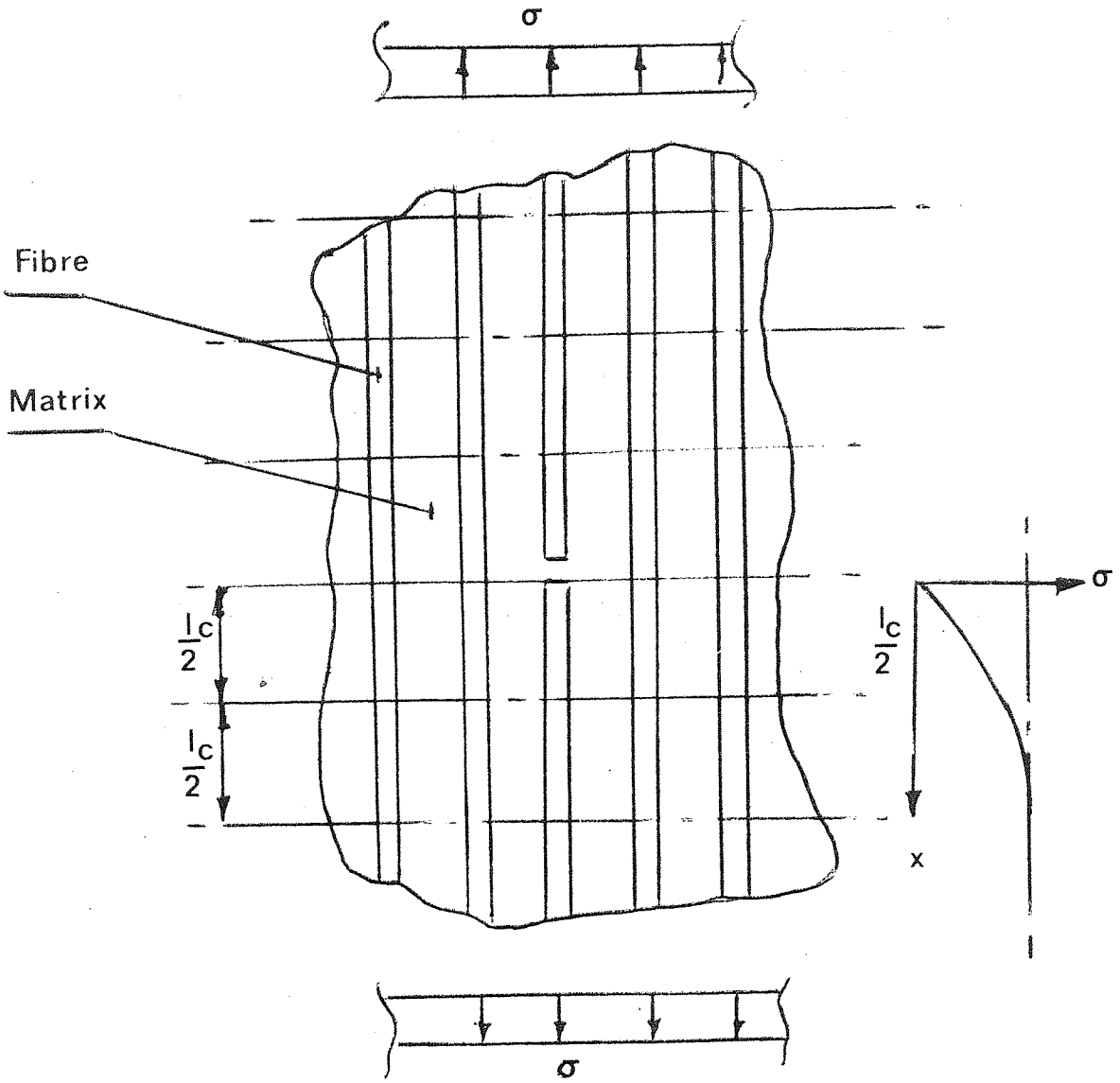

Fig. 6 Failure model of fibre reinforced composite (Rosen)

Rosen, computed the ineffective length by a shear lag analysis, which predicts 1c as a function of the diameter and volume fraction of the fibres and the fibre and matrix stiffnesses. The statistical strength distribution of the links is then expressed as a function of the fibre strength-gauge length relationship (Fig. 7). The results are then used in a statistical study of a series of bundles of links to define the distribution of bundle strengths.

For composite dimensions which are large compared to the fibre cross section Rosen's statistical analysis gives for the composite strength σ_c:-

$$\sigma_c = (\alpha \delta e)^{-1/\beta} V_f \qquad - 2.3$$

where α and β are the Wiebull constants defining the link strength and δ is the ineffective length. (56)

Investigations have been made to study the role of stress concentration effects on the strength of a composite (5, 6, 7). This work demonstrated that a close relationship exists between the probability, that when a fibre fails, it will cause the adjacent fibres to fail and the occurence of composite failure. On this basis a failure criterion was adopted which stated that failure of the composite will occur when the load is such that the first multiple group is expected, that is, when two or more fibres fail together. This analysis gives a more realistic composite strength for glass fibre - epoxy resin composites than Rosen's analysis.

The previous analyses are based on a model in which failure occurs after a significant accumulation of isolated breaks. When perfect bonding exists between the fibre and a brittle matrix, the composite fails without any accumulation of fibre breaks, and such composites do not realise their full strength potential. In this 'noncumulative' mode the failure is probably caused by a fibre break initiating a crack which propagates through

the matrix, resulting in fracture of additional fibres. Recent work on boron fibres in an epoxy matrix has shown such failures (8). The failure criteria would then be the occurrence of the first fibre break. Both Zweben's accumulative and non-accumulative modes of failure imply a size effect. That is, the larger the gauge length, the more likely it is that it contains flawed fibres.

Armenákas et al (9) have made experimental studies of the failure mechanism and strength characteristics of fibre bundles and composites. They were able to plot the strain in adjoining fibres to a broken fibre and showed that large stress concentrations can occur. However these are much reduced in the next nearest neighbours and beyond, which supports the theoretical predictions of Hedgepeth (10). Therefore it is possible that a crack can be propagated after the failure of a single fibre, since adjacent fibres may fail due to stress concentrations. Such a crack will only be stopped by fibres strong enough to survive the stress concentrations.

Armenákas and his fellow workers observed that when unilayer composites failed, the crack tended to follow the path of least resistance, until it encountered a group of strong fibres where it was deflected in the direction parallel to the fibres until it met another crack or weak fibre. They finally concluded that the mode of failure was completely random and no relationship existed between the ultimate load and the mode of failure.

All these analyses are for small specimens and it is not certain whether these criteria are applicable to large volumes of material which are more representative of the real structures considered here. However they demonstrate the important features of the tensile strength of fibrous composite materials which are:-

a) Tensile strength is not an intrinsic property of the material.

b) A stress concentration analysis is required to define tensile strength which can be related to the structural imperfections of the material.

c) The statistical variations in the strength of the single fibres is a governing parameter of composite strength.

d) The resin must be able to transmit, by shear, the load from one fibre to another.

e) If too good a bond exists between fibre and matrix then the crack will propagate through the interface, causing brittle fracture.

f) The mode of failure of unilayer composites is completely random.

2.2 Compressive Theory

Although an exact analytical description of the compressive behaviour of unidirectional C.F.R.P. composites at present does not exist in the literature, various theories have been suggested. Corten (11) has shown that, making the assumption that each fibre acts independently of neighbouring fibres, the critical buckling stress (σ_{crit}) can be defined by:-

$$\sigma_{crit} = \frac{1}{2}\left(\frac{E_f \beta_f}{\pi}\right)^{1/2} \qquad - 2.4$$

(β_f = Spring Constant)

The assumption that each fibre acts independently is over simplified. A majority of the composite materials in use today have fibre volume fractions above 0.2, and with such materials there exists large areas of fibre-fibre contact. In such a composite material it is inconceivable that the spring constant is not influenced by the large areas of closely packed fibres.

Rosen (12) considered a two dimensional model containing unidirectional filaments. When the model is loaded in compression he proposed that the fibres buckled individually, and that for a composite material one fibre interacts with its neighbouring fibres. Rosen analysed local buckling for

two modes of local fibre interaction as shown in Fig. 8, using an energy method. He designated the 'in phase' interaction, the 'shear mode' and the 'out of phase' interaction, the 'extensional mode'. The shear mode occurs when neighbouring fibres buckle with the same wavelength and are in phase. The extensional mode occurs when neighbouring fibres buckle out of phase but with the same wave length. His analysis gave the critical compressive stress (σ_c) for the extensional mode as:-

$$\sigma_c = 2 V_f \left[\frac{V_f E_m E_f}{3(1 - V_f)}\right]^{\frac{1}{2}} \qquad - 2.5$$

and for the shear mode the critical compressive stress was:-

$$\sigma_c = \frac{G_m}{(1 - V_f)} \qquad - 2.6$$

The estimated critical buckling stress for the composite is the stress σ_c computed from equations 2.5 or 2.6, which ever is the lower.

Rosen however commented that strengths of glass-epoxy composites did not achieve the theoretical strengths predicted by his analysis (Fig. 9). This was also found by Ewins (13) who tested unidirectional C.F.R.P. composites in compression, and obtained experimental test results which are several times lower than the strengths predicted by Rosen's analysis.

It is implicit in Rosen's analysis that all the fibres are well bonded to the matrix and that they are uniformly distributed throughout the matrix. However in a realistic composite these assumptions are seldom valid. Fibre-fibre contact and a poor fibre-matrix bond will tend to reduce the shear modulus of the matrix in equation 2.6. Also it will reduce the amount of matrix available to support the buckling ~~matrix~~ fibre. Even assuming that the

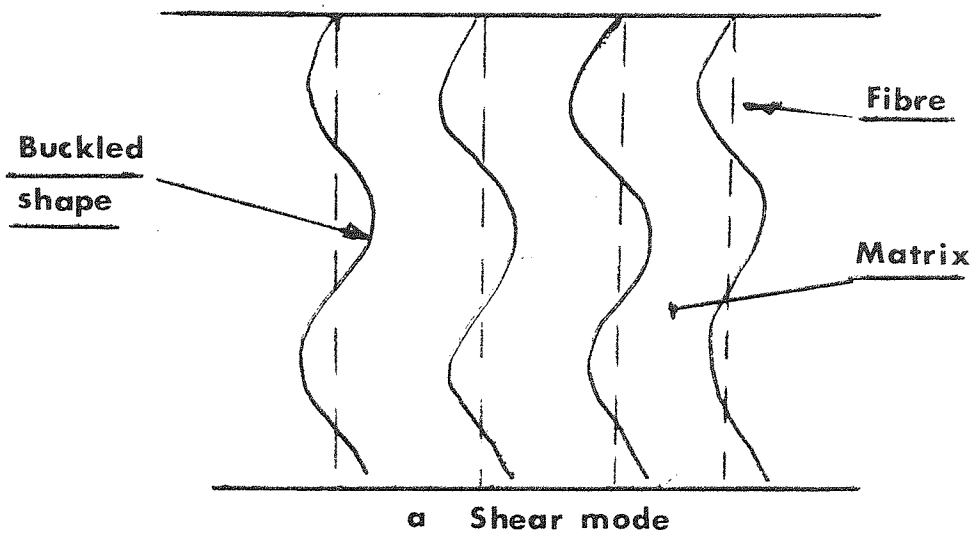

a Shear mode

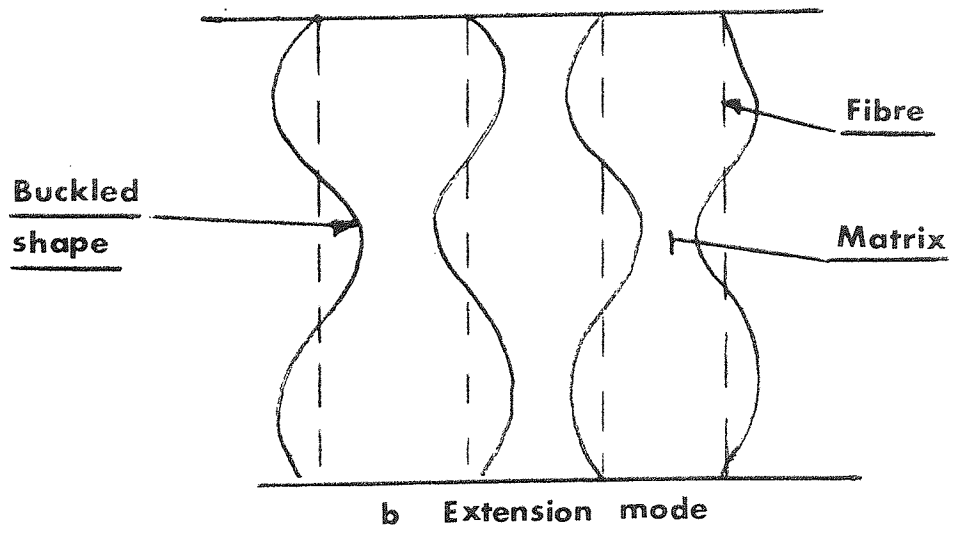

b Extension mode

Fig.8. Rosen's model of fibre buckling.

Theoretical compressive strength v. Fibre volume fraction (V_f)

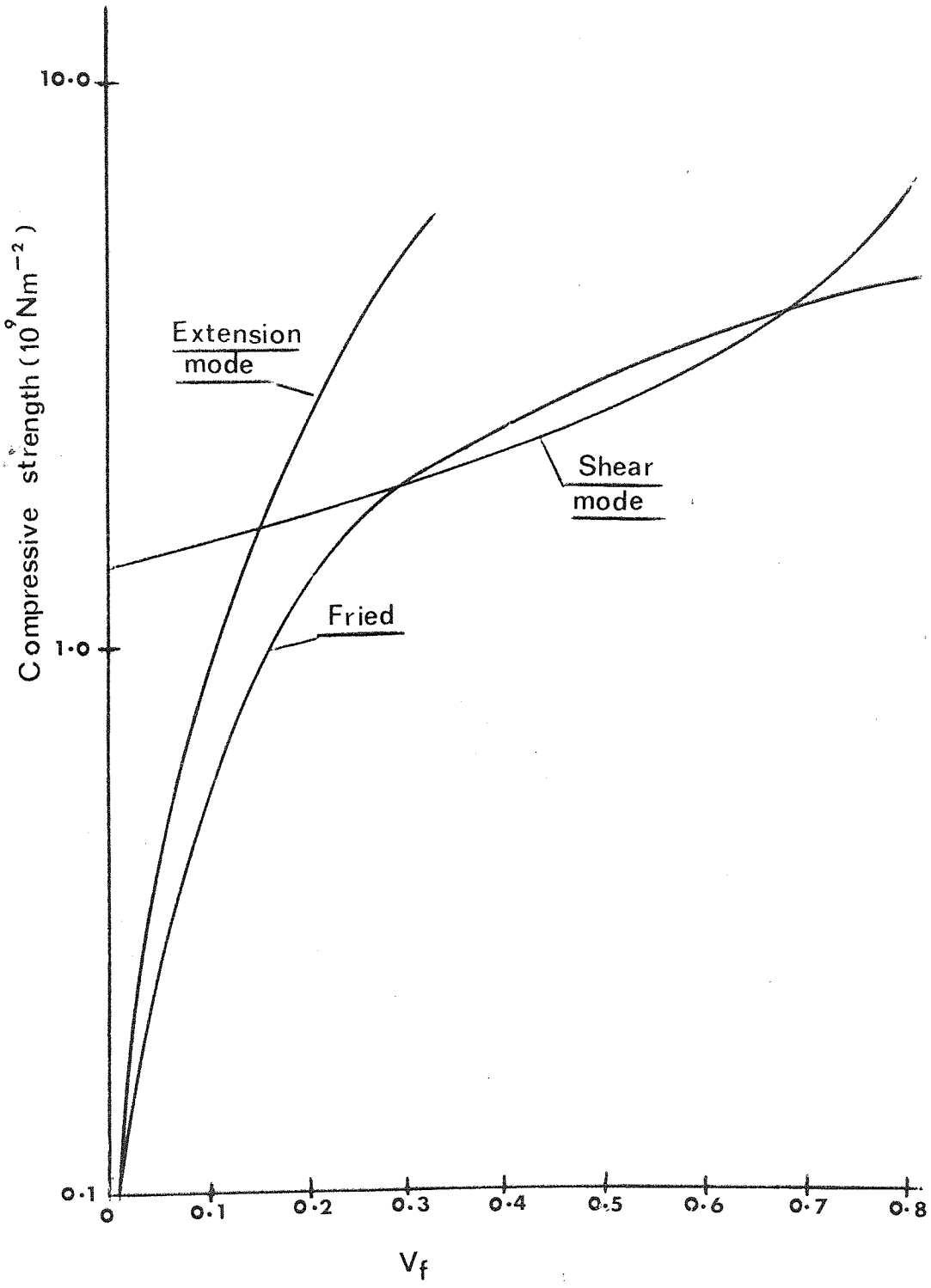

Fig. 9

fibres are perfectly bonded and uniformly distributed, it is doubtful that all the matrix material is effective in resisting buckling of the fibres. However in a three dimensional composite, neighbouring layers of fibres will interfere with each other, reducing the ability for the resin in these regions to resist fibre buckling. Lager and June (14) used this argument to justify the use of a factor of 0.63 to fit Rosen's theoretical analysis to their results for the compressive strength of unidirectional boron-epoxy composites having a square array of fibres. This factor of 0.63 is purely an empirical factor having no theoretical basis, and, as will be shown later, it will vary for different materials. However it is a helpful approach as it shows the large discrepancies between the theoretical and experimental results.

Moncurill et al (15) have compressed single steel wires embedded in polyester blocks. The fibres appeared to buckle into a helical shape rather than into the two dimensional or planer forms postulated by Rosen, and they suggest that the difference between the elastic energy stored in the planer-buckled fibre and in the helically-buckled fibre could be responsible for a large part of the discrepancy between theoretical and experimental compressive strengths. However when they tested single carbon fibres in polyester, the fibres did not visibly buckle but rather a pattern of regularly-spaced breaks occurred along the length of the fibre. The failure mode of a C.F.R.P. shows signs of fibre buckling, (see section 6); this would imply that the matrix becomes unable to support the fibres at a strain lower than that at which the fibres fail in compression. Therefore for C.F.R.P. composites other models must be considered.

Fried (16) postulated a 'yielding' model to describe compressive behaviour. He investigated the mechanism of compressive failure of composite specimens consisting of resin castings containing simple reinforcements. The results of his work led him to the hypothesis that in the limit, the point at which the resin 'yields' or flows, determines the load carrying capacity of the composites. It has been demonstrated that materials such as pyrex glass, stone and steel (17, 18 and 19) are able to withstand very high compressive stresses when they are subjected to hydrostatic pressures. Therefore Fried considered the resin as a fluid which exerts a high hydrostatic pressure on the reinforcement. At the 'yield' point of the resi the hydrostatic pressure falls off, the reinforcement is no longer adequatel supported, and the component fails. Using the 'law of mixtures', Fried suggested that the ultimate compressive strength of the composite would be:-

$$\sigma_c = \sigma_{my} \left(V_m + V_f \frac{E_f}{E_m} \right) \qquad - 2.7$$

(σ_{my} = yield point of matrix)

The yield strain of LY 558 was found to be approxinately 3%. This was used with equation 2.7 to compute the compressive stress shown in Fig. 9. Again this analysis predicts higher compressive strengths than those obtained experimentally. Fried considered the yield strength of the matrix in its solid form. However in a composite the matrix is not homogeneous as it contains fibres which may be poorly bonded and if misaligned cause residual stresses. Hence the effect of the fibres will tend to decrease the yield strength of the matrix, which will give a lower value of the compressive strength. Although Fried's analysis is not very rigorous it is valuable as it introduces a yielding criterion to explain compressive failure.

Employing a macroscopic model, Foye (20) produced a simple analysis of local 'crippling'. Foye recognised the fact that while woven fabric structures possess little or no inherent shear stiffness, their ability to

resist angular distortions can, under the proper circumstances, be increased merely by imposing a tensile stress state on the fibre. A similar stiffening effect can also be predicted for any material by the following argument based on energy principles. (17)

Consider an element of material subjected to a uniform tensile stress σ, in the direction of a principle elastic axis of the material (Fig. 10a). If the element is now subjected to an inplane shearing stress, τ, it is distorted as shown. The additional work done by the external forces must be equal to the additional strain energy stored in the element, i.e:-

$$\frac{\tau\gamma}{2} - \sigma(1 - \cos\gamma) = \frac{G\gamma^2}{2} \qquad - 2.8$$

assuming the material behaves linearly. For small values of γ, $(1 - \cos\gamma) = \frac{\gamma^2}{2}$ then equation 2.8 reduces to the following modified stress-strain law:-

$$\tau = (G + \sigma)\gamma \qquad - 2.9$$

Thus the mechanism, whereby the presence of a tensile stress state may augment the shear stiffness, is evident. For common isotropic materials G exceeds the values of σ that can be applied by such a large amount that any effect on shear stiffness is unnoticed. However in fibre reinforced materials composites, loaded along the fibres, G is often much smaller and comparable with σ

If the direction of the tensile stress were reversed, then the effective shear stiffness $(G + \sigma)$, of the element, would decrease. From equation 2.9 the effective inplane shear stiffness of the element should approach zero when

$$\sigma_c = G_c \qquad - 2.10$$

and the element would be susceptible to crippling in a shear mode.

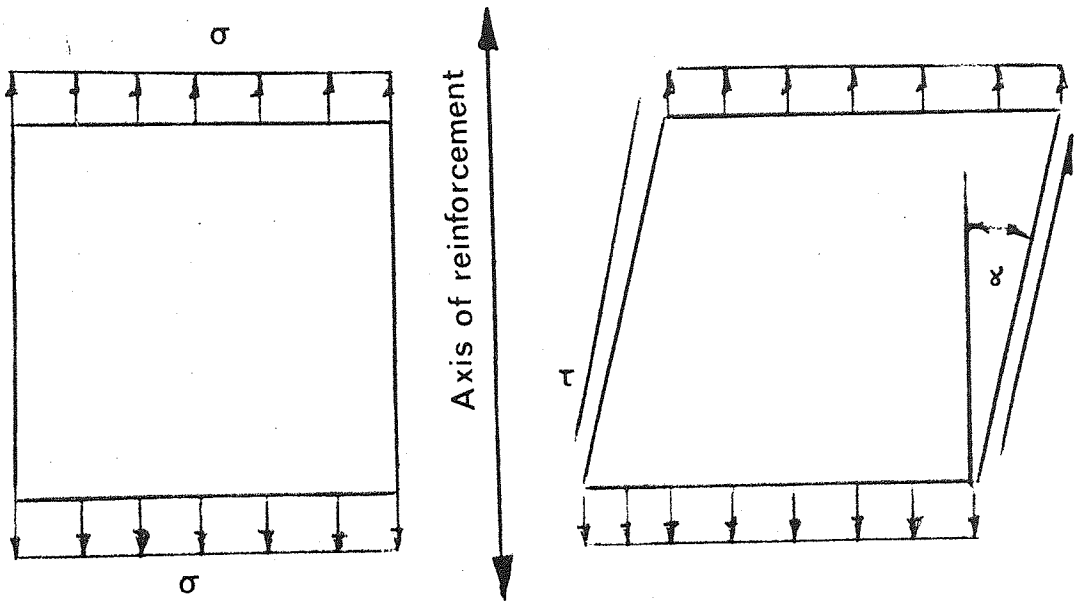

Fig.10a. Unit element of composite.

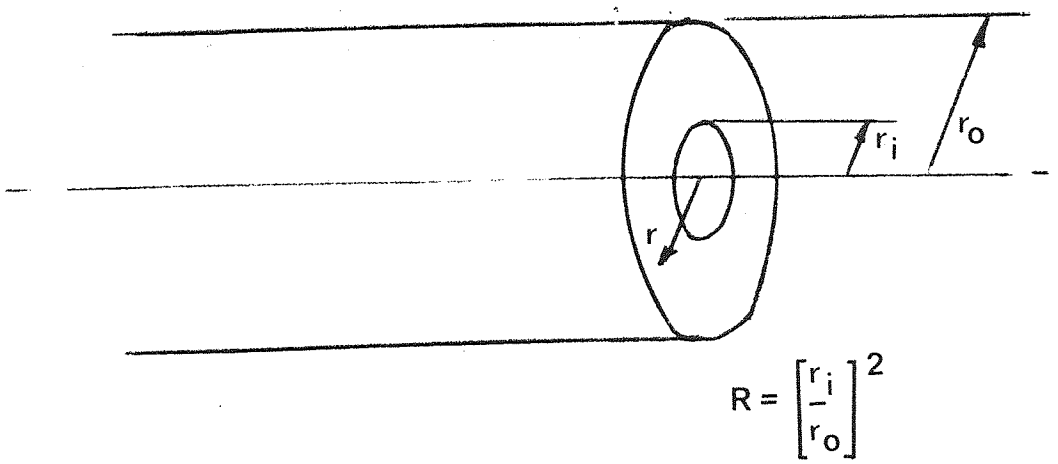

Fig. 10b. Hollow cylinder model .

Adams and Doner (21) have used finite element techniques to obtain numerical results for the shear modulus of unidirectional composites with a variety of fibre arrays, various filament to matrix shear modulus ratios, and a range of filament spacings. The results of their analyses compare favourably with experimental results (22). Using these values of shear modulus the ultimate compressive strengths were determined using equation 2.10 and are plotted in Fig. 11. In contrast to Rosen's model the crippling failure is usually a local phenomena, involving a single crest and trough shaped wave. Foye observed such waves primarily in the plane of the specimen, although there was some evidence of surface ripples.

Foye also demonstrated the importance of voids in reducing the compressive strength; he proposed that a reasonable model to account for the influence of voids on shear stiffness consisted of a hollow cylinder with a ratio of inner radius (r_i) to outer radius (r_o) of $R^{\frac{1}{2}}$ (Fig. 10b). He solved the boundary problem and equated the mean strain energy per unit volume of the hollow cylinder to that of the voided material and found that:-

$$G_v = G_c\left(\frac{1 - 2R + R^2}{1 + R}\right) \qquad - 2.11$$

G_v = modulus of material with voids
G_c = modulus of material without voids

To relate R of the hollow cylinder to the void content (V_v) of the composite, Foye made two assumptions, (a) the fibre volume fraction of the composite is the same in an unvoided area as in a voided area and (b) the reinforcement contained within a void is totally ineffective for resisting longitudinal shear. Then R is related to the void content V_v, by:-

$$R = \frac{r_i^2}{r_o^2} = \frac{V_v}{1 - V_f} \qquad - 2.12$$

combining 2.11 and 2.12 gives the compressive strength of a composite containing voids as:-

$$= G_v = G_c \left\{ \frac{1 - 2\left(\frac{V_v}{1 - V_f}\right) + \frac{V_v^2}{(1 - V_f)^2}}{1 + \frac{V_v}{1 - V_f}} \right\} \qquad - 2.13$$

The compressive strength is plotted against fibre volume fraction for different void contents in Fig. 11. To account for the differences noted between the theoretical and experimental results in terms of voidage, using the above analysis, a composite with a fibre volume fraction of 0.6 would have to contain 15% voids. Although such void contents are possible it is unlikely that the composites considered here are so highly voided. (Typical void contents on C.F.R.P. specimens were approximately 2%). However this analysis is important because it does demonstrate the importance of voids on the compressive strength of composite materials.

Foye also extended his analysis to predict an increase in composite shear stiffness when small quantities of powder and whisker fillers were added to the matrix. The addition of fillers increases the shear modulus of the matrix material which from equation 2.10 and Addams and Doner's work also increases its resistance to compressive crippling (21).

Both Fried (16) and Hand (23) investigated the compressive strength and shear strength of filament wound materials. It was found that the shear and compressive modes of failure were similar. They concluded that voids appear to control the failure process and an inverse relationship was found for shear and compressive strengths against void content. Although these relationships are empirical, it is doubtful whether they define exactly the compressive strength for all composite materials, once again the importance of voidage on the compressive and shear strengths of composite materials is demonstrated.

Foye interpreted this continuin, discrepancy between theoretical and experimental results to mean that the simple analysis did not account for other imperfections in the material such as localised misalignment or poor fibre-fibre bonding. Such imperfections will cause areas of reduced shear modulus.

Hayashi (24) has combined the shear instability model of Foye and the yielding criteria to present a theory of compressive strength of composite materials. The compressive stress in the matrix, σ_m^*, at the shear instabili limit is determined by the condition:-

$$\sigma_m^* = G_m \cdot f(\sigma_m^*) \qquad - 2.14$$

where G_m is the shear modulus of the matrix depending upon the compressive stress σ_m^*. Thus the compressive strength of the composite in the fibre direction σ_c is given by:-

$$\sigma_c = \sigma_f^* V_f + \sigma_m^* (1 - V_f) \qquad - 2.15$$

where σ_f^* is the corresponding fibre stress at the same strain as the matrix strain for σ_m^* Hayashi suggested that the matrix shear modulus at the matrix yield strain is approximately expressed by the empirical formula:-

$$\sigma_m^* = G_m(\sigma_m^*) = G_m \left[1 + \left(\frac{\sigma_m^*}{\sigma_{my}}\right)^n\right]^{\frac{n+1}{n}} \qquad - 2.16$$

$$n \approx 10$$

He observed that the shear instability limit of the matrix material (σ_m^*) is usually greater than the matrix yield stress. Hence to be on the 'safe-side' it was suggested that σ_{my} should be used instead of σ_m^* in equation 2.15, which reduces to Fried's expression for compressive strength (equation 2 Again this does not take into account any localised defects.

From the above the following important facts, concerning compressive strength, emerge.

1) The shear modulus of the matrix material is used by Addams and Doner to determine the shear modulus of the composite, therefore it is the governing variable in both the micro and macrostability analysis defining the compressive strength.

2) Matrix voids will cause a reduction of the shear modulus of the matrix hence there is an inverse relationship between voids and compressive strength.

3) It has been suggested by several workers that other localised discontinuities such as fibre misalignment or poor fibre-matrix bond also reduce the compressive strength of composite materials.

4) The compressive strength may be improved by the addition of small quan of powder or whisker fillers to the matrix, which appear to reinforce the matrix.

2.3 Flexural failure

The flexural strength of a material which does not yield is defined as the maximum stress at failure of a bent beam. For isotropic materials the maximum stress is usually a tensile stress occurring at the outer surfa of the beam. However, as will be shown later, the C.F.R.P. beam, under certain conditions, fails in the compressive zone.

The basic flexural test for a beam of constant rectangular cross secti is set-out in the British Standard B.S. 2782 method 304. The following assumptions are made in calculating the flexural properties:-

1) The material is homogeneous and has the same value of Young's modulus

in tension and compression. Chambers and McGarry (25) have shown that, at high strains, for glass fibre reinforced plastics there is a slight shift in the neutral axis towards the compressive side of the beam. The shift is more pronounced with glass fibre reinforced cement laminates (26) and commences at the onset of crazing of the matrix.

The shift in the neutral axis for both the resin and the cement reinforced composites appears to occur at the onset of matrix crazing. The strain of failure of carbon fibre is less than that of the matrix, hence the fibres fail before the matrix and it was not expected that there would be a difference in the Young's modulus in compression and tension. Workers at Rolls Royce (27) have shown that C.F.R.P. have the same value of Young's modulus in tension and compression up to failure. Therefore it is a reasonable assumption that the neutral axis remains in the centre of the beam until the onset of failure, where it will be displaced as the failure crack begins to run.

2) The beam is initially straight and all longitudinal layers bend into circular arcs with a common centre of curvature. If the beam is long and thin (above an aspect ratio of 40 : 1) it can be shown that the shear deflections are so small that the above assumption is valid.

3) Transverse cross-sections remain plane and perpendicular to the neutra surface after bending. The validity of this assumption will be discussed later when the effect of beam width on the flexural strength is examined.

4) The radius of curvature is large compared with the dimensions of the cross-section. The beam dimensions were so designed to give this condition

5) The stress is purely longitudinal and local effects near concentrated loads are neglected. Evidence will be submitted later showing that Hertzian pressures around the central roller may cause premature failure in compression. However, when the beam fails in tension the strength appears unaffected by the concentrated loads under the roller.

6) Friction at the supports has a negligible effect on the flexural strength. To reduce any possible friction, rollers rather than rods were used at the supports, (Fig. 12).

Making the above assumptions, it can be shown that the maximum tensile or compressive stress at the mid-point of the upper or lower surface of the beam is:- (28)

$$\sigma = \frac{3LW}{2bd^2} \qquad - \ 2.17$$

where:- W = load d = specimen thickness

b = specimen width L = specimen length

and that there is a maximum shear stress along the neutral axis of:-

$$\tau = \frac{3W}{4bd} \qquad - \ 2.18$$

Broutman et al (29) pointed out that when glass fibre reinforced plastics were tested in bending, failure generally starts by buckling of the compressed surface, and they compared this with similar failures found with Douglas fir. In both materials shallower beams have greater flexural strength than that of thick ones. This was believed to be due to the sharper stress gradient in the beam, resulting in the most highly stressed fibres being restrained from buckling by the adjacent fibres under considerably lower stress. Although this is the most likely explanation, the high flexural stress obtained with thin specimens may also be explained by a size effect. That is with the small volume of material under test there is less chance of a

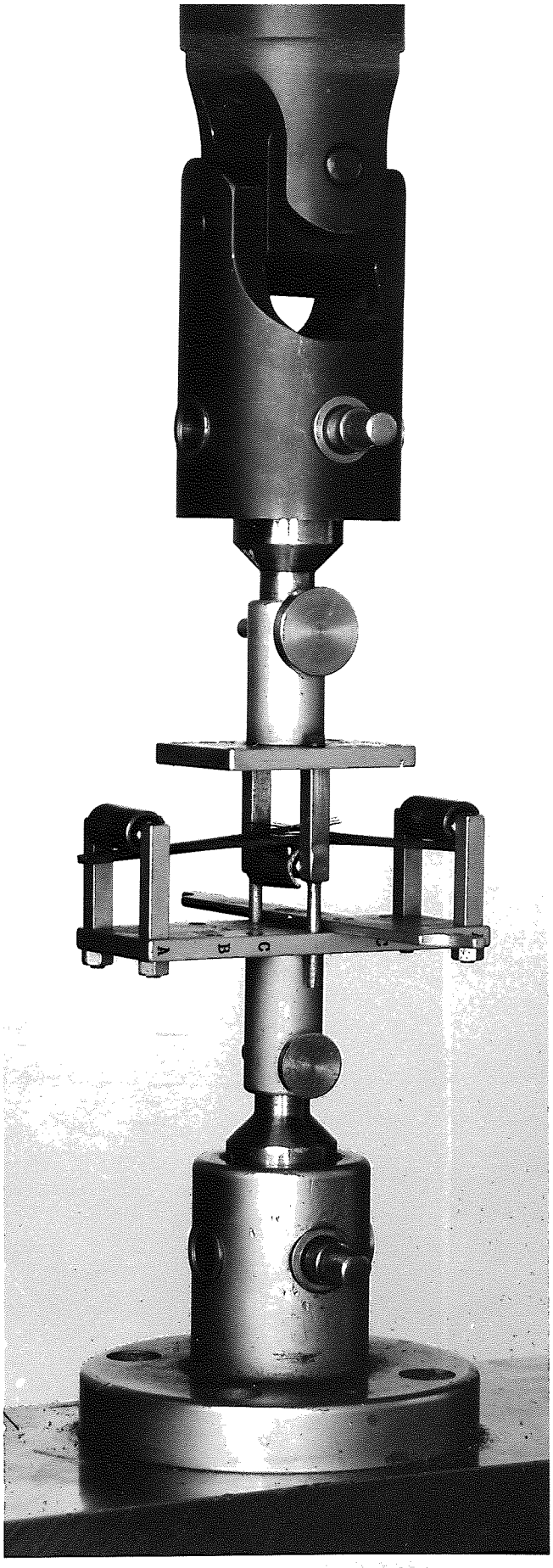

Fig. 12. Three point bending fixture.

flaw causing the beam to fail prematurely.

They also observed that there was a shift of the neutral axis as the beam began to fail in the compressive region. As failure increased there was a progressive shift of the neutral axis until the beam failed catastrophically in tension. As with the observations of McGarry and Chambers this shift in neutral axis did not occur until failure of the matrix had begun.

The fibre buckling in the compressed region of the beam was similar to the compression buckling observed by Bader et al (30) in their studies of carbon fibre composite materials under impact loading. This work has shown that when they fail, as a result of impact, a two stage breakdown frequently occurs. In the first stage, compression buckling takes place on the impacted face which progresses towards the neutral plane. In the final stage failure occurs on the opposite face by fibres pulling out in tension.

Bader's conclusions were that the flexural impact properties could be improved by:-

1) Good fibre-matrix bonding, but avoiding very high bond strengths.
2) Maximum fibre strength.
3) High fibre strain.
4) Maximum fibre content.

From these conclusions they appear to be making the general observation that the impact strength, in bending, will be improved by increasing the

tensile strength of the composite.

The tensile failure was the final failure mode and no mention was made of the possibility that the impact strength may be increased still further by strengthening the matrix so as to inhibit the tendency for the fibres to buckle in compression. If the compressive region was strengthened and fibre buckling eliminated, then there would be no shift in the neutral axis and a greater volume of material would be available to withstand the tensile stresses.

2.4 The role of the interface in stopping cracks.

When the bond between the fibre and the matrix is very good, a tensile crack will propagate rapidly through both the fibre and the matrix, producing a brittle failure, (8, 31). However, when the bond is less than perfect, the material is tougher (31). Cook and Gordon have investigated the effect of the interface on the toughness of glass fibre reinforced plastics (32) and suggested a mechanism for stopping cracks.

Stress distributions, caused by an elliptical crack, were computed at rightangles and parallel to the plane of the crack. The maximum stress concentration which occurs at the crack tip, is approximately 200 in a plane at rightangles to the crack compared to a maximum of approximately 40 in a plane parallel to the crack. The maximum stress, parallel to the crack, is reached at one or two atomic spacings ahead of the crack and also a fairly high tensile stress level exists over a considerable area ahead of the crack.

Cook further suggested that, irrespective of the proportions of the crack or the means by which it is loaded, the ratio of the maximum value of the stress parallel to the plane of the crack, to the peak stress at the tip in a plane at rightangles to the crack, is constant and has a value of one to five.

Therefore, where a weak bond exists between a fibre and matrix the following mechanism can occur, when a crack is approaching the interface at rightangles. When the area of tension stresses ahead of the crack tip reaches the interface it will tend to pull the fibre and matrix apart. If the stress at the interface is greater than one-fifth of cohesive strength of the material, then the interface will remain in tact and the crack will propagate through the interface. If however the fibre-matrix bond is less than one fifth of the cohesive strength of the material, then the interface will be broken before the crack reaches it and an effective crack stopper has been created.

2.5 Modulus

For isotropic materials the modulus is considered to be an intrinsic property of the material and is related to the chemical bonds within the crystal of the material. Any variation in Young's modulus is due to the fact that the chemical bonds can themselves vary considerably. However a composite material is anisotropic and the C.F.R.P. composites have five independent elastic constants. (See appendix I)

The Young's modulus in the longitudinal direction is given by equation 2.2 and experimental results agree with this equation (33,34). The remaining

four elastic constants have been determined by using variational and boundary layer methods using a variety of models such as a monolayer, hexagonal array, etc. (35,36)

All the techniques to determine the elastic constants of composite materials involve a highly complex mathematical analysis, which is beyond the scope of this work. Also many of these demand an exactly defined model, and once the composite departs from the ideal, such as a non-uniform fibre array, then inaccuracies occur in the analysis. However, it is necessary, in the understanding of the mechanisms of failure in bending, to have a knowledge of the elastic constants of the composite beam. In this work an empirical approach has been adopted to determine the elastic constants. (See section 6).

2.6 Summary

1) The tensile strength of a composite material is governed by the statistical variations in the strength of the single fibres and the ability of the matrix to transmit, by shear, the load from one fibre to the other.

2) When a beam is subjected to bending stresses, the final mode of failure is tensile. However if the material has a low buckling strength, then initial failure will occur by buckling with a progressive shift of the neutral axis.

3) The shear modulus of the composite is the governing variable in determining the compressive or buckling strength. Localised discontinuities such as voids, fibre misalignment or poor fibre-matrix bond, reduce the compressive strength of the material.

4) The compressive strength of the composite may be improved by the inclusion of fillers in the matrix.

5) Under impact conditions a mode of failure similar to that of static bending failure was observed.

6) If the fibre-matrix bond is weak, then the composite material is tough; however it will not be able to transfer the load efficiently and as a whole it will be weaker. If however fibre-matrix bond is perfect the composite behaves in an extremely brittle manner. Therefore the strength of the interface needs to be controlled to give the best combinations of strength and toughness.

Chapter 3

Manufacturing Processes

There are three main processes of producing composite materials, filament winding, 'leaky-mould' and prepreg techniques. Filament winding (37) requires sophisticated machinery to obtain a tight control over the fibre volume fraction and distribution; also it is not really suitable for non-circular structures. With the 'leaky-mould' technique, fibres are weighed to give a required fibre volume fraction. Resin is then poured into the mould and left for a period of time to allow the resin to cover the fibres completely. One big disadvantage of this is that it is extremely difficult to vary the direction of the fibre or to 'tailor' the material to give a shape such as a fan blade.

The prepreg method allows quite complicated structures to be produced and the fibre direction can be varied easily. Also the fibre volume can be varied and controlled accurately. Rolls Royce use this method for producing fan blades (38), hence the prepreg technique was used in this project and can be divided into six stages as listed below.

3.1 Impregnation

a) An exact weight of carbon fibre was placed carefully on to a measured area on a sheet of silicone coated release paper. (The release paper could easily be removed from the 'tacky' laminate). The weight of fibre, on a known area, was varied to give a desired volume fraction of fibre.

b) A measured amount of epoxy resin and hardener, diluted in acetone, was poured into a plastic 'squeezy' bottle. Again great care was taken

in measuring out the amount of resin, so as to keep a tight control over the volume fraction of the composite. The amount of resin measured out was the quantity of resin required to give a certain volume fraction of resin, plus 5 to 10% excess by weight which is lost during the moulding operation.

c) The impregnated sheet was placed under infra-red lamps for fifteen minutes, the temperature on the sheet being approximately 70°C. This drove off a certain amount of acetone, which increased the viscosity of the resin. This was necessary, because if the viscosity of the resin was low during the subsequent rolling operation, the fibres could swirl, causing them to be at varying angles to each other. During the fifteen minutes under the I.R. lamps, changes in the surface tension of the resin draws the fibres together into discrete bundles of fibres. To remove these gaps in the fibre, the sheet is lightly smoothed out with a spatula during the fifteen minutes under the lamp.

d) To remove any gaps in the impregnated sheet and smooth out any uneven areas of resin, the sheet was rolled. A second sheet of release paper was placed on top of the impregnated sheet. The sheet was placed between a $^{1}/_{8}$" thick aluminium plate and a thin sheet of steel, which were both slightly larger than the sheet. Both the metal sheets and the impregnated sheet were rolled between the rollers of a domestic mangle. The rolling operation was continued until there were no gaps between the fibres of the impregnated sheet. To maintain the viscosity of the resin at the level which permits the gaps between the fibres to be removed, the metal sheets were heated to approximately 70°C. Excessive heat reduced the viscosity of the resin, allowing the fibres to move around when pressure was applied.

3.2 'B' Staging

Some acetone had already been removed during the fifteen minutes under the I.R. lamps and the rolling operation. The remaining acetone was removed by heating the sheet to 80°C for 75 minutes. After this heat treatment the sheet was in a 'B staged' condition. In resin technology a 'B staged' material is one which is soluble in such solvents as acetone, and hard at room temperature but softens when heated. However it may not entirely dissolve or fuse (39).

After 75 minutes at 80°C the resin had not hardened completely, and the laminates were sufficiently 'tacky' for them to stick together.

3.3 Laminating

a) The impregnated sheet was cut into strips, to the exact size of the mould cavity. Care was taken in measuring and cutting, as any variation would cause a variation in the moulded volume fraction.

b) The strips of laminate were carefully layed on each other until the laminated block was the required thickness. The resin-fibre formulation was designed to give a thickness of 0.005 in, for each strip of laminate, when moulded, hence the number of laminates required to produce a moulded block of certain thickness, can easily be determined. The laminated block is referred to as the preform. By cutting the strip out of the impregnated sheet, at various angles relative to the plane of the fibres, it was possible to design a moulded composite with layers of fibres at varying angles to each other.

c) The preform was weighed. This was a further check to ensure that the laminates had the correct fibre to resin ratio.

d) Finally the prepreg was stored in a refrigerator, until it was required for moulding. By keeping the prepreg at low temperatures the 'shelf life' of the resin was considerably increased. The 'shelf life' is defined as the time available for use of the epoxy system after the resin and the curing agent have been mixed. (40)

3.4 Precure

When significant masses of resin are involved, the use of an initial high cure temperature results in exotherms, which may be enough to degrade the physical properties of the resin. Because of the exotherm, it is customary to gel the BF_3 - MEA - epoxy resin systems at approximately $120^{o}C$. (41) (Gel is the initial jelly-like solid phase that devlops as the liquid resin cross-links to form a solid (39)). This partial curing operation is referred to as the precure.

With the LY 558 resin system the precure was probably necessary for other reasons. Later, evidence will be offered to suggest that precure increases the viscosity of the resin so that when a pressure is applied to it, during the moulding operation, voidage within the composite is reduced. Another possible reason for the precuring operation is that it will effectively remove any traces of acetone that may remain in the system after the 'B' staging operation.

The precuring temperature, for the LY 558 - BF_3 - MEA system, was $125^{o}C$. At this temperature the BF_3 and MEA dissociate and the BF_3 begins to catalytically cure the epoxy resin. (See Appendix II).

The gel time for the HX4C system, at the moulding temperature is so short that the precuring operation is omitted. A precure will increase the viscosity of the resin making it very difficult for the preform to be moulded down to the design thickness.

3.5 Moulding

Two different types of presses have been used for this work, a hand and an automatic press. The hand press used a mould which sat between two hot plates. The temperature of the hot plates was controlled by a 'Honeywell' recorder from a thermocouple which was located in the top plunger of the mould. The depth of the moulding cavity can be varied by changing the spacers under the lugs of the plunger (Fig. 13)

One disadvantage with this press was that the mould had to be removed from the heat source when the preform was loaded into the mould. This caused a fall in the temperature of the working faces of the mould. Another disadvantage was that as it was a hand press the pressure was applied hydraulically by pumping a lever, consequently it was extremely difficult to get a constant application of pressure.

With the automatic press, the two halves of the mould were fixed to the top and bottom bolsters of the press which were heated, their temperature being controlled by proportional controllers. The temperature on both the working faces of the mould was checked and found to be within $2^{o}C$ of the recorded temperature. The prepreg was placed in the moulding cavity and the mould closed, by a hydraulic pump, the rate of approach of the two halves of the mould was controlled through a needle valve. As the mould approached

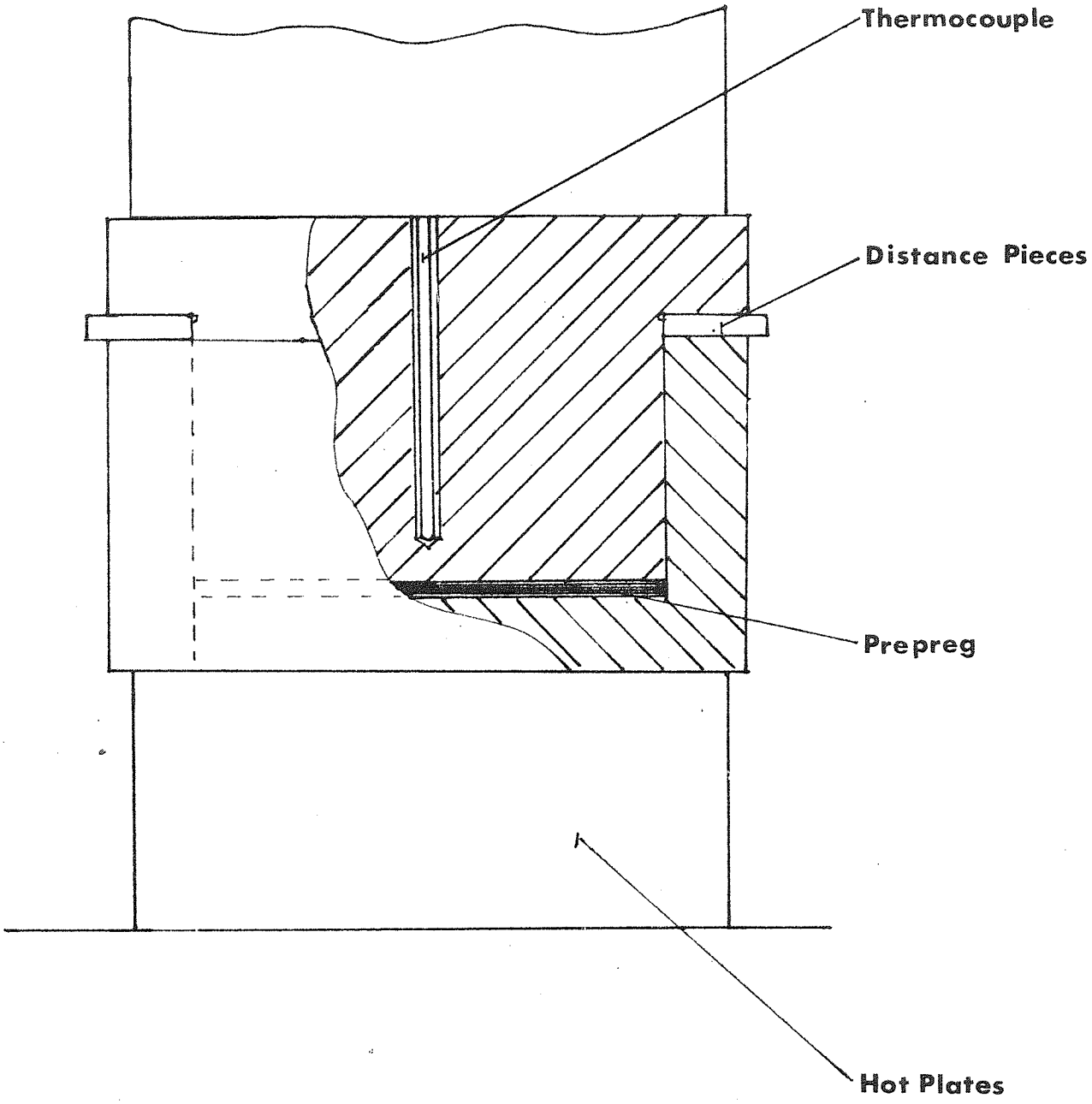

Fig13. MOULD USED ON HAND PRESS.

the fully opened condition, injector pins came up through the bottom half of the mould lifting the moulding clear. (Fig. 14) Because the mould is not removed from the heat source, the temperature of the working faces, of the mould, was accurately controlled throughout the moulding cycle. With this design of press both the rate of approach of the two halves of the mould and moulding pressure were controlled accurately. The depth of the moulding cavity can be varied by changing the pressure pads on the top half of the mould. (Fig. 14)

The moulding process was as follows:-

a) The working faces of the mould were coated with a thin film of release agent. This provides for clean removal of the moulded block from the mould.

b) The prepreg was placed in the moulding cavity, the temperatures of which were 150°C for LY558 and 165°C for HR4C.

c) A short length of time was allowed to pass (dwell time) before the moulding pressure was applied. This allowed the temperature at the centre of the prepreg to reach the moulding temperature. The length of the dwell time depended upon the volume of the prepreg.

d) The mould was closed and a pressure applied to the specimen. If the moulding was to be made to a fixed volume then the fixed stops were used. The laminate was left under pressure and the moulding temperature, for 30 minutes. During this period the BF_3 was reacting further with the epoxy resin and cross-linking of the resin structure was taking place. After 30 minutes the moulded block was rigid enough to be removed from the mould.

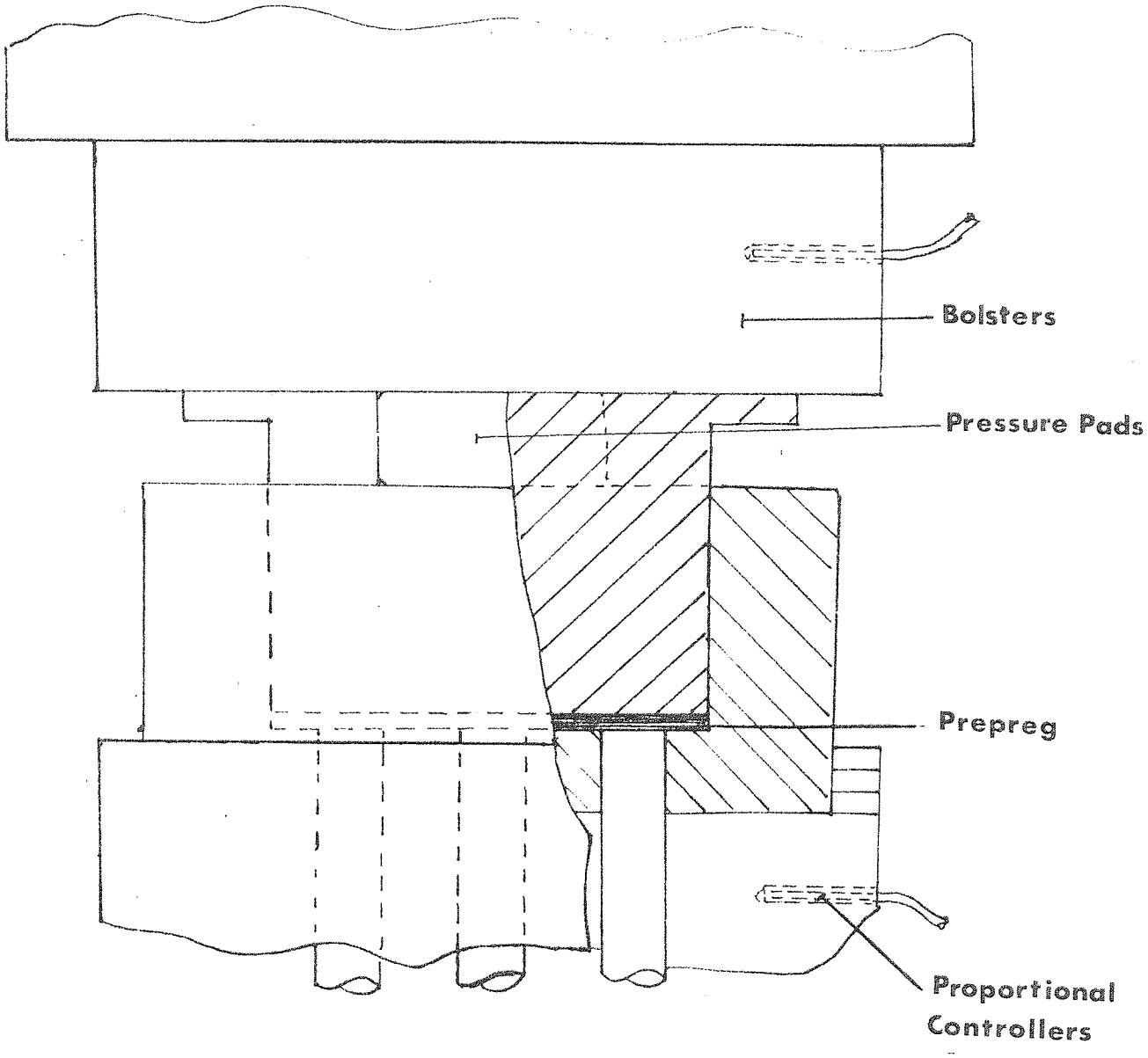

Fig.14 MOULD USED ON AUTOMATIC PRESS.

3.6 Moulding Trials

Initial moulding trials were conducted to determine which of the moulding parameters were the most important. The prepregs were produced from sheets impregnated with the LY558 - BF_3 resin system.

The prepreg measured 152 mm x 12.7 mm and contained 20 laminates which gave a moulded specimen 2.54 mm thick. The following parameters were kept constant throughout the initial series of tests.

Precure temperature	=	$125^{o}C$
Dwell time	=	0.75 mins.
Moulding temperature	=	$150^{o}C$
Moulding pressure	=	3.8 MNm^{-2}

It was shown that although the resin flow (i.e. the percentage weight loss of the specimen during moulding) decreased with increasing precure time (Fig. 15), the amount of voidage present in the specimen also decreased. (Fig. 16) Increasing the precure time increases the viscosity of the resin and shortens the time the resin is in the mould before it gels and therefore reduces the amount which can be squashed out during the moulding process.

3.7 The dependence of mechanical properties on void content

The existence of an ~~inverse~~ linear relationship between interlaminar shear strength and void content, has been observed by various workers investigating the mechanical properties of glass fibre reinforced plastics. (Chapter 2 of this Thesis) (42-44) W. Hand (23) determined an empirical expression for interlaminar shear strength (I.L.S.) in terms of the volume of voids (V_v) present in the composite:-

$$I.L.S. = 66 - 5.5\ V_v \quad \text{(where the units are } MNm^{-2})$$

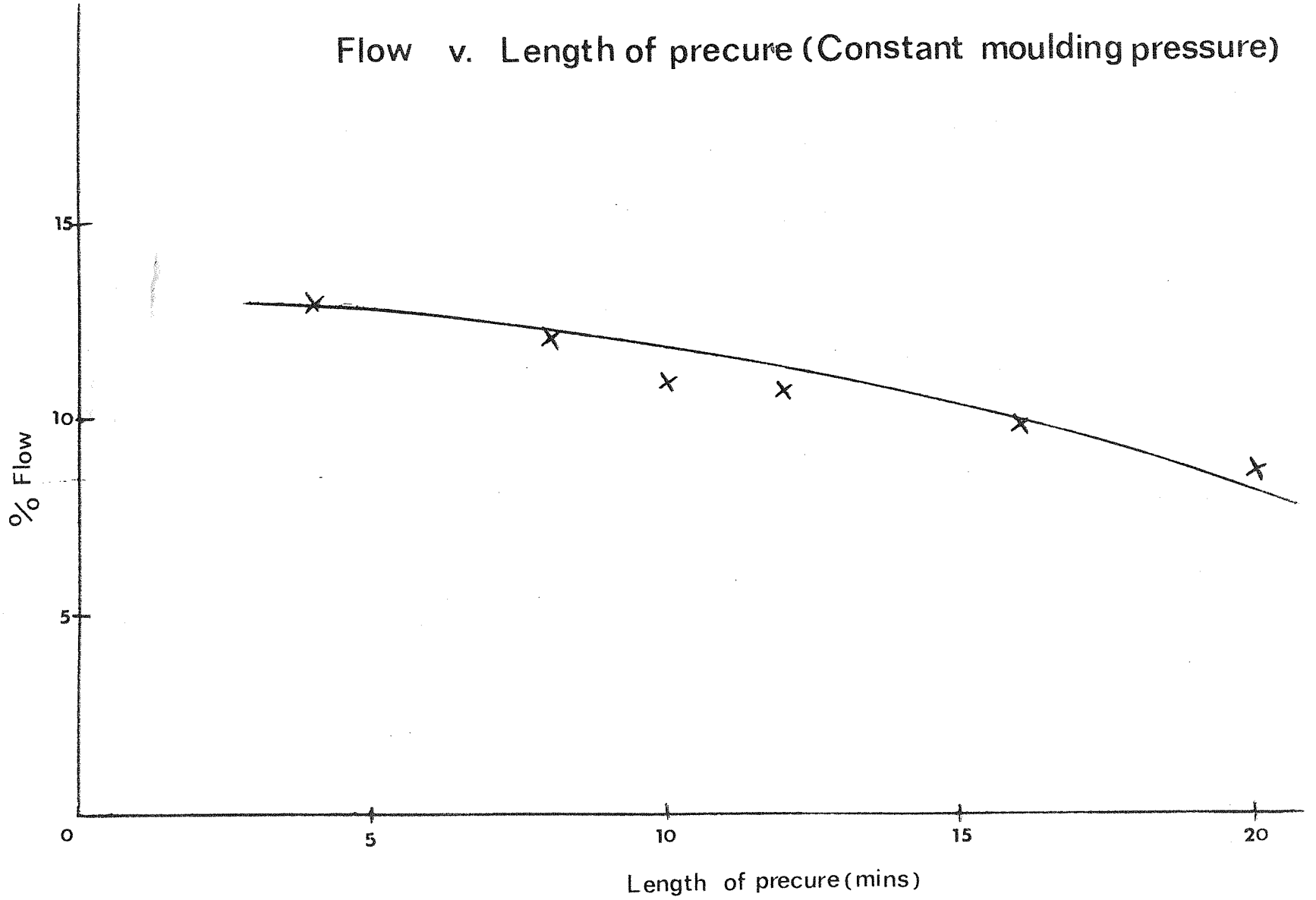
Flow v. Length of precure (Constant moulding pressure)
% Flow
15
10
5
0
5
10
15
20
Length of precure (mins)

Fig.15.

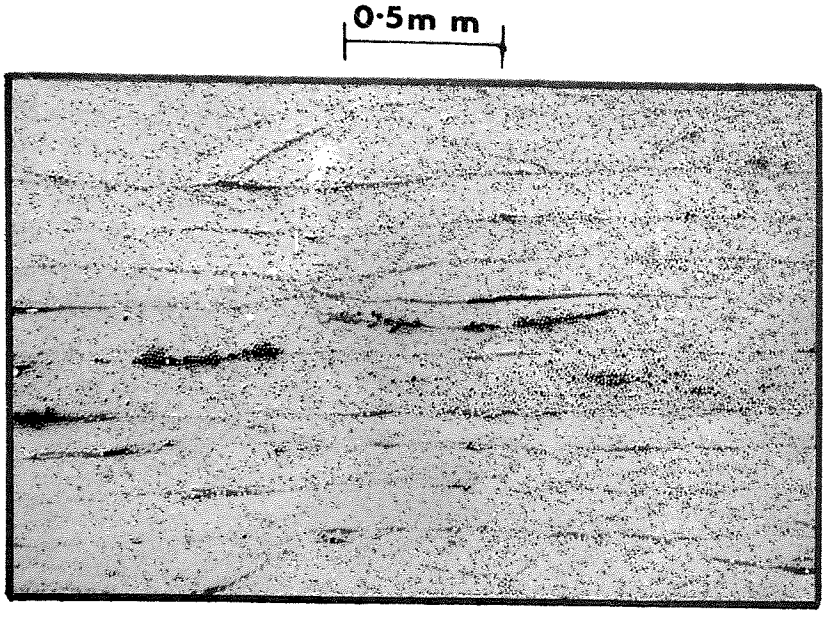

12 min.

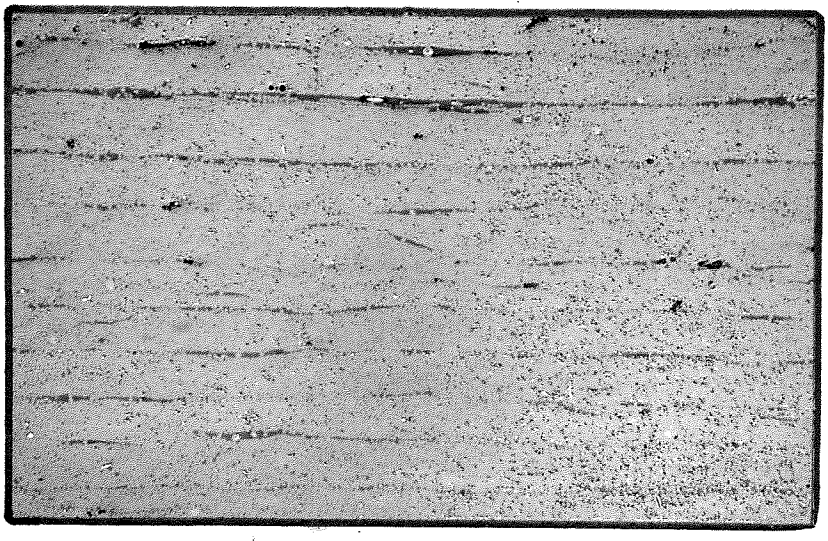

18 min.

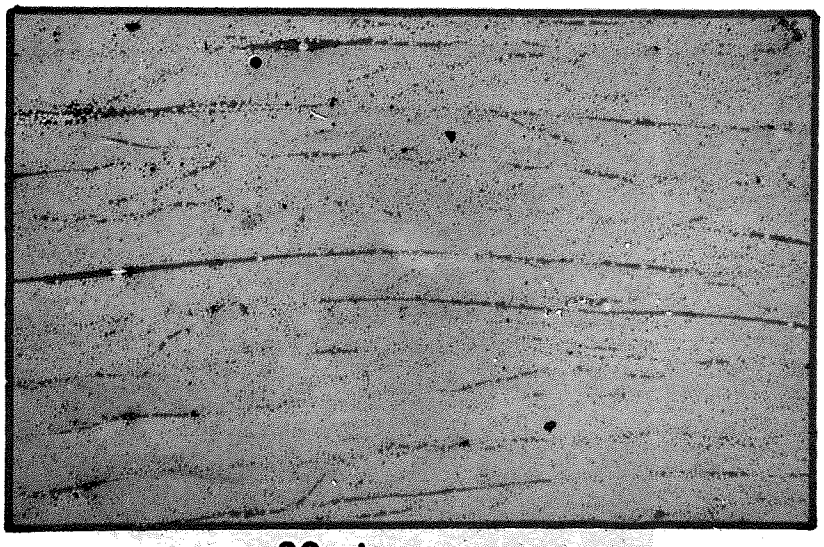

20 min.

Fig. 16. SPECIMENS PRECURED IN AIR FOR VARYING LENGTHS OF PRECURE, MOULDED WITHOUT FIXED STOPS

By assuming an 'equivalent crack length' which was proportional to the cube root of the void content, Corten (11) applied a fracture mechanics analysis to the results obtained by Hand. Both analyses fit the results well but Corten's approach is preferred primarily because it appears to provide a sound theoretical basis for the trend of horizontal shear strength with void content. This is only a crude analysis as it does not take into account the irregular size of the void.

The automatic press was used to investigate whether the inverse correlation between voidage and precure time, discussed briefly in section 3.6, still applied, when specimens were moulded to a fixed volume under well controlled conditions. The moulding conditions were as above apart from the pressure which was 8.3 MNm^{-2} on the specimen. The specimens so produced were 203 mm x 25.4 mm x 2.54 mm in size. After post cure the following tests were made on each specimen:- interlaminar shear strength, using the short beam shear test; flexural strength test (span to depth ratio of 40 : 1) to measure the maximum tensile or compressive stresses the outer layers of the beam will withstand prior to failure; and the dynamic longitudinal modulus. Both the interlaminar shear test and the dynamic modulus test are described in Appendix III.

Figures 17, 18 and 19 show the relation between interlaminar shear strength, flexural strength and dynamic modulus as a function of precure time. Micrographs (Fig. 20) of the cross section of the specimens showed that voidage decreased with increasing precure time. Whereas the dynamic modulus and flexural strength were little affected by variations in precure time or void content, the interlaminar shear strength was significantly affected. Maximum interlaminar shear values were attained for those specimens which had

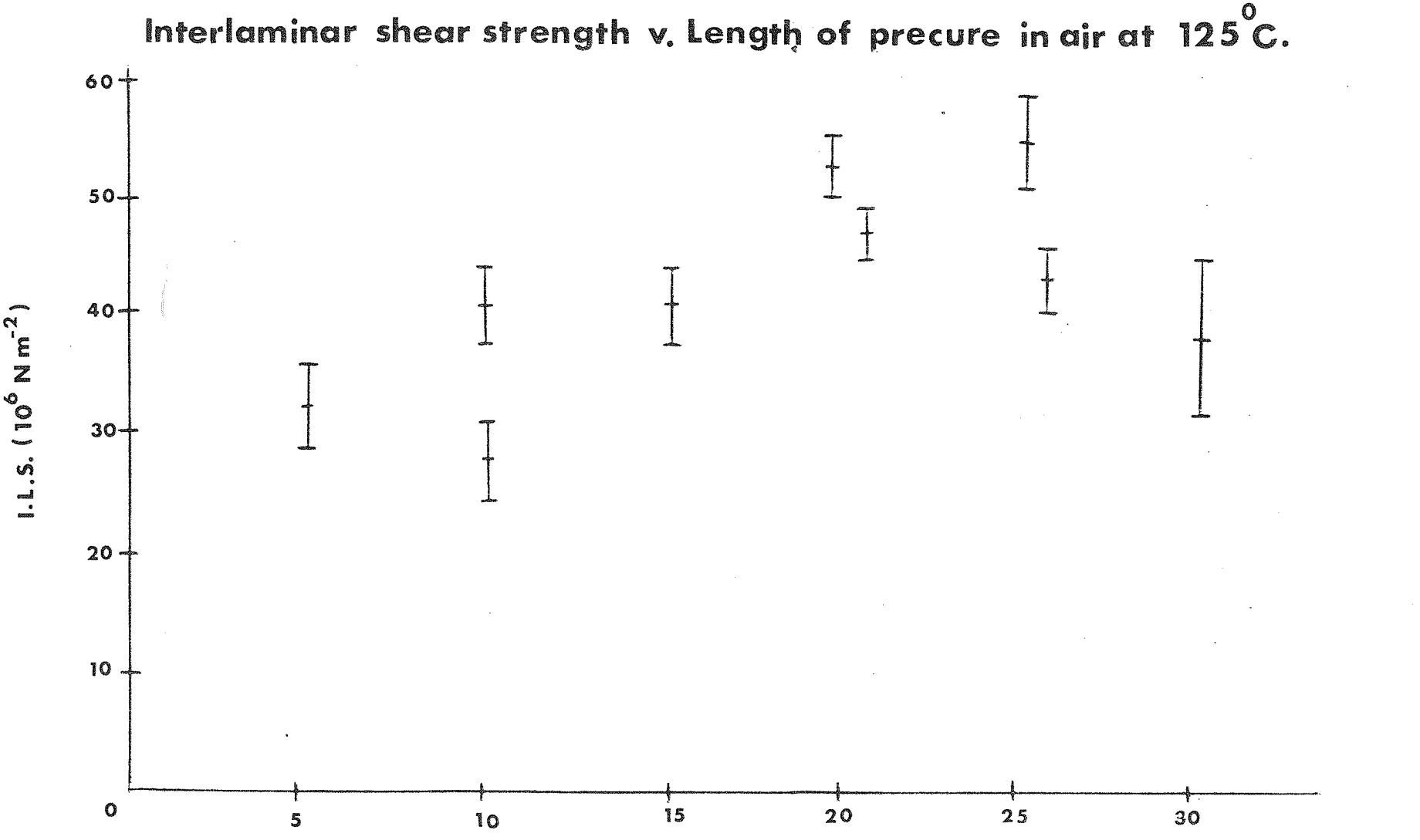
Interlaminar shear strength v. Length of precure in air at 125°C.
I.L.S. (10^6 N m^{-2})
60
50
40
30
20
10
0
5
10
15
20
25
30
Precure time (mins)

Fig.17.

Flexural strength v. Length of precure in air at 125° C.

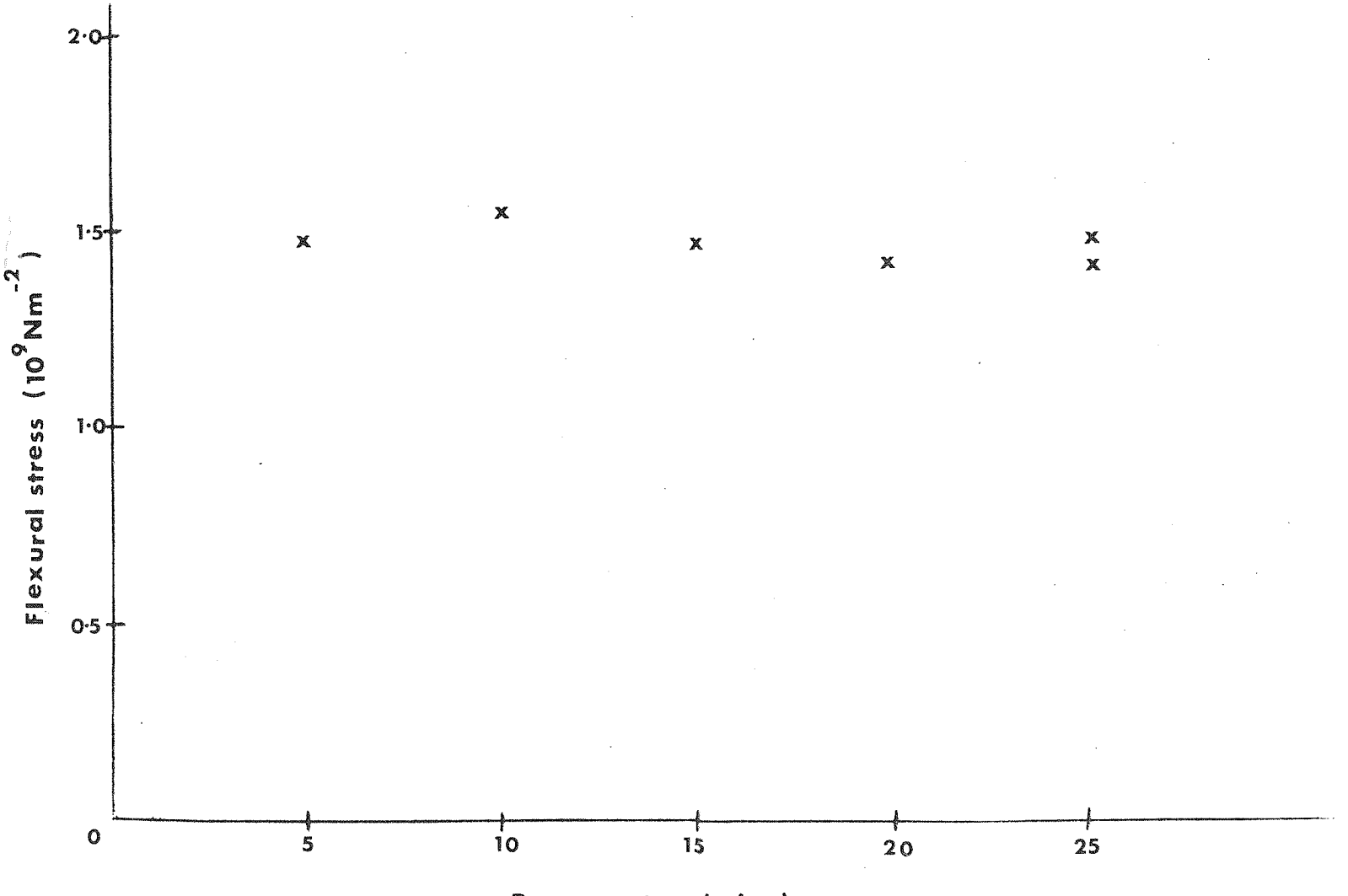

Fig·18.

Modulus v. Length of precure in air at 125°C.

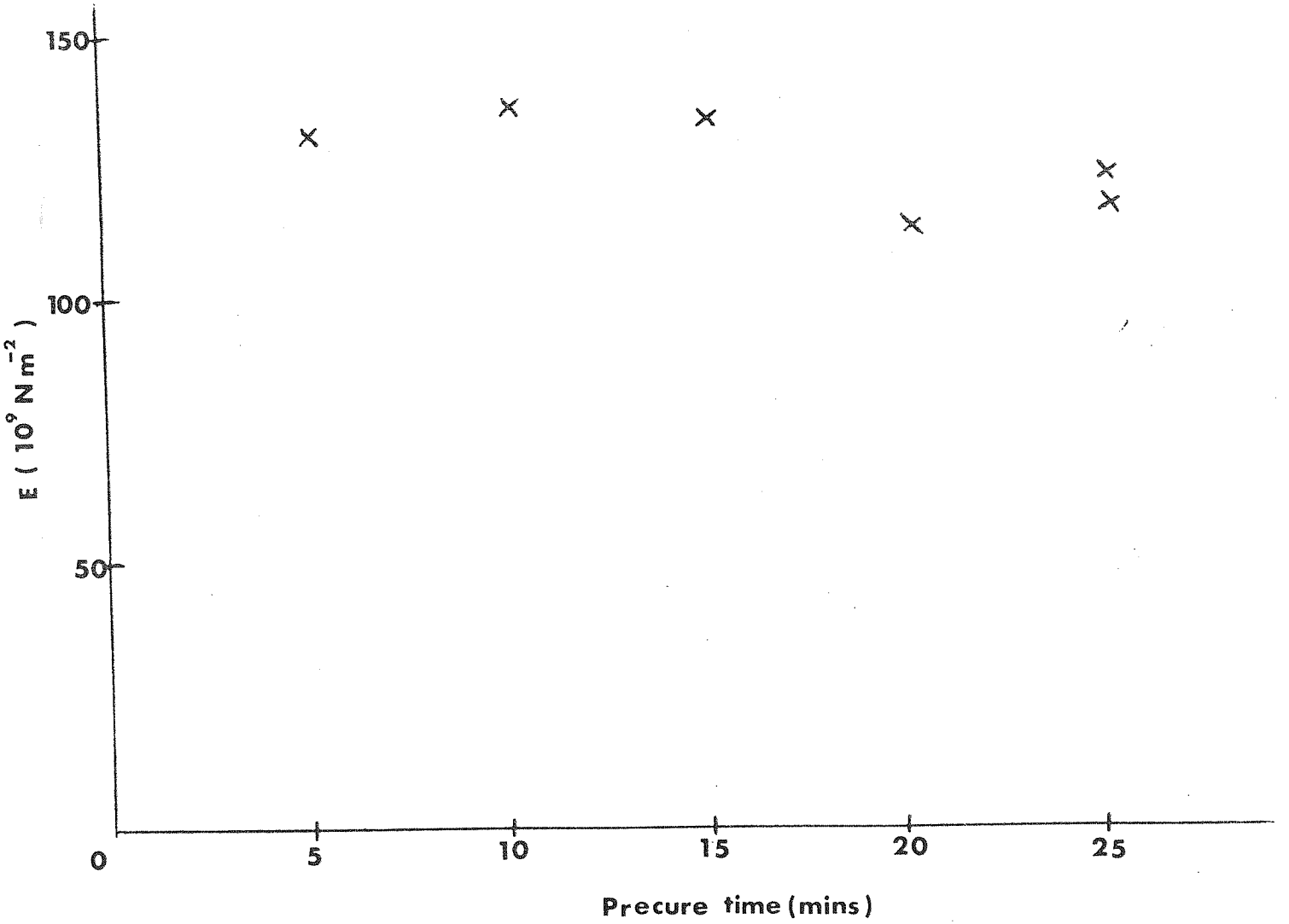

Fig. 19.

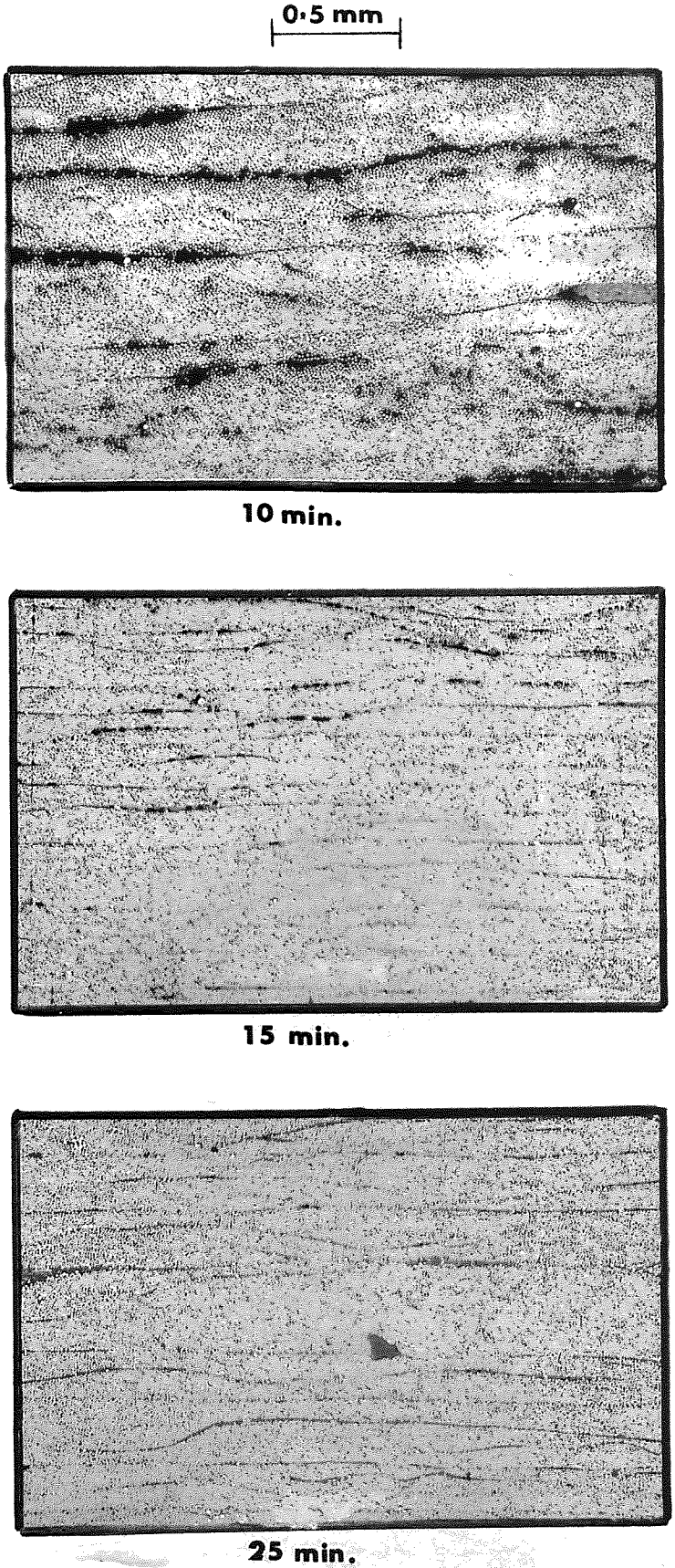

Fig.20. SPECIMENS PRECURED IN AIR FOR VARYING LENGTHS OF PRECURE.

the lowest void contents, that is for the specimens which had only just or not quite moulded to fixed stops. Excessive precure (approximately 30 mins.) prevents any compaction taking place in the mould and thus leaves a specimen with a large amount of voidage whilst insufficient precure also produces a voidy specimen.

Using the same moulding conditions but a different batch of impregnated laminate, a more direct correlation between I.L.S. and void content was sought. The precure time was varied from 10 to 25 minutes in 3 minute increments so as to provide a varying void content. From the specimens so produced, interlaminar shear strength and flexural strength test pieces were cut. The cut faces adjacent to each end of a specimen were metallographically mounted and polished and the area void content was measured using the Metals Research 'Quantimet' (Q.T.M.) The Q.T.M. is an analysing microscope connected to a television screen which can provide quantitative information on size and number of microscopic features of different optical intensity. Using the Q.T.M. it was possible to estimate the void content of each test specimen by taking the average void content of the two end faces of the specimen.

Void content as a function of precure time is plotted in figure 21 and again an inverse relation is apparent. Individual values of interlaminar shear strength are plotted against void content in figure 22, and a least squares quadratic fit has been made to these points. The effect of modest amounts of voidage (2-4%) is clearly not insignificant on the interlaminar shear strength. In figure 23 although there is no clear dependence of flexural strength on void content, there is a change in the mode of failure at the higher void contents. For low void contents the beams failed in tension, at void contents above 4% the specimens failed by a crack which

Void content v. Precure time in air at 125° C.

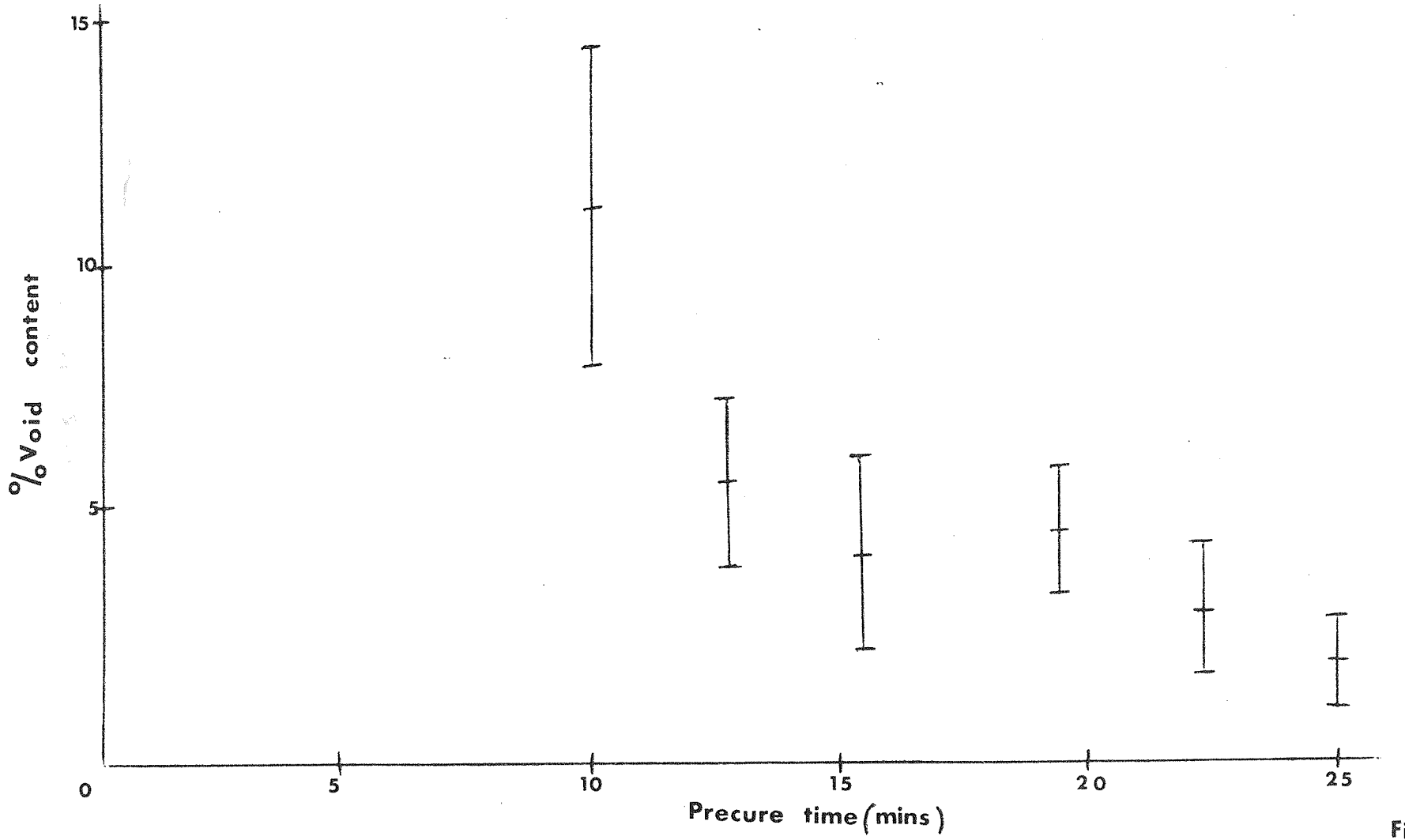

Fig. 21.

Interlaminar shear strength v. Void content.

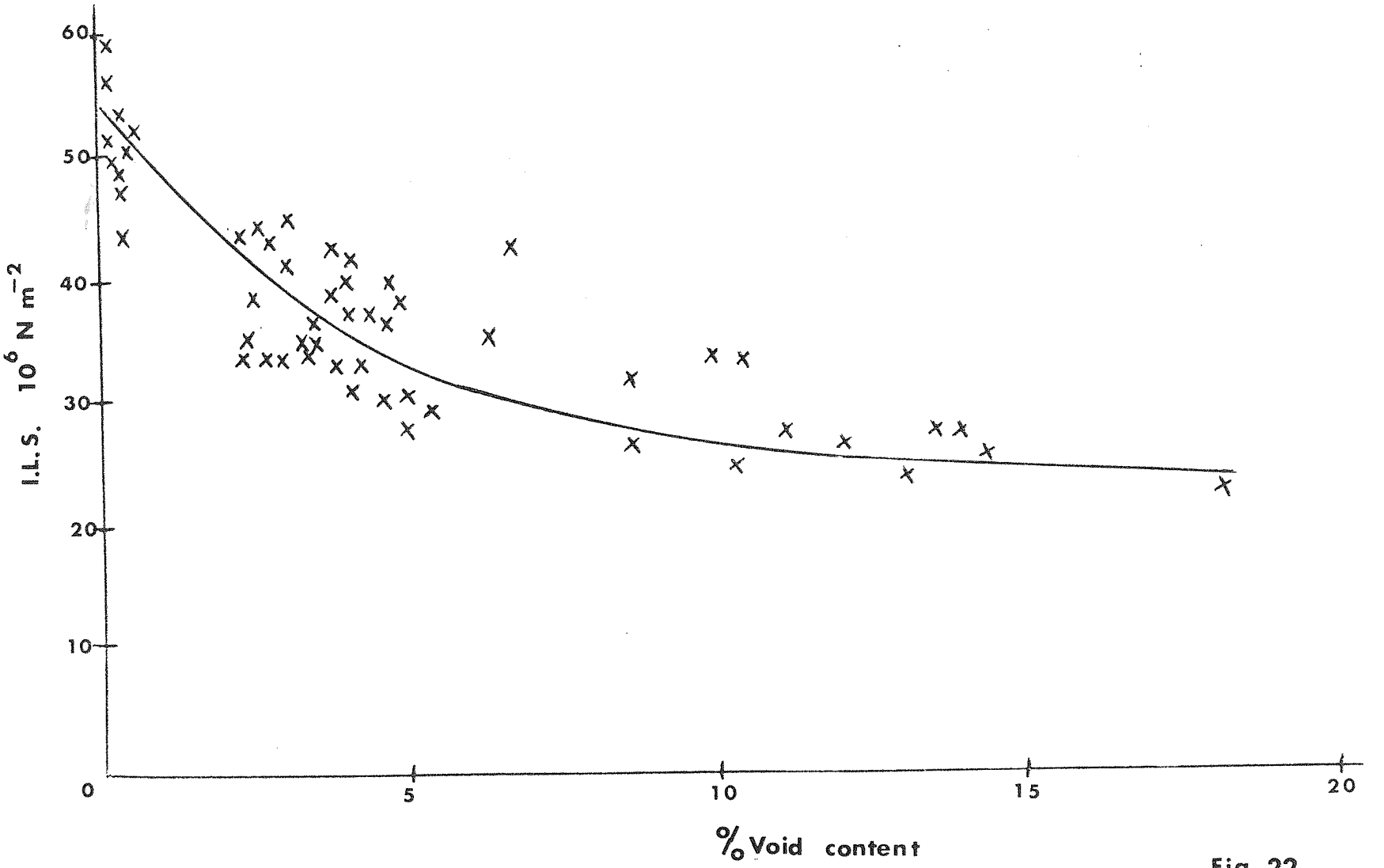

Fig. 22.

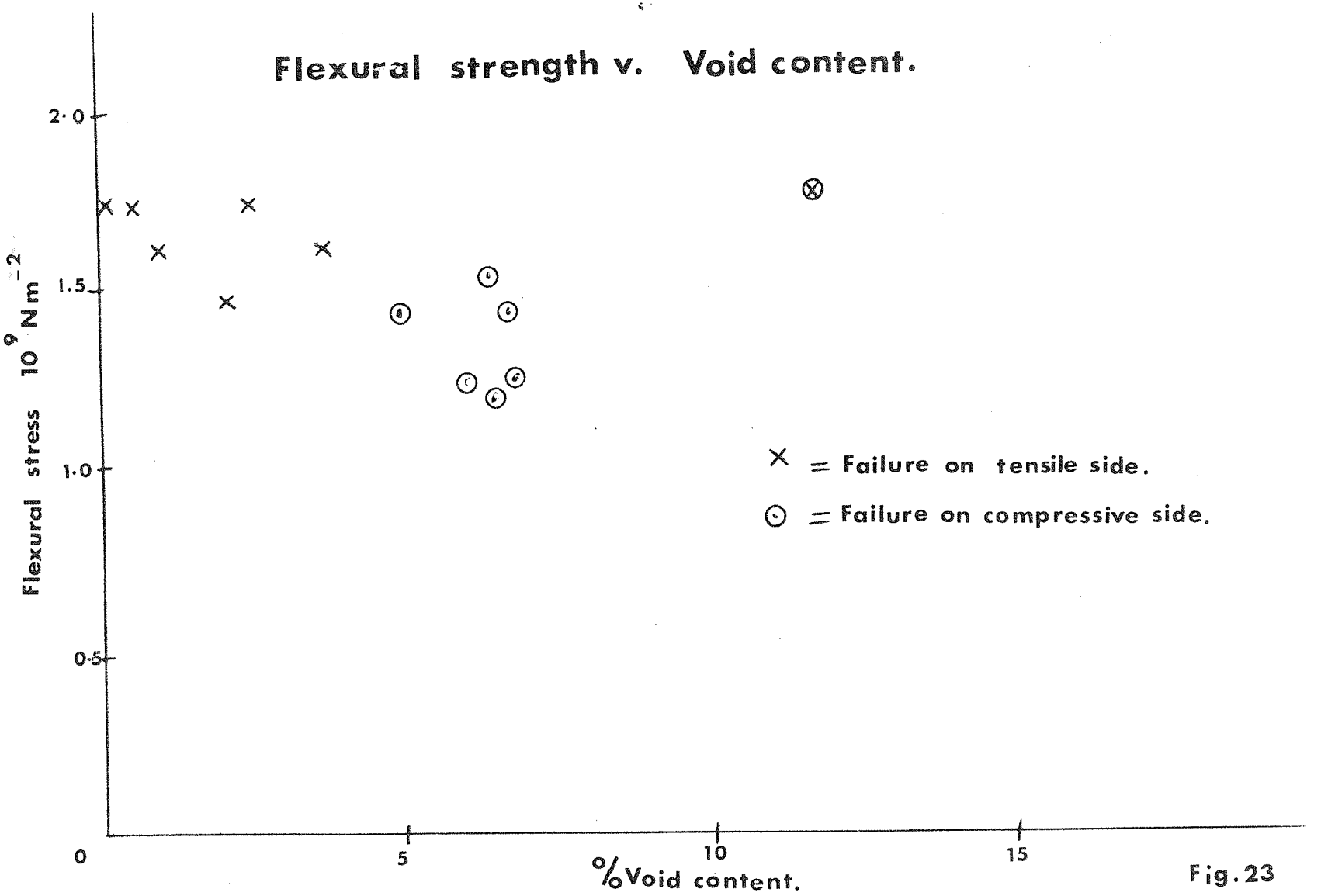
Flexural strength v. Void content.
2·0
1.5
1·0
0·5
0
5
10
15
Flexural stress $10^9 Nm^{-2}$
%Void content.
× = Failure on tensile side.
⊙ = Failure on compressive side.

Fig.23

was initiated in the compressive side of the beam and was stopped at the neutral axis by shear cracks. The reasons for this behaviour will be discussed in more detail later.

3.8 Methods of reducing void content

In view of the inverse correlation between void content and interlaminar shear strength it was of interest to investigate further means of producing void free mouldings. The void most frequently found was one which had an eliptical cross-section (Fig. 20), which extended several filament diameters across the fibres. The position of these voids is usually in the resin rich bands between the laminates. One explanation as to the cause of voidage could be that pockets of air are trapped between the laminates during the manufacturing process, and these remain within the prepreg throughout the curing operation. Another possible cause of voidage is that any volatiles, present in the resin, are boiled off and form discrete gas bubbles within the composite.

3.8.1 Acetone free specimens

The main contributor to the volatiles, which are present in the LY558-BF_3 resin system, is the acetone which is used as a solvent for the LY558. To examine the effect of acetone, laminates were produced using resin which had not been diluted by acetone. These specimens were made using a thin resin film impregnation technique.

In this technique a thin film of resin is melt coated onto a sheet of release paper and directly transferred to the fibres by a hot rolling process, to produce an impregnated sheet, without the use of any acetone. This sheet is then cut, preformed and moulded in the usual way.

Typical cross-sections taken from specimens after being precured for times varying from 5 to 25 minutes and then moulded in the normal way are shown in figure 24. The only specimen which was free of voids was the specimen precured for 25 minutes, and moulded when the resin had gelled, and consequently the specimen did not reach fixed stops. This would suggest that acetone, used as a solvent in the production of the laminated sheet, is not the main contributor to voidage in the moulded composite.

3.8.2 Rolled Specimens

Initially two laminates were stuck together and warm rolled between a mangle. Localised bubbles of entrapped air could then be seen preventing the laminates from bonding together over their total possible contact area, suggesting the importance of air entrapment during the laminating process.

In view of this, attempts were made to put laminates together without allowing pockets of air to be trapped. To do this laminates were rolled on top of one another using the technique illustrated in figure 25. By keeping the laminate being rolled on to the preform stack under tension it was hoped to apply the laminate with a single advancing area of contact and thus avoid the formation of gross air pockets. These carefully made preforms were pre-cured along with control preforms stacked in the usual way. One pair of specimens was precured for 15 minutes and the other two pairs were precured for 20 minutes in air at $125^{o}C$.

Micrographs (Fig. 26) of the two specimens precured for 15 minutes, showed that the specimen which was carefully laminated contained appreciably less voidage. The specimens which had been carefully laminated and precured for 20 minutes were free of voids and those specimens which had been precured for 15 minutes contained only a small percentage of voids.

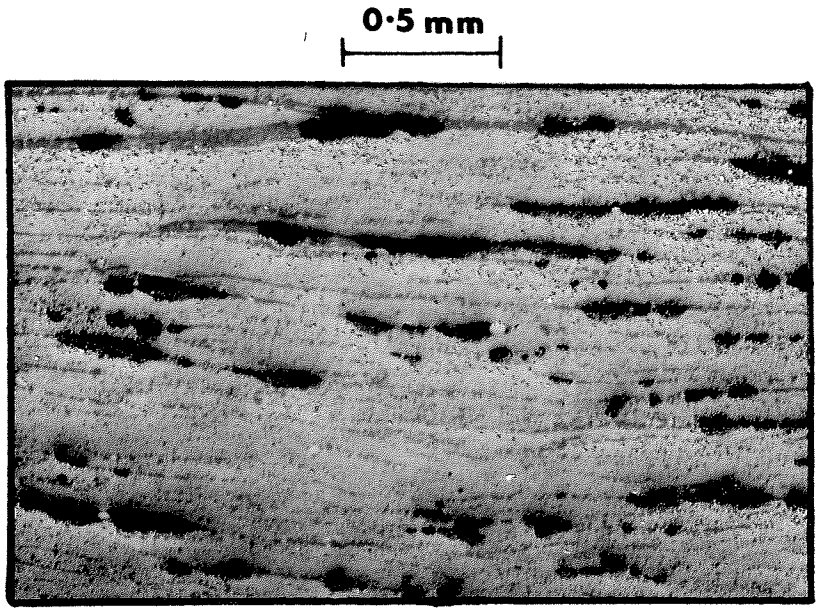

10 min.

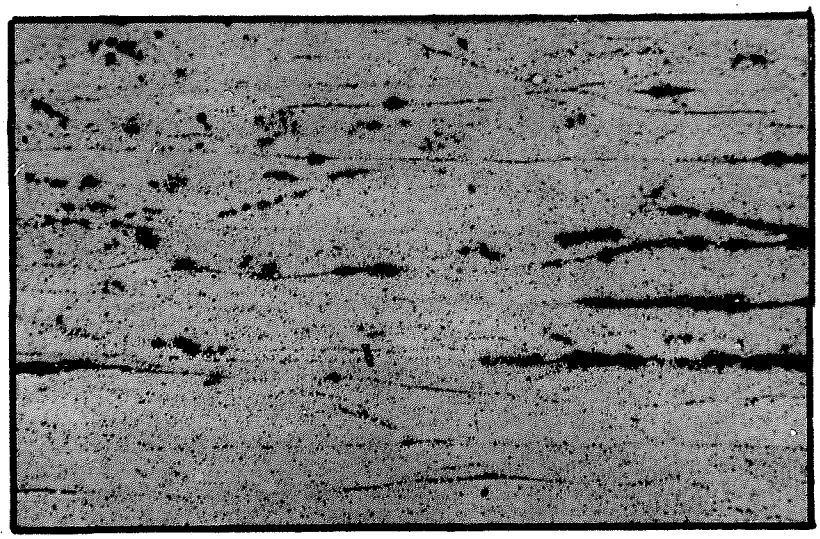

20 min.

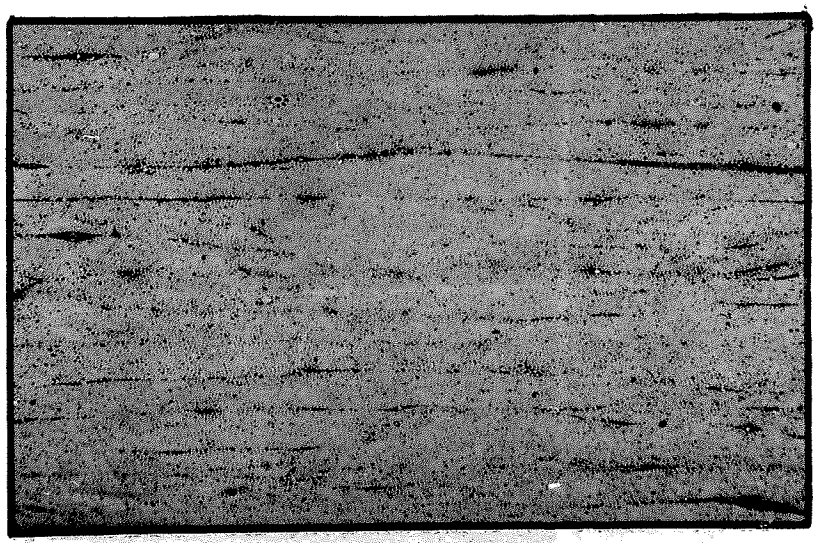

25 min.

Fig. 24. ACETONE FREE SPECIMENS PRECURED IN AIR FOR VARYING LENGTHS OF PRECURE.

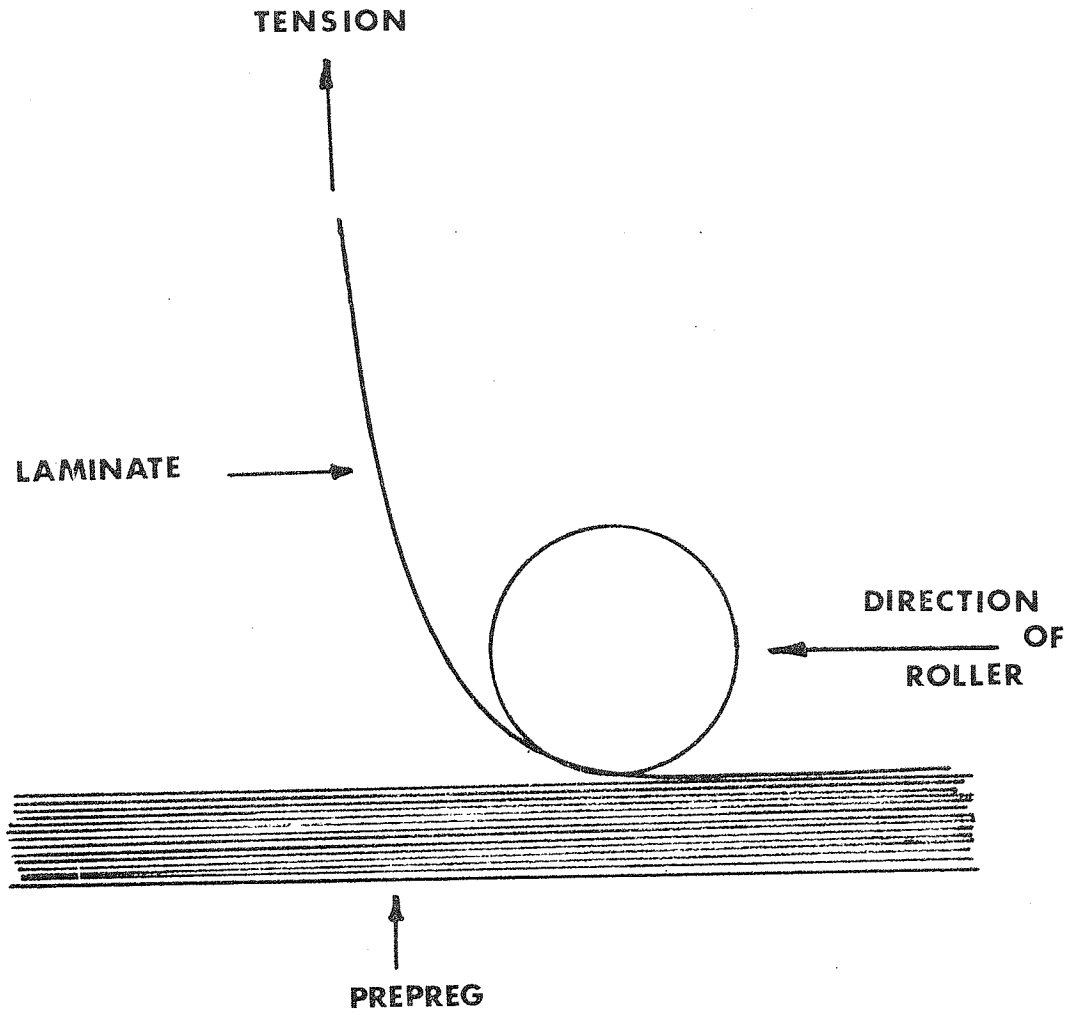

Fig. 25. Rolled laminates

UN ROLLED

ROLLED

0·5mm

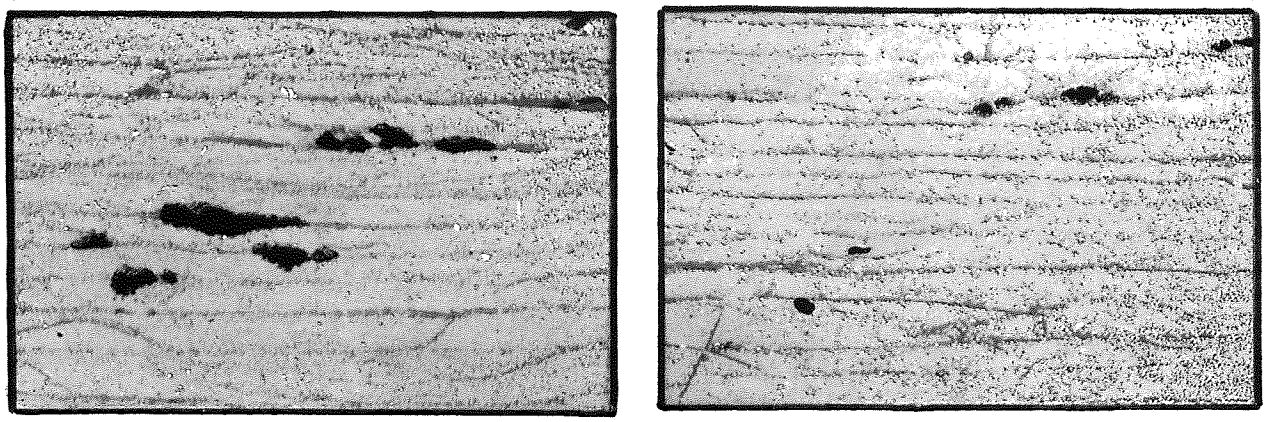

15 min.

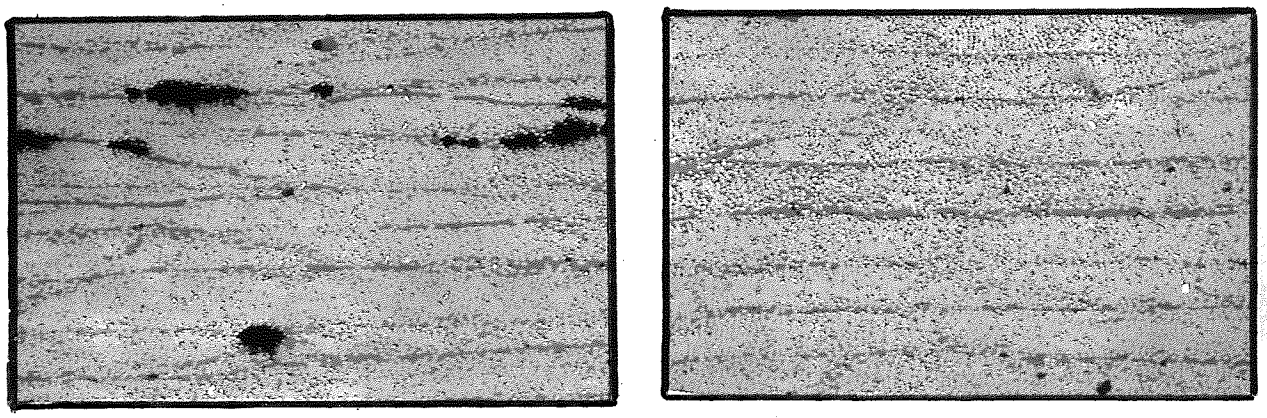

20 min.

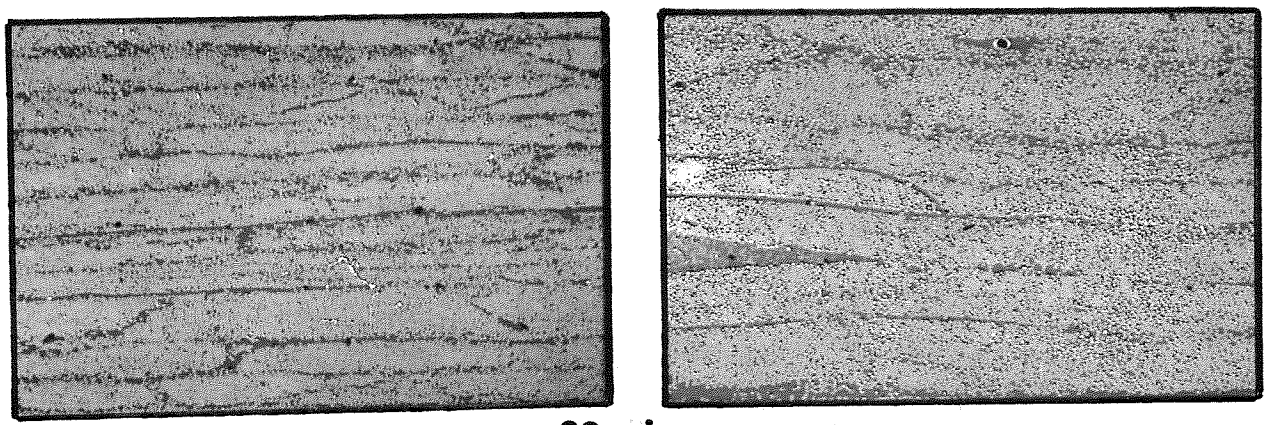

20 min.

Fig.26.ROLLED AND STANDARD LAMINATES PRECURED IN AIR FOR 15 AND 20 MINUTES.

Fig. 27 is a graph of the interlaminar shear of these rolled specimens together with controls plotted against precure time. The higher values of interlaminar shear strengths were obtained by the specimens which had been carefully laminated and consequently obtained fewer voids.

The fact that voidage appears to be reduced by carefully rolling the laminates together suggests that entrapped air is at least a contributory factor. This impression is reinforced by the observation that almost invariably voids lie between laminates and that they have an elongated cross section. Voidage due to the boiling off of volatiles during the curing process might be expected to ~~any~~ lie anywhere within the matrix and be circular in cross-section. From the above results it appears that acetone does not significantly contribute to voidage in composites. For both the above sets of results the specimens which were free of voids were those subjected to a length of precure which advanced the polymerisation of the resin to such a stage that as the moulding pressure was applied, the resin began to gel.

A series of specimens were prepared which had been precured and moulded in a vacuum (Appendix IV). However this was a very long process and as the results obtained were no better than the best results discussed above, it was decided that the specimens which were to be used for this project would be produced in the following way:-

i) The preform was prepared by carefully rolling the laminates together.

ii) The specimen was precured for such a time so as to ensure that the resin began to gel just as the moulding pressure was being applied.

Interlaminar shear strength v. Length of precure(Rolled laminates)

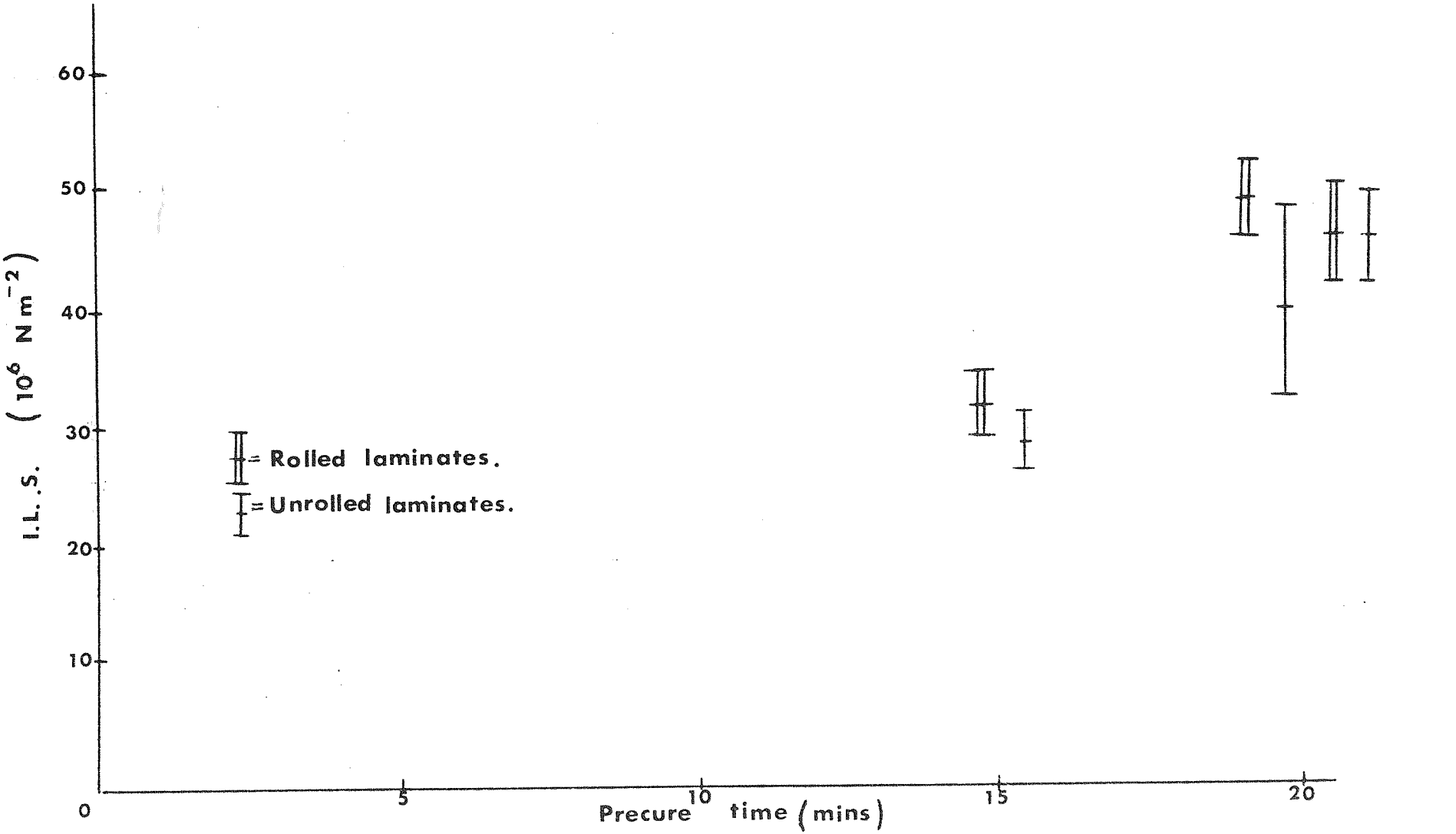

Fig. 27.

3.9 Possible reasons for scatter in mechanical properties of reinforced plastics

In principle the ideal composite would consist of an array of perfectly spaced fibres of constant diameter and strength, perfectly orientated within a matrix of constant properties. In practice carbon fibre reinforced materials deviate from this ideal in several respects. The wide strength distribution of carbon fibres, and the difficulty of achieving a completely uniform fibre distribution because of the very small and variable diameter of carbon fibres have to be accepted for the moment but there are some more easily controlled factors which can introduce variability into composite properties. These are dealt with below.

3.9.1 Fibre volume fraction

The Young's modulus of carbon fibre is so much higher than that of resin, hence when a load is applied, in the direction of the fibres, a large percentage of the load will be carried by the fibres. Consequently the fibre volume fraction of a composite is directly proportional to its load bearing capacity.

Experience has shown that for a unidirectional carbon fibre composite the expression $\sigma_c = V_f \sigma_f$ approximately defines the tensile strength in the fibre direction, where the symbols have the same meaning as in section 2.1.

Good control over V_f is therefore essential to reduce scatter and, as discussed below, fabrication methods have been developed to produce composites with a volume fraction to within $\pm$ 2%.

3.9.2 Fibre orientation

Misaligned fibres will reduce the tensile properties of the composite, depending on the number of fibres and the angle of misorientation. To determine the effect of misaligned fibres, two series of mouldings were manufactured using standard production LY558 - BF_3 400 prepreg material. In one set of mouldings all the fibres were lying at an angle θ to the axes ($+\theta$ specimens), and another set had alternate layers of fibres at angles $+\theta$ and $-\theta$ to the axis ($\pm\theta$ specimens). The two central layers of the $\pm\theta$ specimens were at the same angle so that forces, due to thermal contraction on cooling from the curing temperature, were balanced. The following properties were investigated for both the $+\theta$ specimen and the $\pm\theta$ specimens:-

(a) Dynamic Young's modulus (E_D)

(b) Dynamic Torsional modulus (G_T)

(c) Static Young's modulus (E_s)

(d) Ultimate tensile strength

(e) Interlaminar shear strength

(a) Dynamic Young's Modulus

When the $+\theta$ specimens were vibrating, at their fundamental bending frequency, the node positions were displaced by an angle ϕ from the true position (see Appendix III). A maximum displacement angle of approximately 56^{o} was measured for the specimens with their fibres at $+5^{o}$. The reason for nodes being displaced is because a twisting moment is induced when composites of this orientation are bent. (45) The dynamic Young's modulus is plotted in Fig. 28 together with a theoretical plot, obtained from the generalised Hooke's law. (46)

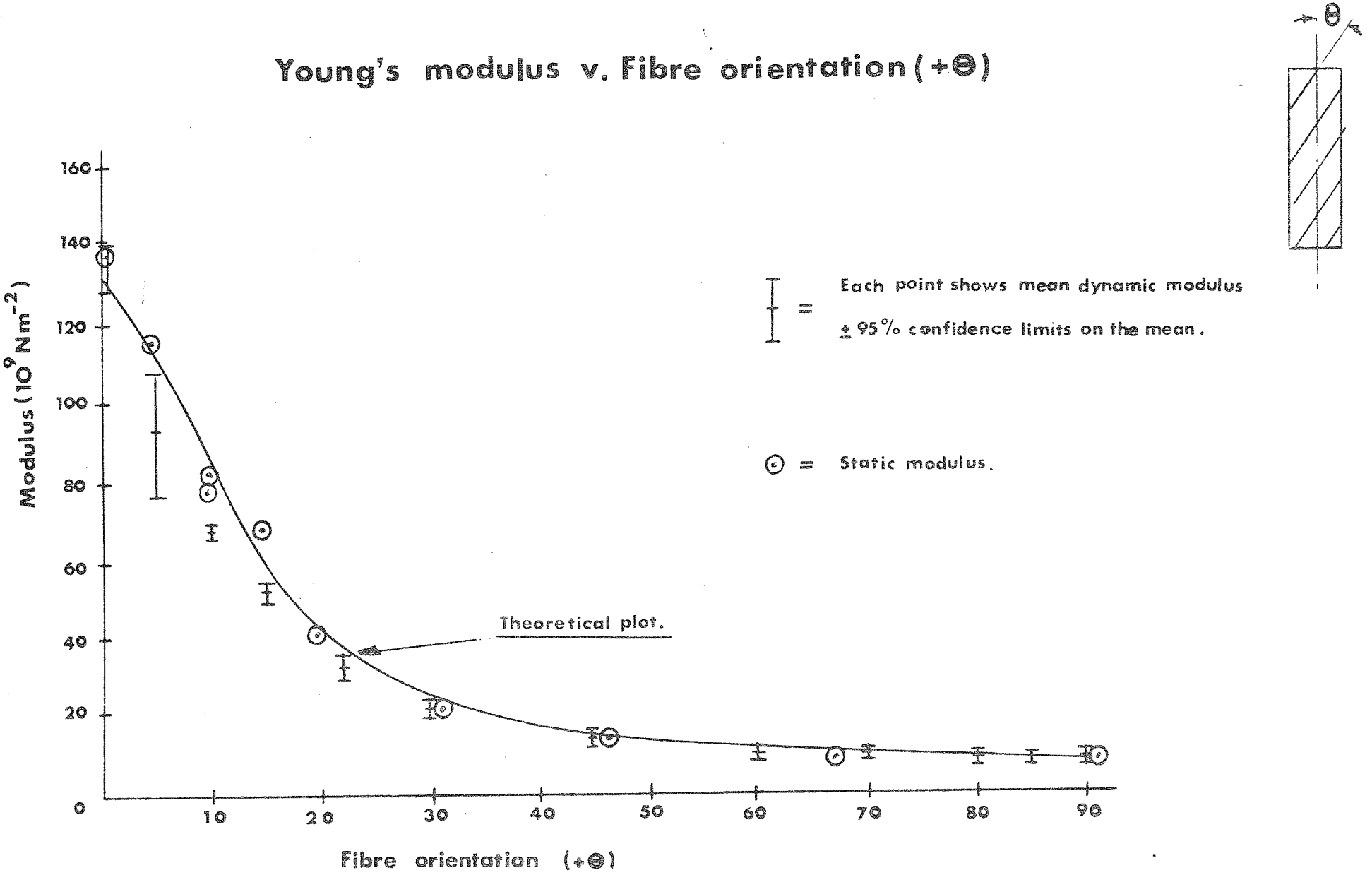
Young's modulus v. Fibre orientation (+Θ)
Modulus ($10^9 Nm^{-2}$)
160
140
120
100
80
60
40
20
0
10
20
30
40
50
60
70
80
90
Fibre orientation (+Θ)
Theoretical plot.
= Each point shows mean dynamic modulus ± 95% confidence limits on the mean.
= Static modulus.
Θ

Fig. 28.

The equation from which the dynamic modulus is calculated (see Appendix III), does not take into account any twisting moment and assumes that the displacements across the width are constant. Hence it does not define the $+\theta$ modulus and the results are low.

The nodes were not displaced when $\pm\theta$ specimens were vibrated at their resonant frequencies. The dynamic moduli for the $\pm\theta$ specimens are plotted in Fig. 29 together with a theoretical plot obtained from the generalised Hooke's law. The experimental results compare favourably with the theoretical plot.

(b) Dynamic Torsional Modulus (see Appendix III)

As with the bending vibration the nodes of the $+\theta$ specimens were displaced by an angle from the position expected with an isotropic specimen, the maximum displacement occurring with specimens with a fibre orientation of 30^{o}. Therefore, because the nodes were displaced no significance can be attributed to the results (Fig. 30).

The $\pm$ specimens vibrated about their expected nodes at their torsional resonant frequency. The torsional modulus increased with increasing angle, up to a maximum at 45^{o}, where the fibres were lying in the plane of principal shear stress. At angles above 45^{o} the modulus decreased with increasing angle (Fig. 31). The torsional modulus for unidirectional composites was $6.9\ GNm^{-2}$.

(c) Static Young's Modulus

To measure the static Young's modulus, percentage elongation at failure and the ultimate tensile strength in one test, both the $+\theta$ and $\pm\theta$

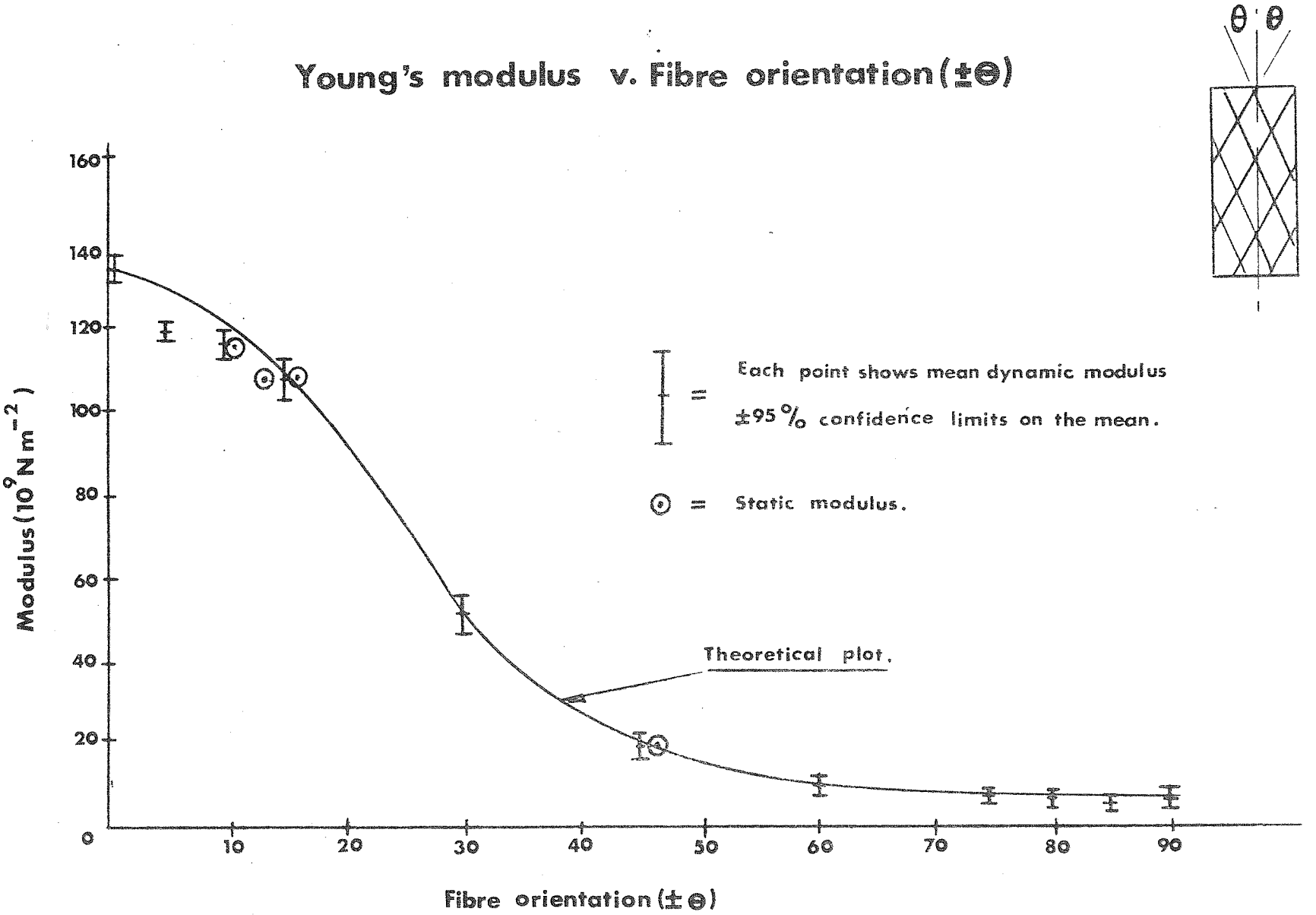
Young's modulus v. Fibre orientation (±θ)
θ θ
Modulus (10^9 N m^{-2})
160
140
120
100
80
60
40
20
0
10
20
30
40
50
60
70
80
90
Fibre orientation (±θ)
Each point shows mean dynamic modulus
±95% confidence limits on the mean.
= Static modulus.
Theoretical plot.

Fig. 29.

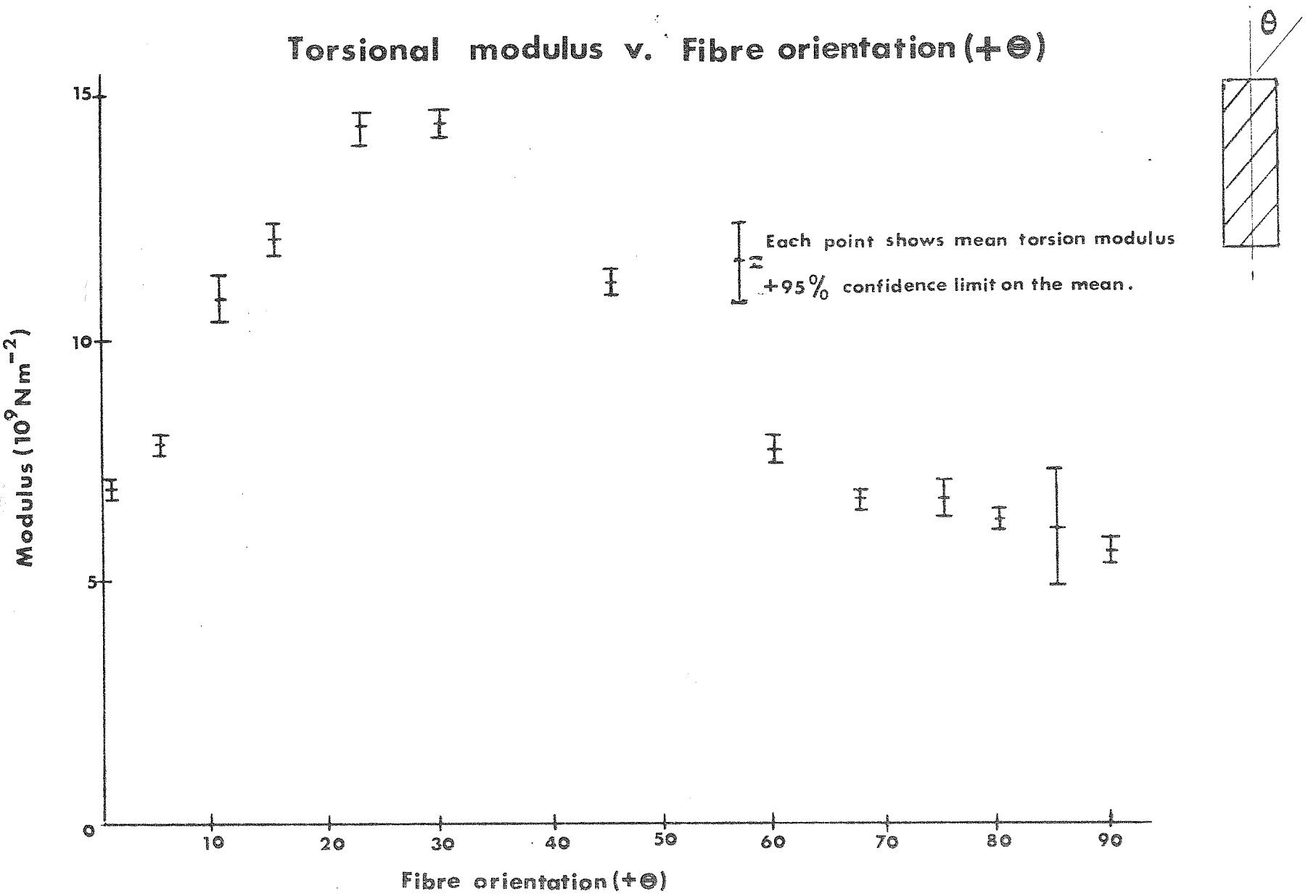
Torsional modulus v. Fibre orientation (+Θ)
θ
Each point shows mean torsion modulus
+95% confidence limit on the mean.
Modulus ($10^9 Nm^{-2}$)
15
10
5
0
10
20
30
40
50
60
70
80
90
Fibre orientation (+Θ)

Fig. 30.

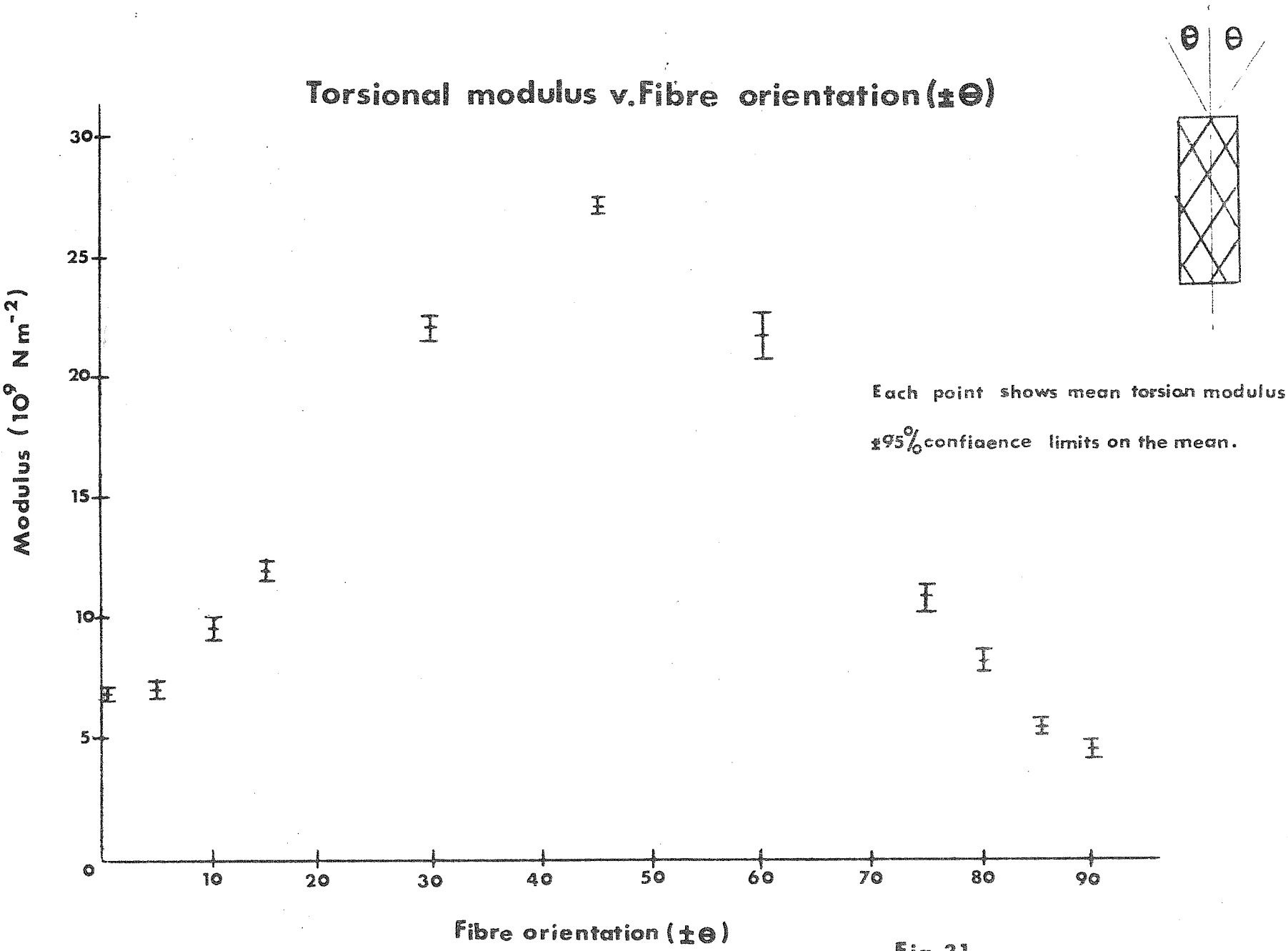
Torsional modulus v. Fibre orientation (±Θ)
Modulus (10^9 N m^{-2})
30
25
20
15
10
5
0
10
20
30
40
50
60
70
80
90
Fibre orientation (±Θ)
Θ Θ
Each point shows mean torsion modulus
±95% confidence limits on the mean.

Fig. 31.

specimens had a reduced cross section in the gauge length (Fig. 32). The specimens were tested on the Instron at a strain rate of 1 mm/min. The strain was measured using an extensometer with a gauge length of 10 mm, which was capable of measuring a maximum strain of 10%.

The specimens were cycled a number of times, up to a maximum load within the limit of proportionality, with the extensometer on one side. The extensometer was then taken off and replaced on the opposite side, and the specimens cycled again up to the maximum load. This was done to take account of any bending of the specimens due to misalignment. The specimens were then loaded to failure and their percentage elongation and ultimate tensile strength noted.

The static modulus is plotted, in Fig. 28, against the fibre orientation for the $+\theta$ specimens. There was good agreement between the experimental results and the theoretical plot, which emphasises the inadequacy of the formula that gives the dynamic modulus. The anisotropy of such materials is noteworthy.

There was good agreement between the static, dynamic and theoretical, Young's modulus for the $\pm\theta$ specimens. The decrease in modulus with fibre orientation was not so sudden, compared with the $+\theta$ specimens (Fig. 29)

(d) Ultimate Tensile Strength

The experimental results of the tensile strength of the $+\theta$ specimens compare favourably with a theoretical plot computed using a strain energy theory (47). At an angle of only 5^{o} the tensile strength has decreased to approximately 25% of the unidirectional strength (Fig. 33). However, when

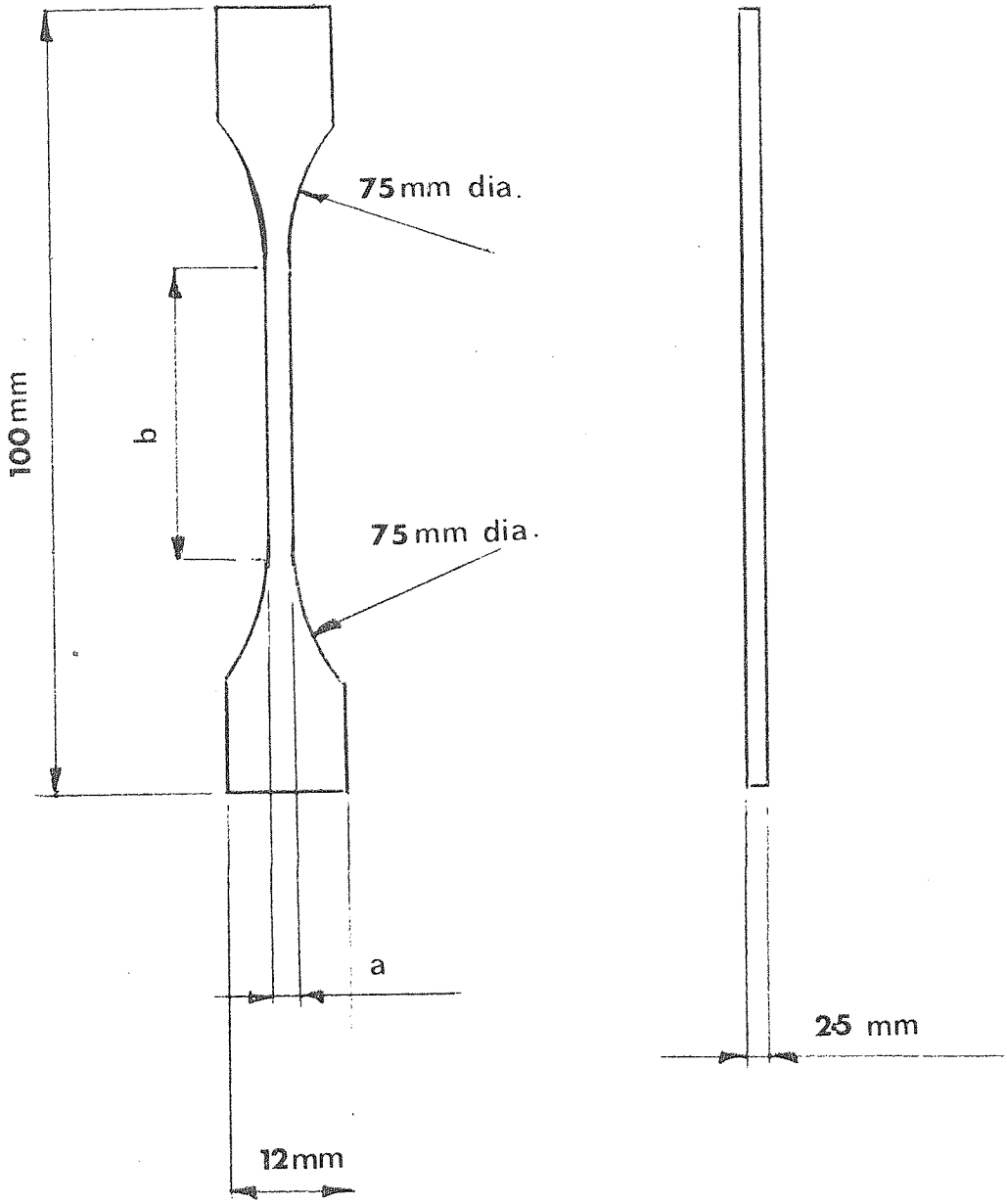

Fibre angle θ	a	b
5	30	4·5
10	20	2·5
15 → 90	20	2·0

Fig. 32. Tensile test shape for θ and ± θ specimens.

U.T.S. v. Fibre orientation (+ Θ)

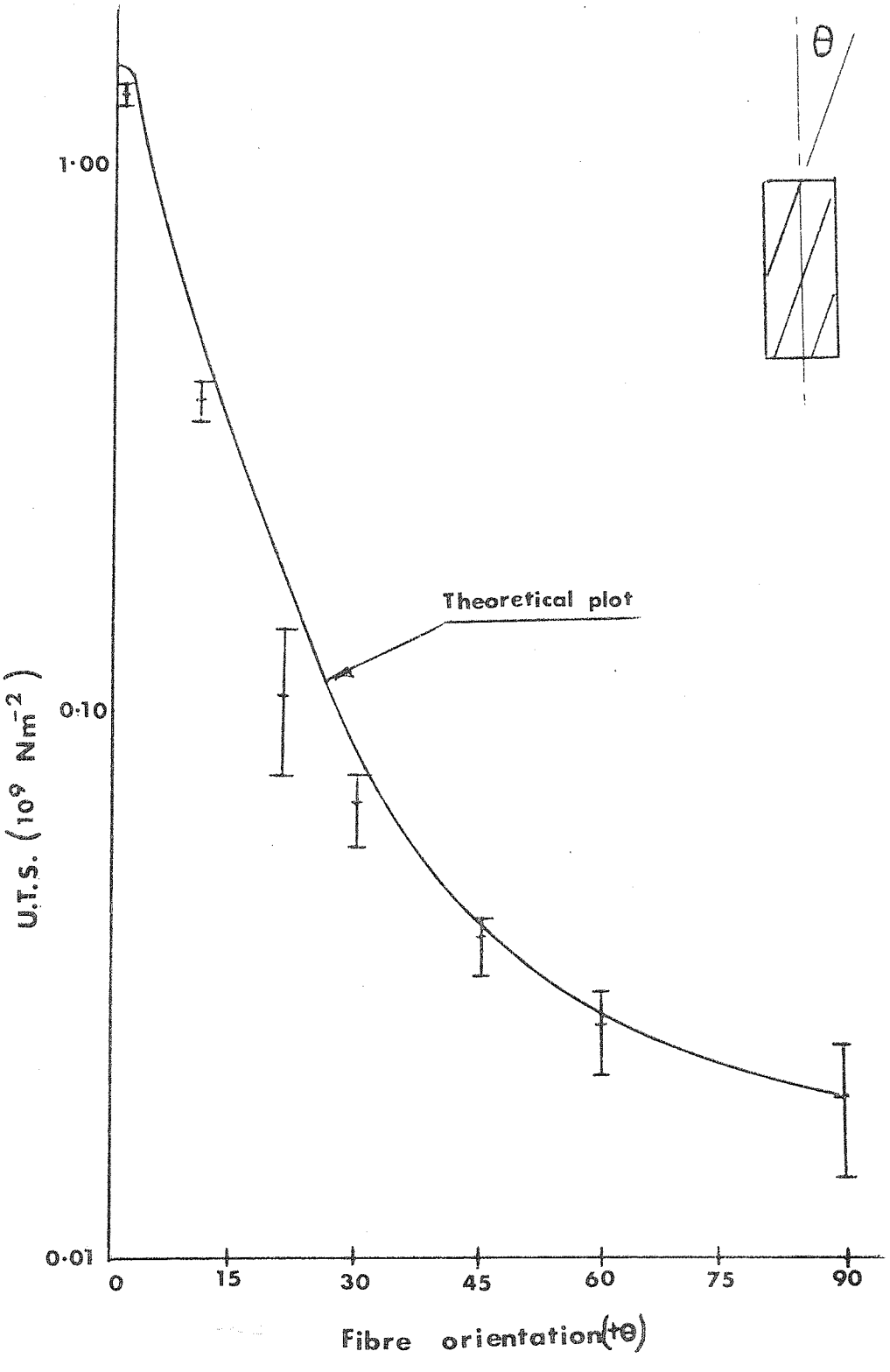

Fig. 33.

failure has occurred between fibres the composites can still bear load on the area between the $+\theta$ and $-\theta$ layer, hence the drop off is not so large with the $\pm\theta$ specimens at low angles. At a fibre orientation of $\pm$ 5% it is approximately 60% of the unidirectional strength (Fig. 34).

The stress-strain curves for the $+\theta$ specimens were linear up to failure, where there was a sudden drop in load (Fig. 35). The composite failure was due to resin failure along a plane parallel to the fibre direction. (Fig. 35).

The stress-strain curves for the $\pm\theta$ specimens were linear up to the ultimate strain of the $+\theta$ specimen of equivalent angle, where they began to curve over (Fig. 35). At final failure there was a sudden drop in load. To investigate the mode of failure three $\pm 45^{o}$ specimens were loaded to 18, 52 and 62 MNm^{-2} respectively. These were sectioned along the longitudinal axis, mounted and polished. The specimens showed, beyond the limit of proportionality, an increasing amount of resin failure along planes parallel to the fibre direction within each laminate. There was no sign of interlaminar shear failure even just before final failure (Fig. 36). The final failure is shown in Fig. 37.

(e) Interlaminar shear strength

The shear test used was the short beam shear method discussed in Appendix III. However with the specimens tested with different fibre orientations, the flexural strength was decreasing rapidly with increasing angle of fibre orientation, therefore at a certain orientation the mode of failure changed from shear to tensile. All the $+\theta$ specimens, with a fibre orientation above 5^{o} (Fig. 38) and the $\pm\theta$ specimens, with a fibre orientation above 20^{o} (Fig. 39) failed in tension. All specimens which

U.T.S. v. Fibre orientation (±θ).

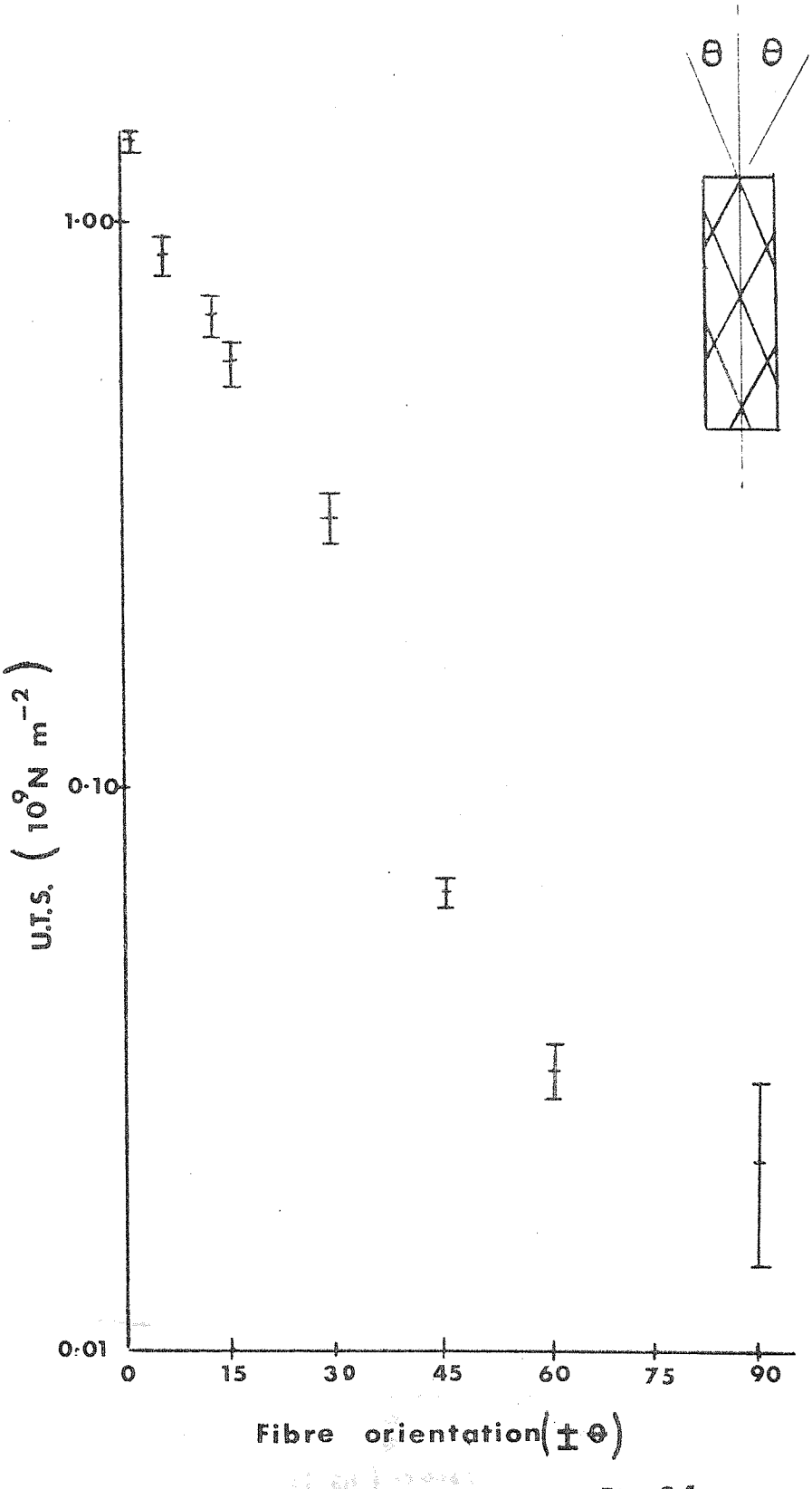

Fig. 34.

Stress-Strain plots for off-axis tensile tests.

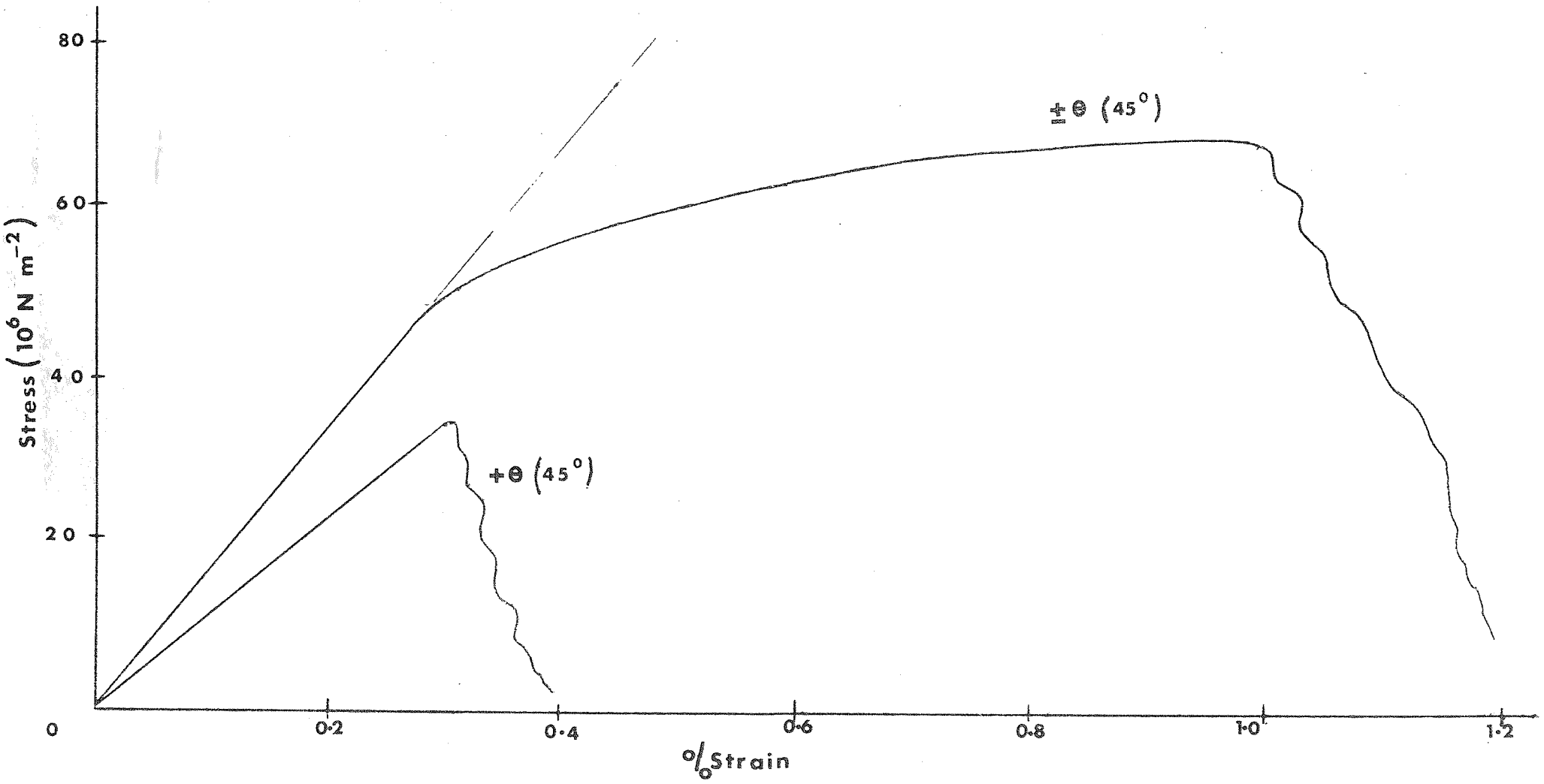

Fig. 35.

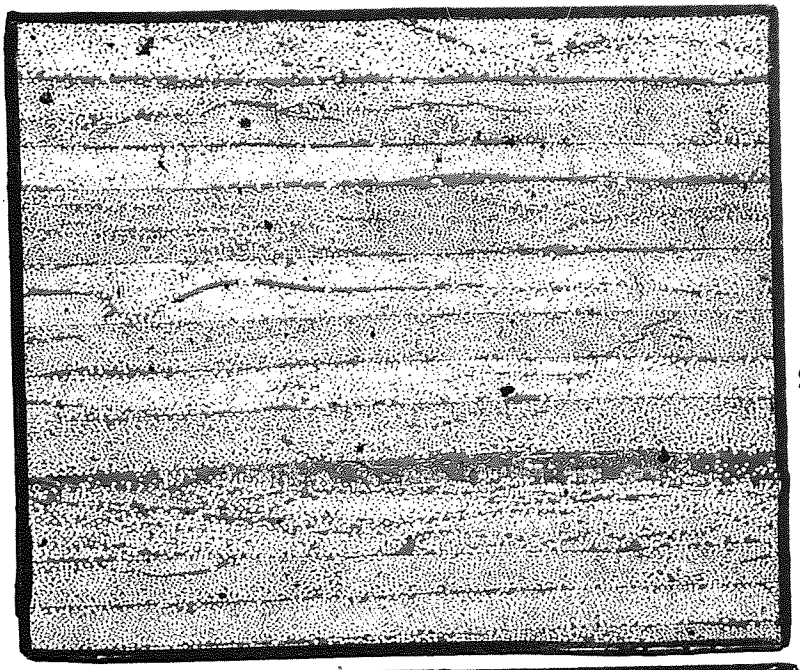

Stress = 19 $10^6 Nm^{-2}$

Stress = 52 $10^6 Nm^{-2}$

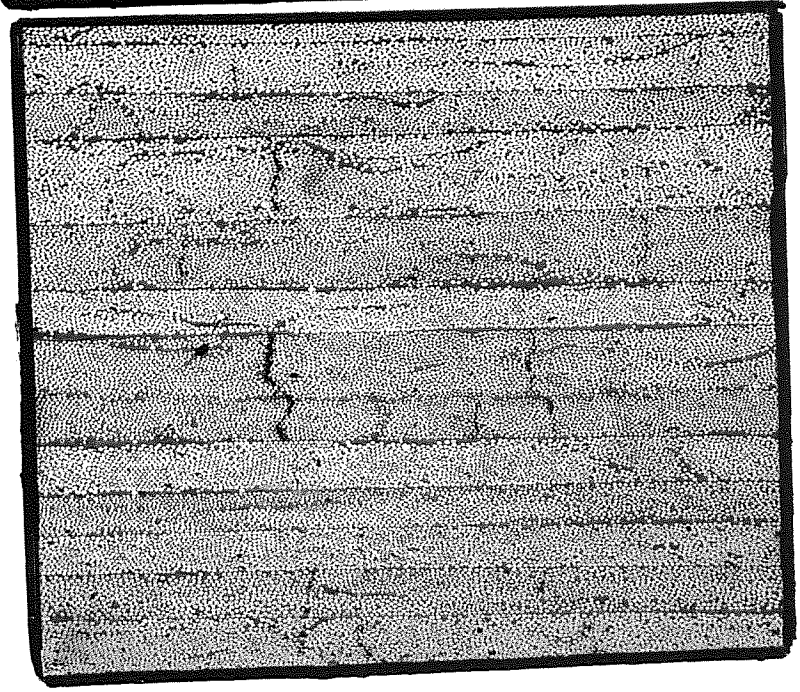

Stress = 62 $10^6 Nm^{-2}$

0·5mm

Fig.36.SEQUENCE OF TENSILE FAILURE OF ±Θ SPECIMENS.

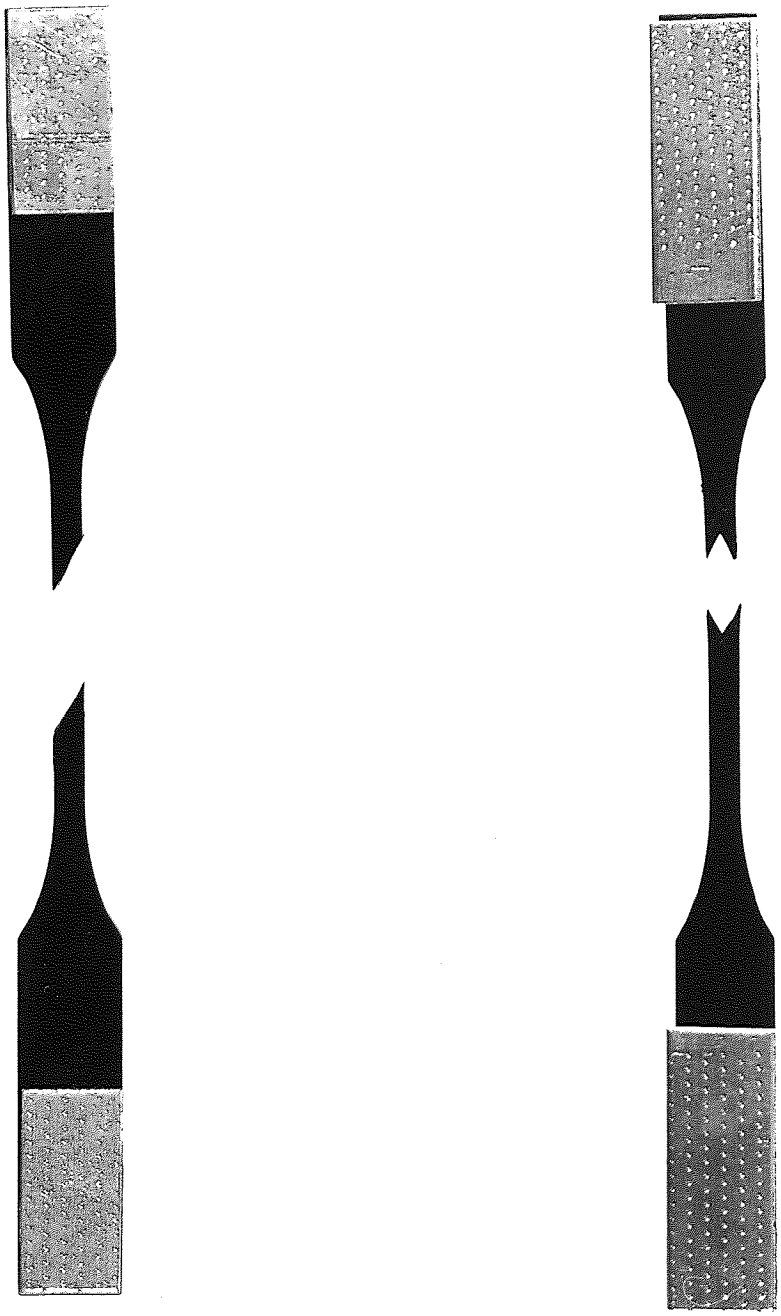

Fig.37. TENSILE FAILURE OF OFF ANGLE SPECIMENS.

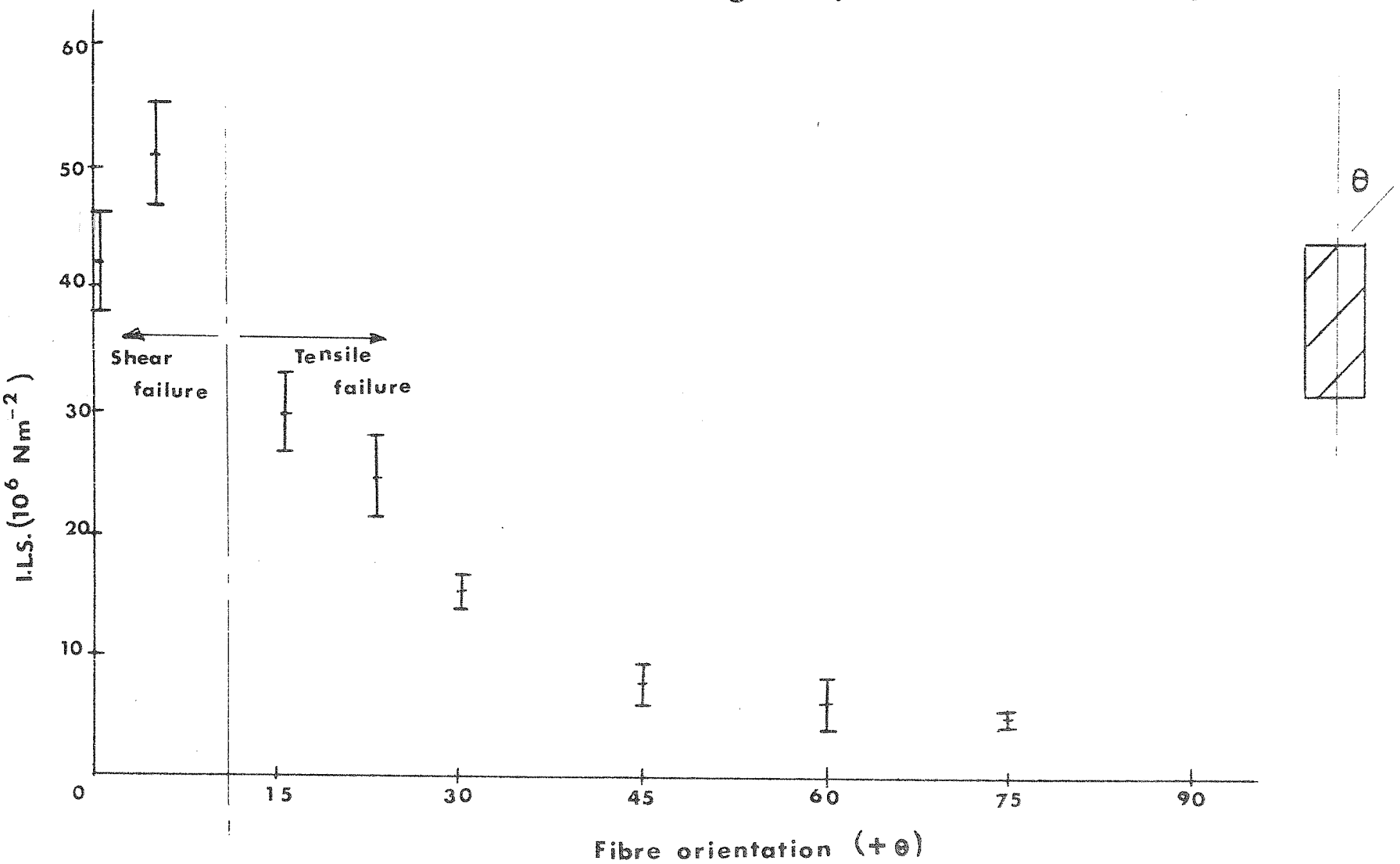
Interlaminar shear strength v. Fibre orientation +θ .
I.L.S. (10^6 Nm^{-2})
60
50
40
30
20
10
0
Shear failure
Tensile failure
15
30
45
60
75
90
Fibre orientation (+θ)
θ

Fig. 38.

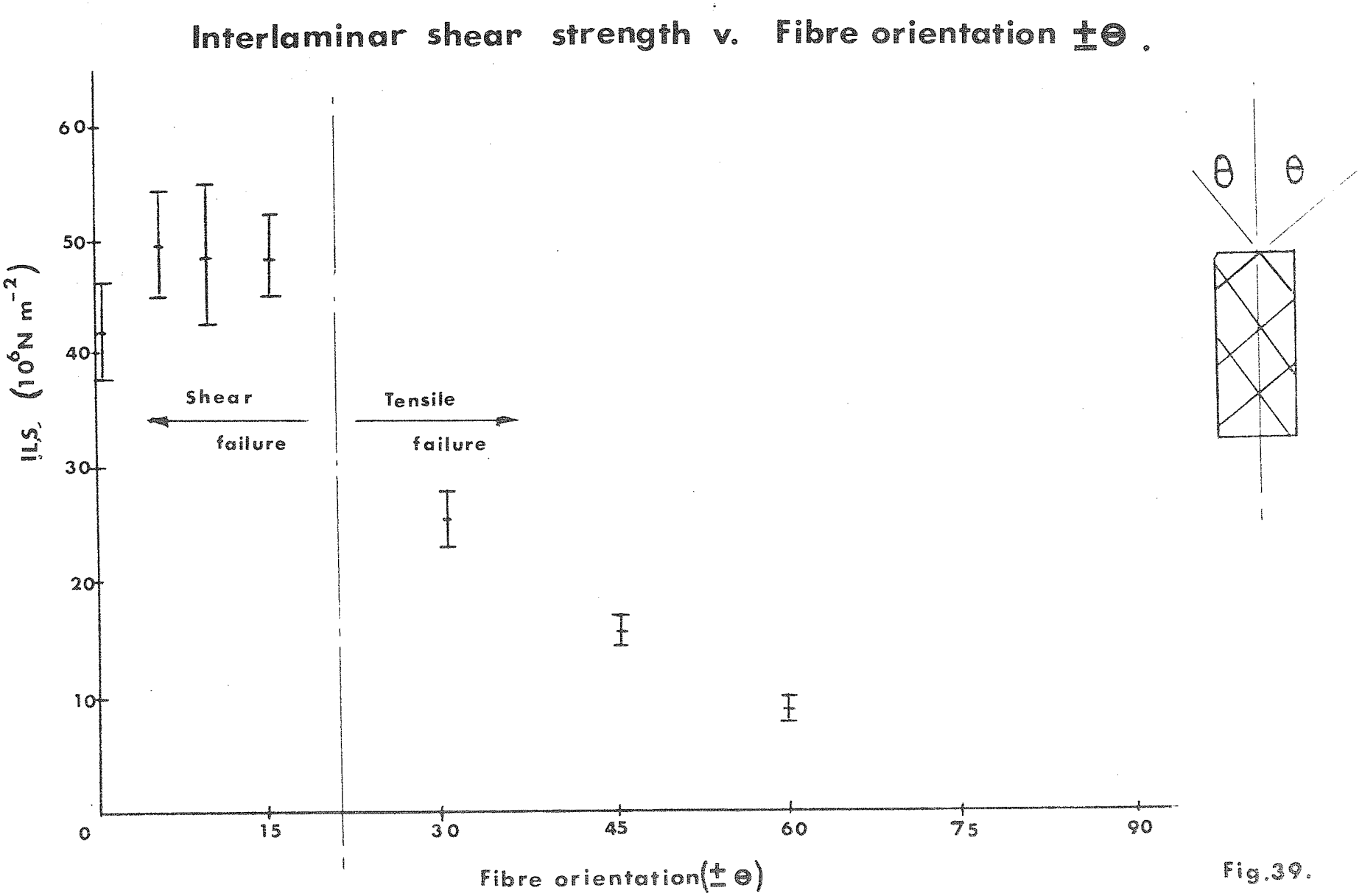
Interlaminar shear strength v. Fibre orientation ±θ .
ILS ($10^6 N m^{-2}$)
60
50
40
30
20
10
0
15
30
45
60
75
90
Shear
failure
Tensile
failure
Fibre orientation(± θ)
θ
θ

Fig.39.

failed in shear had a shear strength of 48 MNm^{-2} which is the optimum value for the LY558 - $BF_3$400 System. Hence over the limited range of angles ($\pm \theta$) in which shear failure occurred, no decrease in interlaminar shear strength was observed. However, a plot of interlaminar shear strength at failure for increasing values of $\pm \theta$ shows an apparent decrease because of the onset of tensile failure, and the decreasing tensile strength with increasing θ values.

3.9.3 Errors associated with fibre misalignment

Fibre misalignment may occur either at the 'prepreg' stage or when cutting the composite plate into the test shape.

Fibre misalignment of an angle of approximately 5^{o} has been observed in the prepreg sheet. When such sheet is made into a composite the fibres will tend to lie at an angle either side of the axis because of the random way in which they are stacked together. In the extreme case where all the fibres in each layer are at an angle of 5^{o} to the axis the composite will be similar to the $\pm \theta$ specimens where $\theta = 5^{o}$ giving the following errors.

Table 3.1

Property	Approximate error
Tensile Strength	- 25%
Young's Modulus	- 12%
Torsional modulus	0
I.L.S.	0

Such a high degree of misalignment of each layer is unlikely and in practice only one or two layers would be so misaligned with a pro-rata reduction in the properties. However table 3.1 provides an approximate upper limit on the errors that may occur.

The second cause for misalignment is likely to occur when the test specimen is being prepared from the moulded plates. It is extremely difficult to cut the specimen in an exact line, with the fibres, and an error of about 3^{o} can be expected. This will give a + θ specimen, where $\theta = 3^{o}$, with the following reduction in mechanical properties:-

Table 3.2

Property	Approximate error
Tensile strength	- 25%
Young's modulus	- 10%
Torsional Modulus	+ 3%
I.L.S.	0

Even in a specimen where the fibres are misaligned by a small angle such as 3^{o} the tensile strength will be reduced by as much as 25%. Such a large error is obviously undesirable, and extreme care must be taken both in the laying out of fibres to produce the impregnated sheet and in the preparation of the test specimen.

3.9.4 The mechanical properties of the resin matrix

The intrinsic mechanical properties of a given resin system are likely to depend on the degree of cure of the resin (that is on the amount of cross-linking within the resin which will in turn depend on the amount of

hardener used and the thermal history of the resin) prior to testing. (The observed strength of brittle resins will also depend on the extent and magnitude of flaws, such as voids, within the resin). Whereas longitudinal properties of a composite may be dominated by fibre behaviour, the transverse properties are likely to be affected by the physical condition and cure of the resin. Consequently the resin hardener composition, the mixing and the times and temperatures of the curing process need careful control.

Chapter 4

Single Fibre Properties

The carbon fibres used in this project were produced from polyacrylonitile (PAN) fibres, which were supplied by Coutaulds Ltd., under the brand name Courtelle, in 1½ den. form. The PAN fibres were pyrolysed according to the method described in the Rolls Royce patents for the production of carbon fibre. (48).

Figure 40 (49) shows the variation of Young's modulus of carbon fibres as a function of the carbonising temperature. There is a large improvement in modulus, beginning at very low heat treatment temperatures, which continues up to 1000°C beyond which the rate of increase is reduced.

Jones and Johnson (50) have shown that at heat treatment temperatures above approximately 1600°C carbon fibres produced from PAN begin to exhibit a marked non-Hookean behaviour. For 1000°C material the stress-strain curve is linear up to failure, but fibres heat treated to 1600°C, at high strains show a stress-strain curve which begins to curve away with a reducing modulus. With 2800°C material the stress-strain curve is non-linear almost from the beginning of the test.

Data has been obtained by Johnson (49) and by Watt and Johnson (51) showing that the fibre strength increases with increasing temperature up to a maximum at approximately 1200°C where increasing temperature produces a reduction in strength. (Fig. 41) Hence proportionality between tensile strength and Young's modulus is not maintained above 1000°C

A complete furnance load of fibre, which weighed approximately seven Kilograms, was obtained to be used in the project. The fibre was heat treated

Fibre modulus v. Processing temperature.

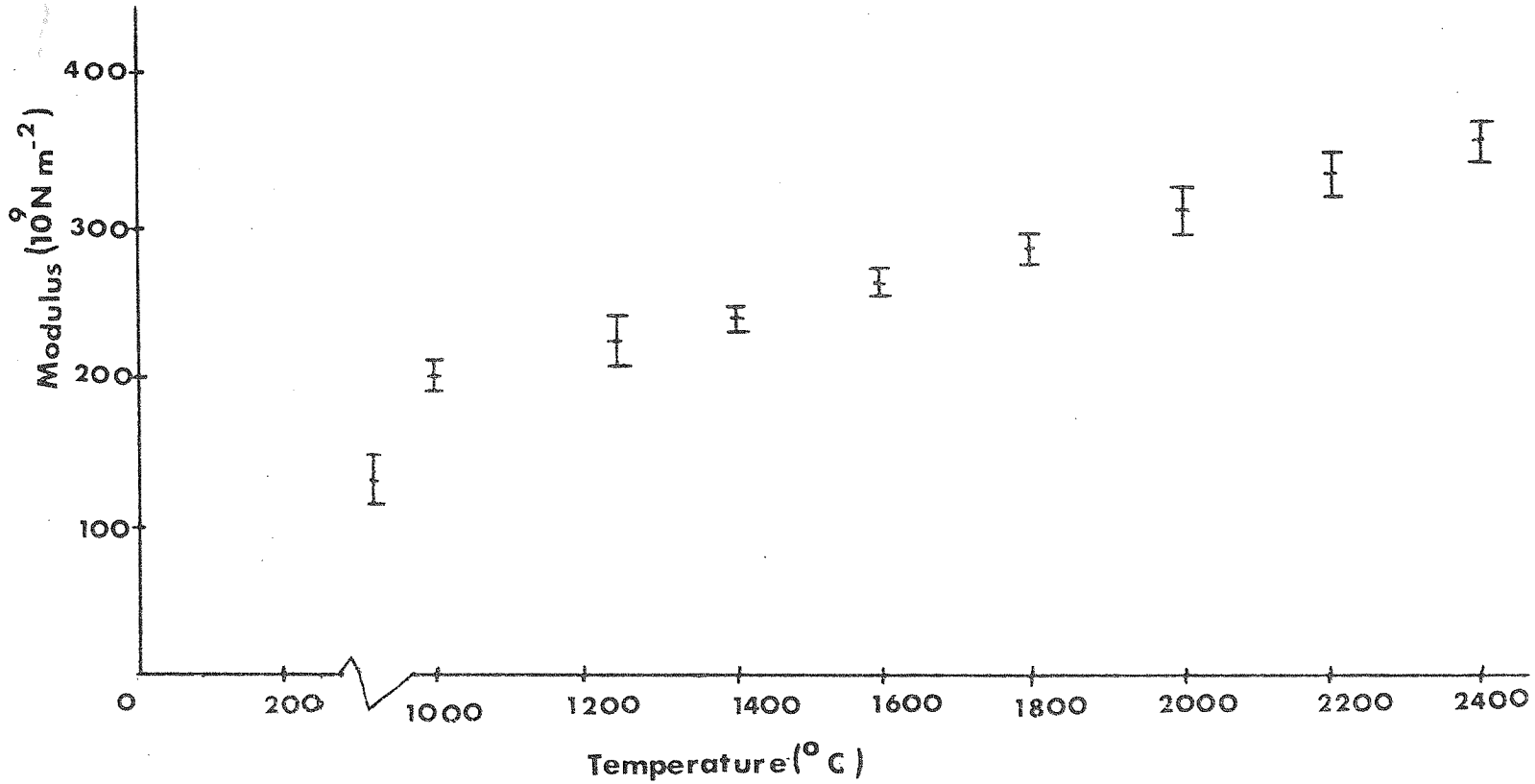

Fig. 40.

Fibre U.T.S. v. Processing temperature.

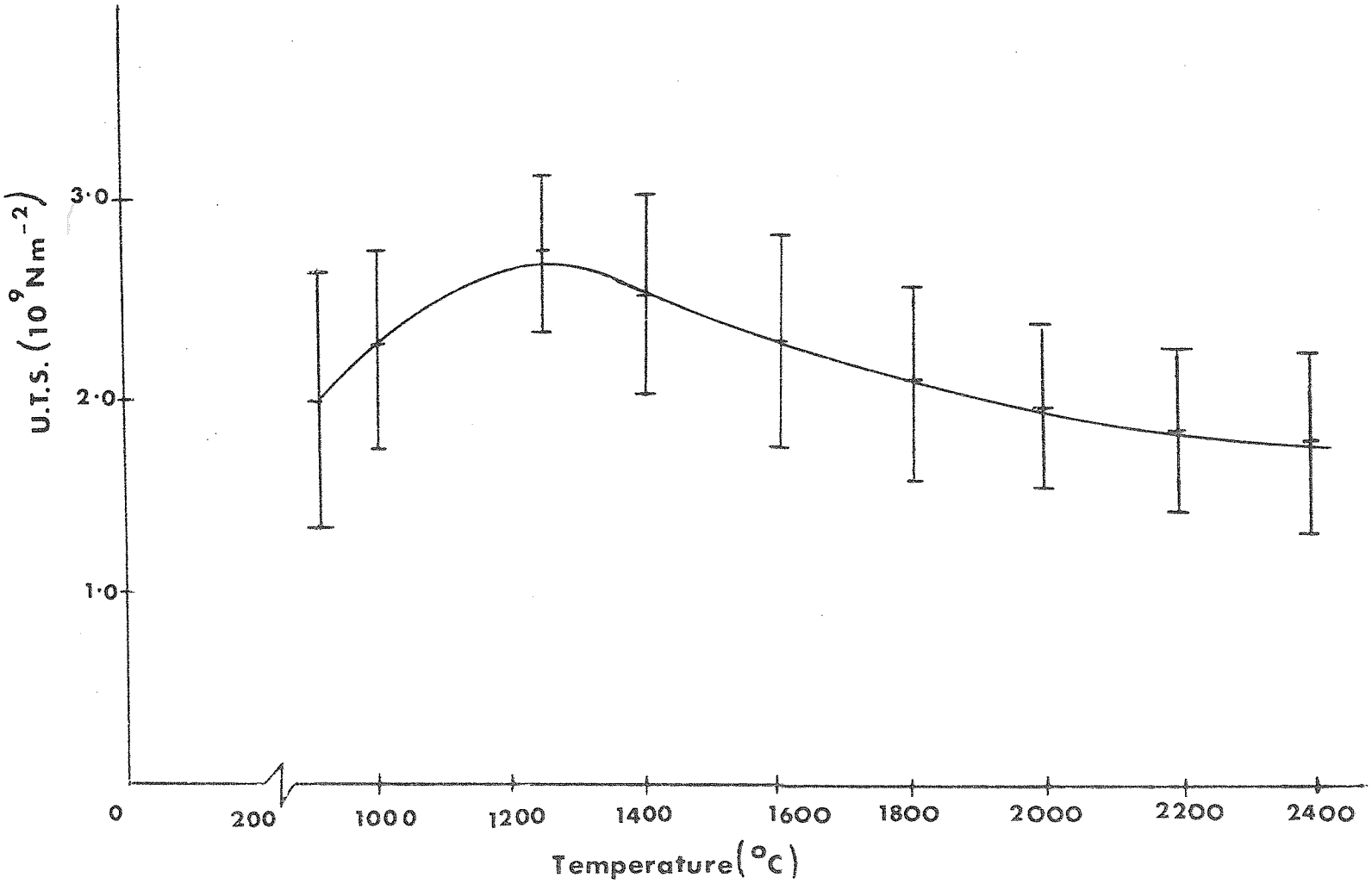

Fig. 41.

to a temperature of 1100°C. A survey of the fibre's mechanical properties was conducted, which could be used in a statistical analysis of the composite strength.

The furnace load was split up arbitrarily into three at the fibre manufacturing unit, each part being identified by three batch numbers (2343/4/5). It will be shown later that there was no significant difference in the mechanical properties of the three batches tested.

The mechanical properties of the single fibres measured were the tensile strength, Young's modulus and the torsional modulus. The effect of varying the gauge length on the tensile strength of the fibres was observed. The tensile strength and Young's modulus were determined for approximately 100 fibres from each batch using a gauge length of 25 mm. From the results of the testing of these 300 fibres an indication was given of the distribution of the modulus and strength of the total furnance load.

4.1 Methods of Testing

Methods of measuring single fibre properties have been evolved by various workers at Rolls-Royce (49). These standard techniques were used to define the properties of Batch 2343/4/5.

4.1.1 Tensile strength and Young's modulus

To facilitate handling and diameter measurement each fibre to be tested was mounted on a punched card (Fig. 42). A line was drawn on to the card which was parallel to the direction of the applied load and the fibre aligned against it and gripped by sealing wax. If there was poor alignment of the fibre to the direction of the load, then bending forces at the gripped ends

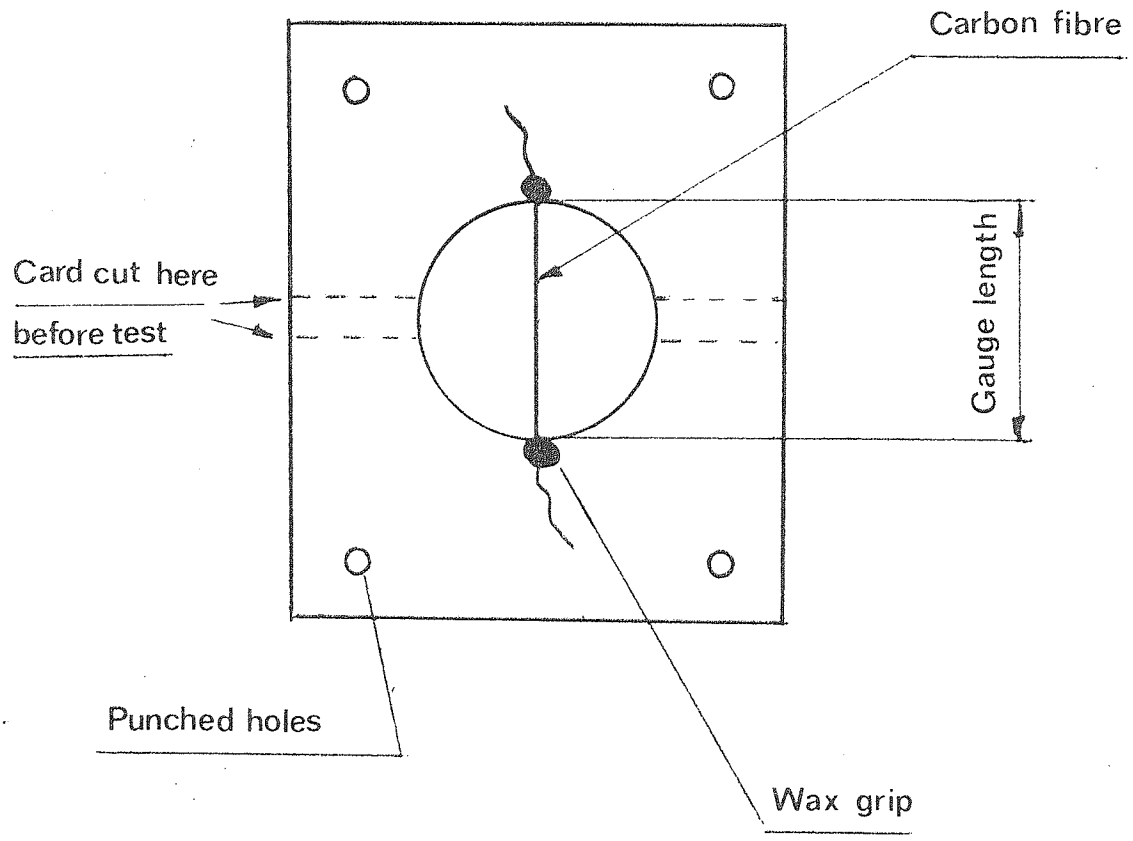

Fig.42. Carbon fibre mounting.

would have caused the fibre to fail at a lower load.

Before testing, the fibre cross-sectional area was determined. The fibres are reasonably round in section and it was considered justifiable to compute the area of the cross-section from the mean fibre diameter. The diameter of the fibre was measured by a bench microscope fitted with a Watson Image Shearing Eyepiece, (WISE). This produces two images which could be moved relative to each other by rotating a calibrated knob. The images were crossed over from side to side until the opposite edges of the image just touched and the respective readings taken. The total movement provided a measure of twice the fibre diameter; the scale on the WISE having been calibrated against tungsten wires of known diameter. Three readings were made on each fibre and the average reading taken as the diameter.

The card and fibre were mounted on to the test rig (Fig. 43) by brass clamps. One of the clamps was fixed to the base of the rig and the other was connected to a micrometer screw which was driven by a low geared motor. The load and the displacement were measured by a load cell and displacement transducer mounted in series, which were calibrated with balance weights and a dial gauge respectively. The output of the transducers was displayed on an X-Y recorder. Variable amplifier gains were adjusted to give an optimum load-displacement slope of approximately 45^{o}.

The card was cut along the dotted lines shown in Fig. 42 and a slight load was applied to the fibre to remove any kinks. The gauge length (defined as the length of fibre between the sealing wax blobs) was measured using a cathetometer.

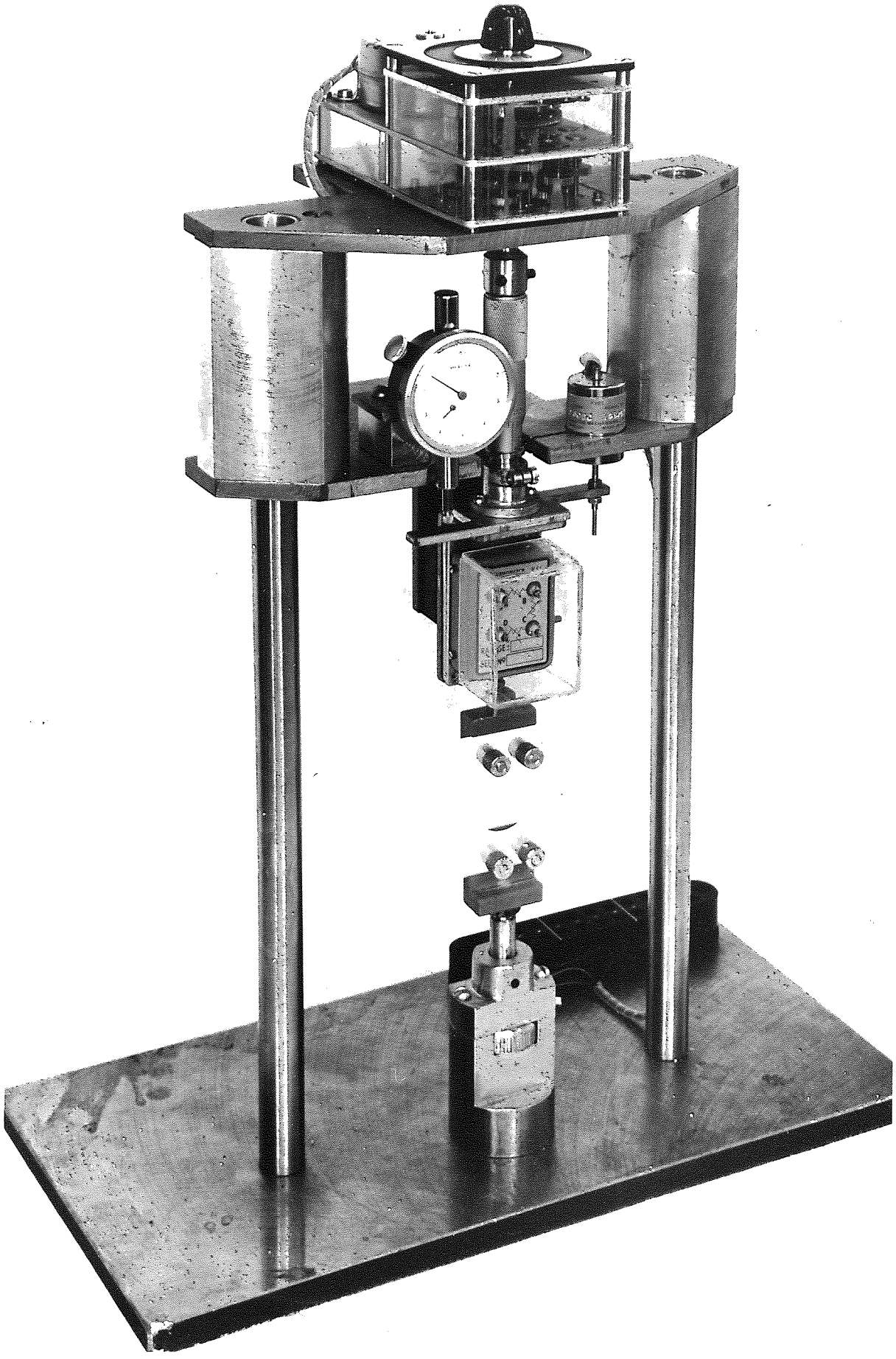

Fig.43.SINGLE FIBRE TEST RIG.

4.1.2 Errors

It has been shown that there were significant errors in the measurements described above (52). Considerable errors arise in the fibre diameter measurements because of diffraction effects in the microscope and these errors increase with decreasing diameters. As a consequence, for fibres of lower diameters than 10 μ (the diameter of carbon fibres is approximately 7 μ), the diameter is probably over estimated rather than under estimated. Hence this would tend to give values for the modulus which were an under estimate. Previous work on tungsten wires suggested that errors on the diameters may be as high as $\pm$ 5%. (42)

Machine errors could have existed in the transducers, and recorder, although it is thought that any such errors would be small when compared to the errors incurred in measuring the fibre diameter. The displacement transducer and the load cell were mounted in series. Therefore any extension of the load cell would also be measured by the transducer. However, at the fibre failure load the errors in extension from this effect were calculated to be about 0.3%.

The calibration factor for the strain measurement has been shown to be within 1%. The errors in the measurement of the load have been estimated to be within 0.25%.

Additional errors in the modulus determination were found in the gauge length measurements. During the mounting of the specimen the wax wicked down the fibre. This small effect was difficult to evaluate. The total error in the gauge length measurements, which included the errors in the cathetometer measurements, have been estimated to be $\pm$ 2%.

Hence the errors in the modulus measurements are:-

Diameter error	2 × 5%	= 10%
Extension error		= 1%
Gauge length error		= 2%
Load error		= $\frac{1}{4}$%
Total error	= ±	13$\frac{1}{4}$%

Similarly it can be shown that the errors in the breaking strength are approximately ± 10% (52).

4.1.3 Elastica

Carbon fibres have been shown (53) to possess a gauge length effect, which is an indication that the fibres contain flaws. A statistical model of composite strength demands a knowledge of the strength of the fibres as a function of gauge length. This gauge length effect was investigated by varying the length of the fibre tested, using the method described above. Because of alignment problems and experimental difficulties at short gauge lengths, the minimum length that could be tested using this technique was 10 mm. To get an indication of the intrinsic strength of the fibres, (the strength of a flaw-free region) a bending test was employed.

If a fibre behaves elastically when it is twisted into a loop, the shape that the fibre takes up is well defined mathematically and known as the elastica (54).

The elastica treatment has been applied to glass fibres (55) and the modulus and strength determined. This technique has been employed by Rolls Royce on carbon fibres (50). One end of a fibre was connected to a

spring. The length of the unlooped fibre was measured, and a loop twisted into it. A load was applied to the specimen and the spring displaced. Between the spring and the fibre was a plate, which was partially covered by a system of photo-electric cells. The change of out-put of the cells was proportional to the load applied (P). The extension was recorded as a resistance change on a slide wire potentiometer. The slide wire was connected to a micrometer attachment for calibration purposes. The fibre was loaded to fracture.

Sinclair has shown that the minimum radius of curvature (Rm) is proportional to the difference between the length of the fibre and the distance between the two ends of the looped ~~wire~~ fibre (L). (Fig. 44).

$$\text{i.e.} \quad Rm = \frac{L}{8}$$

The strain in the fibre $\epsilon = \frac{r}{Rm} = \frac{8r}{L} = \frac{4d}{L}$ (d = fibre diameter)

The maximum tensile stress σ in the fibre is:-

$$\sigma = \frac{16\ PRm}{r^3} = \frac{16\ PL}{d^3}$$

Hence the Young's modulus is:-

$$E = \frac{\sigma}{\epsilon} = \frac{4\ PL^2}{d^4}$$

The errors of this test are difficult to estimate, but from the above equation for modulus the fibre diameter is raised to the fourth power and as an estimate of the errors of the fibre diameter is $\pm$ 5% the possible error in the modulus is at least $\pm$ 20%.

As large errors could occur because of inaccuracies in the fibre measurement, the assumption was made that there was no effect of gauge length

on the modulus and if the calculated modulus from the elastica test was within the distribution of modulus of the tensile tests, (172 to 240 GNm^{-2}) then the computed value of the strength was reliable. Approximately half the results fell outside this distribution and were not considered in the analysis.

4.1.4 Torsional Modulus

Small pendulums were made by securing a carefully weighed bar onto fibres of 4 to 5 cm in length. The pendulums were made to oscillate under free oscillation conditions in a draught free enclosure and the periodic time (T) was measured. Knowing the inertia of the bar (I) the fibre diameter, the pendulum length (ℓ) and the periodic time, the torsional modulus (G) was evaluated using the following equation:-

$$G = \frac{2 I \ell}{T^2 a^2} \quad (a = \text{area of cross section of fibre})$$

4.2 Results of Single Fibre Tests

4.2.1 Young's modulus for the three batches tested with a 25 mm gauge length

No significant difference in the Young's modulus of the fibres taken from different positions within the three batches was found. The histogram of the Young's modulus is shown in Fig. 45. The mean fibre modulus of 350 tests was 196 GNm^{-2} with a standard deviation of 14 GNm^{-2}. There was a slight skew on the histogram which could be caused by individual fibres not reaching the carbonizing temperature and consequently having a reduced modulus as in Fig. 40. Also any slight variations in carbonizing temperatures could be responsible for the large scatter recorded in the Young's modulus.

4.2.2 The breaking strength of the three batches tested with a 25 mm gauge length

Again there appeared to be no significant difference in the breaking strengths of fibres taken from different positions within the three batches. The histogram of all the breaking strengths is shown in Fig. 46. The mean fibre breaking strength of 363 tests was 2.3 GNm^{-2} with a standard deviation of 0.5 GNm^{-2}. As the histogram is quite heavily skewed towards the low results a Weibull distribution curve was found for the breaking strengths (Fig. 47). The equation for the cumulative function of the Weibull distribution is (56):-

$$F(x) = 1 - e^{-\left(\frac{x - \sigma_o}{\sigma_u}\right)^m}$$

where:-

σ_u = scale parameter, any positive real number,

m = shape parameter, any positive real number

σ_o = location parameter, any real number where $x \geqslant \sigma_o$

The weibull cumulative frequency function reduces to a straight line with a double logarithmic transformation. That is:-

$$\ln \ln\left(\frac{1}{(1 - F(x))}\right) = -\ln \sigma_u + m \ln (x - \sigma_o)$$

Regarding this as a relation between the variables $\ln \ln\left[\frac{1}{(1 - F(x))}\right]$ and $\ln(x - \sigma_o)$ it is a straight line with the intercept $-\ln\sigma_u$ and slope m. Hence σ_u and m can be found. An estimate is made for σ_o so as to give a straight line.

When the Weibull distribution is plotted there appear to be two distinct straight lines. This indicates that there are two distinct distributions, one governing the low results up to a cumulative frequency function of 20% and another for the remaining higher values. The Weibull constants for both these curves are:-

σ_u (low)	= 49.2	σ_u (high)	= 500
m (low)	= 3.32	m (high)	= 6.9

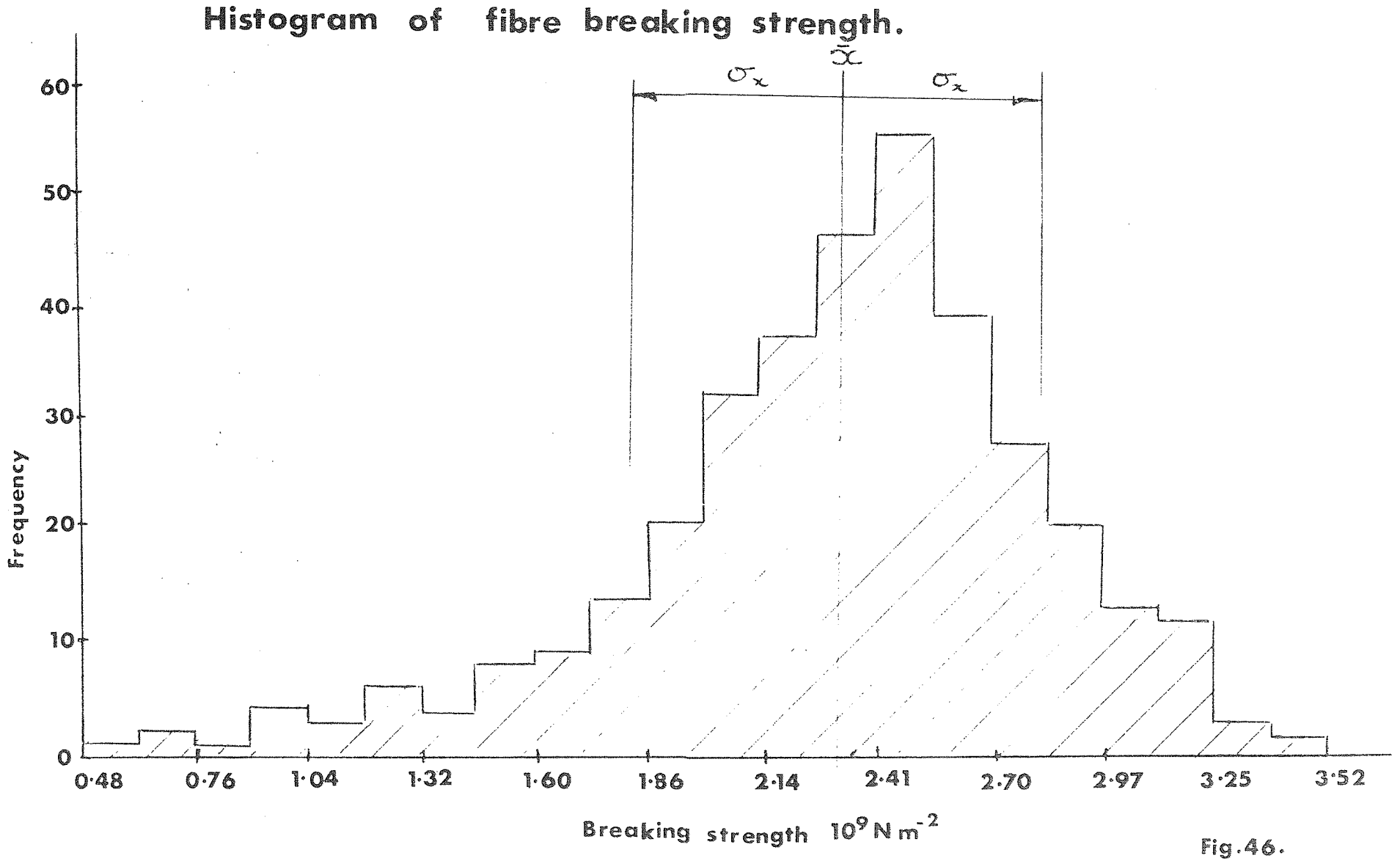
Histogram of fibre breaking strength.
$\bar{x}$
σ_x
σ_x
60
50
40
30
20
10
0
Frequency
0·48
0·76
1·04
1·32
1·60
1·86
2·14
2·41
2·70
2·97
3·25
3·52
Breaking strength $10^9 N m^{-2}$

Fig.46.

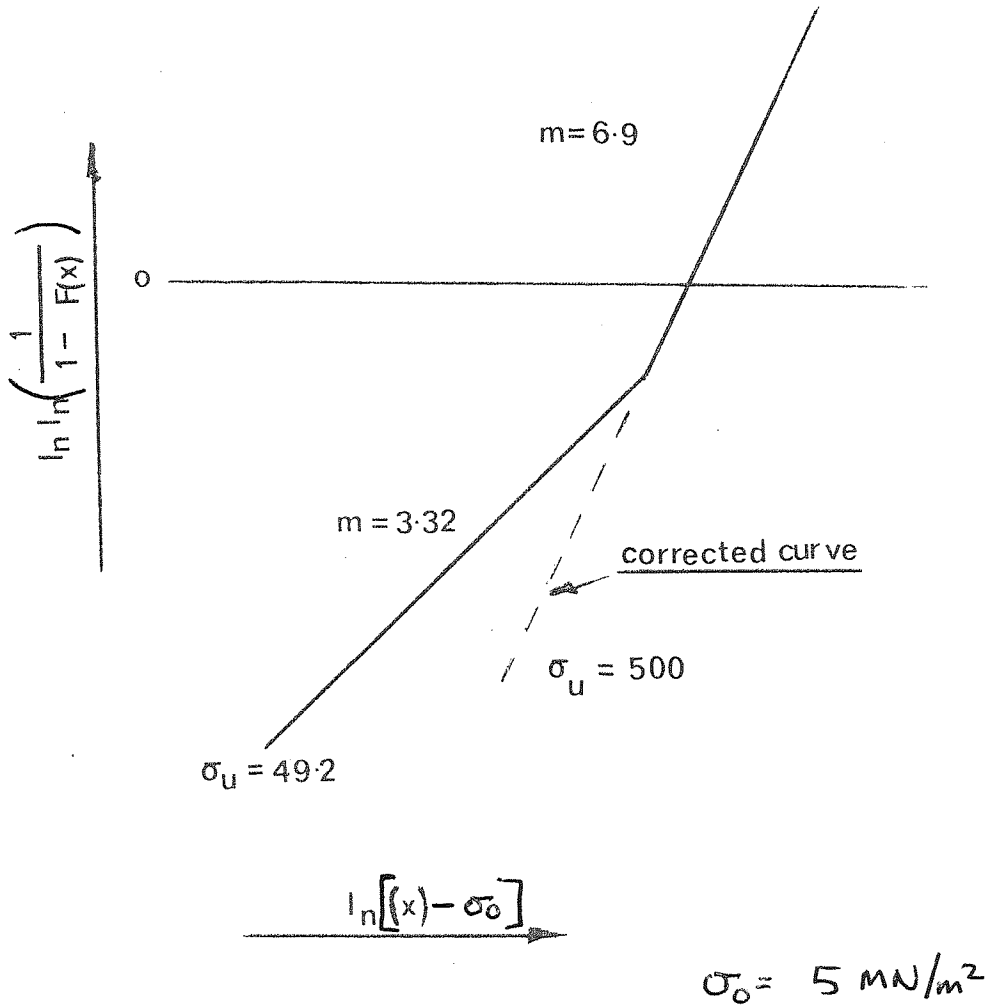

Fig. 47. Weibull distribution of fibre failure stress.

Johnson and Thorne (57) have shown that two types of flaws exist in carbon fibres. Firstly fracture may be initiated by surface flaws with a certain strength distribution. Secondly internal flaws within the fibre initiate failure and are associated with a slightly higher strength distribution. Hence this may be the reason for the bimodal distribution observed in Fig. 47.

It can be shown that there is a 20% probability of a serious flaw occurring up to 1 mm away from the gripped ends of the specimen (49). If such a flaw coincided with a region of high stress, produced by stress concentration effects of the grips, it would cause premature failure. From Fig. 47 it was calculated that a stress concentration factor of 2 would account for the low results. Therefore it is likely that failure at the grips may also give a bimodal distribution.

4.2.3 Strength as a function of gauge length

The gauge lengths tested were the elastica, 10, 25 and 100 mm. The elastica gauge length was calculated on the basis of the volume in which failure is likely to occur. This has been calculated taking an arbitrary proportion of the maximum applied tensile stress, of 80%, and calculating the prismatic volume of material subjected to stresses above this level. Calculations have shown that the length of fibre under such a stress was approximately 0.6 mm, however the volume of material is very much smaller than in the tensile test. The volume under test has been estimated to be approximately 2,000 times less than that of the tensile test with a gauge length of 25 mm. A nominal value of approximately 13 μm has been suggested, (50), for the gauge length of the elastica.

From the graph of breaking strength against gauge length (Fig. 46) there is a clear indication that the tensile strength of a fibre increases as the gauge length decreases.

As shown by the results of Fig. 46 repeated measurements of the tensile strength of a material often produces a wide spread of results. In addition, the average tensile strength varies with specimen volume and method of test. Griffith (58) found that the breaking strength of the glass fibres was strongly dependent on the diameter of the fibre. A statistical approach to this problem considers the probability of failure of a specimen at a given stress level. The specimen is to be considered to be a network of elements each having a certain probability of failure. If the stress is uniform throughout the specimen, each element will have the same probability of failure. If the failure of one element dictates total failure a weakest link model can be developed.

Using Weibull's theory and basing it on the weakest link model the mean tensile strength (σ) for specimens of different volume (V) can be related by the formula $\left(\sigma_1/\sigma_2\right)^m = \frac{V_2}{V_1}$ (59) when $\sigma_0 = 0$.

The single fibre breaking strength results, measured with a 25 gauge length were used with the above formula, to predict the breaking strengths of fibres of different gauge lengths and plotted together with the experimental results (Fig. 48). There is a reasonably good agreement between the experimental and the predicted results. The elastica results were higher than expected which may be because of the arbitary way in which the volume under test was determined. However the trend in the results indicates the validity of using a Weibull distribution to describe the breaking strength of single fibres and as it was shown, in the review of the theoretical concepts, it may be used to describe the composite strengthening mechanism.

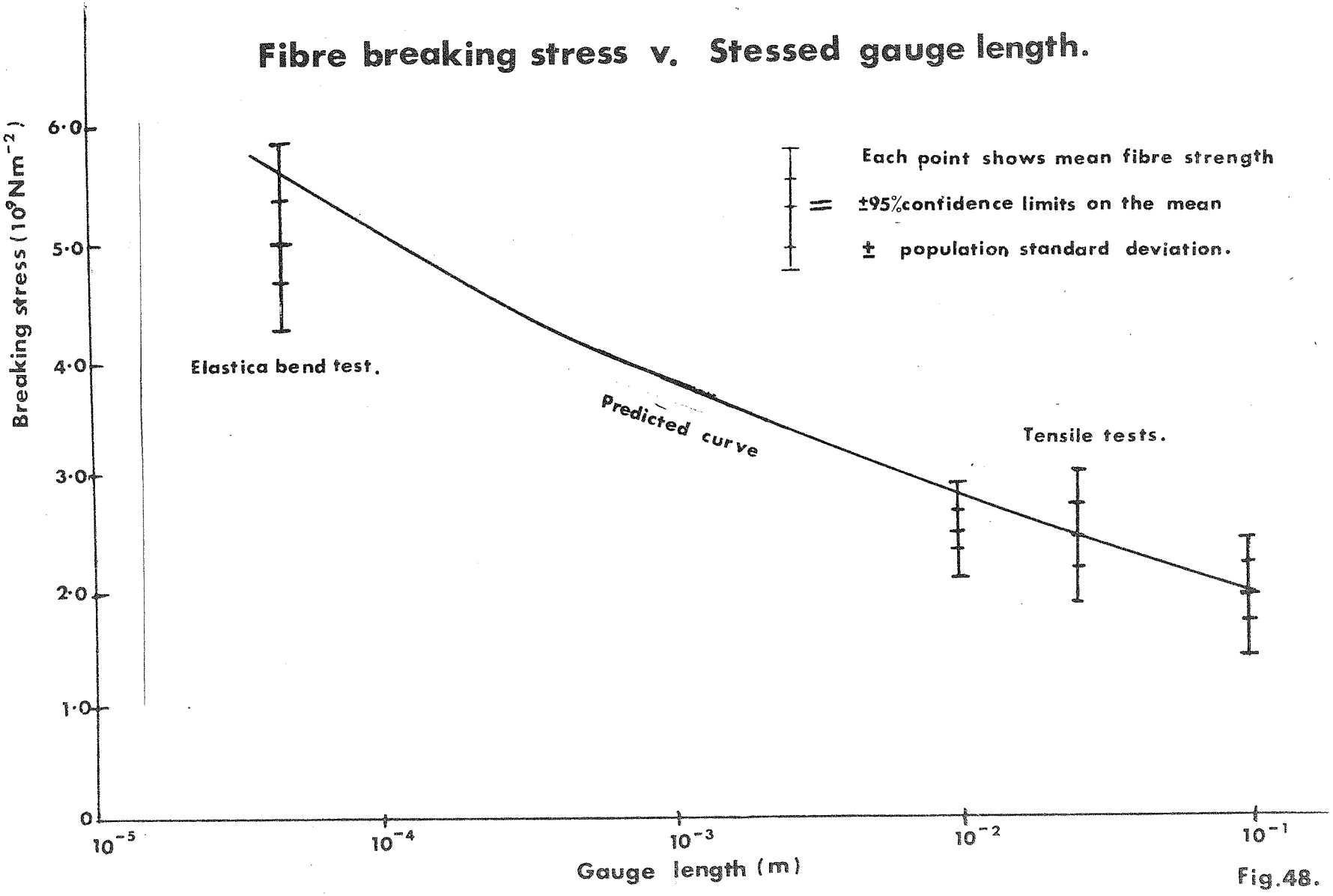
Fibre breaking stress v. Stessed gauge length.
Breaking stress ($10^9 Nm^{-2}$)
6·0
5·0
4·0
3·0
2·0
1·0
0
Each point shows mean fibre strength
= ±95% confidence limits on the mean
± population standard deviation.
Elastica bend test.
Predicted curve
Tensile tests.
10^{-5}
10^{-4}
10^{-3}
10^{-2}
10^{-1}
Gauge length (m)

Fig.48.

Chapter 5

Optimisation of Test procedures

5.1 Composite tensile strength

Earlier workers (25) studying the flexural strength of composite materials observed that the specimens failed in either tension or compression, which ever is the weaker of the two properties. Hence before any detailed study of the flexural strength it is necessary to fully understand how composite materials behave under tensile and compressive stresses, and to assess the best method of determining these properties.

5.1.1 Tensile Test procedure

A 10 000 N Instron testing machine was used to load the specimen. The rate of strain was 1 mm/min and the load range varied to suit the cross-section area of the specimens. Aluminium strips were stuck on to the ends of the specimens to protect them from damage by the jaws of the testing machine. To ensure that the specimens were properly aligned, they were lined up to a plumb-line at the beginning of the test.

5.1.2 Optimum tensile shape

Carbon fibre-epoxy resin composites, like most other resin matrix composite materials, have a low shear strength, when compared with their axial tensile strength. This causes the predominant mode of failure, with a specimen of the conventional shape (60), to be one of shear cracking away from the necked region right back into the gripped end. This raises doubts

as to what effect the grips have on the tensile strength of the composite. Hence an attempt was made to find a shape of tensile specimen that failed away from its gripped ends. For convenience standard production LY558/$BF_3$400 'prepreg' material, with a moulded fibre volume fraction of 0.65, was used in this study.

5.1.2.2 Flat parallel strip (Shape 1)

Straight un-necked strips 150 mm x 6 mm x 1 mm were tested, the distance between the gripped ends being approximately 80 mm (Fig. 49, 1), As the test progressed, the jaws dug into aluminium strips, and there was a change in the slope of the load-time curve. After this initial 'knee' the plot was straight. When approximately 60% of the load had been applied, faint cracks could be heard coming from inside the composite. These cracks were most probably individual fibres failing. However, the drop-off in load, because of fibre failure, was insignificant until just before final failure, when the cracks became more audible and numerous. At failure there was a sudden drop-off in load. The fracture of the specimen was fibrous and extended over the whole length of the specimen, between the gripped ends, (Fig. 50, 1). The mean stress at failure was 1.11 GNm^{-2} (Fig. 51, 1).

5.1.2.2 Specimens necked down in the width (Shape 2)

In an attempt to confine failure to a gauge length removed from the grips, flat strips (210 mm x 13 mm x 2.5 mm) were necked down to 0.8 mm in their width (Fig. 49,2) and tested. Again there was a definite 'knee' in the load-time curve as the jaws dug into the aluminium shims, after which it was linear up to approximately 40% of the total load. At this load, shear cracks began to propagate back from the necked portion into the gripped ends

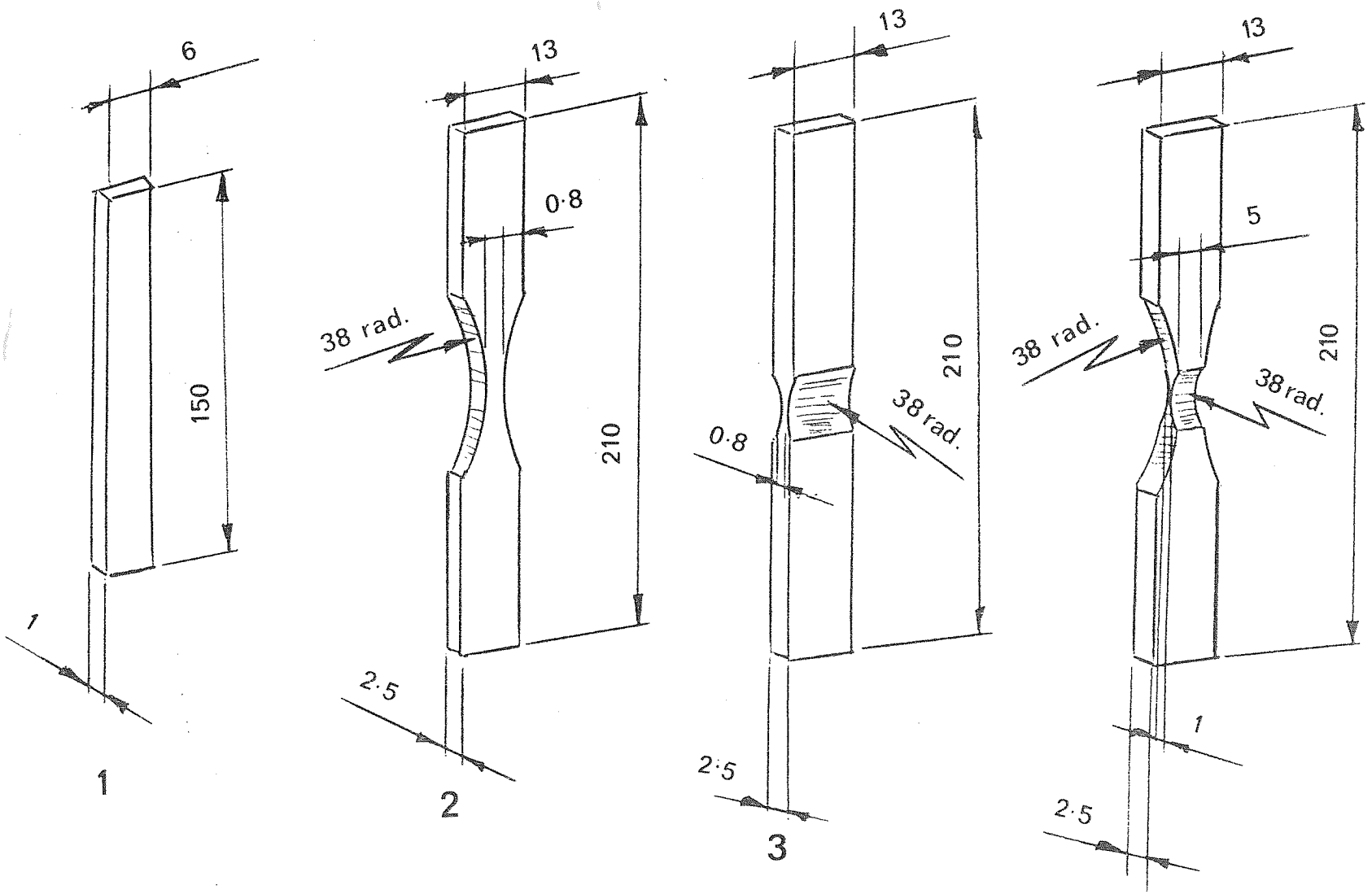

Fig. 49. Tensile test specimen shape.

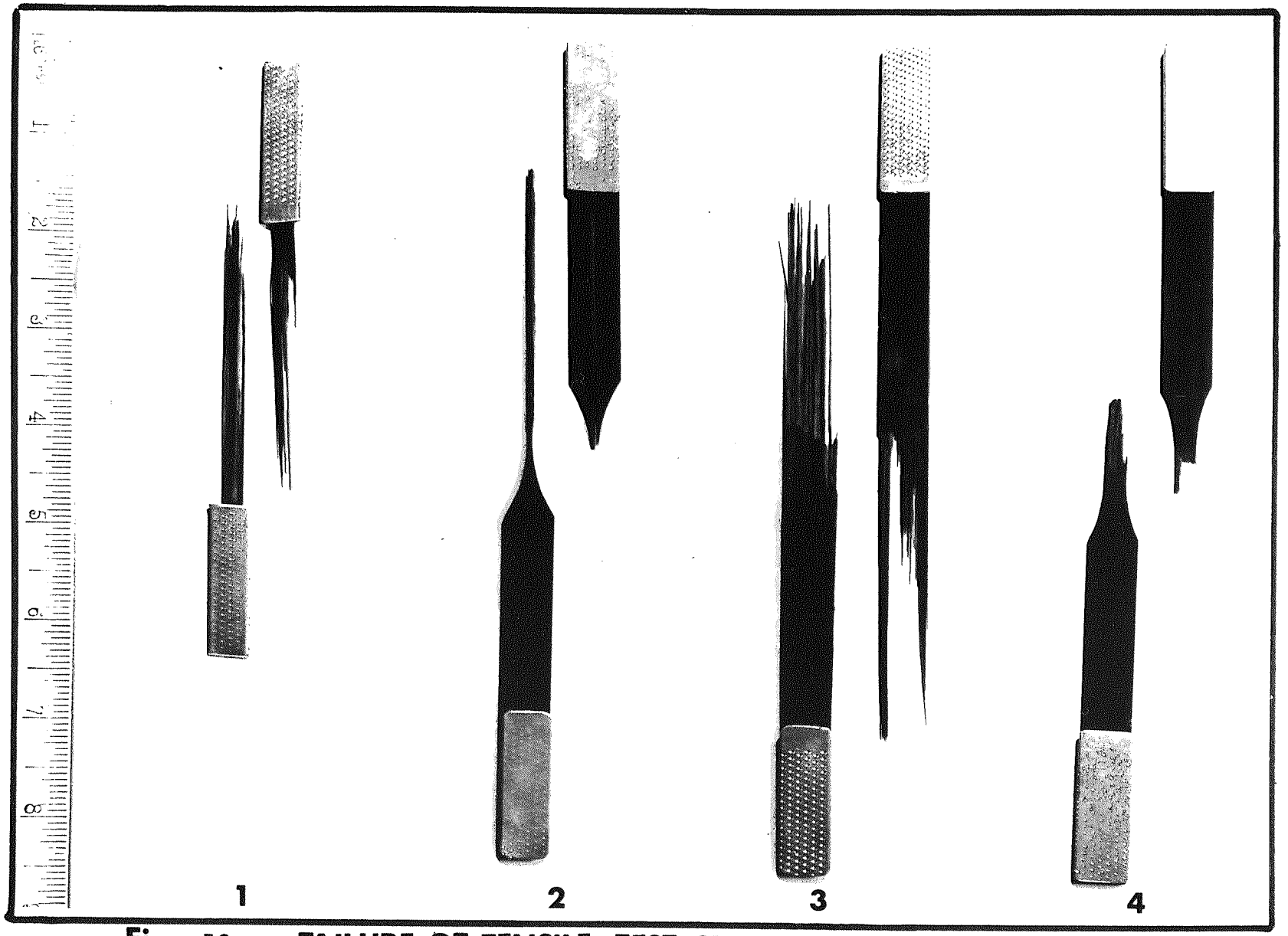

Fig. 50 FAILURE OF TENSILE TEST SPECIMENS OF DIFFERENT SHAPE.

Tensile strength for different test shapes.

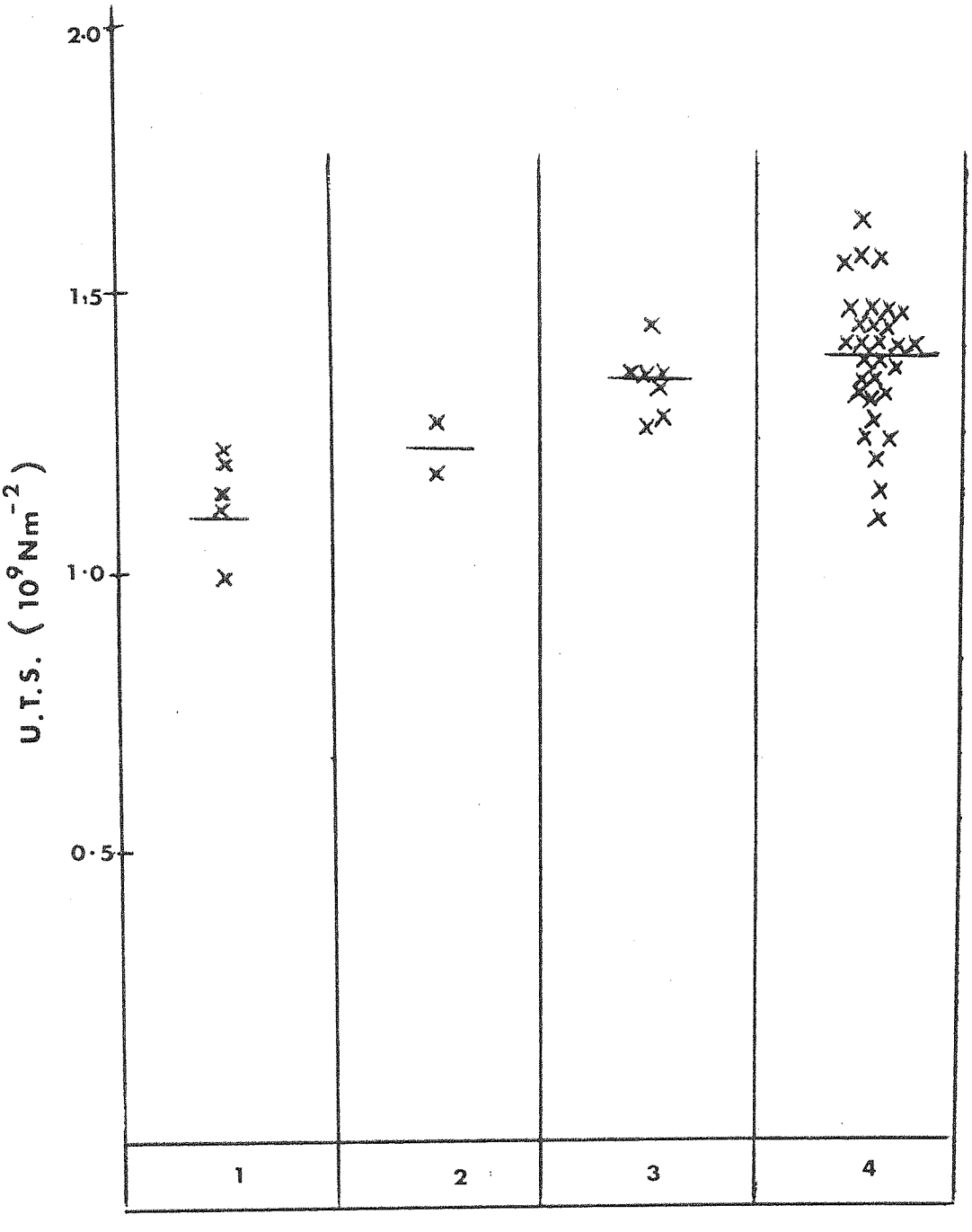

Fig. 51.

shown in Figure 52 was as follows:-

Fig. 52 a The unloaded specimen

Fig. 52 b Shear cracks began to propagate back from the necked region. (The cracks show as the lighter areas).

Fig. 52 c The shear cracks propagated right back to the grips.

Fig. 52 d The final fracture of the specimen was fibrous and extended over the whole length of the specimen between the grips.

The mode of failure of the carbon fibre/resin specimens was very similar to that of the G.R.P. specimens.

5.1.2.4 Specimens necked down in both the width and thickness (Shape 4)

The specimens necked down in the thickness (shape 3) began to fail in shear at approximately 50% of the load. Hence it was thought that if the specimens (210 mm x 13 mm x 2.5 mm) were necked down in the width to 5 mm as well as being necked down in the thickness to 1 mm (Fig. 49, 4), the part of the specimen away from the necked region would be able to support the shear stresses at the failure load. At approximately 40% of the failure load, shear cracks propagated back from the radii in the thickness, but they did not appear to reach the grips. After this shear failure, cracks appeared on the surface of the specimen. It was thought that these cracks were caused because the core of the specimen was being contracted by Poisson's ratio effects, while some layers were 'relaxing' because of shear failure. Before final failure there was an appreciable drop-off in the load as groups of fibres failed. The final fracture was fibrous, but although failure had not been confined to the necked region it was away from the grips (Fig. 50, 4). As with the previous specimens, there was some evidence that the fibres had failed in groups.

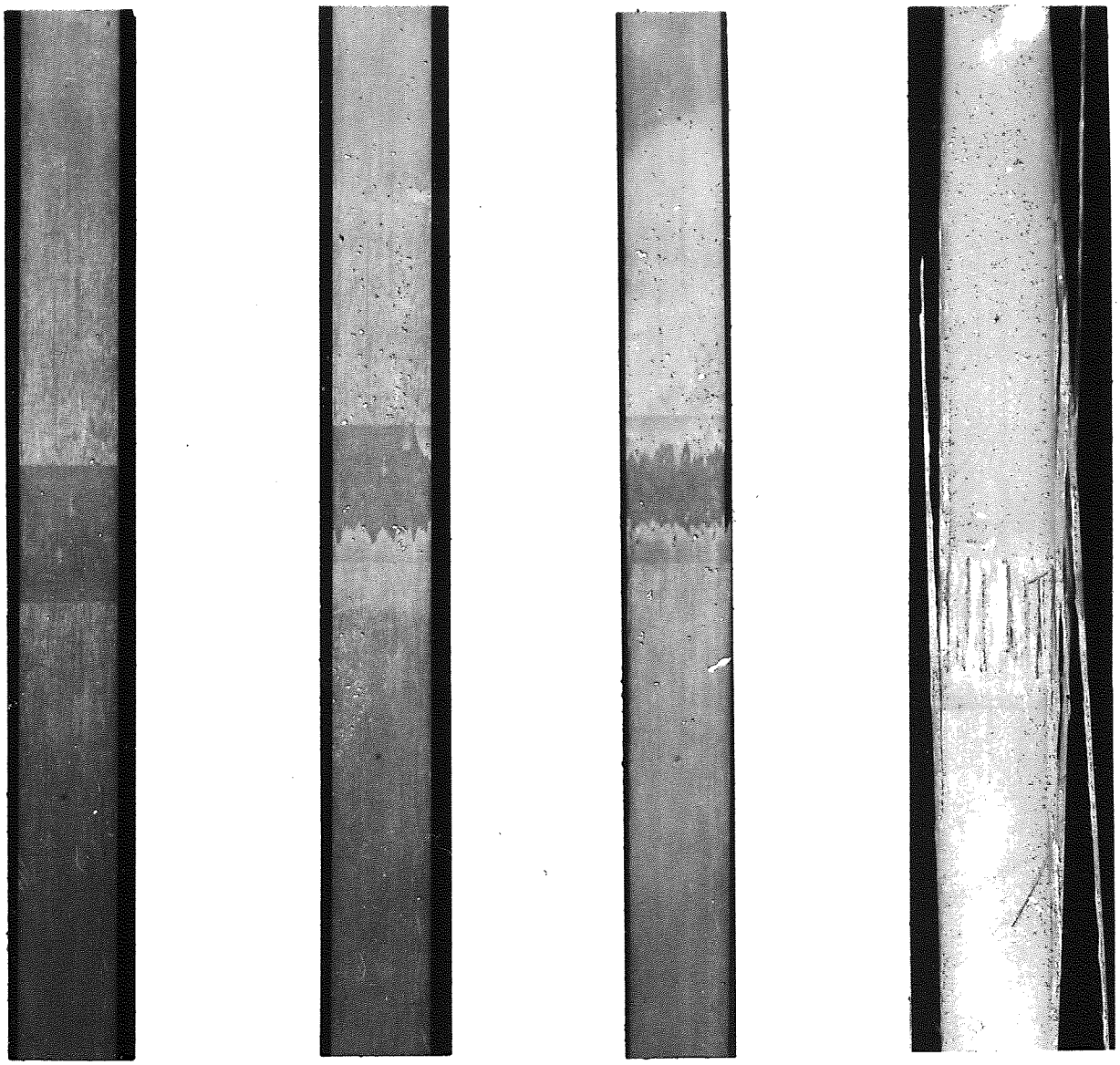

Fig.52. FAILURE OF G.R.P OF TENSILE TEST SHAPE 3.

To understand more about the mode of failure, a G.R.P. specimen was machined to shape 4 and tested. The untested specimen is shown in Figure 53 a. At approximately 30% of the load shear cracks propagated back from the radii in the thickness (Fig. 53 b) right back into the grips (Fig. 53 c). As with the carbon composites, when the shear cracks were propagating longitudinal cracks appeared in the 'sheared' layers. The final tensile failure was over the whole region of the specimen between the grips. (Fig. 53 d). Although the mode of failure of the G.R.P. composite was different, in that there was shear failure back to the grips, it illustrates clearly how the specimens with this shape fail. A number of specimens, having this shape, were tested and a histogram of the results is shown in Figure 54. The mean breaking strength of 48 specimens was 1.40 GNm^{-2} with a standard deviation of 0.12 GNm^{-2}. This was higher than the other three specimen shapes.

5.1.2.5 Specimens necked down in the thickness with varying radii

One disadvantage of specimen shape 4 is that, because of its double radii, some time is taken in machining. Machine time would be cut by half if the specimens were necked down in the thickness only. Specimens of shape 3 failed because the material, at the radii, could not support the shear stress generated at the neck. Using the equations of equilibrium (51) (See Appendix V) the shear stress was found at different points on the radius for various radii. (Fig. 55). The short beam shear strength of the material is 45 MNm^{-2}, therefore assuming that the specimen can withstand this stress at the radius, Figure 55 suggests that if the radius was 250 mm or above the specimens will not fail in shear. So that more specimens could be taken from one moulding, 6 mm wide strips were cut from a 2.5 mm thick panel and

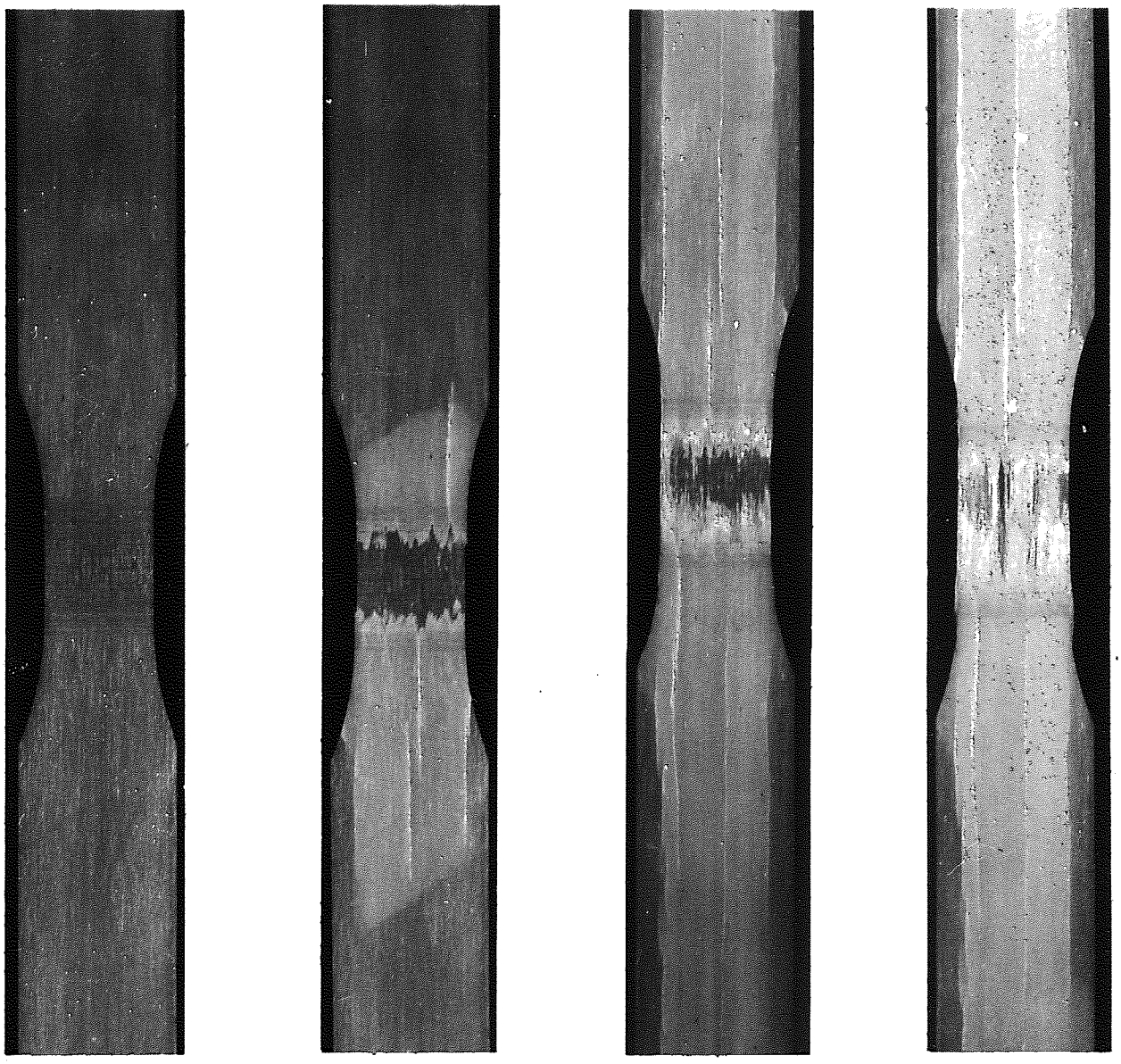

Fig.53. FAILURE OF G.R.P. OF TENSILE TEST SHAPE 4 .

Histogram of the U.T.S. for shape 4

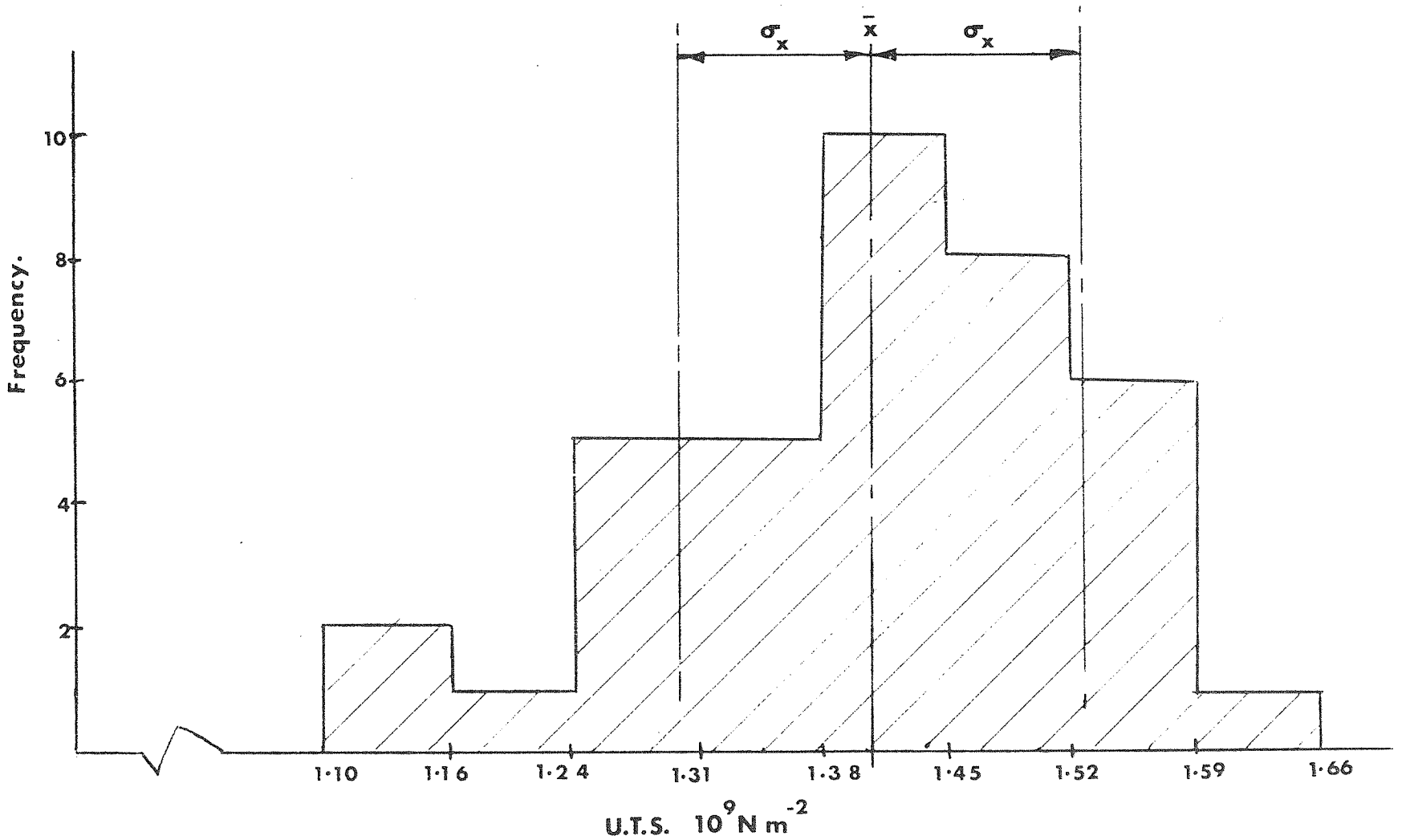

Fig.54 .

Shear stress at different points on the radius

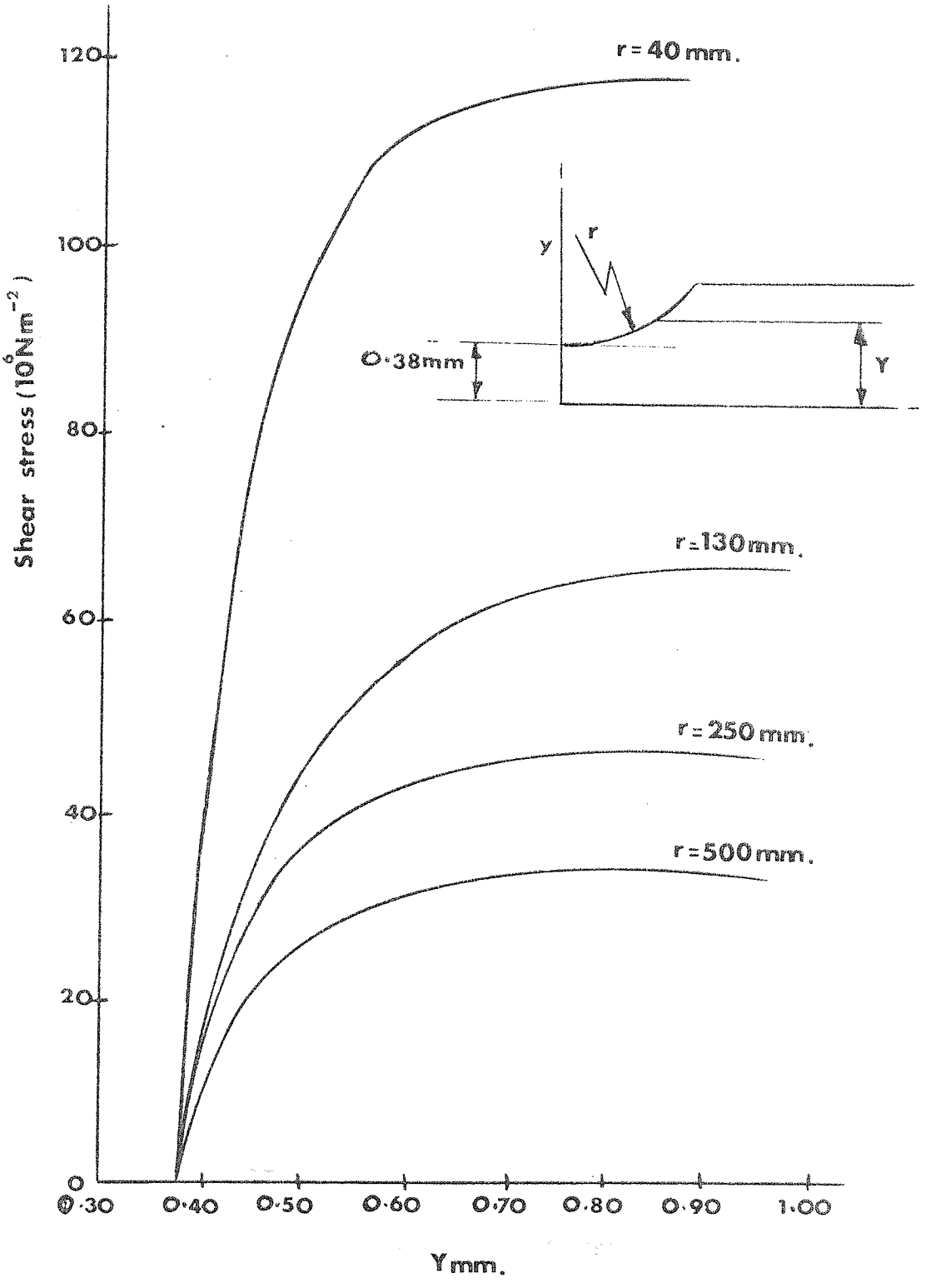

Fig.55.

machined with varying radii to a necked thickness of 0.5 mm. It is thought that this reduction in width should not affect the mode of failure.

When tested all the specimens failed in shear right back to the grips. Their mode of failure was fibrous and extended over the whole length between the grips, similar to the mode of failure of specimens of shape 3. (Fig. 50, 3).

From Figure 55 it can be seen that 75% of the specimen is bearing the peak stress. With the 1.5 mm thick specimens only a small section of the radius is subjected to a peak stress. Specimens 165 mm x 6 mm x 1.5 mm were necked down to 0.8 mm in the thickness with 250 mm radii. The mode of failure of these specimens was exactly the same as the others of shape 3.

There was no significant difference in the breaking strength of the specimens of shape 3 with different radii (Fig. 56). The breaking strength was in the region of 1.31 GNm^{-2} for all the specimens. This would suggest that the shear strength along the specimen length is lower than that found in bending, by the interlaminar shear strength test. A further explanation would be that the method for determining the shear stresses around the radius was not adequate. However as the object of this section of the research was to determine an optimum test shape, and that this shape appeared to be unsatisfactory it was decided not to seek a more rigorous stress analysis.

Workers at R.A.E. Farnborough have issued a note on the preferred specimen shapes of carbon fibre reinforced plastic test pieces (62). For testing the strength of unidirectional material in the direction of the fibres they suggest a blank (154 mm x 6 mm x 1.6 mm) necked down to 1.0 mm by means of a 50 mm radius in the specimen thickness, similar to the type 3 specimen. The failure of the R.A.E. specimens was reported to be away from the gripped

U.T.S. for shape 3 with different raddii .

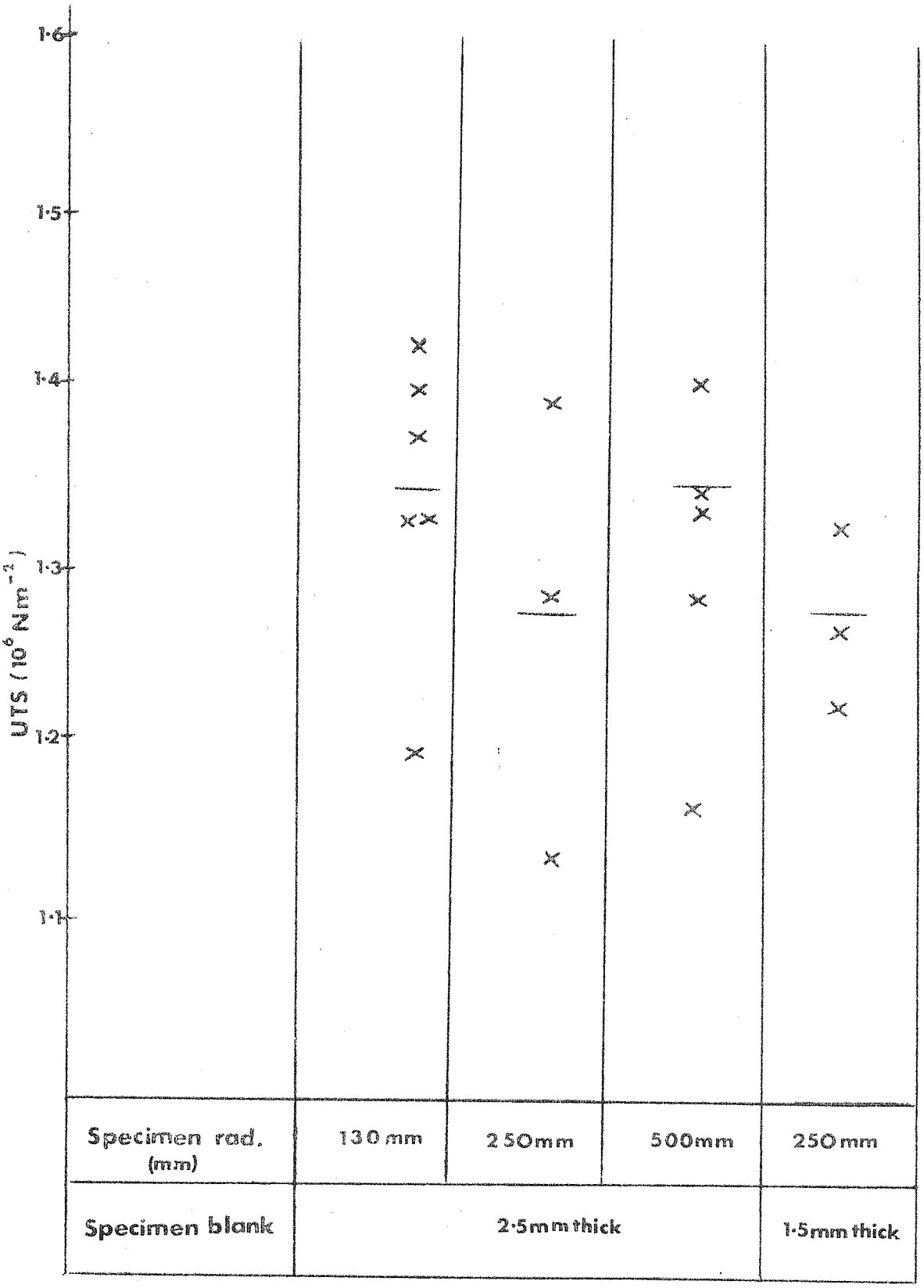

Fig. 56.

ends whereas the type 3 specimens tested, even those with a radius of 250 mm have failed in shear back to the grips.

Reasons for this apparent contradiction could possibly be found in the different manufacturing techniques and in the different fibre volume fractions. The fibre volume fraction of the test pieces used in the R.A.E. note varied from 0.5 to 0.6 compared with 0.6 to 0.7 for the composites used in the above exercise. It will be demonstrated later that the lower fibre volume fraction specimens have a marginally higher interlaminar shear strength and a proportionally lower tensile strength. R.A.E. produce their composites using a leaky mould technique. The fibres are simply laid into a mould, the resin poured on and moulded. With this technique the fibres are not grouped together in close packed bonds, hence because there is possibly a better bond between the fibres the R.A.E. composites can sustain a higher shear load at the radius than the Rolls Royce composites and the failure is in tension away from the gripped ends.

5.1.2.6 The choice of an optimum specimen shape

Shape 4 was chosen as the optimum specimen shape because it gave for all fibre volume fractions:-

a) A failure, which although extended beyond the region of minimum cross section area, was away from the grips.

b) Specimens which failed at higher stress than the specimens of shapes 1, 2 and 3.

Although there was some shear failure with this specimen shape, particularly at the higher fibre volume fractions, it was used to evaluate the tensile strength of the composite.

5.1.3 Gauge length effects in the composite

The breaking strengths of specimens of shape 3, in which tensile failure was observed to take place over the whole length of specimen between the grips are lower than those for specimens of shape 4 which fail over a shorter length. Assuming that the grips do not affect the strength of the composite, there appears to be a gauge length effect. To check this, specimens 108 mm long were machined to shapes 3 and 4 and tested.

The mode of failure of the short specimens of shape 3 was similar to that of the longer specimens, but because the aluminium grips were closer, 62 mm instead of 150 mm, it was confined to a smaller length. The mean breaking strength of the shorter composites was 1.49 GNm^{-2}, this compares to a mean strength of 1.34 GNm^{-2} for the 216 mm long specimen. (Fig. 57).

When the shorter specimens of shape 4 were tested, although the mode of failure was similar to that of the long specimens, there was fibrous failure at the grips. This was because the distance between the grips was approximately the same length as the extent of failure. The mean strength of 1.44 GNm^{-2} is similar to that of 1.40 GNm^{-2} for the longer specimens, which is not surprising as the extent of fibre failure was similar for both sizes of specimens (Fig. 57).

Although only a limited number of tests have been carried out, there does appear to be a size effect as predicted by Rosen and Zweben (6).

U.T.S. v Specimen length.

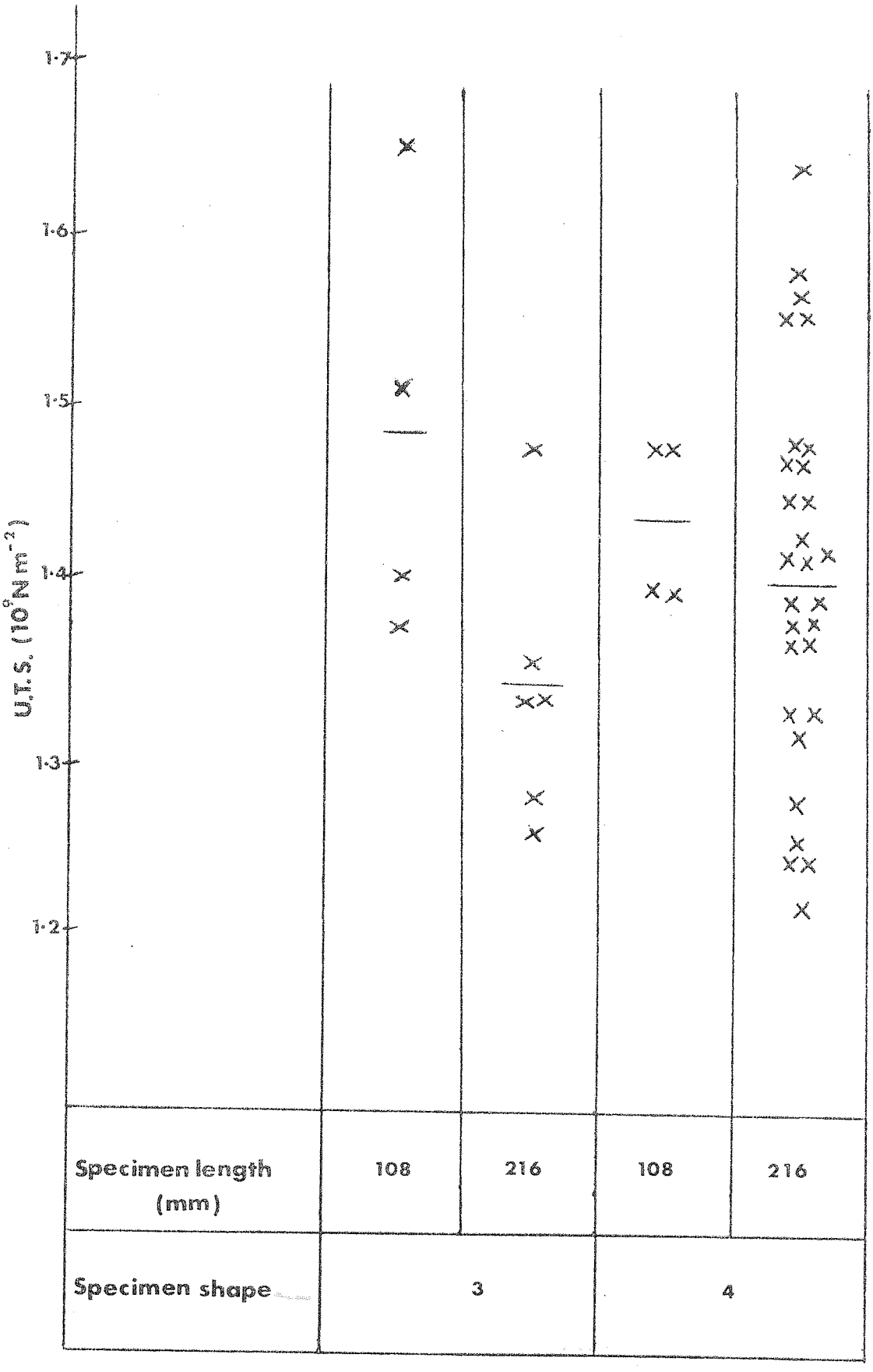

Fig. 57.

5.2 Compression testing

For many years the standard test used for measuring the compressive strength of plastics and other materials was similar to that specified by ASTM test 695 (63). This method uses a test specimen in the form of a right cylinder or prism whose length is twice its principal width or diameter. The ends of the specimen are machined flat and normal to the direction of the applied load. The specimen is loaded from the anvils of the testing machine through the flat ends of the test piece.

Similar test methods have been applied to fibre reinforced plastics and without exception the test specimens failed by crushing at the ends with a complete breakdown of the matrix, giving them a brush like appearance (64, 65).

Transverse loads set up in the ends of the test specimen under a compressive load are small compared with the ultimate transverse strengths of more traditional homogeneous materials. However, carbon fibre reinforced plastics have a low transverse strength because of their dependence upon the properties of the weak resin matrix and the fibre-resin bond. Hence the premature failure, at the ends of the composite material test specimens, are probably caused by the relatively high transverse loads set up by the loading anvils.

To reduce the end constraints caused by the loading anvils, a series of tests were conducted by Fried and Winans (65) in which the loaded end faces between the specimen and anvil were lubricated. The compressive strength results were slightly higher but, the specimens again failed prematurely by a crushing of the ends.

Fried and Winans came to the conclusion that, to prevent load crushing, an attempt must be made to reinforce the specimens at the ends. Ewins (64) has taken this concept and developed it to produce a compressive test specimen for unidirectional carbon fibre reinforced plastics. This specimen consists of a rod which is waisted at the centre section to approximately 80% of the nominal diameter. The ends of the specimen are bonded into mild steel collets. After the adhesive has cured, the steel ends are machined flat and normal to the test piece axis. Tests on specimens of this design gave results which were capable of being reproduced and the failures were apparently not influenced by end effects.

The main disadvantage of this test specimen is that considerable time and care is required in its preparation. Therefore a more simple test method was sought.

The ASTM have developed a method for testing thin laminated plates (66). With this method the specimens are given lateral support by a jig, to prevent premature failure by 'Euler' buckling, the load being applied through its ends which are required to be flat and normal to the loading anvils. This, with thin plates, makes alignment difficult.

Workers at Bell Areosystems Co., have developed a fixture for measuring the compressive strength of carbon fibre resin matrix composites (67). The specimens were necked down by 50% in the width using a 13 mm radius on each side. The compression tests were conducted using a specially designed fixture, which aligned and supported the specimen. With this arrangement they found that over 90 per cent of the specimen failures occurred in the reduced-width gauge length

The Bell Areosystems compression test configuration fulfilled the basic requirements for this project which are (a) the failure was not influenced

by end effects and (b) that it can accommodate thin flat specimens. Also, because the load was transmitted to the specimen through the fixture, it was not necessary to carefully machine the ends of the specimen.

A fixture, which was similar to the above, was designed to determine the compressive strength of unidirectional carbon fibre reinforced plastic test pieces (Figs. 58 & 59). The ends of the specimen were clamped between recessed blocks. The fixture was so designed that there was a gap of 2.5 mm between the blocks on both sides of the specimen to allow for compressive deformation. The gaps on either side were offset by 25 mm. There were cavities in the longer blocks on either side of the specimen to accommodate strain gauges. In order to minimise bending and to maintain alignment throughout the test, the blocks and specimen were gripped in a vice like fixture. To ensure uniform load distribution across the specimens, the fixture was loaded through a simple universal joint, which consisted of a ball bearing between two blocks.

5.2.2 Optimum specimen shape

Various shapes have been recommended by different workers ranging from flat plate (68) to a waisted bar (64). All these workers were achieving compressive strengths for a carbon fibre composite machined to their 'best' shape, of approximately 1.10 GNm^{-2}. This would appear to indicate that there is no unique optimum specimen shape and that it is dependent upon the design of the fixture used in the test, and the material being tested. The following series of tests were conducted to determine the optimum compressive test piece configuration for the fixtures described above. A 10 000 N Instron testing machine was used to load the specimen at a strain rate of 1 mm/min.

Fig.58. General view of compression fixture.

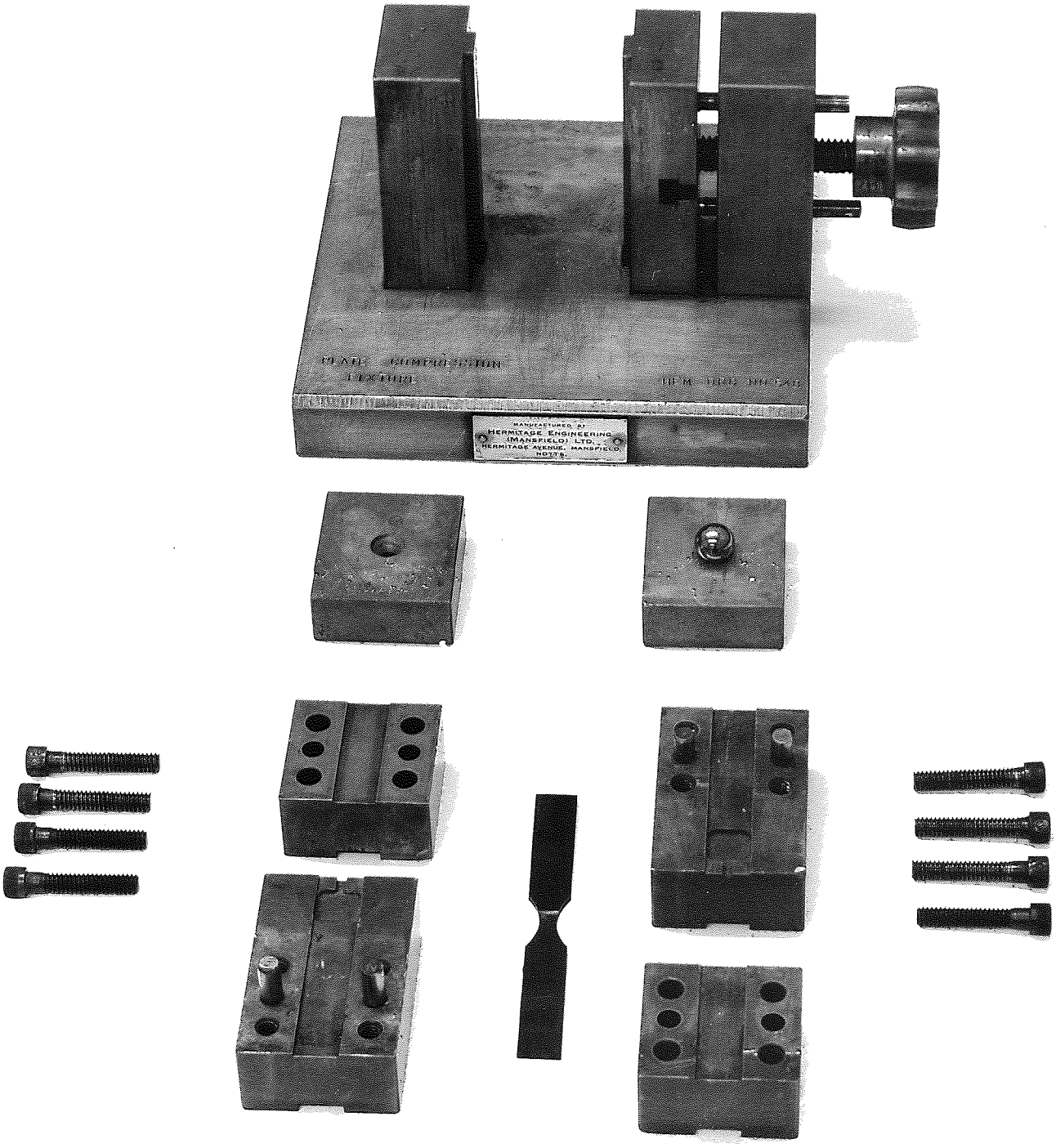

Fig.59. Exploded view of compression fixture.

5.2.2.1 Flat plate strip

A flat parallel strip (100 mm x 13 mm x 2.5 mm) was placed in the fixture and a load applied. As the test progressed the load-time curve began to curve away as the specimen slipped between the blocks. The test was stopped and to improve the frictional force between the specimen, strips of fine emery paper were placed in the recesses of the blocks. The specimen was returned to the fixture and the load applied. At approximately 80% of the maximum load applied there was a reduction in the slope of the load-time curve. At failure there was a sudden drop--off in load.

Study of the final fracture showed that there was a sharp crack in the specimen and pronounced shear damage up to a distance of about 12 mm away from the crack. (Fig. 60, 1). The failure occurred adjacent to the strain gauge cavity. Hence the mode of failure, its position and the load time curve suggest the following sequence of failure. The plate was loaded uniformly up to 80% of the load where it became unstable and buckled into the strain gauge cavity in the blocks. The final failure was a mixture of bending and compression with an ultimate compressive strength of 0.57 GNm^{-2}.

5.2.2.2 Specimens necked down in the thickness

In an attempt to confine the failure to a particular gauge length, the specimen blank was necked down in the thickness to 1.2 mm by a 50 mm diameter on either side (Fig. 61, 1). As the load was applied the load-time curve was linear up to approximately 60% of the maximum load where shear cracks began to propagate back from the necked region causing a change in slope. At failure there was a sudden drop off in load and the fracture was confined to the gauge length. The mean breaking strength of 5 specimens was 0.90 GNm^{-2} which was low, possibly because of the early shear failure.

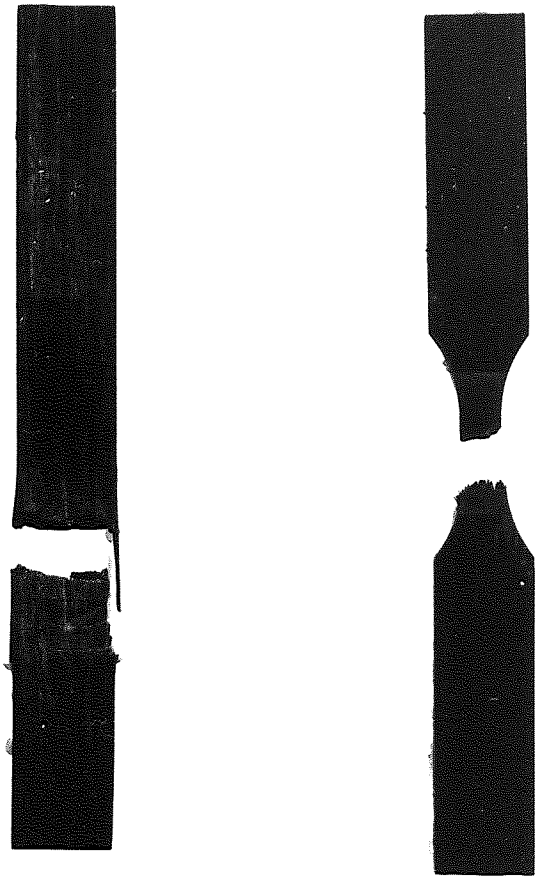

1 2

Fig.60. COMPRESSION FAILURES

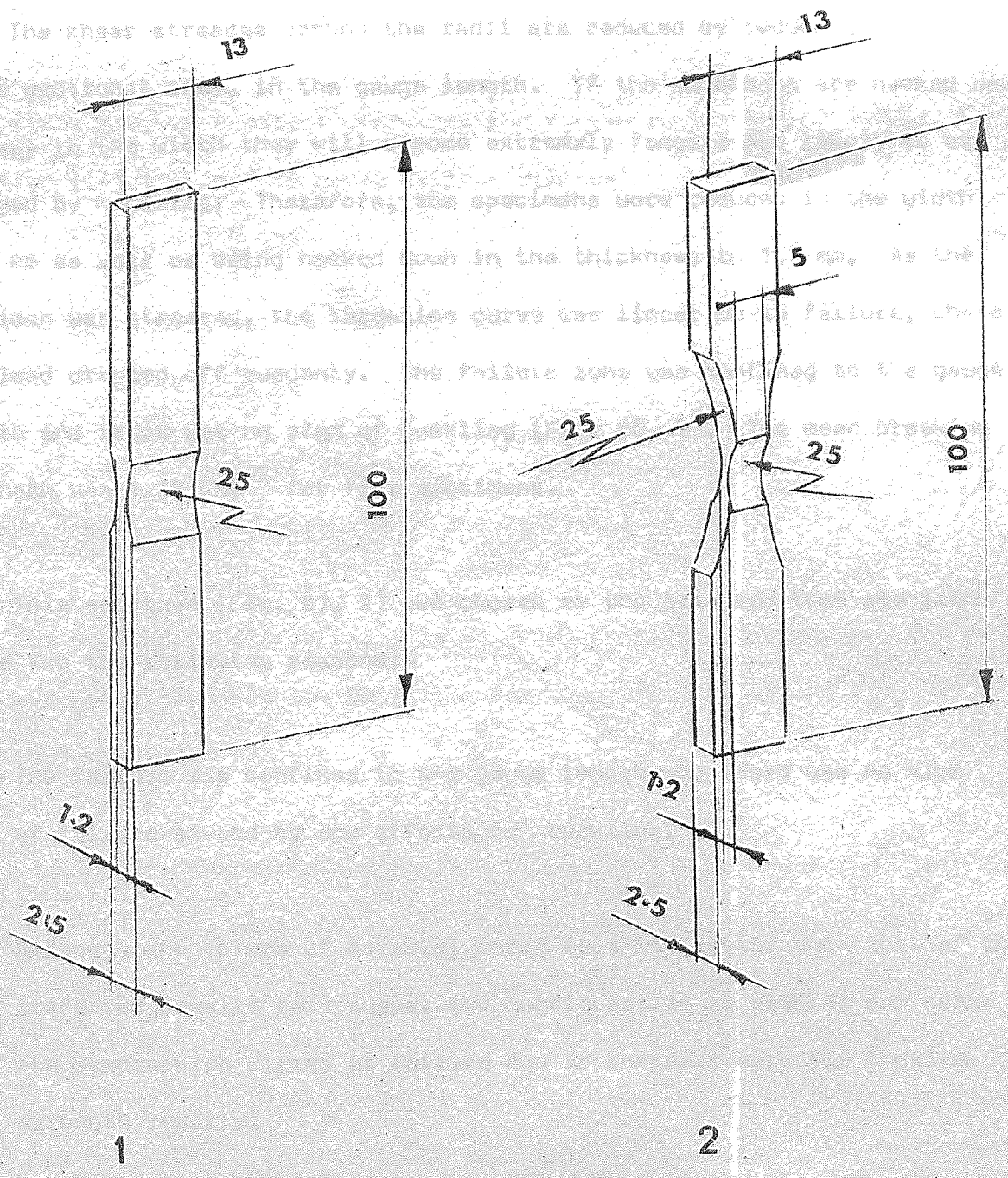

Fig.61. Compression test specimen shape

5.2.2.3 Specimen necked down in the width

The shear stresses around the radii are reduced by reducing the cross sectional area, in the gauge length. If the specimens are necked down further in the width they will become extremely fragile and likely to be damaged by handling. Therefore, the specimens were reduced in the width to 5 mm as well as being necked down in the thickness to 1.2 mm. As the specimen was stressed, the load-time curve was linear up to failure, where the load dropped off suddenly. The failure zone was confined to the gauge length and there was no sign of buckling (Fig. 60, 2). The mean breaking strength was 1.12 GNm^{-2} for five specimens.

This specimen (Fig. 61, 2) was chosen as the standard test specimen shape for the following reasons:-

(1) The failure was confined to the gauge length and there was no sign of failure caused by end effects or buckling.

(2) Although the volume of material under test is greater than that of the preferred tensile test shape, the configuration is similar and hence the compressive stress at failure can be compared with the tensile strength results.

(3) The compressive stress obtained was at least as high, if not higher than those obtained by other workers (54, 67 & 68).

5.3 Flexural Strength

The test used here to measure the flexural strength at failure was a three point bending test similar to B.S.2782 method 304, of a constant rectangular section beam.

The shear strength is not normally of great concern when dealing with isotropic materials, but because C.F.R.P. composites have low shear strengths it cannot be neglected here.

For a beam of constant cross-section tested over a span (L) from equation 2.17 the load to cause failure will be

$$W_T = \frac{2\hat{\sigma}\, bd^2}{3L} \qquad - 5.1$$

and that to cause shear failure will be

$$W_S = \frac{4\hat{\tau}\, bd}{3} \qquad - 5.2$$

where $\hat{\sigma}$ is the lower of the tensile or compressive strength,
$\hat{\tau}$ is the shear strength of the material.

Then the beam will fail in shear if $W_T > W_S$ or in tension-compression if $W_T < W_S$. This leads to the condition for shear failure $L/d < \frac{\hat{\sigma}}{2\hat{\tau}}$ and for tensile-compressive failure $L/d > \frac{\sigma}{2\tau}$

The shear and tensile-compressive stress at failure as a function of aspect ratio are shown in Figure 62. To the left of the diagram the beam fails in shear at a constant value of shear stress (according to simple theory) while the tensile stress at shear failure increases with increasing aspect ratio. To the right of the diagram the beam fails in tension or compression at a constant tensile stress, while shear stress decreases with aspect ratio. The critical aspect ratio at which the change in failure mode occurs for a given material clearly depends on the ratio of the smaller of the tensile or compressive strength and the shear strength for that material.

5.3.1 The effect of changing the aspect ratio on the flexural strength

For convenience the specimens used to determine the optimum aspect ratio were moulded from standard production LY558-BF$_3$400 prepreg material with

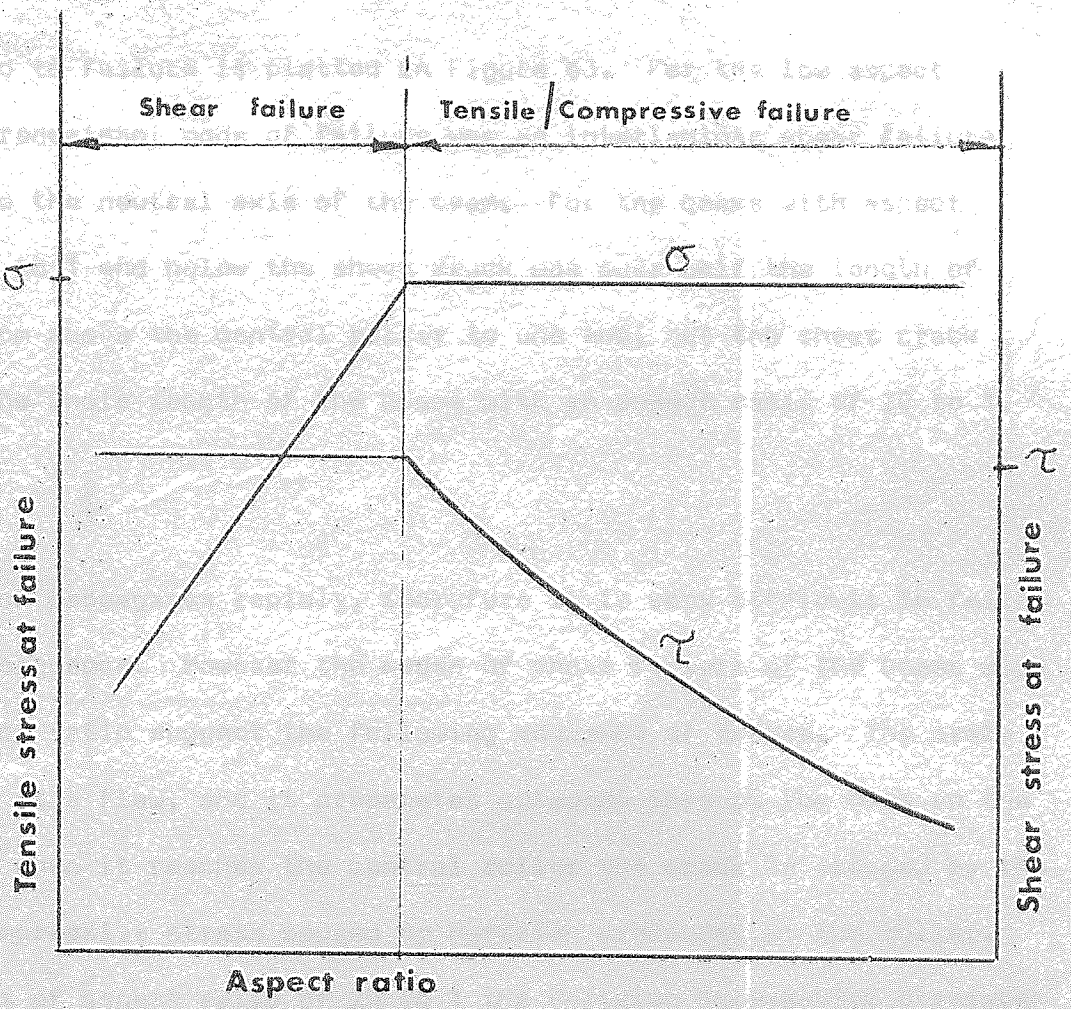

Stress at failure v. Aspect ratio.

Fig. 62.

a fibre volume fraction of 0.65. The aspect ratio was increased from 6 : 1 to 70 : 1. The width of the beams was kept constant at 6.3 mm throughout the test and the varying aspect ratio achieved by varying the length and keeping the depth constant at 2.5 mm. The load was applied to the specimens with a constant cross head movement of 100 mm/min.

The load to failure is plotted in Figure 63. For the low aspect ratios the predominant mode of failure was an interlaminar shear failure at or near to the neutral axis of the beam. For the beams with aspect ratios of 12 to 1 and below the shear crack was over half the length of the beam, from above the central roller to one end, but the shear crack propagated the whole length of the beams with an aspect ratio of 20 to 1. (Fig. 64).

The crack propagates rapidly, therefore it is very difficult to follow the failure sequence. However the modes of shear failure of the beams with varying aspect ratio suggest the following sequence of events. The crack is initiated at a flaw, and it propagates outwards through the beam on the same plane. When it reaches the central roller the crack is stopped by the region of compressive stress caused by Hertzian pressures at the roller. With the beam of aspect ratio of 20 to 1 the Hertzian compressive stresses are lower, because of reduced load to failure (Fig. 63) and are not sufficient to stop the crack and consequently it propagated the whole length of the beam.

As the aspect ratio was increased, the load at failure decreased and the mode of failure changed to failure in the compressive region of the beam. The compressive failure was a sharp crack under the central roller which propagated up to the neutral axis of the beam where it was stopped by localised

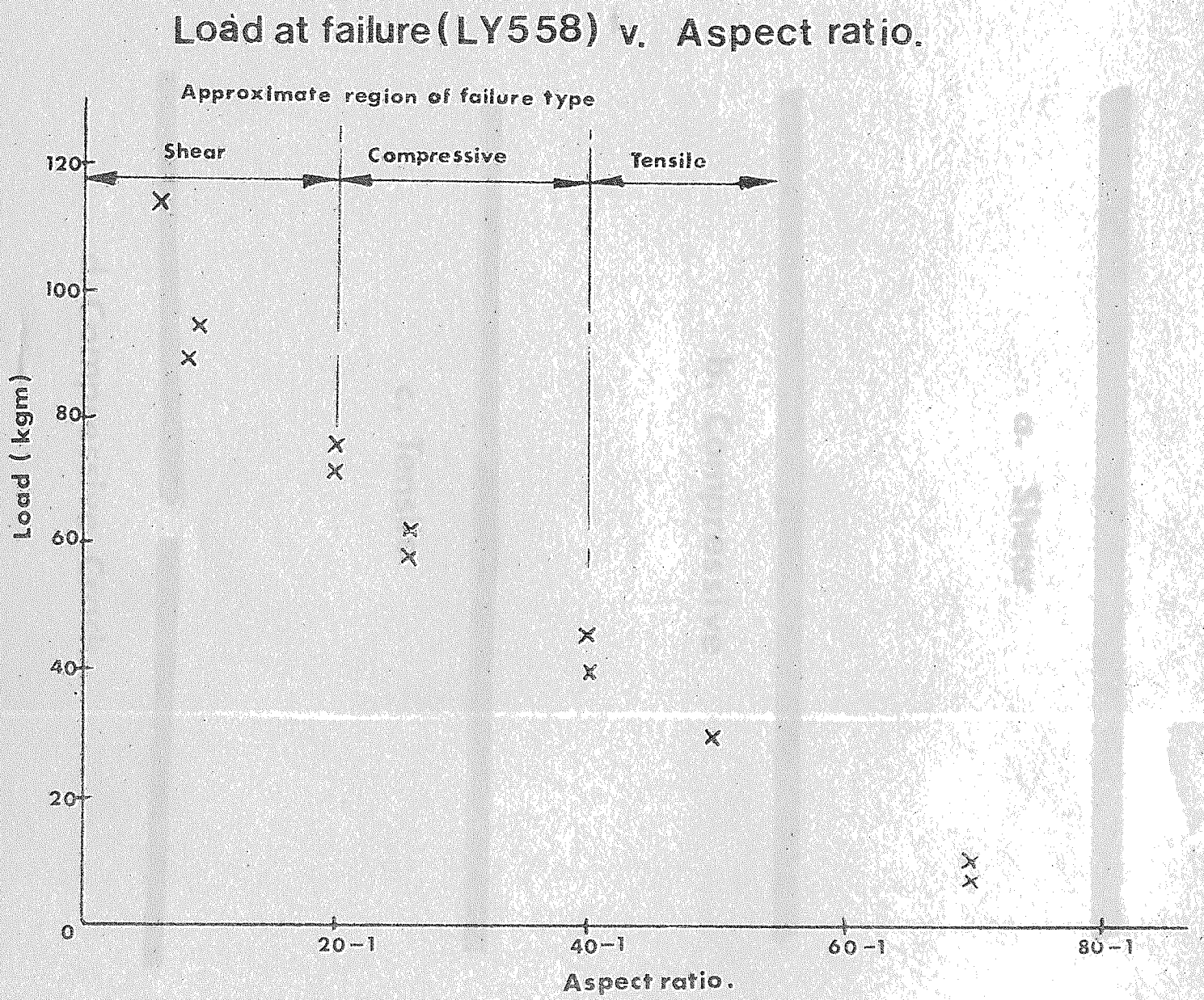
Load at failure (LY558) v. Aspect ratio.
Approximate region of failure type
Shear
Compressive
Tensile
120
100
80
60
40
20
0
Load (kgm)
20 – 1
40 – 1
60 – 1
80 – 1
Aspect ratio.

Fig. 63.

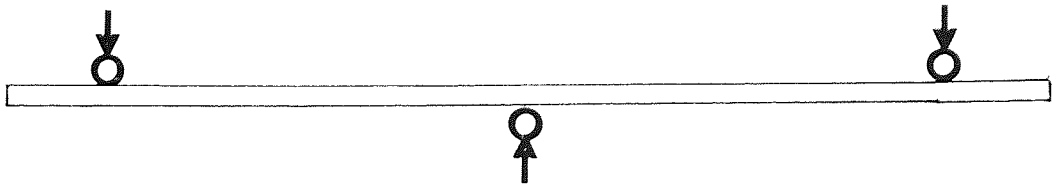

a. Shear

b. Compressive

c. Tensile

d. Compressive Crack

Fig.64. DIFFERENT MODES OF FLEXURAL FAILURE.

delamination (Fig. 64). At failure there was a sudden drop in load as the crack propagated.

Tensile failures (Fig. 64) were not observed until the aspect ratio was increased to 40 to 1 but even then some of the specimens failed in compression. When the specimens failed in tension there was a gradual drop in load as individual groups of fibres failed. The final mean load of specimens which failed in tension was slightly higher than those which failed in compression. This would seem to suggest that the governing mode of failure was the compression mode, but if a specimen had a high compressive strength then it failed in tension.

With aspect ratios of 50 to 1 and 70 to 1 the predominant mode of failure was tensile. However, with these aspect ratios there were large deflections at failure. With large deflections loading faces are no longer normal to the beam and the horizontal components not measured by the testing become significant. Also the span length changes as the beam 'wraps' round the rollers. These effects are illustrated in Figure 65 together with multiplication factors calculated by Freeman (69) and others to correct the stresses calculated using simple theory. There is little difficulty in detecting the bending of linearly elastic C.F.R.P. into the large displacement region ($\Delta/L = 0.1$) as the normally linear load-displacement curve begins to curve towards the load axis, showing a pseudo yield.

The flexural strength is plotted in Figure 66 against aspect ratio, with the approximate regions of predominant failure. The specimens with aspect ratios of 40 to 1 gave a maximum value of flexural strength. Although the failure was a mixture of tension and compression, the horizontal component of force was insignificant.

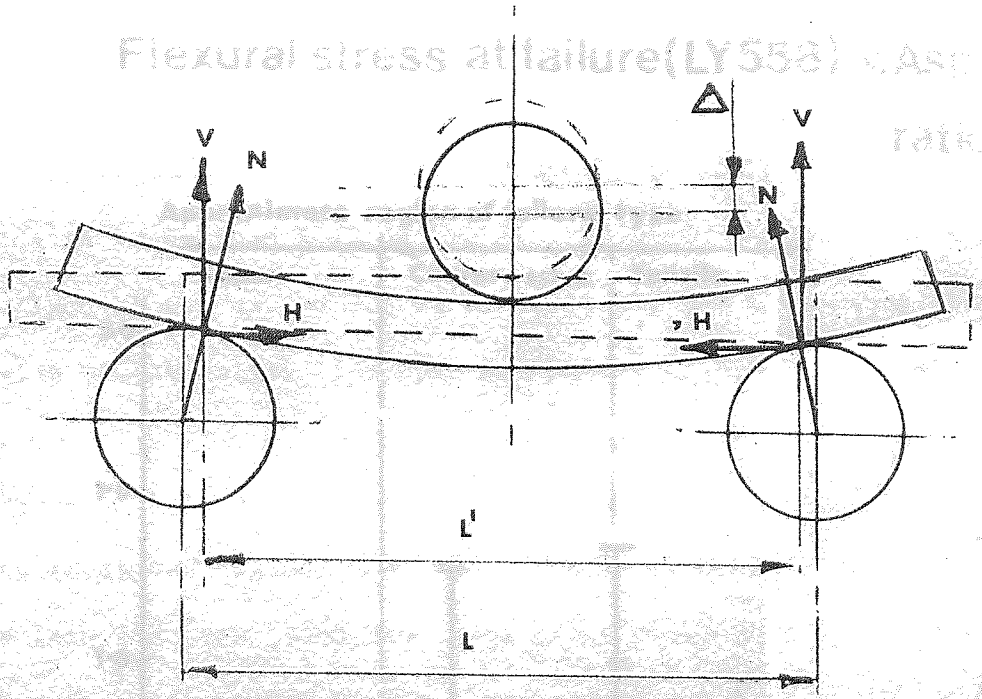

Magnification factor to correct stress (After Freeman)

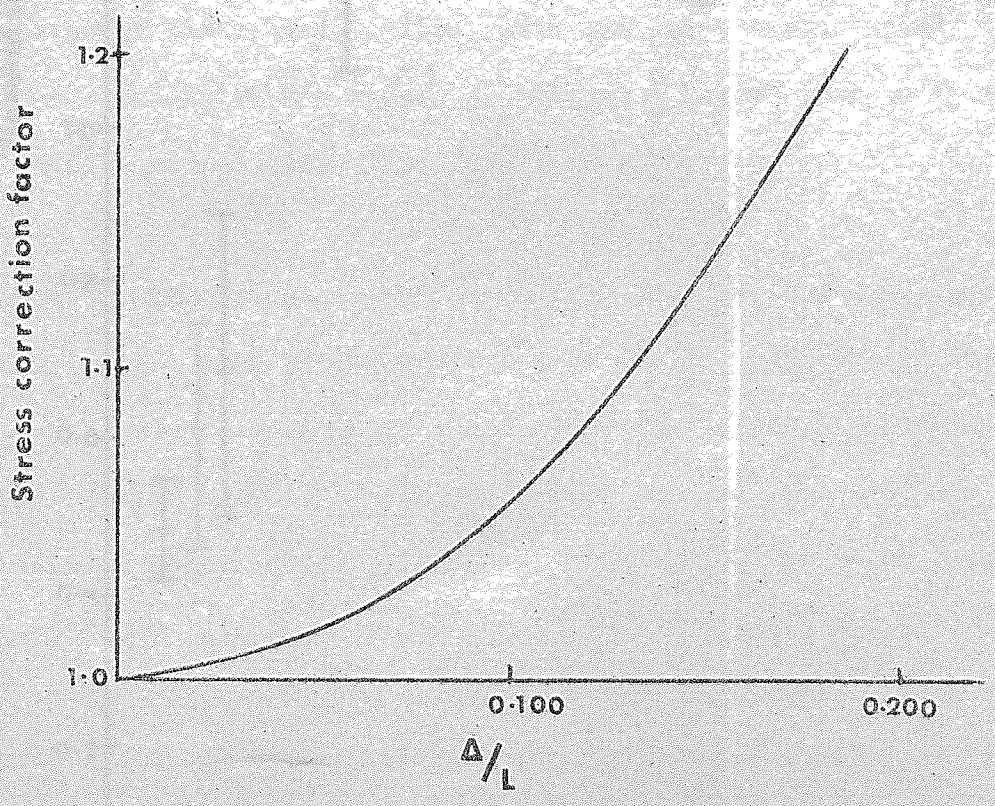

Three point bending — Large deflections.

Fig 65.

Flexural stress at failure(LY558) v.Aspect ratio.

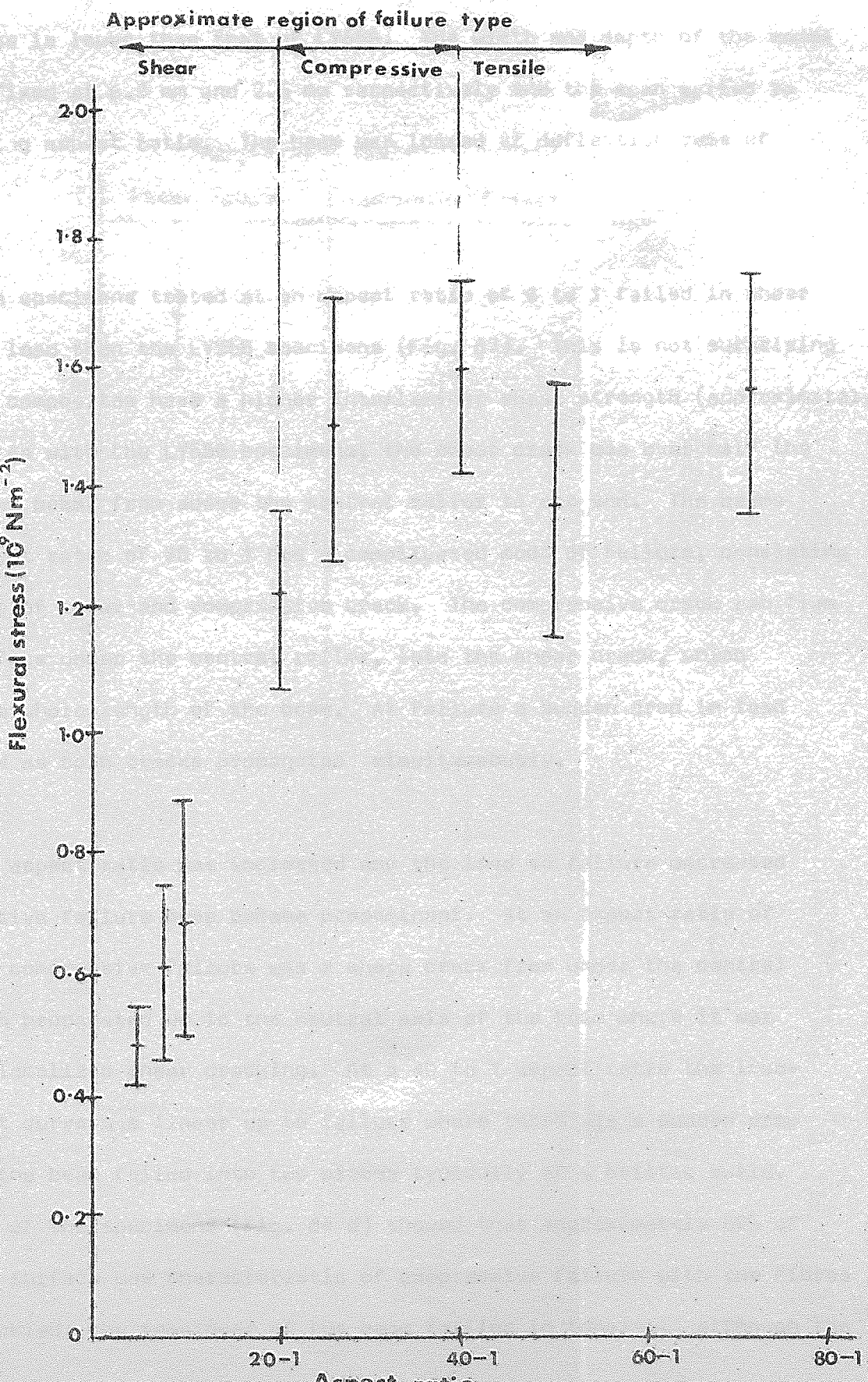

Fig.66.

The aspect ratio is clearly dependent upon the physical properties of the beam so it was necessary to repeat the above work using carbon-fibre HR4C matrix beams having a fibre volume fraction of 0.65. The HR4C cast resin modulus is lower than that of LY558. The width and depth of the beams were again fixed at 6.3 mm and 2.5 mm respectively and the span varied to give a varying aspect ratio. The beam was loaded at deflection rate of 100 mm/min.

All the specimens tested at an aspect ratio of 6 to 1 failed in shear at a higher load than the LY558 specimens (Fig. 67). This is not surprising as the HR4C composites have a higher interlaminar shear strength (approximately 55 MNm^{-2}). As with the LY558 specimens, the shear crack was over half the length of the beam, from above the central roller to one end. The beams with an aspect ratio of 20 to 1 had a complicated mode of failure, consisting of a mixture of shear and compressive crack. The compressive crack ran from the bottom face under the central roller, into the shear crack, which extended the whole length of the beam. At failure a sudden drop in load was observed as both cracks propagated simultaneously.

As the aspect ratio was increased and the load to failure decreased the compressive failure mode became predominant. At an aspect ratio of 30 to 1 the compressive failure was a sharp crack from under the central roller which propagated up to the neutral axis of the beam where it was stopped by localised shear cracking. At a 40 to 1 aspect ratio the load-displacement curve was linear up to failure where there was a sudden drop in load as the beam failed into two pieces typically of a brittle solid. Observation of the specimens (Fig. 64 d) showed that approximately 80% of the failure surface was characteristic of compressive failure with the fibres severely buckled; the remainder of the beam failing in tension. Although the

Aspect ratio v Load at failure(HR4C)

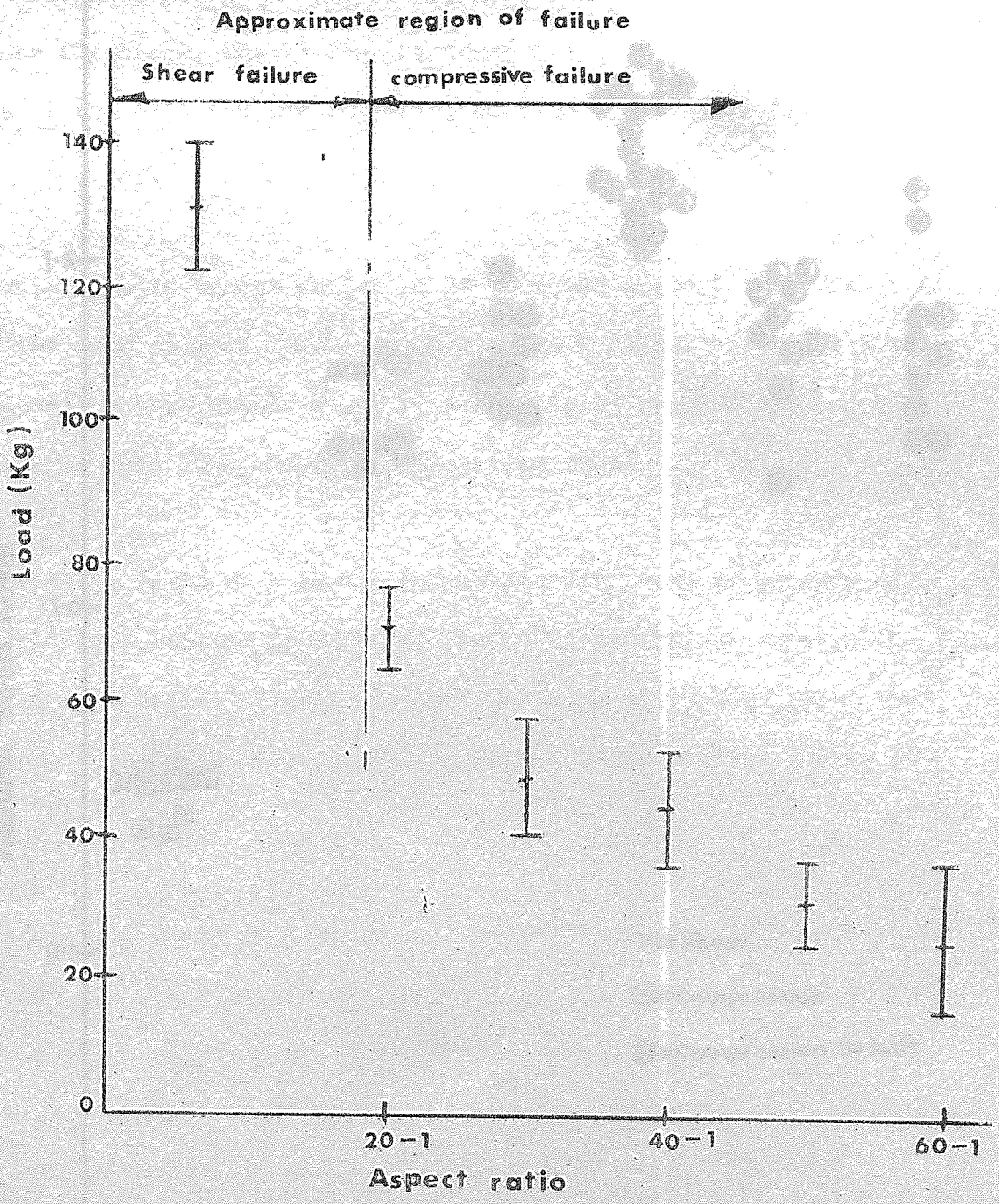

Fig. 67.

Flexural stress at failure(HR4C) v. Aspect ratio.

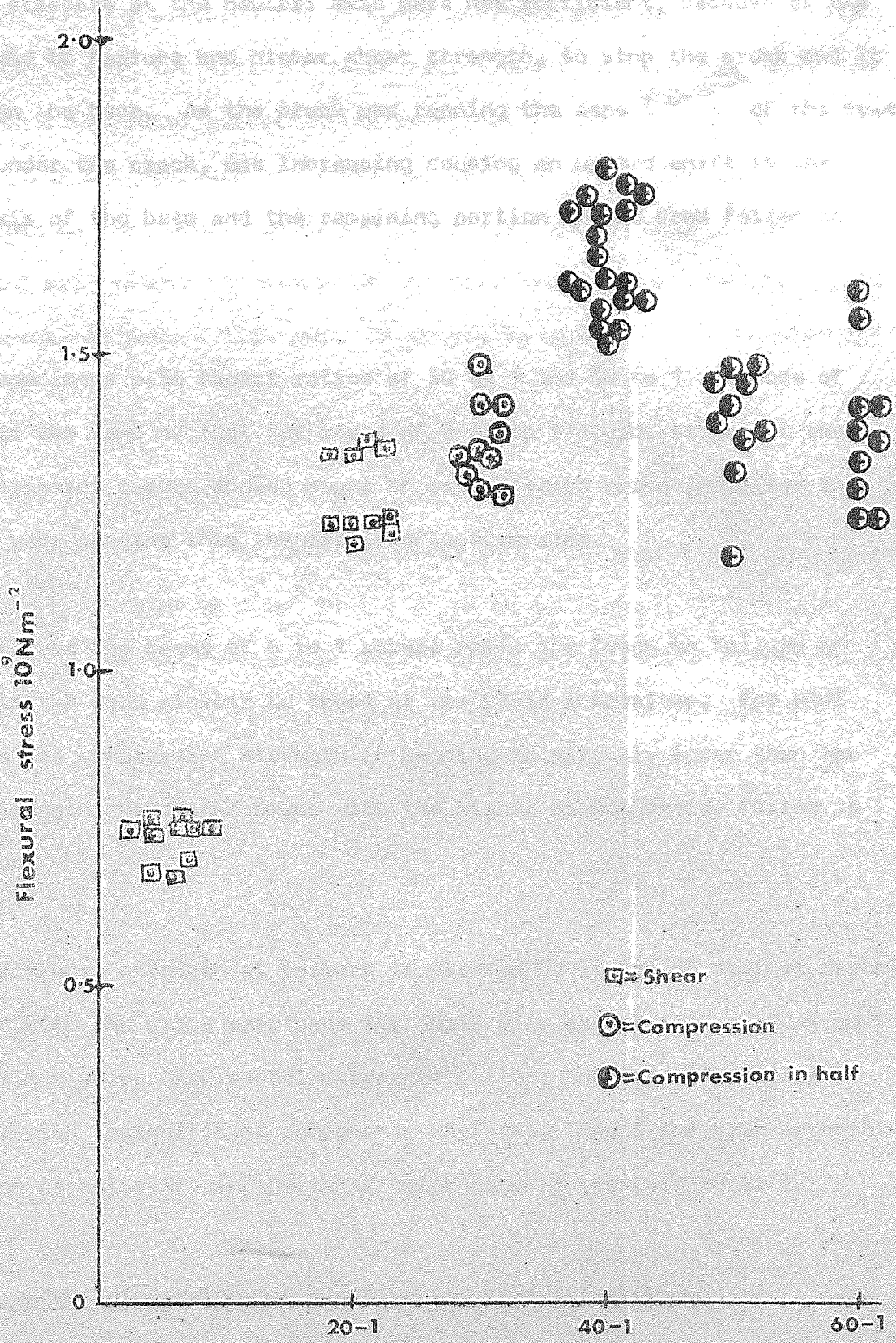

Fig. 68.

crack propagated rapidly and was consequently difficult to observe, the following sequence of failure is suggested. The specimen failed in compression near to the central roller and the crack began to run up through the beam. The shear stresses at the neutral axis were not sufficient, because of the reduced load to failure and higher shear strength, to stop the crack and it ran through the beam. As the crack was running the aspect ratio of the beam, directly under the crack, was increasing causing an upward shift in the neutral axis of the beam and the remaining portion of the beam failed in tension.

For specimens with aspect ratios of 50 to 1 and 60 to 1 the mode of failure was the same as that for beams of a 40 to 1 aspect ratio but the load-displacement curves showed signs of pseudo yield which indicated that the beams were bending into the large deflection zone.

Apart from the beams of 6 to 1 aspect ratio the loads to failure of HR4C composites were similar to those of the LY558 composites. For HR4C composites the compressive strength in bending is slightly lower than the tensile strength, hence the beams with the higher aspect ratios failed in compression.

The flexural strength at failure is plotted in Figure 68 against aspect ratio. As with the LY558 specimens the beams with aspect ratios of 40 to 1 gave a maximum value of flexural stress at failure and the deflections were small with insignificant components of force. Hence for both materials the optimum aspect ratio in the three point bending test was 40 to 1.

5.3.2 The effect of varying the width on the flexural strength

Experimental work carried out within Rolls Royce (70) showed that the short beam interlaminar shear strength is dependent upon the width of the

test specimen. As the width was increased the interlaminar shear strength decreased. Kellog and Sattor (71) have developed a solution for an orthotropic beam which shows a significant effect of high width to depth on the magnitude and distribution of shear stresses in a short beam. This theory predicts that for width to depth ratios above approximately 2.5, for unidirectional composite materials the interlaminar shear stress is highest at the edges of the specimen and lowest at the middle with the mean value being similar to that predicted by simple theory (eqn. 2.18). Whitney (72) has analysed beam theory for highly anisotropic materials and has shown that it is necessary to have a high ratio of length to width for the simple beam theory to be valid.

A series of experiments were conducted to determine the effect of varying the span to width ratio. The span and depth were kept constant at 100 mm and 2.5 respectively. Span to width ratios of 40 to 1, 16 to 1, 8 to 1 and 4 to 1 were cut from unidirectional carbon fibre - HR4C matrix plates having a fibre volume fraction of 0.65, and tested in three point bending at a deflection rate of 100 mm/min. The loading nose and supports were 6 mm cylinders.

The 40 to 1 span-width ratio beams failed brittlely in half from under the central roller and the fracture surface showed a predominantly compressive failure with a small amount of tensile failure on the top face. The mode of failure remained the same for the 16 to 1; however with some of the 8 to 1 span-width ratio the compressive crack was stopped at the neutral axis. With the 4 to 1 specimens the sharp compressive crack was stopped every time at the neutral axis by localised shear cracking. The flexural stress at failure is plotted in Figure 69 against the span to width ratio. The flexural stress at failure increased with increasing width up to a maximum for specimens with

Specimen width v. Flexural stress at failure.

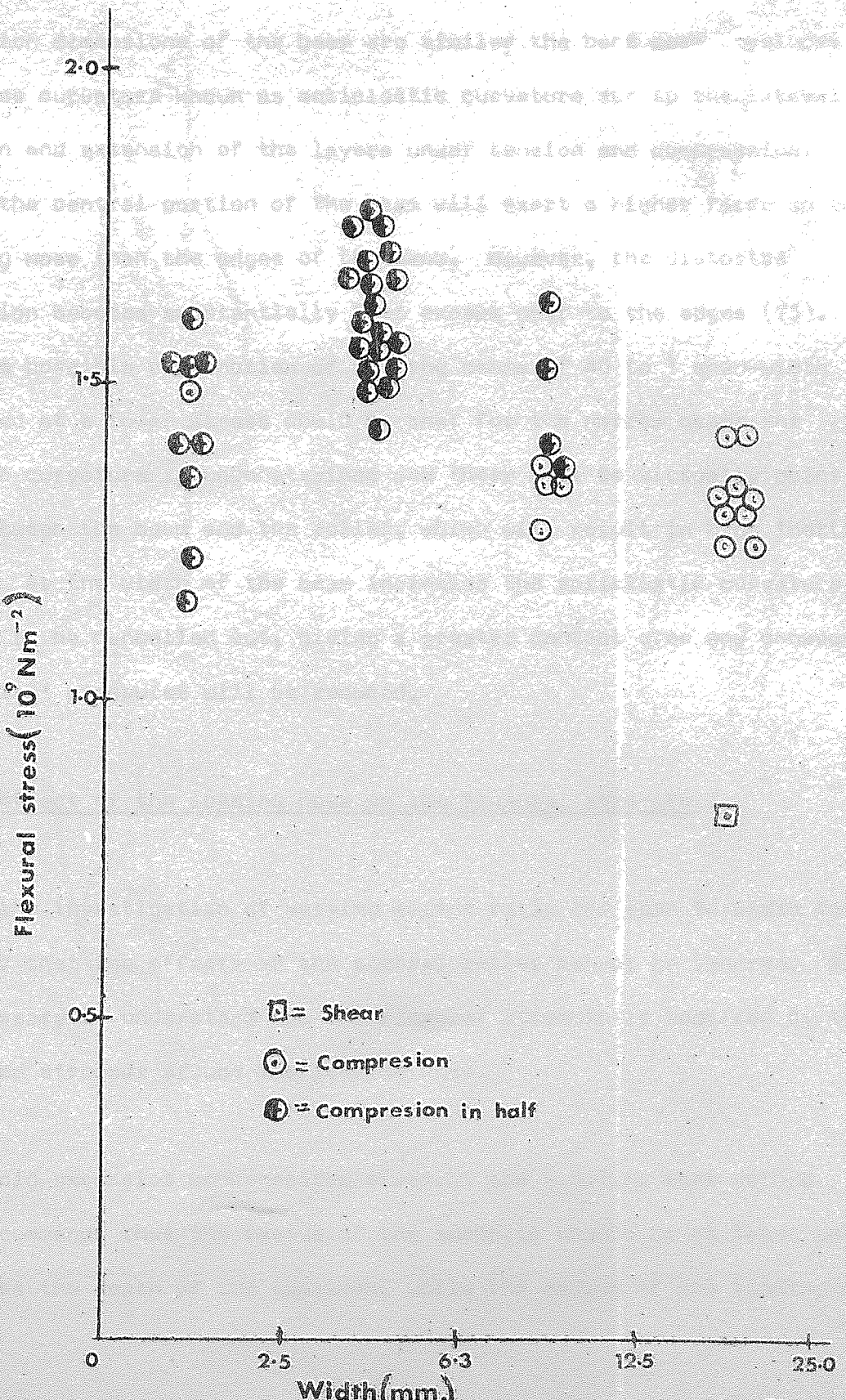

Fig. 69.

a 16 to 1 span-width ratio then began to decrease as the width was increased further.

The mode of failure is further evidence that the concentrated load under the central roller is affecting the mode of failure. When the cross-section dimensions of the beam are similar the bent beam developes a transverse curvature known as anticlastic curvature due to the lateral contraction and extension of the layers under tension and compression. Therefore the central portion of the beam will exert a higher force on to the loading nose than the edges of the beam. However, the distorted cross-section becomes substantially flat except near to the edges (73). Therefore a possible explanation of why the beams of 40 to 1 span-width ratio failed at a lower stress could be that for the narrow beams the anticlastic curvature is unconstrained and there will be virtually point contact between the beam and the roller, which will result in high 'Hertzian' pressures. As the width of the beam increases the anticlastic curvature will begin to be cancelled out, giving a greater contact area and consequently the 'Hertzian' pressures will be reduced.

5.3.3 The effect of the loading nose on the flexural strength

From the investigation of varying aspect ratio and span to width ratio, it is clear that the effects of the central roller cannot be ignored. Hence it is necessary to understand how the flexural strength is modified by the concentrated stresses around the loading nose.

To avoid excessive concentrated stresses the A.S.T.M. test method D790-66 recommends that the radius of the supports should be at least one and a half times the depth of the specimen, while the radius of the loading nose

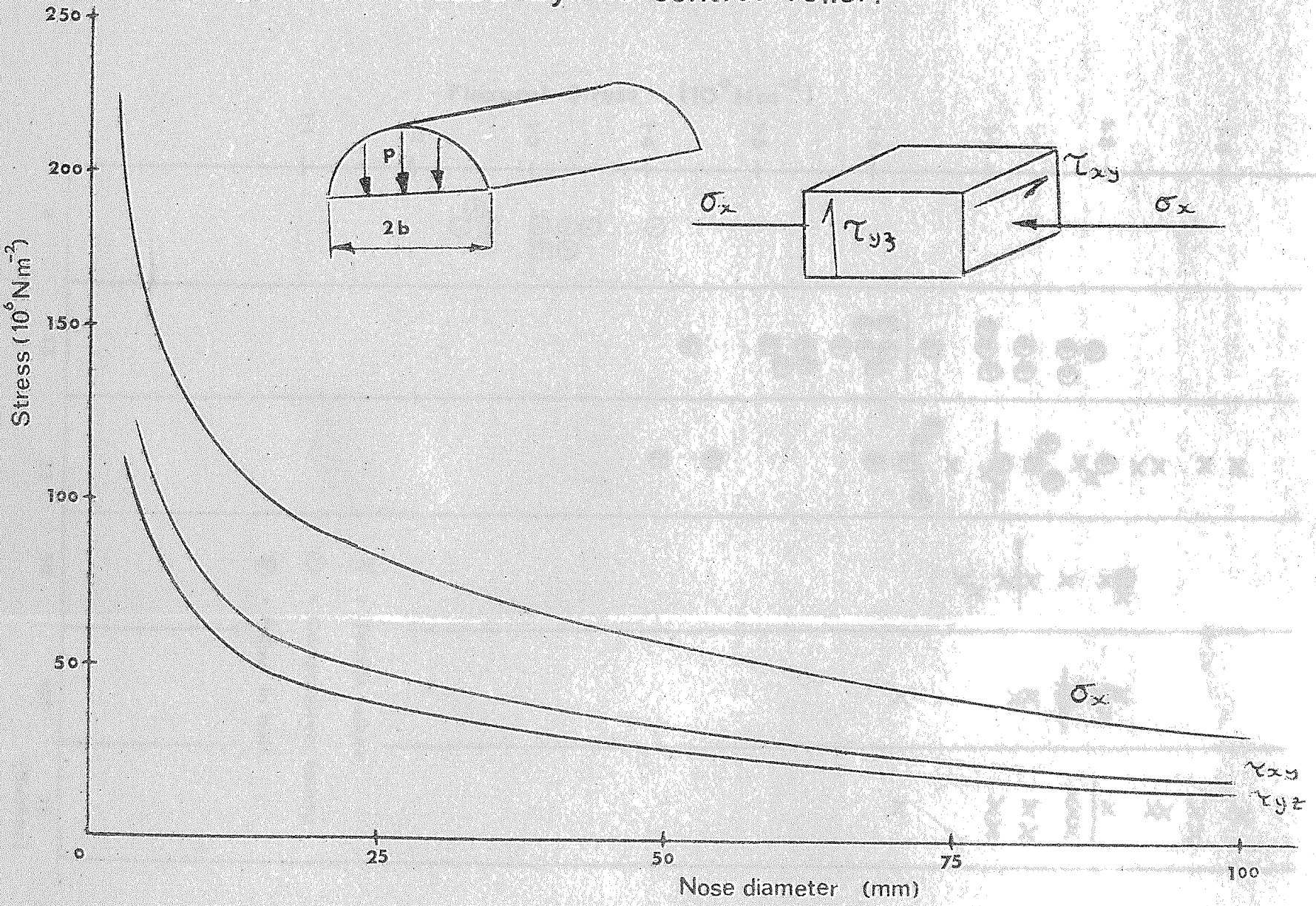
Stresses caused by the central roller.
250
200
150
100
50
0
Stress ($10^6 Nm^{-2}$)
P
2b
σ_x
τ_{xy}
τ_{yz}
σ_x
σ_x
τ_{xy}
τ_{yz}
25
50
75
100
Nose diameter (mm)

Fig.70.

Nose diameter v. Flexural stress at failure.

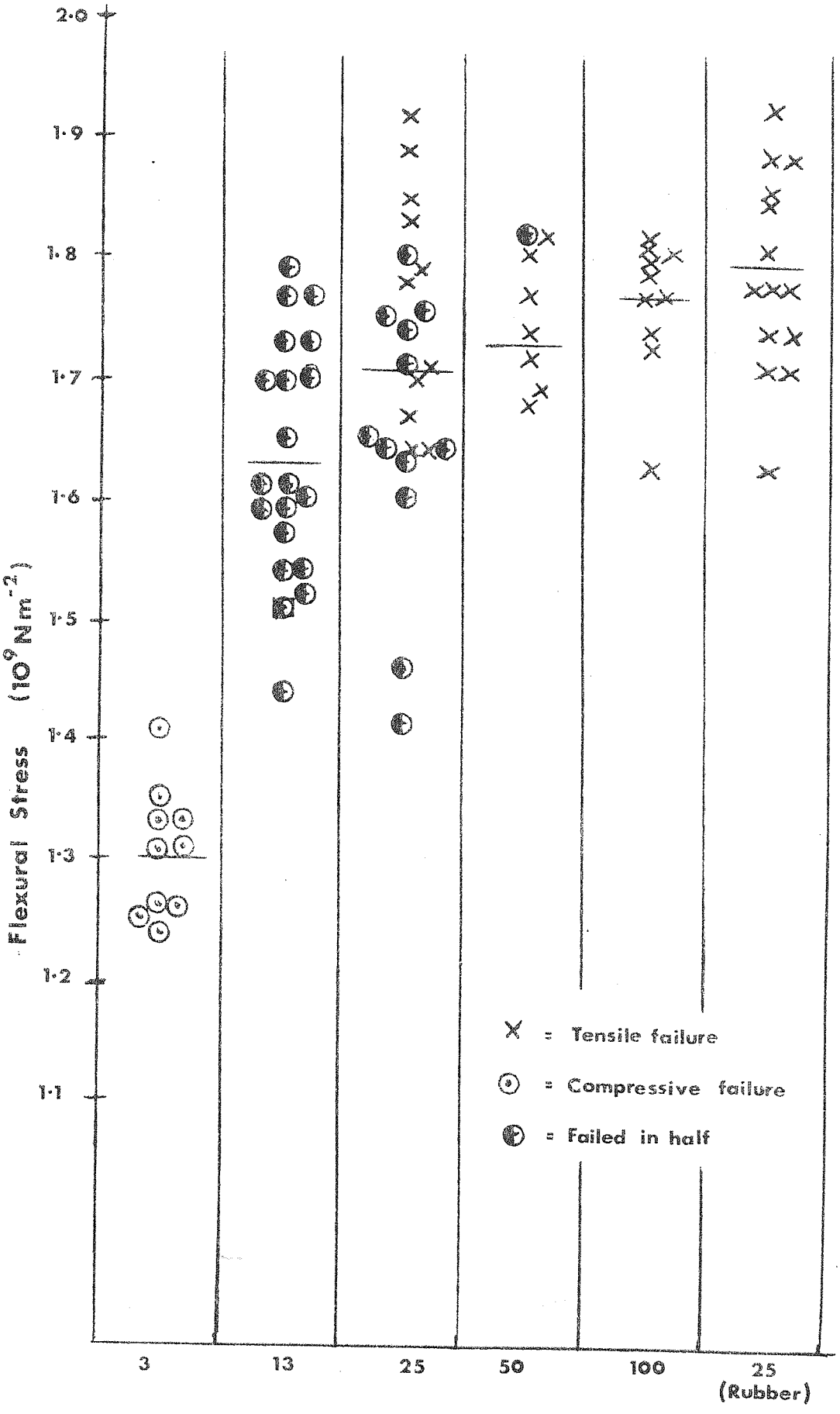

Fig. 71.

should be up to 4 times the specimen depth. Duckworth (74) eliminated the effect of localised stresses on the flexural strength of ceramics by using a dumb-bell shaped specimen in four-point bending. However, with this shape of specimen, although it may give a realistic value of the flexural strength of ceramics, it is probable that there would be significant shear failure around the dumb-bell shape when testing C.F.R.P. because of its low shear strength. Recent work at RAPRA (75) has shown that the flexural strength of 'Perspex' may be increased by as much as 10 per cent if rubber pads are placed between the loading nose and the beam.

The stresses caused by the pressure between elastic bodies are of importance in connection with the design of bearings, gears, etc. Hertz (76) developed the mathematical theory for the surface stress and the deformations produced by pressure between curved bodies. For an isotropic body the half width (b) of a rectangular contact area for a cylinder in a circularly bent beam is:-

$$b = \left(\frac{4 \omega R_1 R_2}{\pi (R_2 - R_1)} \left[\left(\frac{1 - \nu_1^2}{E_1} \right) + \left(\frac{1 - \nu_2^2}{E_2} \right) \right] \right)^{1/2} \qquad - 5.3$$

where ω = load per unit length of the surface of contact

R_1 = radius of loading nose roller

R_2 = radius of curvature of the beam

ν = Poisson's ratio

E = Young's modulus

and that the maximum pressure exerted by the contact q_o is

$$q_o = \frac{2P}{\pi b} \qquad - 5.4$$

where P = load per unit length of the surface of contact.

Knowing b and q_o the stress at any point can be calculated.

No exact solution exists at the present for the pressure distribution caused by anisotropic bodies under direct contact. However an approximate solution, which is sufficient to indicate the magnitude of the stress may be obtained if the transverse values of Young's modulus and Poisson's ratio are used in equation 5.3. The maximum stress components are plotted in Figure 70. The maximum shear stress in the y-z direction (τ_{yz}) is at a depth of 0.7 b and its magnitude is 0.3 q_o but the maximum shear stress in the x-y direction (τ_{xy}) is at the surface and has a value of 0.25 q_o. The roller also imparts a compressive stress in the direction of the fibres (σ_x) which will add to the bending compressive stress and a compressive stress normal to the direction of the fibres.

Specimens (l = 100 mm, b = 6 mm, d = 2.5 mm) were loaded in three point bending at a deflection rate of 100 mm/min with varying sizes of loading nose. All the specimens tested with a 3 mm nose radius failed in the compressive region of the beam. This compressive failure was a sharp crack under the central roller which propagated up to the neutral axis of the beam, where it was stopped by localised shear cracking. As the nose diameter increased, the compressive failure changed. With the 12 mm diameter loading nose the specimens failed in a brittle fashion in half from the compressive face. Tensile failures were not observed until the loading nose diameter was increased to 25 mm, but even then some of the specimens failed brittlely in half from the compressive face. As the nose diameter increased, the mode of failure become predominantly tensile and at a diameter of 100 mm all the specimens failed in tension. The flexural stress at failure is plotted in Figure 71.

Equation 5.3 shows that band width may also be increased by reducing the Young's modulus of the loading nose. The 25 mm steel roller gave a mixture of tensile and compressive failures, by using a hard rubber roller of the same

diameter equation 5.3 predicts that the Hertzian pressures will be halved. When the beams were tested with a rubber nose they all failed in tension.

Simply adding the compressive strength in the fibre direction does not fully explain the low flexural stresses at failure, for the beams tested with small nose rollers. For example, the beams tested with a 3 mm diameter roller failed at a stress of 1.31 GNm^{-2} which means, by adding the Hertzian stress (σx), the fibres were subjected to a compressive stress of 1.40 GNm^{-2}, which is still much lower than the stress at failure for the 25 mm roller (1.71 GNm^{-2}).

An extremely complicated stress condition exists under the central roller. However, the presence of shear cracks, which stopped the compression crack, in the specimens tested with a 3 mm loading nose, implies that the specimens are indeed being subjected to high shear stresses. Work by Hand (23) has suggested that the interlaminar shear strength may be directly proportional to the compressive stress. Then if this is so as the roller diameter increases the Hertzian shear stress is reduced, which will increase the compressive strength of the beam, in addition to the Hertzian compression stress being reduced, and the mode of failure changes from compressive to tensile. The stresses at failure for all the specimens which failed in tension were similar, therefore it would appear that if a beam fails in tension then the loading nose has little effect on the strength.

The above investigations suggest that the optimum configuration for a three point bend test of C.F.R.P. is:-

length	=	100 mm
breadth	=	6 mm
depth	=	2.5 mm
loading nose	=	Rubber cylinder with a 25 mm diameter.

Chapter 6

Test Results

6.1 Fibre volume fraction

Composites with fibre volume fractions varying from 0.2 to 0.7 were manufactured from LY-558-BF_3 400 prepreg. The error in fibre volume fraction was estimated to be within $\pm$ 2½%.

6.1.1 Tensile strength

Composite plates were machined to the optimum specimen shape (see section 5.1.2) and tested in an Instron testing machine at a strain rate of 1 mm per minute.

In figure 72 the tensile strength is plotted against increasing fibre volume fraction, together with a plot of the theoretical strength, computed from the single fibre properties and the law of mixtures. The law of mixtures is but a crude method for predicting the tensile strength, and it is only included here as an indication of the relationship between the experimental tensile strength and the volume fraction.

The specimens having a fibre volume fraction of 0.2 failed in a brittle manner within the gauge length (Fig. 73). As the volume fraction of fibres increased, the failure region became more fibrous. The specimens with fibre volume fractions of 0.7 failed in an extremely fibrous way and the failure region extended over almost the whole length of the ungripped portion. Electron micrographs (Fig. 74) of the failed regions showed that as the fibre volume

Tensile-compressive strength for LY558.

v.

Fibre volume fraction.

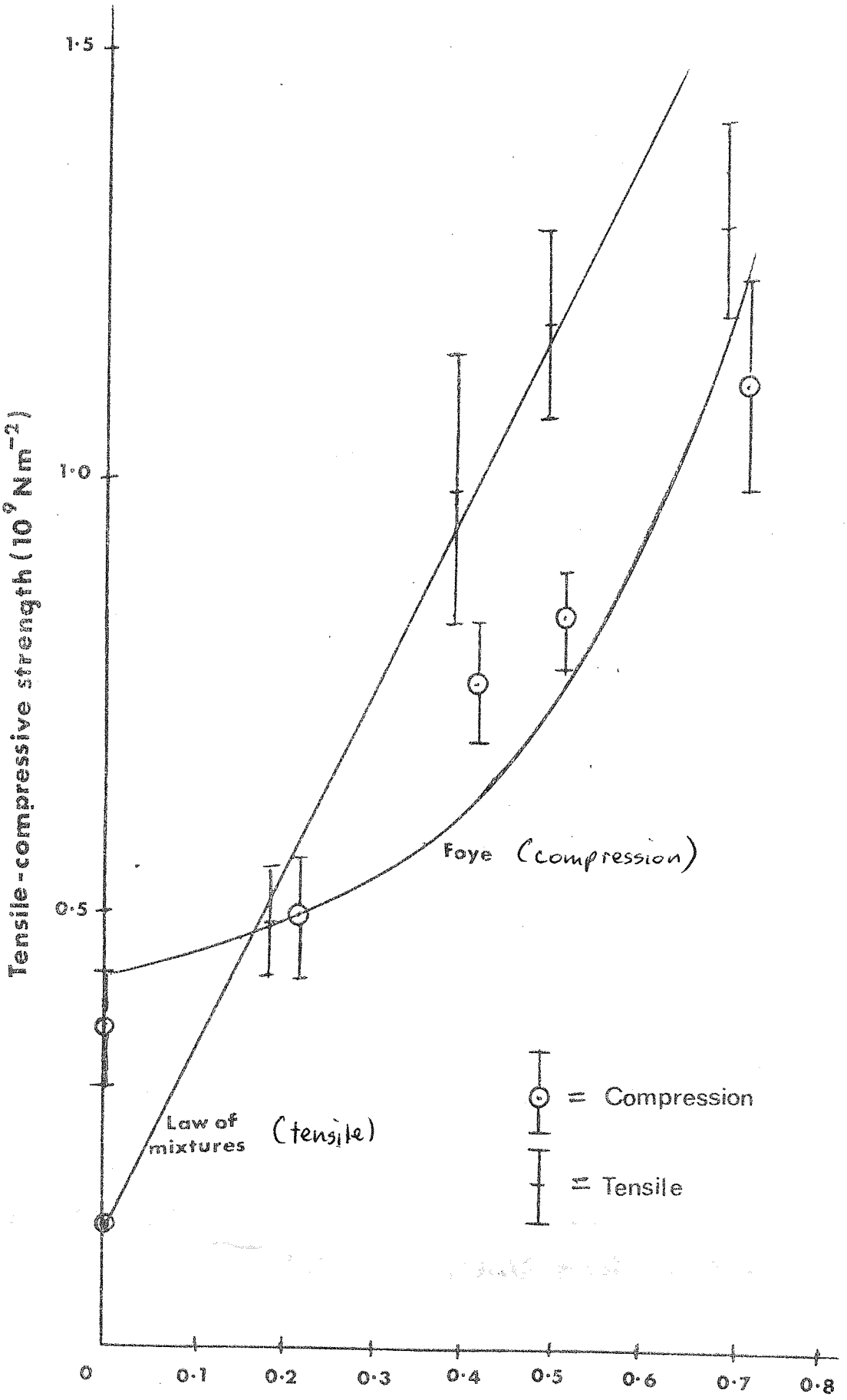

Fig.72.

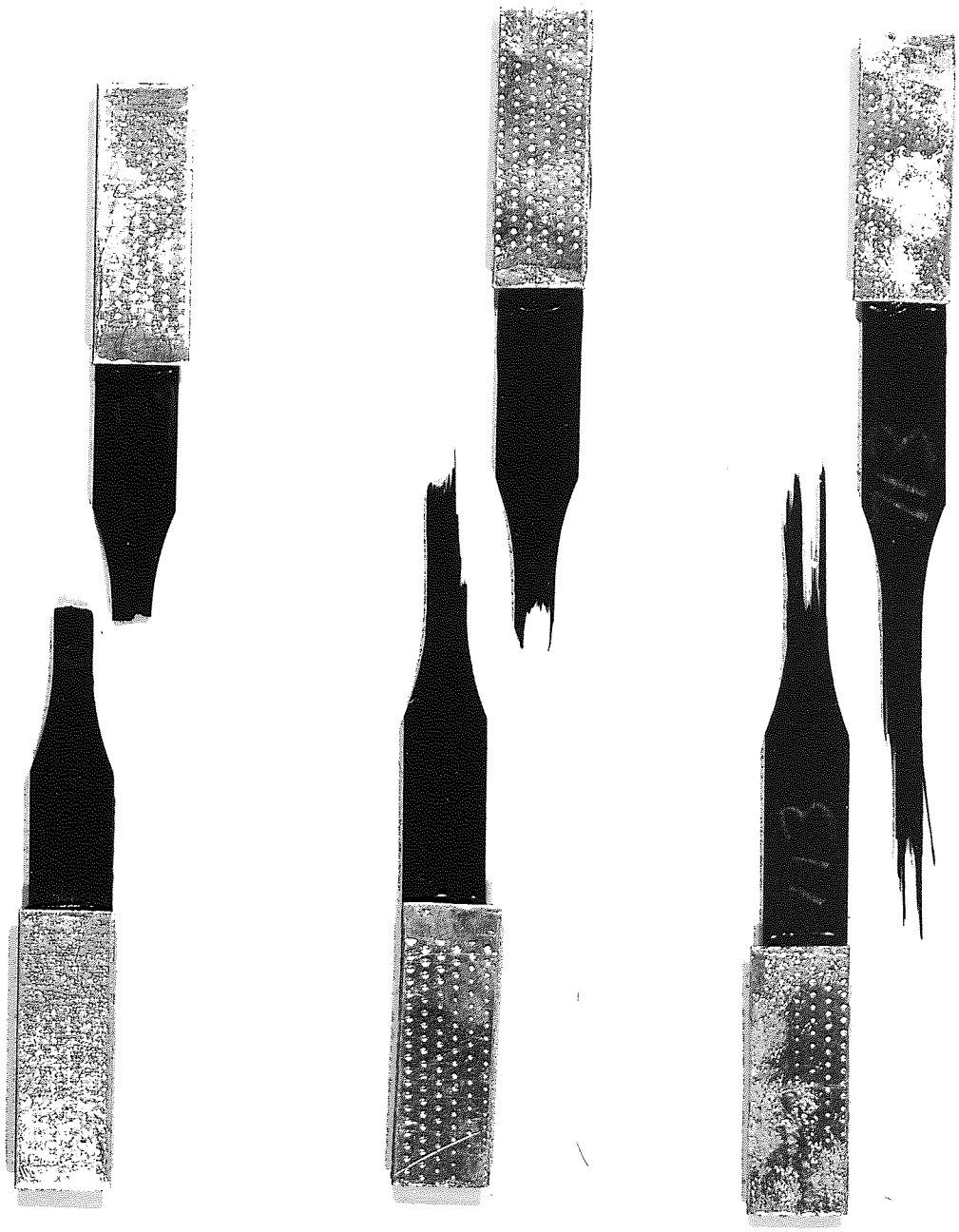

Fig. 73. TENSILE FAILURE OF SPECIMENS WITH DIFFERENT FIBRE VOLUME FRACTIONS.

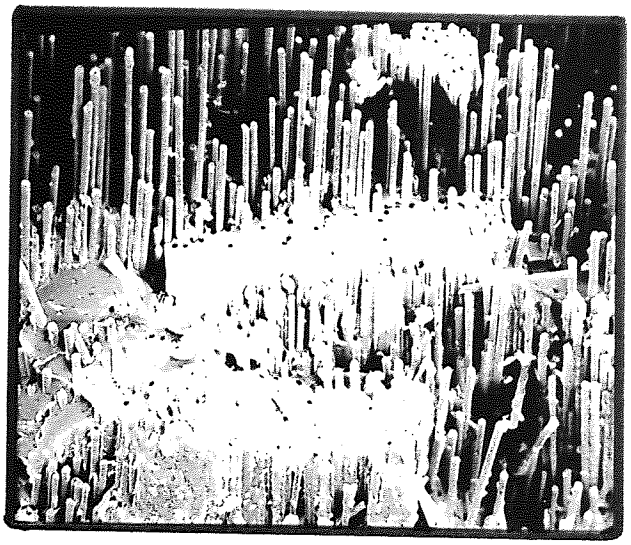

V_f = 0·2

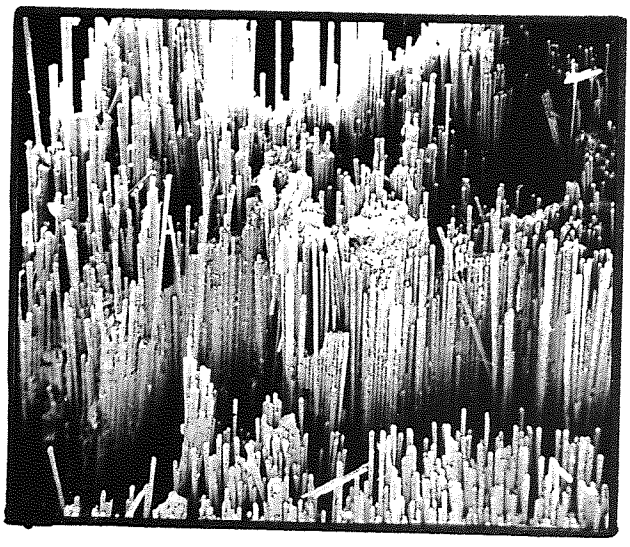

V_f = 0·7

Fig.74. TENSILE FRACTURE FACES FOR DIFFERENT FIBRE VOLUME FRACTIONS (V_f).

fraction increased there was a higher probability of fibre-fibre contact. The fibre fracture faces were very similar to the fracture faces of sapphire single crystals (77). The most notable feature of both fracture surfaces was the appearance of straight cleavage lines, radiating from a source which pin-pointed the location of the stress raising flaw responsible for fracture. High magnification electron micrographs showed that where there were a group of fibres in contact with each other, then the fracture of those fibres originated from the points of contact. (Fig. 75). This implies that fibre-fibre contact acts as a stress raiser.

For the specimens with a low fibre volume fraction the tensile strength was very close to that predicted by the law of mixtures. At 0.7 fibre volume fraction, the strength was significantly lower than the law of mixtures values. There are two possible reasons for this loss of efficiency in reinforcement at the higher fibre volume fractions.

1. At the higher volume fractions there is an increased probability of the higher incidence of fibre-fibre contact, causing stress concentrations within the fibres.
2. Fibre-fibre contact will also reduce the fibre matrix bond causing the fibres to have a longer ineffective length. Assuming that Rosens equation (4) defines the tensile strength, then as the ineffective length increases the tensile strength will decrease.

6.1.2 Compressive strength

From the same mouldings that the tensile test specimens were taken, compressive test specimens were machined. The specimens were waisted down in both the thickness and width, as described in Chapter 5 and tested in the

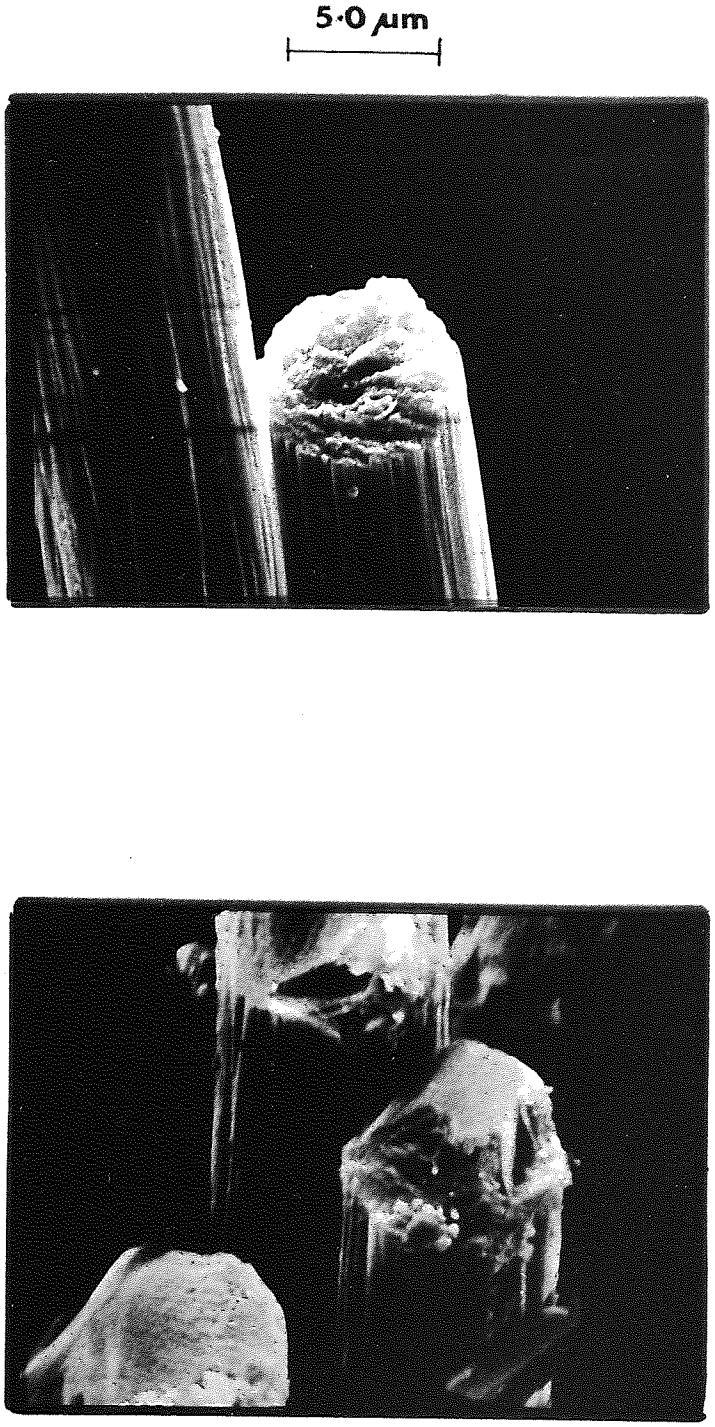

Fig.75. FIBRE - FIBRE CONTACT .

compressive fixture (Fig. 58) using an Instron testing machine at a strain rate of 1 mm/min. The compressive strength of the cast resin was obtained by compressing rectangular prisms (10 mm x 10 mm x 20 m) similar to the ASTM test method D695-61T. Graphite paste was applied to the loading faces of the prism, in an attempt to prevent friction. The stress-strain curve was linear up to a strain of approximately 3% where the specimen began to "barrel" and the stress-strain curve flatten out. The strain at failure was approximately 25% with a mean breaking strength of 0.25 GNm^{-2}.

The cast resin strength is plotted in Figure 72, together with composite compressive breaking strength as a function of fibre volume fraction and a theoretical plot. The 'theoretical' plot was derived using Foye's analysis with a correction factor of 0.25. No theoretical explanation is offered for this correction factor, and it is only included to 'high light' any trend in the experimental results.

For the specimens with fibre volume fractions of 0.2, 0.4 and 0.5 the load-time curve was linear up to failure, where there was a sudden drop in load as the specimen failed within the gauge length. The specimens failed by the fibres all buckling together in the same direction and plane. At the edges of the buckle the fibres were fractured (Fig. 76). For specimens with a fibre volume fraction of 0.7 the load-time curve was linear up to approximately 80% of the maximum applied load, where shear cracks began to propagate from the waisted region. At failure there was a sudden drop in load. Some of the specimens failed away from the gauge length, within the body of the specimen. (Fig. 77). A possible sequence of failure could be that as the shear cracks ran back from the waisted cross-section they produced a highly stressed region, extending the length of the shear crack, with the final failure probably occurring at a flaw within the modified gauge length.

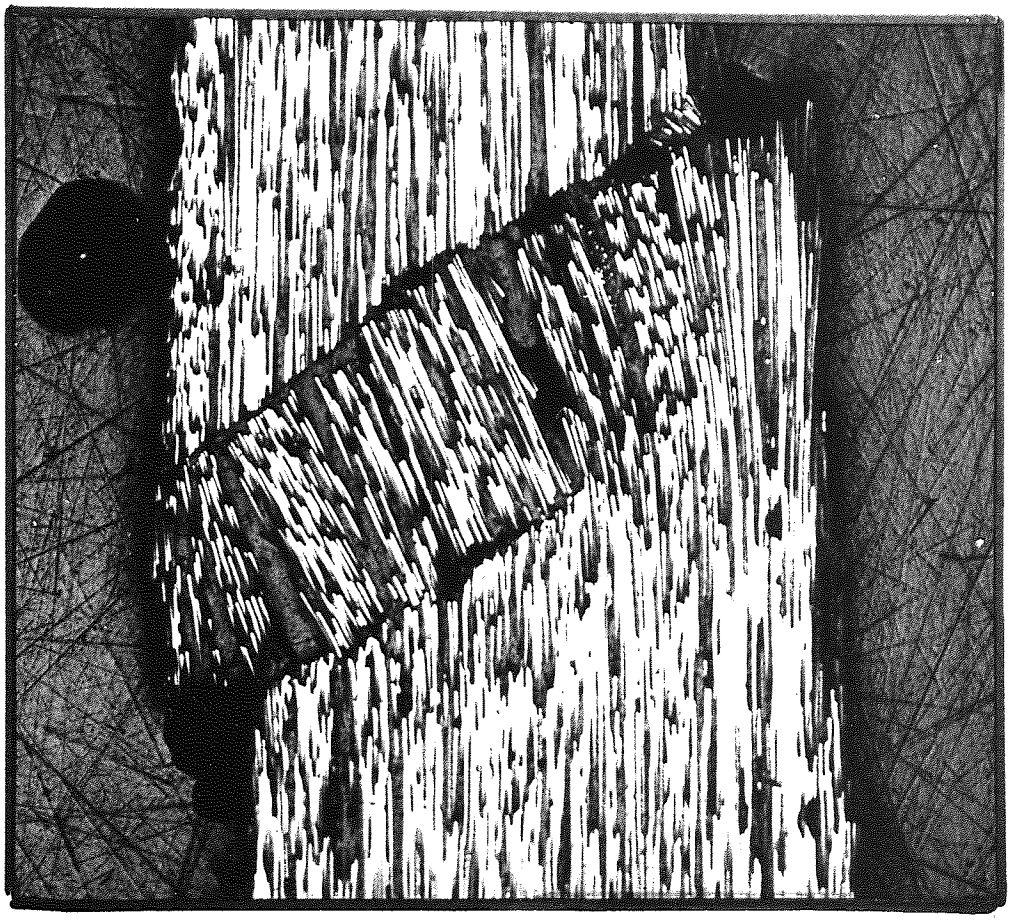

0·5 mm

Fig.76. COMPRESSION FAILURE.

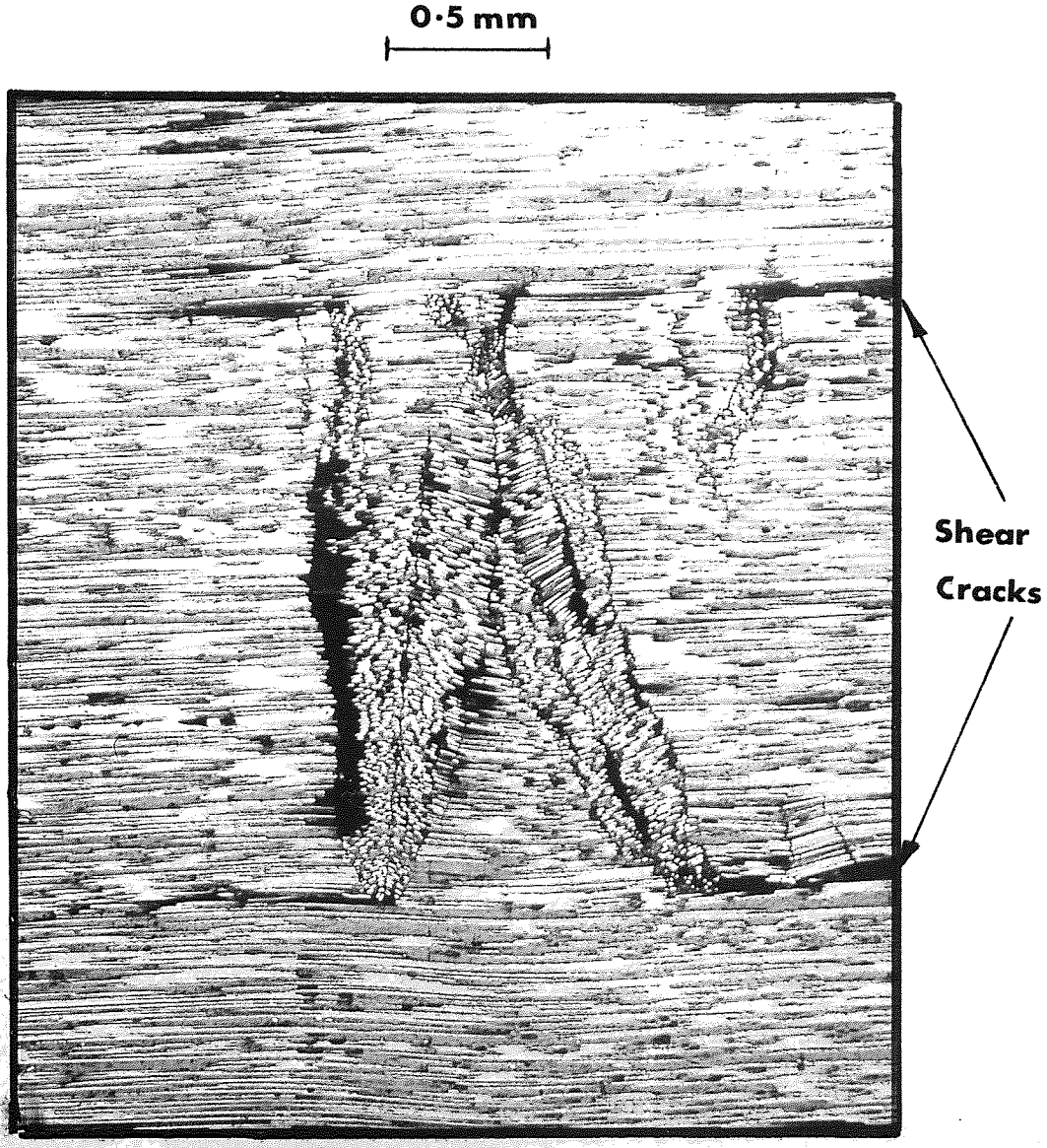

Fig. 77. COMPRESSION - SHEAR FAILURE .

The failure was surrounded by unstressed areas of composite which reacted against the buckled region, producing a hydrostatic stress, causing the specimens to fail at a stress higher than the breaking stress of the specimens of the same volume fraction that failed in the gauge length.

The compressive strength of the composites with low fibre volume fractions follow the modified theoretical plot closely, then for volume fractions above 0.5 the strength begins to fall away. Assuming the validity of the theoretical plot here is a further indication that the fibres are less efficient at reinforcing the composite at the higher volume fractions. Again there are two possible reasons for this loss in efficiency.

1. At the higher fibre packing densities, the increased fibre-fibre contact reduces the fibre's ability to withstand buckling.
2. The shear cracks propagating back from the waisted cross-section increase the gauge length. The fact that the specimens failed in a random way along the modified gauge length would imply a size effect for the compressive strength of composite materials. Hence the specimens with a fibre volume fraction of 0.7, because they were tested over a greater volume of material, failed at a stress lower than predicted by the modified analysis of Foye, although this would be offset by the supporting role of the unstressed fibres when failure occurred in the body of the specimen.

The fracture faces of the fibres are very distinctive (Fig. 78) and are very similar to the fracture face of a fibre which has failed in bending as in the Elastica test (50). The fracture face consists of two distinct areas (Fig. 79). The bottom half of the fibre shows tensile failure with the cleavage lines radiating from the highly stressed outer edge. The top half of

10 µm

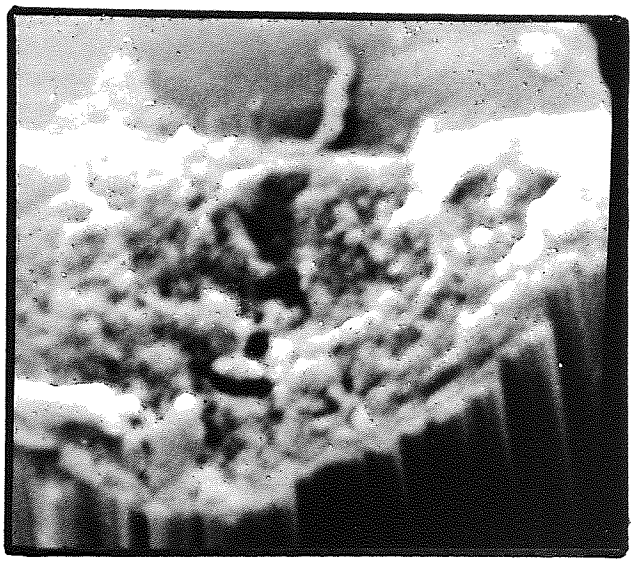

1·0 µm

Fig. 78. FRACTURE FACE OF COMPRESSIVE SPECIMEN.

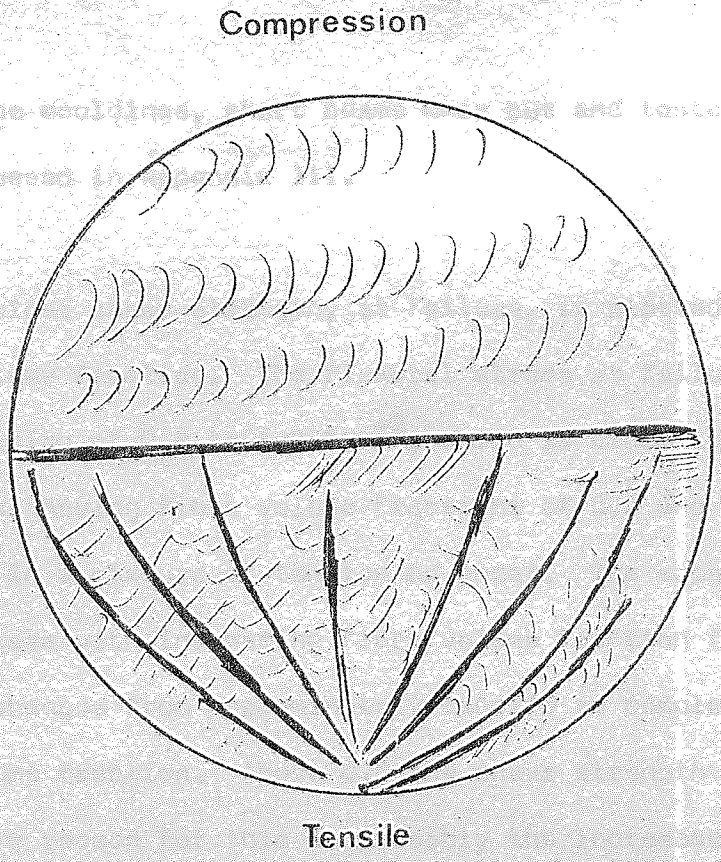

Fig. 79. Sketch of compressive fracture face.

the fibre failed in compression with deep grooves in the fibre, running at right angles to the axis of the buckle. The axis of fracture of the fibres were in the same direction confirming that the fibres, at failure, all buckled together in the same direction.

6.1.3 Interlaminar shear strength

From the same mouldings, short beams were cut and tested in three point bending, as discussed in Appendix III.

The interlaminar shear strength, at failure, is plotted in Figure 80 against fibre volume fraction. The flexural stress at failure for the beams was within the region of 0.8 to 1.2 GNm^{-2}, which is close to the failure stress of the composites, having fibre volume fractions of 0.2 and 0.4. Hence these specimens failed in a mixture of tension and shear. The apparent shear stress at failure increases with increasing fibre volume fraction from 0.2, as the mode of failure changes from predominately tensile to completely shear failure at 0.5 fibre volume fraction. Above 0.5 the shear strength begins to fall away. As above, a reason for this is probably the increased fibre-fibre contact reducing the effectiveness of the bond. Also, as the resin content reduces, any voidage within the resin will become more significant, which will cause a reduction in the interlaminar shear strength (23).

The load-time curve was linear up to failure, where the load suddenly dropped to approximately 80% of the maximum load. At failure the crack propagated instantaneously and it was impossible to follow it. The crack extended from one edge of the specimen to just under the central roller.

To determine the influence of the machined edge on the mode of failure, specimens which had 50 mm overhang each side of the outside roller, were tested

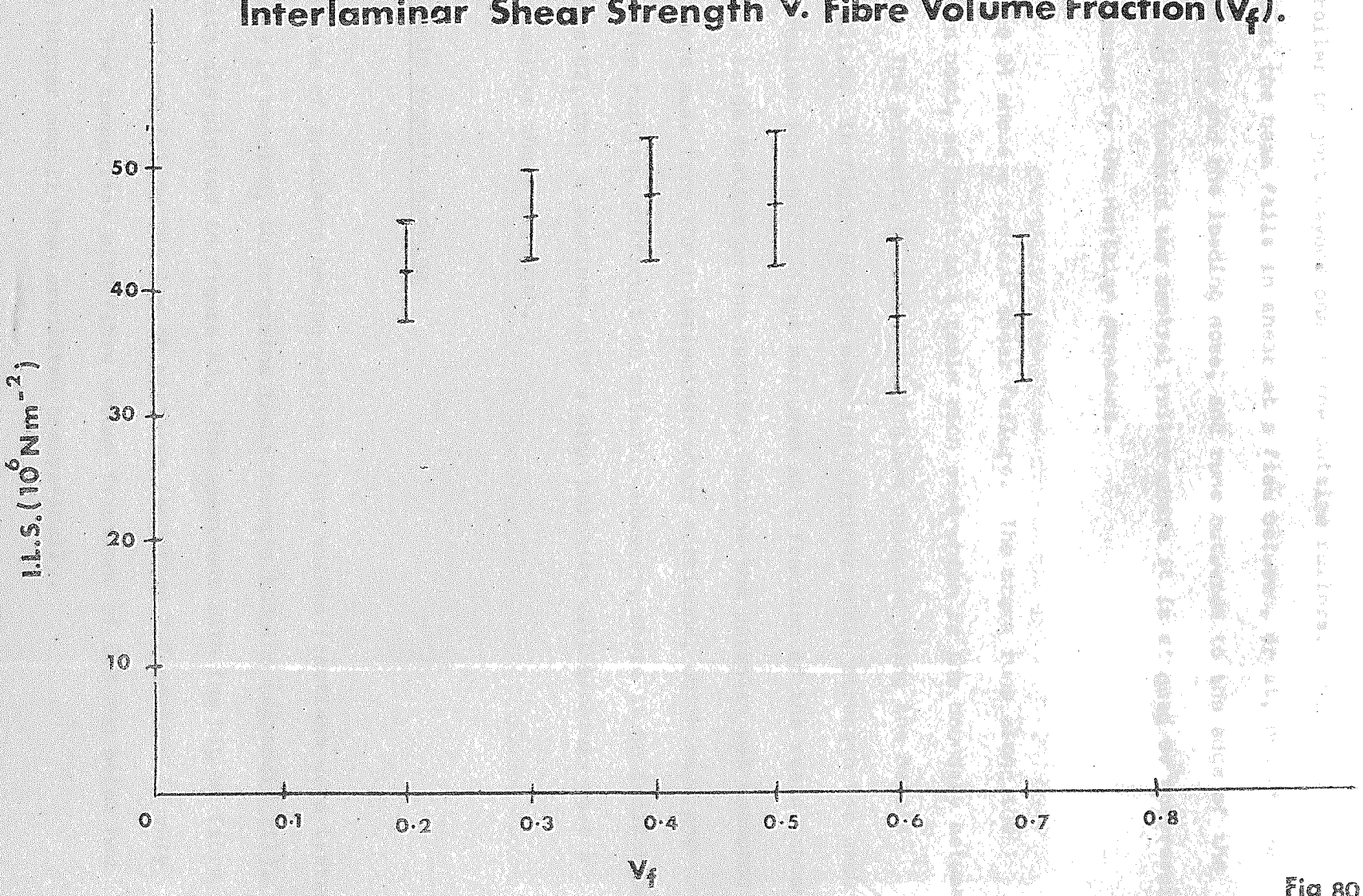
Interlaminar Shear Strength v. Fibre Volume Fraction (V_f).
I.L.S. ($10^6 Nm^{-2}$)
50
40
30
20
10
0
0·1
0·2
0·3
0·4
0·5
0·6
0·7
0·8
V_f

Fig 80.

in three-point bending as above. The shear stress at failure was similar to that of the shorter standard beams and the failure crack ran from under the central roller to just beyond one of the outside rollers. This would suggest that the beam fails in shear at a flaw between, or at, one of the outside rollers and the loading nose, and runs outwards to the edge of the specimen, and in towards the central roller where it is stopped by compressive stresses caused by the Hertzian pressure.

Figure 81 shows a typical shear failure. The crack runs along the fibre resin bond, adjacent to a resin rich area which is the boundary between laminates. The porosity of each moulding was measured using the Metals Research O.I.M. In figure 82 the mean interlaminar shear strength for each moulding against the void content measured as a fraction of the resin content. There was a large scatter on the results, because the porosity was measured some distance away from the interlaminar shear specimens, which made any trends in the results, difficult to detect. However, there is an indication, from figure 82, that a specimen with a high porosity will probably have a low interlaminar shear strength.

6.1.4 Dynamic Young's Modulus

A series of specimens having varying fibre volume fractions were tested dynamically in bending, to determine their Young's modulus (Appendix III). The results are plotted in figure 83. The specimens with the higher fibre volume fractions follow the law of mixtures (equation 2.2 section 2) very closely. The composites with fibre volume fractions of 0.5 and below had slightly higher moduli than predicted theoretically.

Micrographs (Fig. 84) of the composites with low fibre volume fractions show that the fibres tend to be together in discrete bands, the fibre packing

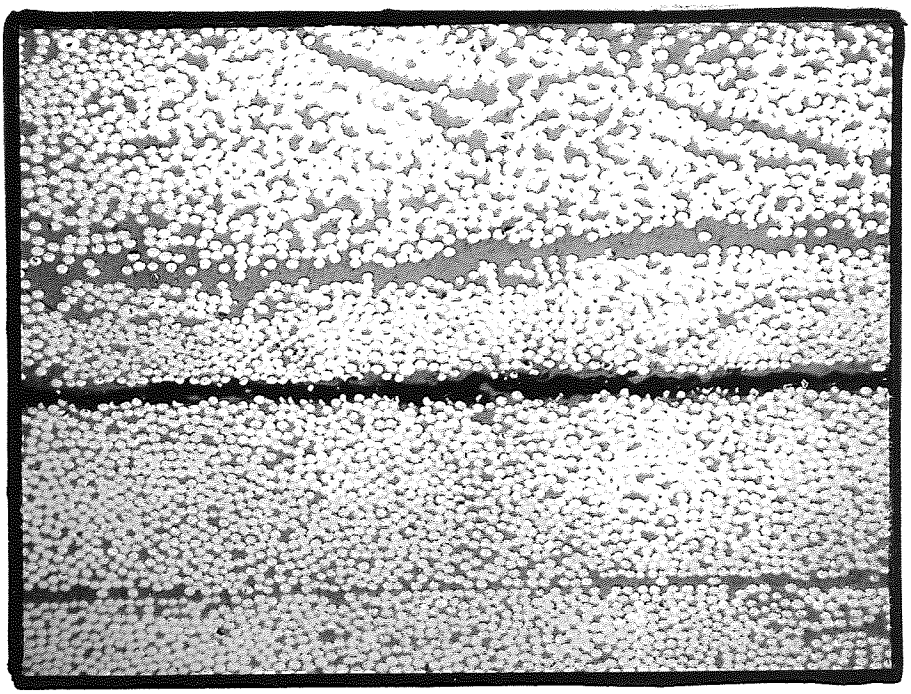

Fig.81. INTERLAMINAR SHEAR FAILURE.

Inter laminar shear strength v. Void content as a fraction of resin volume.

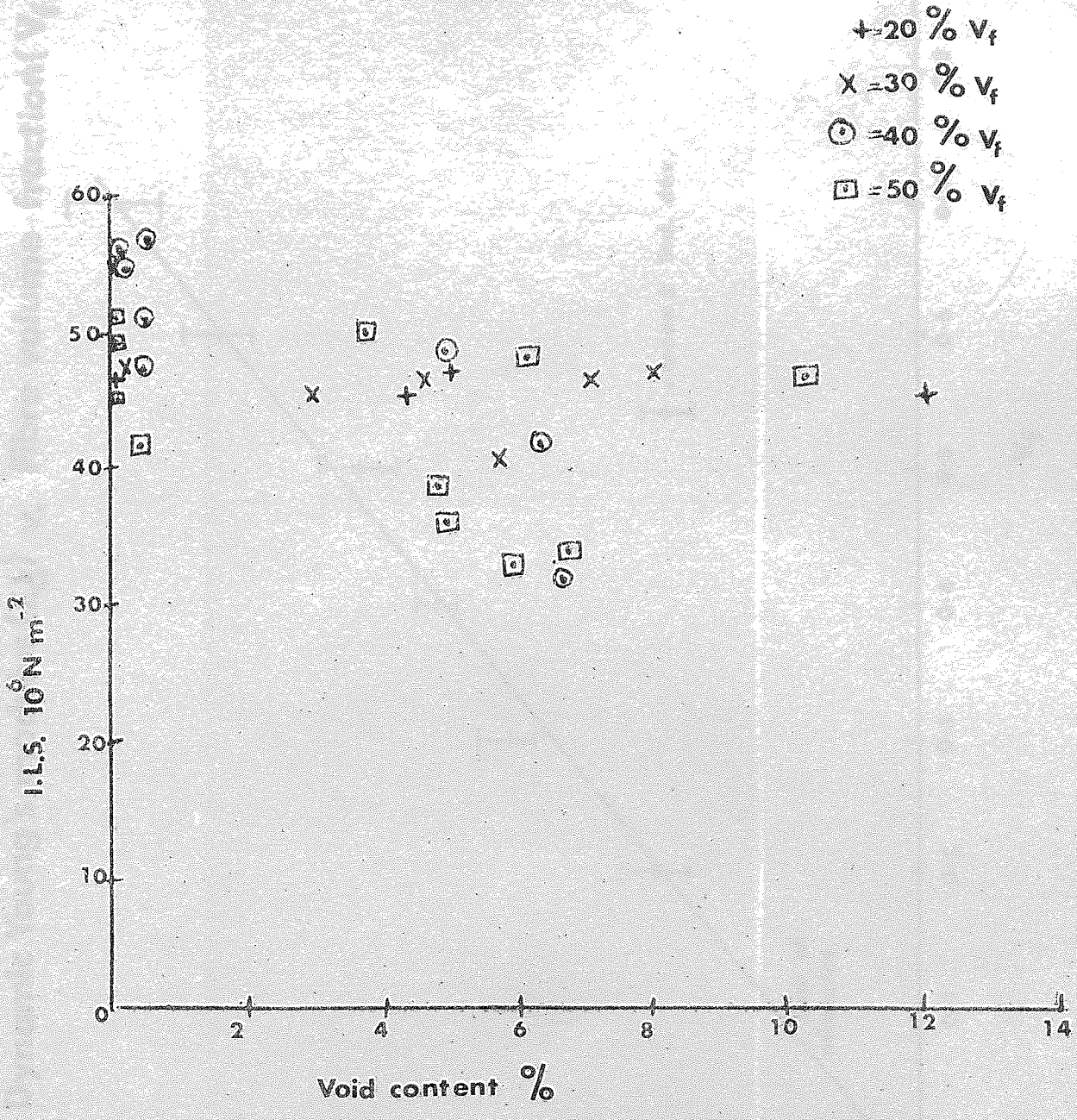

Fig. 82.

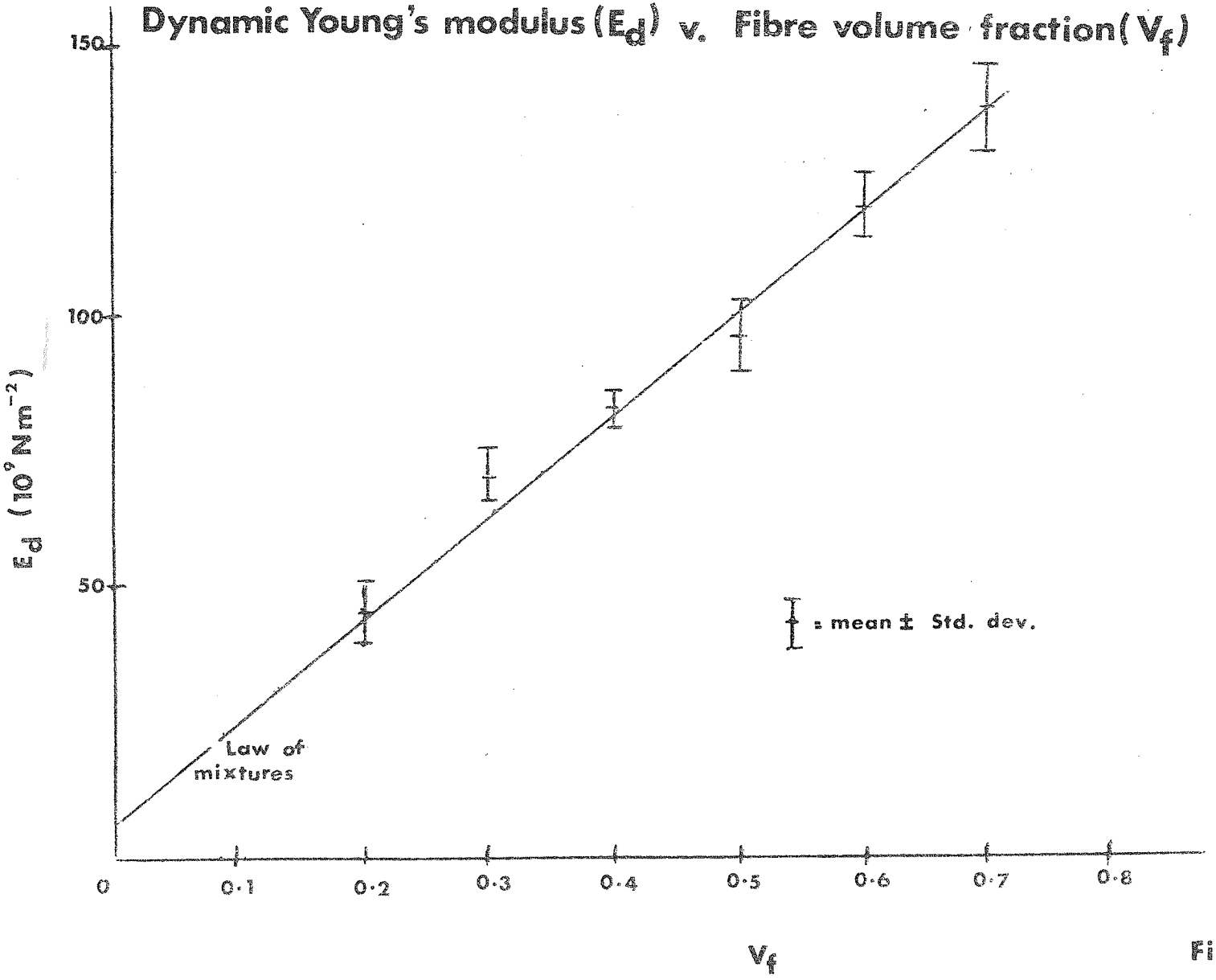
Dynamic Young's modulus (E_d) v. Fibre volume fraction (V_f)
150
100
50
E_d ($10^9 Nm^{-2}$)
Law of mixtures
= mean ± Std. dev.
0
0·1
0·2
0·3
0·4
0·5
0·6
0·7
0·8
V_f

Fig. 83.

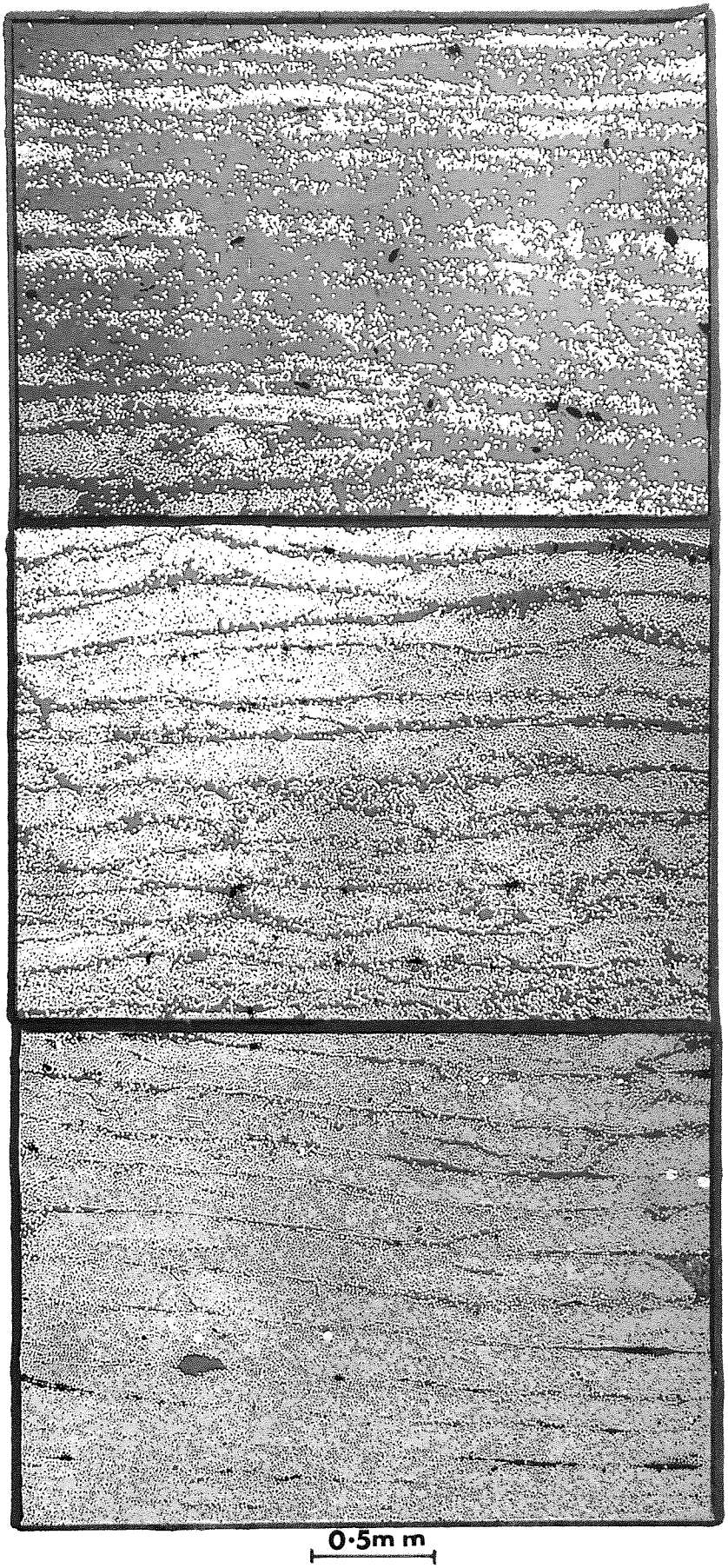

Fig84:CROSS SECTIONS OF CARBON-RESIN COMPOSITES WITH VARYING VOLUME FRACTIONS (V_f).

of these bands being higher than the mean fibre volume fraction. If these bands tend to lie on the outside of the specimen, then because the beam is in bending, the test will tend to give a high modulus. Above 0.5 fibre volume fraction these bands of fibres are not so noticeable. Hence an explanation of the results in figure 83 would be that the low fibre volume fraction results are slightly high because of fibre distribution within the composite and that when the fibre distribution becomes more even at fibre volume fractions above 0.5, the results are as predicted theoretically.

Another explanation of figure 83 would be that there had been a systematic error in the calculation of the single fibre modulus and the low fibre volume results were the true moduli. A collaborative experiment has been conducted to compare the single fibre property results obtained, in different laboratories, on the same batch of carbon fibre (78). Rolls-Royce consistently measured the diameter of the fibre approximately 4½% higher and the modulus 12% lower than the other laboratories. This discrepancy was thought to be due to the use of a different calibration standard for diameter measurements. All the laboratories, except Rolls-Royce use tungsten wires measured by R.A.E. as their standard, whereas Rolls-Royce have measured their own calibration wires.

Adding 12% to the results obtained in chapter 4 gives a modulus of approximately 250 GNm^{-2}. Using this corrected value in the law of mixtures, a modulus of 126 GNm^{-2} is predicted for a composite with a fibre volume fraction of 0.5. This compares with 115 GNm^{-2} using a single fibre modulus of 224 GNm^{-2} which is confirmed by the experimental results with the composites of 0.5 fibre volume fraction. However, the composites with fibre volume fractions of 0.2 and 0.3 are well defined by the modulus predicted using a single fibre modulus of 250 GNm^{-2}. If it is assumed that there is a systematic error in calculating the single fibre modulus, then this would imply a loss of

efficiency for the composites, which have higher fibre packing, caused by an increasing amount of fibre-fibre contact.

6.1.5 Dynamic Torsional Modulus

The same specimens, used in the above investigations were dynamically vibrated into their fundamental torsional mode, and the torsional modulus determined (Appendix III).

The torsional modulus is plotted against fibre volume fraction in Figure 85 together with a theoretical curve obtained using the cast resin and fibre shear modulus in Adams' analysis. All the specimens, except those with a fibre volume fraction of 0.7 had a torsional modulus which was 25% higher than predicted by Adams. The specimens with a fibre volume fraction of 0.7 had a torsional modulus similar to the theoretical value.

A possible explanation of the higher results is that the analysis of Adams does not adequately define this system. However, evidence will be presented later (Section 6.2) which suggests that when a unidirectional beam is twisted, the fibres wrap round each other making the beam stiffer. This "wrapping" constraint would give a higher observed torsional modulus and could account for the 25% discrepency between the two results. However, no matter which explanation is correct, the specimens with a fibre volume fraction of 0.7 appear to have a torsional modulus lower than predicted by the trend in results. This is possibly further evidence of a loss in efficiency for composite materials which have a high fibre volume fraction, where there is increased fibre-fibre interaction.

6.1.6 Flexural strength

Composites with fibre volume fractions from 0.2 to 0.7 were manufactured,

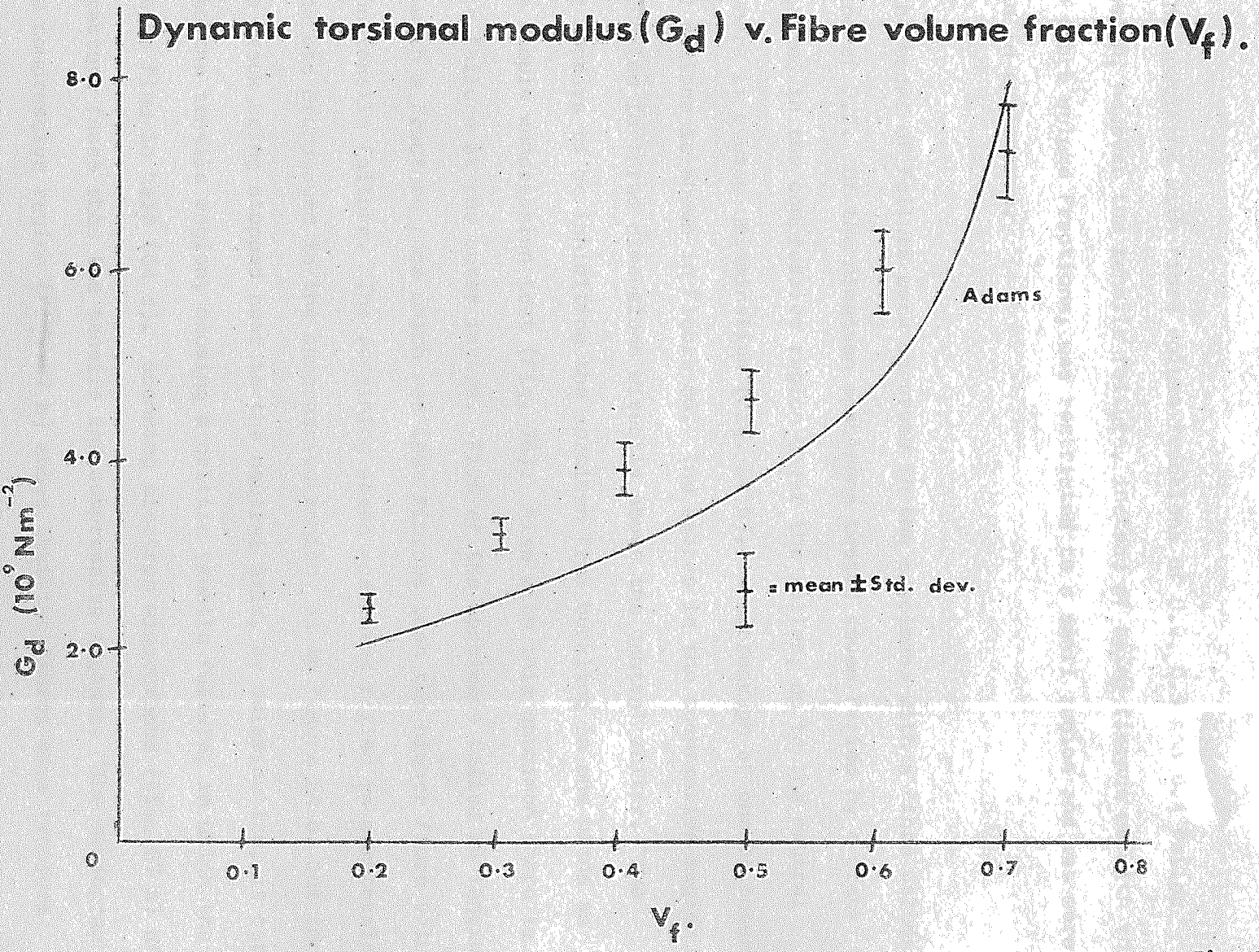
Dynamic torsional modulus (G_d) v. Fibre volume fraction (V_f).
8·0
6·0
4·0
2·0
0
G_d ($10^9 Nm^{-2}$)
Adams
= mean ± Std. dev.
0·1
0·2
0·3
0·4
0·5
0·6
0·7
0·8
V_f.

Fig. 85.

The specimens were cut into strips (ℓ = 125 mm b = 6 mm d = 2.5 mm) and loaded in three point bending, with an aspect ratio of 40 : 1, at a deflection rate of 100 mm/min, with a 13 mm loading nose made of brass. This type of loading nose was used so as to induce a compressive-tensile failure typical of fan-blade failure.

The specimens with fibre volume fractions of 0.2, 0.3 and 0.4 failed in tension, however the tensile failure, instead of being fibrous as with the higher fibre volume fractions, was restricted to a small region and was more brittle in appearance.

The modes of failure were observed in the specimens with a fibre volume fraction of 0.5. Of the nineteen specimens tested seven failed by a crack propagating in the compressive region under the roller, up to the neutral axis where it caused delamination (Fig. 64 b). A micrograph of one of these failed regions is shown in Figure 86. The fibres in the compressive region have buckled in three dimensions directly above the central roller. The roller appears to be inhibiting the specimen from buckling in one plane as in the simple compression test (Fig. 76). Also with this specimen there is tensile failure at the outer layers. Five of the specimens failed in tension, again with a fracture face which was less fibrous than the higher fibre volume fraction tensile failure. The remaining seven specimens failed in compression. A crack was propagated in the compressive region, as in figure 64 b, but instead of the crack being stopped near to the neutral axis, by delamination, it carried on into the tensile region, causing a brittle tensile failure, in which the specimens flew in half (64 d). Scanning electron micrographs (Fig. 87 a) of the fracture faces show the tensile and compressive regions. The micrograph of the compressive region (Fig. 87 b) shows that the fibres have fracture faces similar to those of the compressive fracture faces (Fig. 78). The tensile fractures faces (Fig. 87 c) are typical of tensile failure.

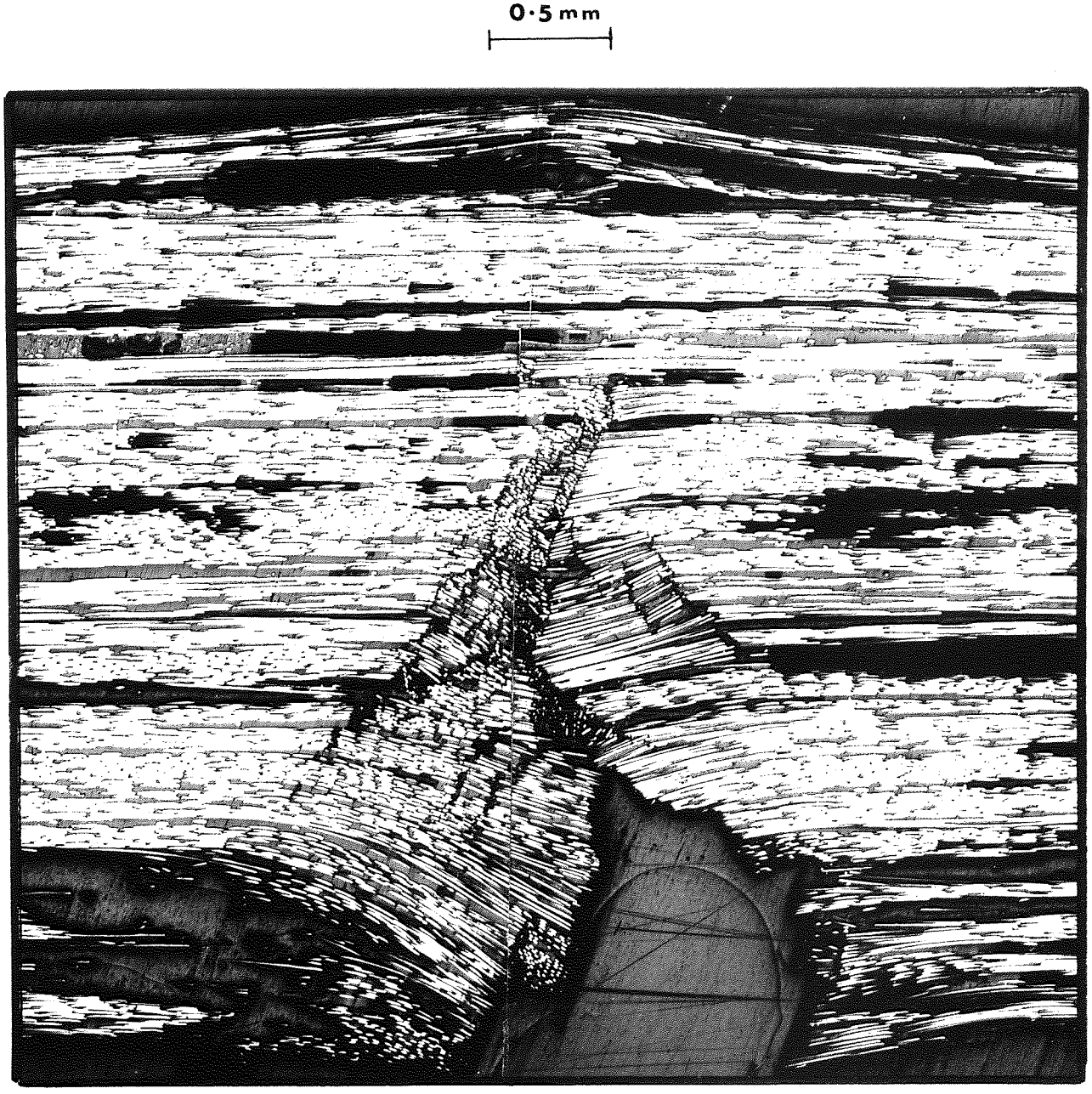

Fig.86.FLEXURAL FAILURE.

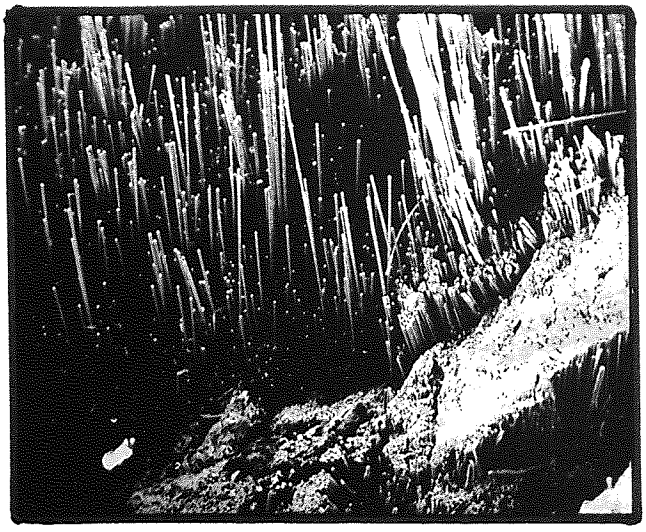

(a) Tensile-Compressive Region.

(b) Compressive Region

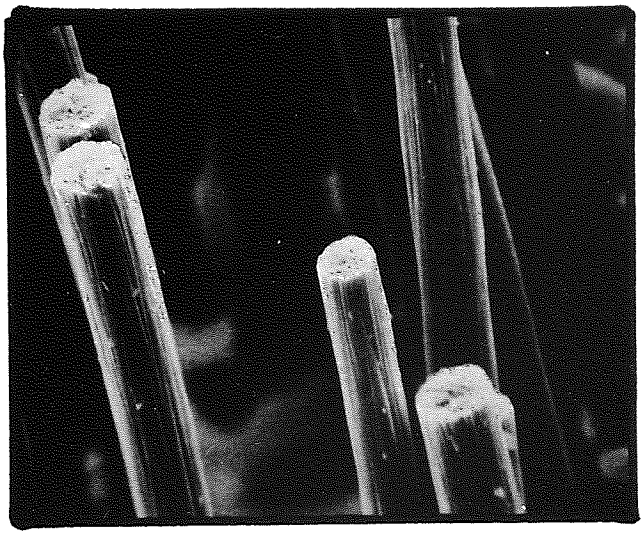

(c) Tensile Region.

Fig. 87. FRACTURE FACE OF A FLEXURAL SPECIMEN.

The composites with fibre volume fractions of 0.6 and 0.7 failed in a mixture of tension and compression, the compressive crack being stopped near to the neutral surface by delamination. Two of the specimens, with a fibre volume fraction of 0.7, failed by an interlaminar shear crack running near to the neutral axis, along the length of the beam.

In figure 88 the flexural strength is plotted against increasing volume fraction, together with a plot of the theoretical strength computed from the single fibre properties and the law of mixtures. Also plotted is an estimate of the theoretical compressive strength of the composites in bending, tested with the above three point bending configuration. The curve was obtained by correcting Foye's results for a 0.5 fibre volume fraction composite to the experimental results. It was assumed that the specimens failed by a compressive crack running through the specimen without being stopped by shear cracking which gave an indication of the compressive strength for this test configuration. A correction factor of 0.37 was required to fit the theoretical curve to the experimental results; this compares to the correction factor of 0.25 required to fit Foye's analysis to the compression test results. This would suggest that either the roller is producing a hydrostatic stress which would improve the compressive properties of the specimen, which would be offset by the effect of the higher Hertzian shear stresses, or that the compressive strength is dependent upon the specimen geometry.

The load to failure of the beam is directly proportional to the stress at failure, therefore as the stress increases with increasing fibre volume fraction, the load under the central roller will increase and hence the Hertzian stresses become more significant. Consequently as the fibre volume increases, the mode of failure changes from tensile to compressive. Also at the higher fibre volume fractions the interlaminar shear strength, compressive

Flexural strength for LY558.

v.

Fibre volume fraction

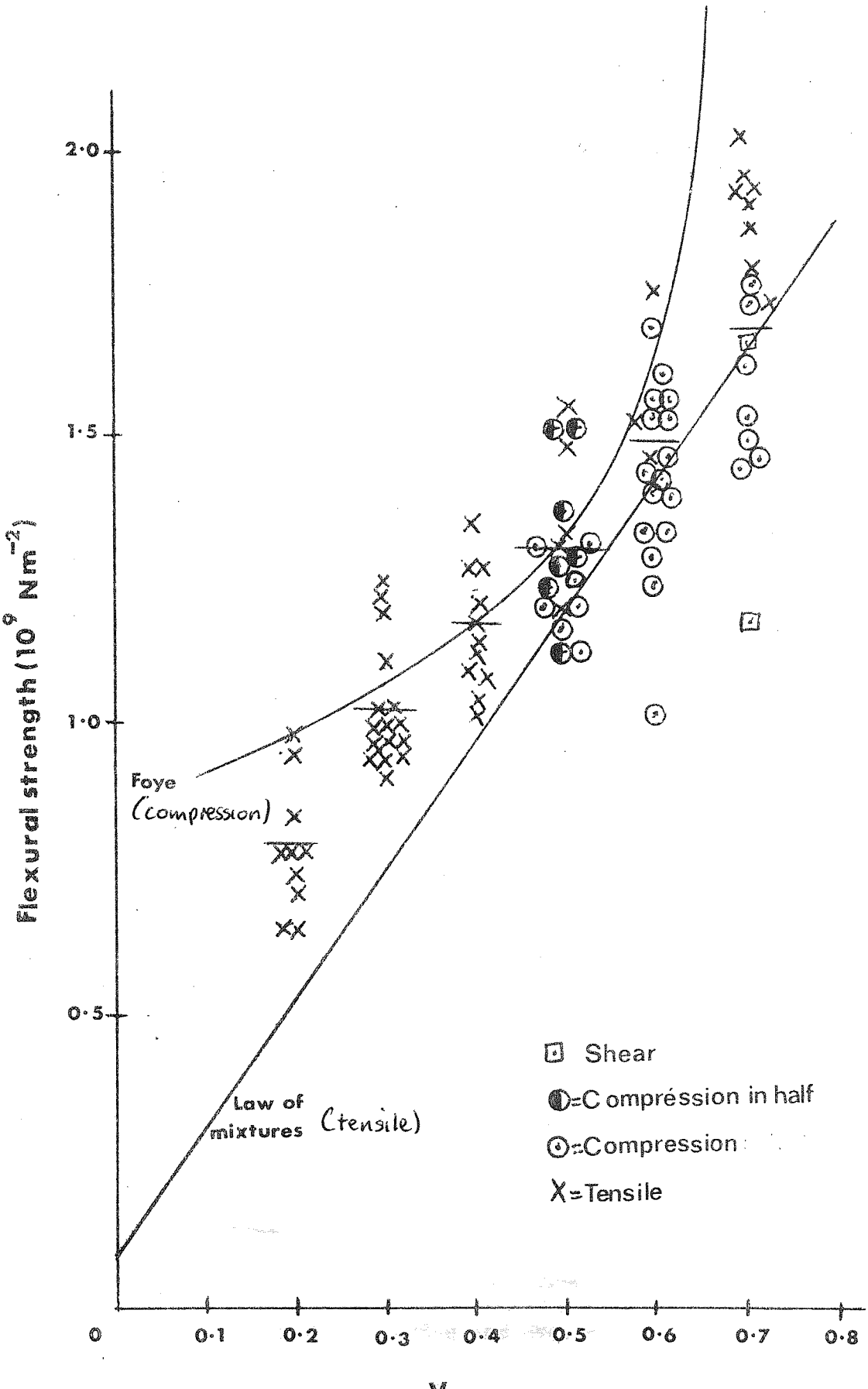

Fig.88.

and tensile strengths of the beam are probably falling away because of a loss of composite efficiency, hence the fracture mode is a mixture of compression and shear and tension.

6.2 Modulus of the matrix

Both the Rosen (12) and the Foye (20) models predict that the compressive strength is directly proportional to the matrix shear modulus. As the resin modulus is dependent upon the test temperature, a series of tests were conducted to determine the effect of varying the modulus of the resin by varying the test temperature.

A series of LY558 and HR4C cast resin blocks were produced and tested dynamically to determine their Young's and torsional modulus. The dynamic modulus apparatus was placed in the "Instron" environmental chamber and the moduli were found over a range of temperatures.

The Young's modulus of LY558 falls rapidly as the temperature increases from $-60^{o}C$ to room temperature (fig. 89) where there is a change in slope and the modulus reduces at a slower rate up to $200^{o}C$. This reducing modulus with increasing temperature is caused by an increase in molecular activity. The curve of Young's modulus against test temperature for HR4C (Fig. 90) is similar to that of LY558 except that at $100^{o}C$ there is a sudden drop off in modulus. The softening point of this resin system is near to $100^{o}C$. Above a test temperature of $125^{o}C$, the resin became very soft and the exciting frequency was so heavily damped that the beam was not able to vibrate at its fundamental bending frequency.

The shape of the curves of a plot of torsional modulus against test temperature (Figs. 91 & 92) for both the LY558 and HR4C systems were very

Dynamic Young's modulus for cast LY558 v. Test temperature.

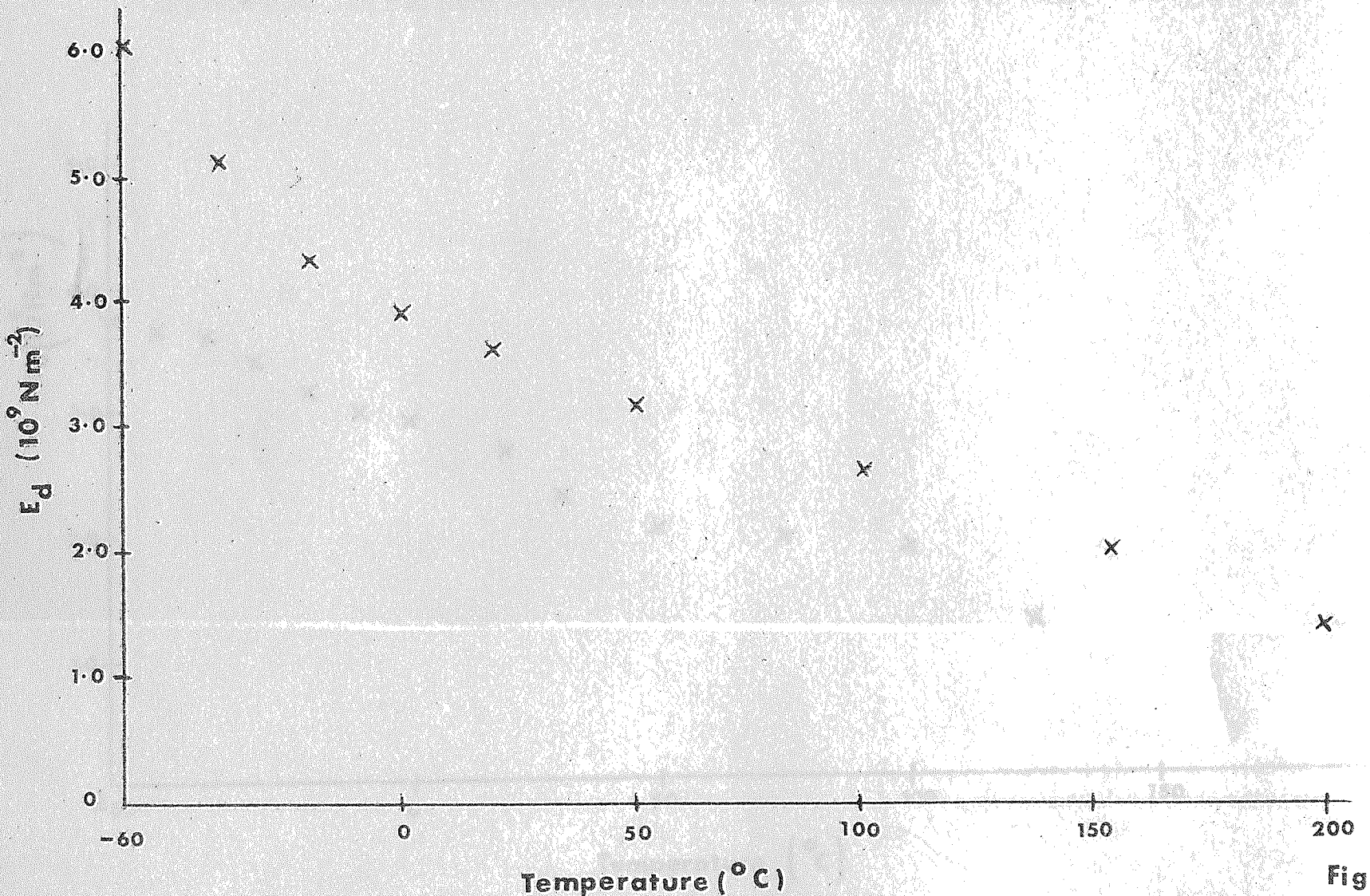

Fig. 89.

Dynamic Young's modulus for cast HR4C v. Test temperature.

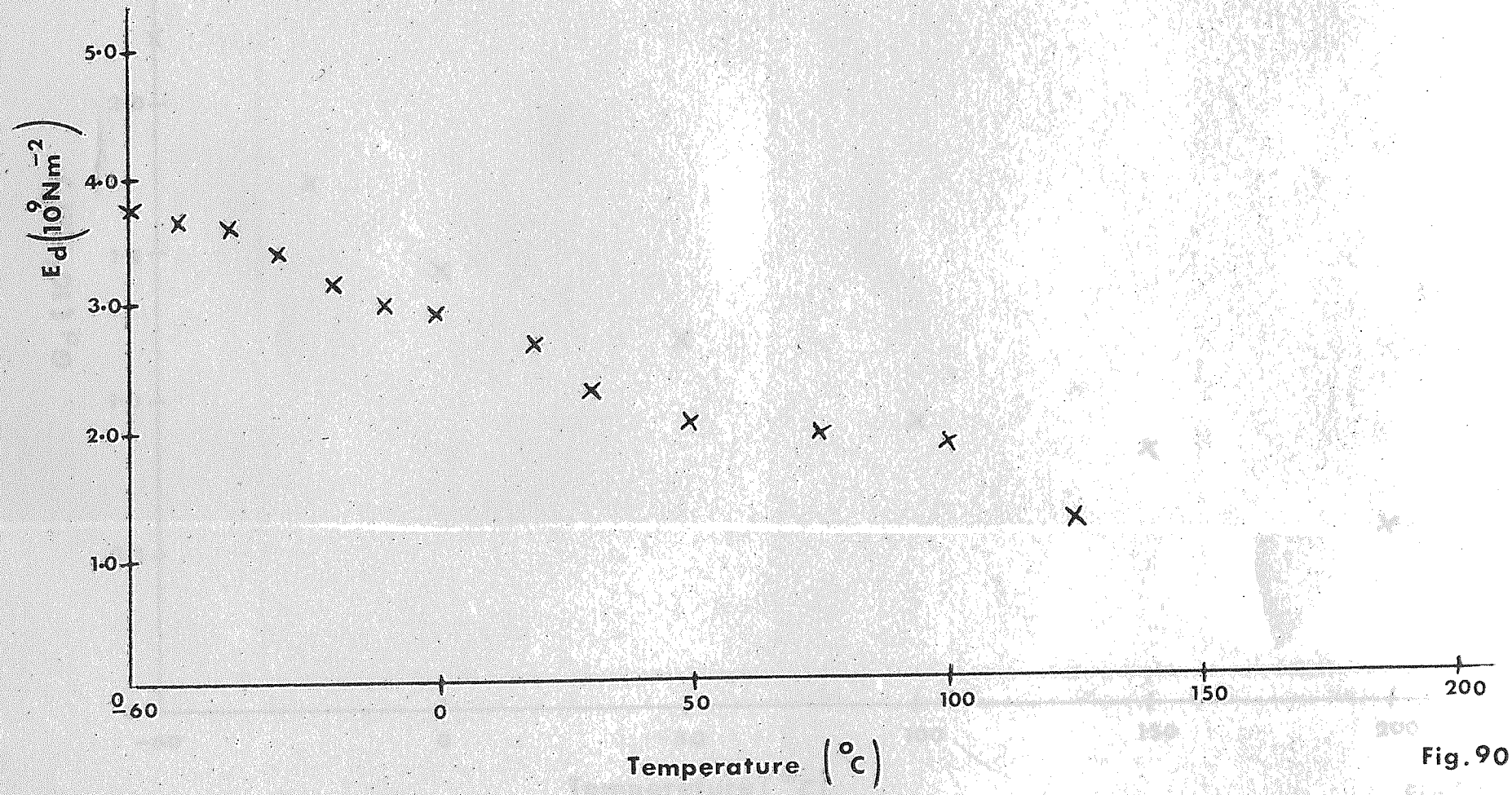

Fig. 90.

Dynamic torsional modulus for cast LY558 v. Test temperature.

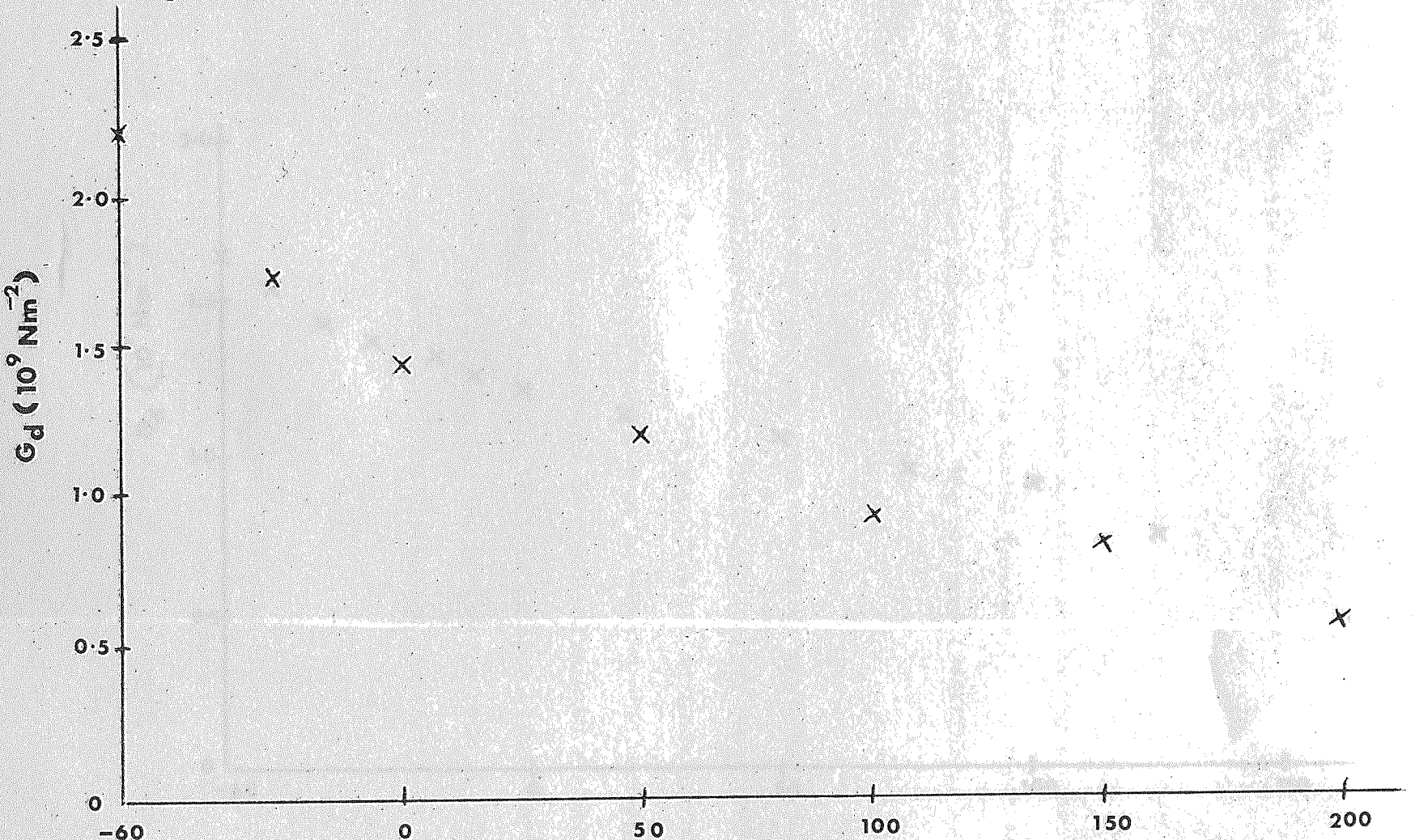

Fig.91.

Dynamic torsional modulus for cast HR4C v. Test temperature.

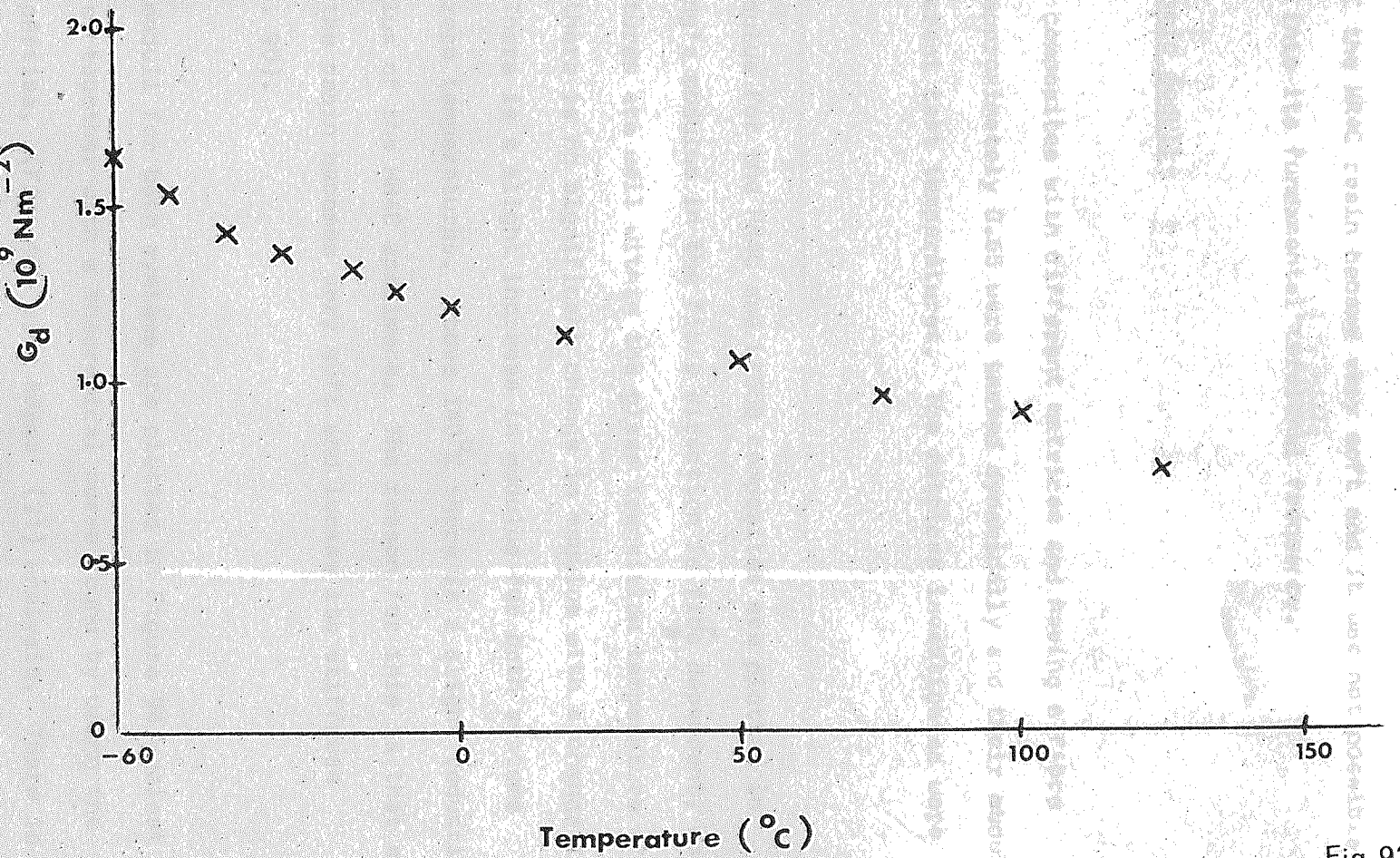

Fig.92.

similar to those of the Young's modulus against temperature (Figs. 89, 90). The torsional modulus of HR4C, however, did not fall off so rapidly as did the Young's modulus, above a test temperature of 100°C. Again, above a temperature of 125°C the HR4C resin became very soft and it was not possible to vibrate the beam into its fundamental torsional frequency.

6.2.1 Composite dynamic moduli

Unidirectional composites with different matrices and having a fibre volume fraction of approximately 0.65 were tested dynamically and their moduli determined for different test temperatures. The matrices investigated were LY558 and HR4C.

The Young's modulus for the HR4C and LY558 composites are plotted in Figure 93. The Young's modulus in the fibre direction is fibre dependent, and as the test temperatures are well within the glass transition temperature of the carbon fibres, there is no significant change in modulus with a change in test temperature. There is a slight increase in modulus for both systems when tested at sub-zero temperatures. Above 140°C there is a slight reduction in the Young's modulus of the HR4C specimens. The reason for this is that at these temperatures the resin becomes very soft and looses its stiffness dramatically. (Fig. 90).

The torsional moduli for both systems are plotted in Figure 94 against the test temperature, together with a theoretical curve found by using the HR4C cast resin properties, (Fig. 92) with Adams' (21) analysis. There is no significant change in torsional modulus with changes in test temperature for the composites with the LY558 matrix, and only a slight decrease above a temperature of 125°C for the HR4C composites. The experimental curve is completely different from the theoretical plot which predicts a constantly reducing modulus

Dynamic Young's modulus v. Test temperature.

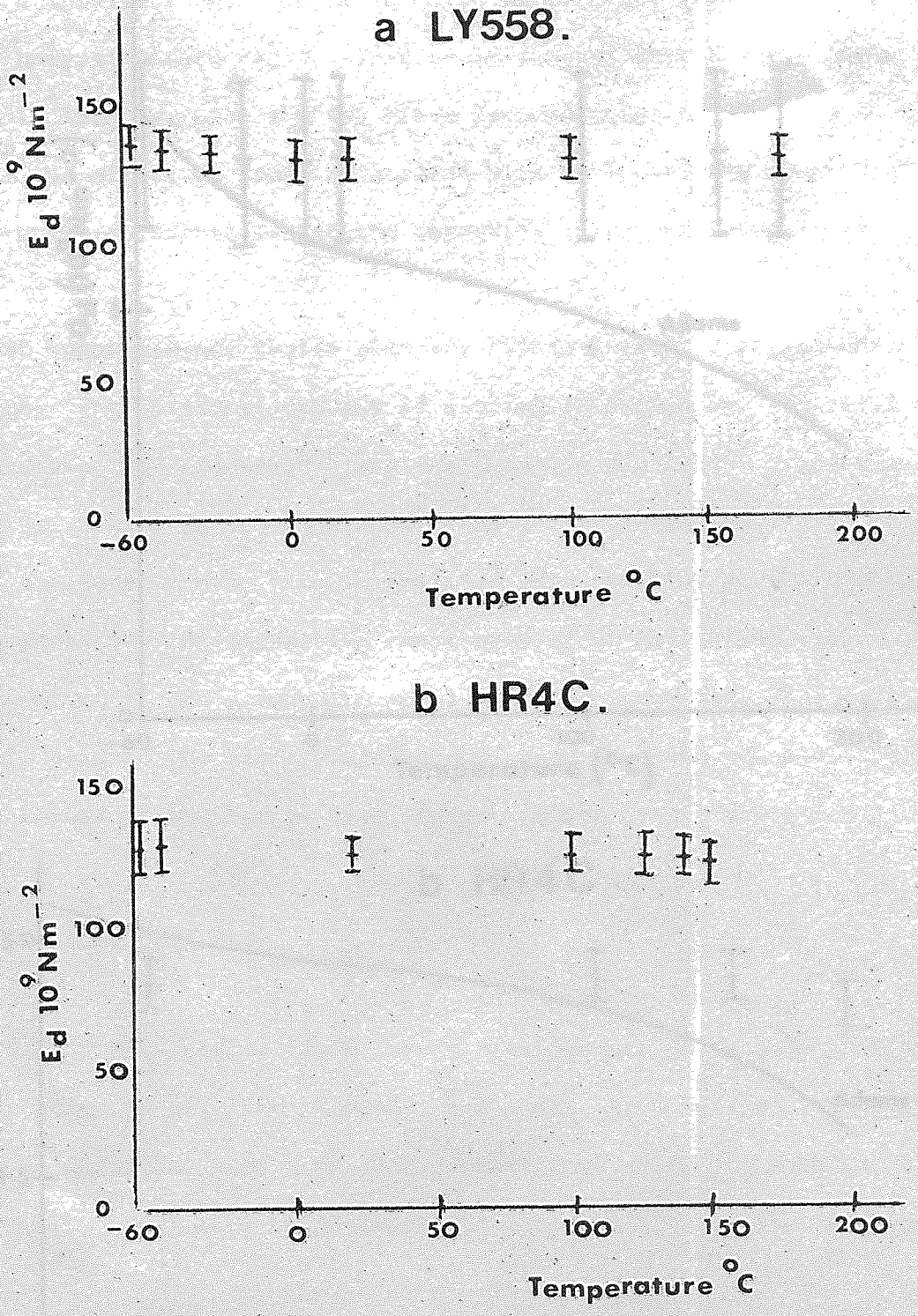

Fig. 93.

Dynamic torsional modulus v. Test temperature.

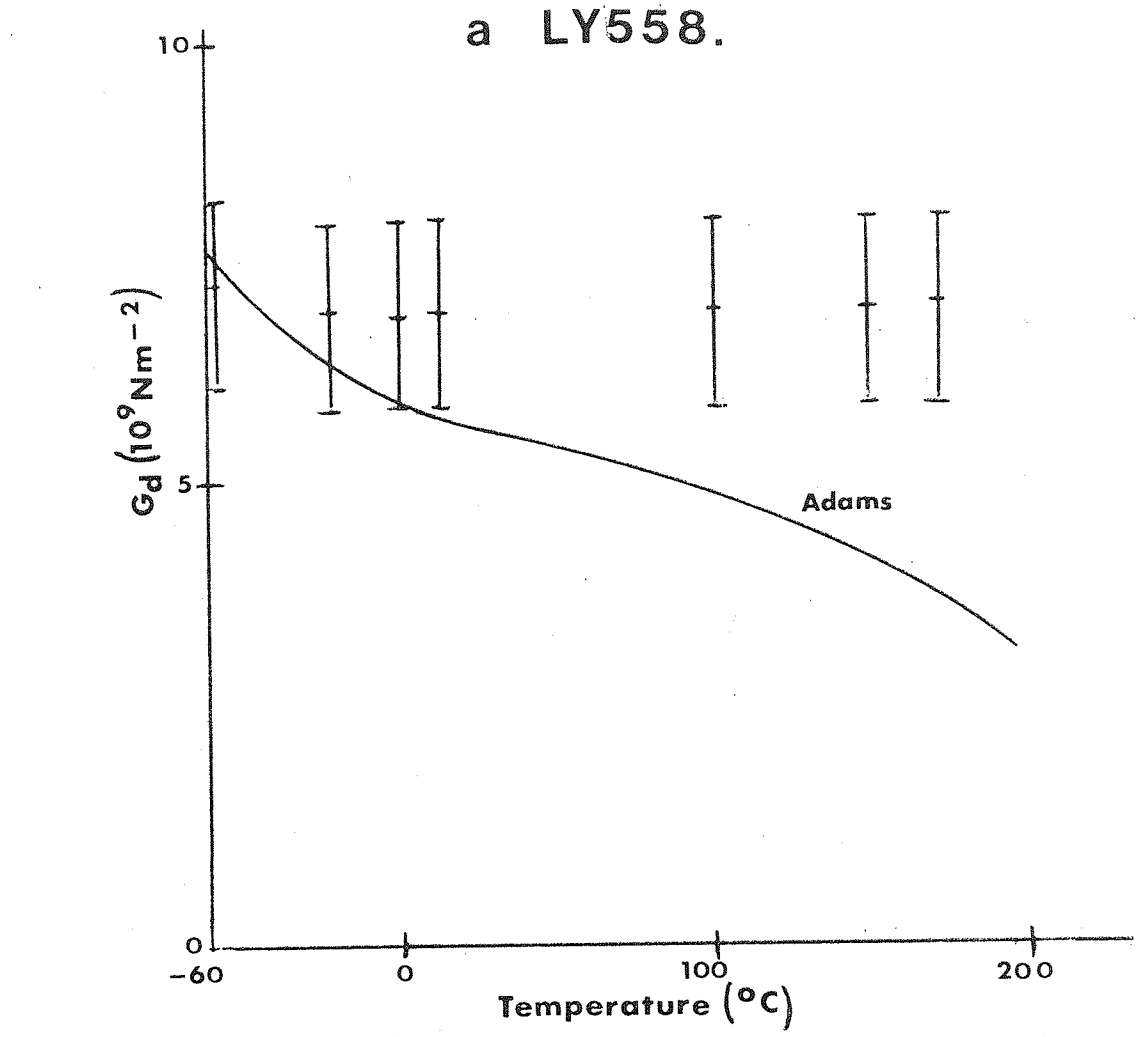

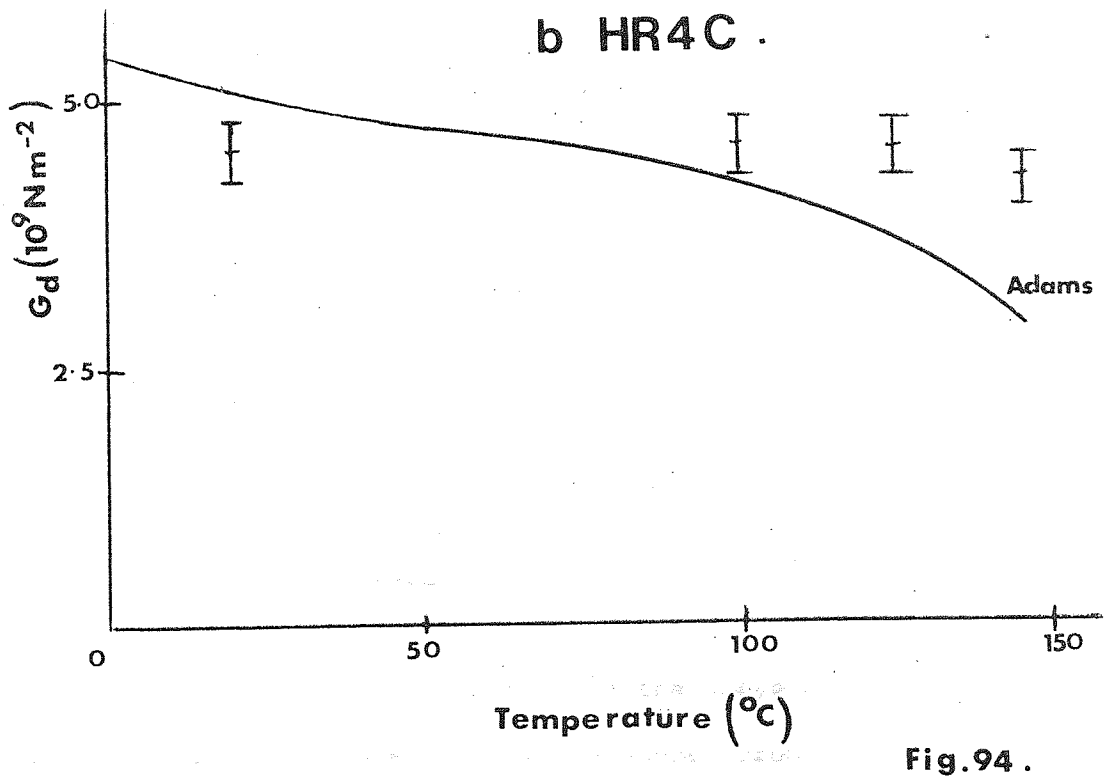

Fig.94.

with increasing test temperature.

As discussed in the previous chapter there is an indication that the fibres, in a unidirectional composite which is twisted, wrap round each other, making the composite more rigid. This would suggest that the specimens, which are tested in torsion, with the the fibre perpendicular to the axis of the test, where the effect of fibre constraint will be lower, the torsional modulus is more representative of the composite shear modulus.

An HR4C composite was tested with the fibres perpendicular to the axis of vibration. The torsional modulus is plotted in Figure 95. There is good agreement between the transverse torsional modulus and Adams' prediction for shear modulus. There is a strong dependence of transverse torsional or shear modulus of the composite on the torsional or shear modulus of the matrix. As the test temperature increases, the shear modulus of matrix reduces, causing a similar reduction in the transverse modulus of the composite. The implication here is that because the fibre wrapping constraint has been reduced, the transverse torsional modulus is more representative of the shear modulus.

6.2.3 Compressive strength

Composite plates with a fibre volume fraction of 0.65 and an HR4C matrix were waisted down in both the thickness and width, as described in Chapter 5, and tested in compression at different temperatures using the compressive fixture (Fig. 58) inside an environmental chamber on the Instron (Fig. 96).

At test temperatures below 100^{o}C the stress-strain curve was linear up to just before the maximum load, where shear cracks began to propagate back from the waisted region of the test specimen and the curve continued increasing, but at a reduced rate. At failure there was a sudden drop in load and all the

Transverse torsional modulus(dynamic) v. Test temperature.

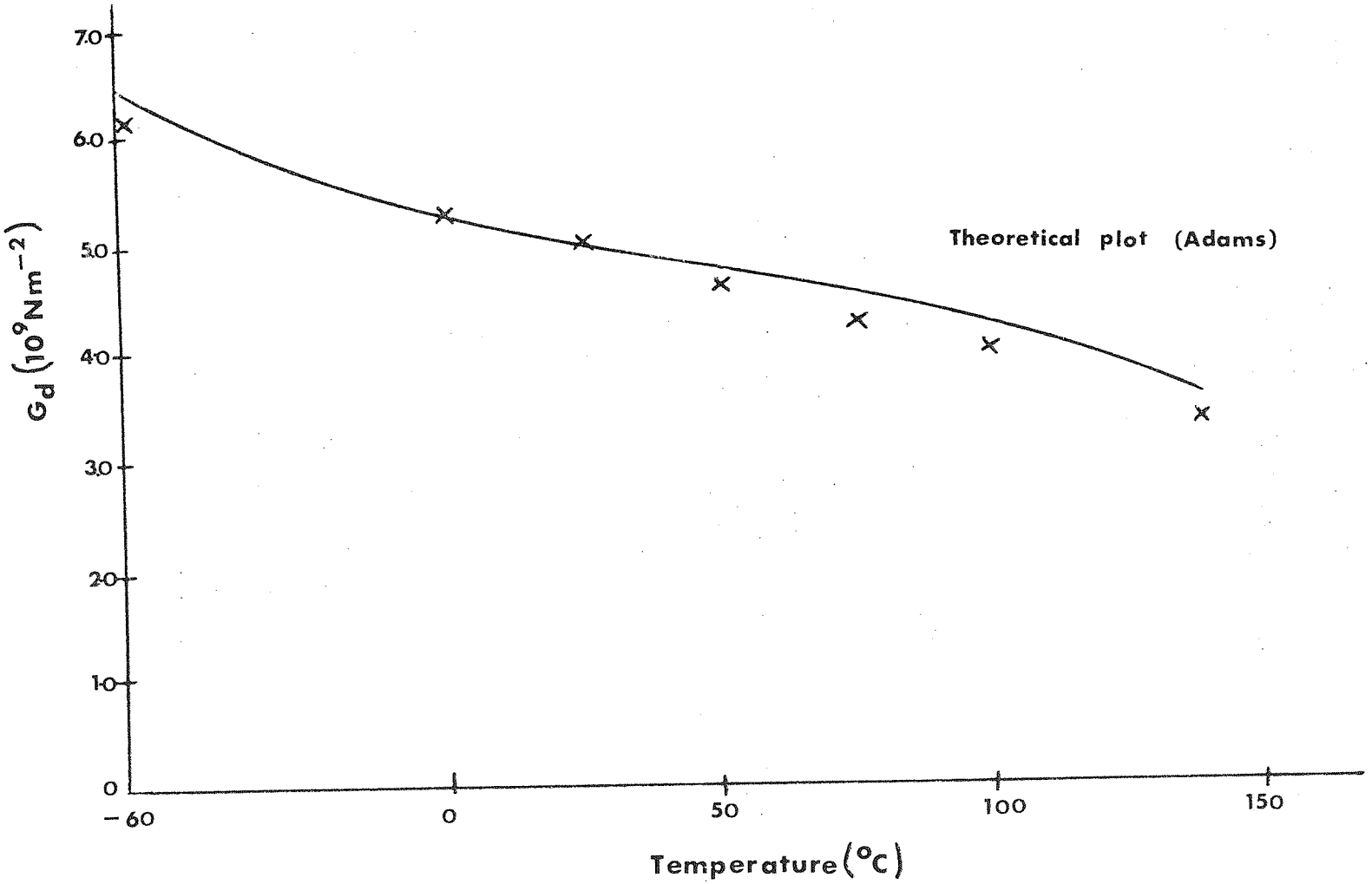

Fig.95.

Fig.96. Environmental Chamber.

specimens failed within the gauge length. At a temperature of 100°C, the load time curve was linear up to approximately 80% of the maximum, where it slowly began to curve away until the specimen failed. This change in slope appears to be associated with the softening of the matrix and it is similar to a yielding mechanism in metals. As the test temperature increased this 'yielding' became more pronounced and at a temperature of 150°C the matrix is very soft and the composite continually 'yields' as soon as the load is applied.

The breaking strengths at failure are plotted in Figure 97 against test temperature together with a theoretical plot. The theoretical plot was derived using Foye's analysis with a reduction factor of 25%. No theoretical explanation is offered for this correction factor, other than it is the factor required to fit Foye's analysis, for a composite with a fibre volume fraction of 0.65, to the experimental results in Figure 72. The 'theoretical' curve is in very good agreement with the experimental results up to a test temperature of 100°C. At temperatures above 100°C the theoretical plot increasingly over-estimates the experimental values. This descrepancy between the two results coincides with the change in behaviour of the composite to failure. At these elevated temperatures the resins are known to behave visco-elastically, where the modulus is both a function of strain and time at a given temperature, which would cause a reduction in the modulus.

6.2.4 Tensile strength

Specimens were machined to the optimum tensile test shape and loaded on the Instron in an invironmental chamber at a strain rate of 1 mm/min. As before the specimens investigated were carbon fibres with a volume fraction of 0.65 in an HR4C matrix.

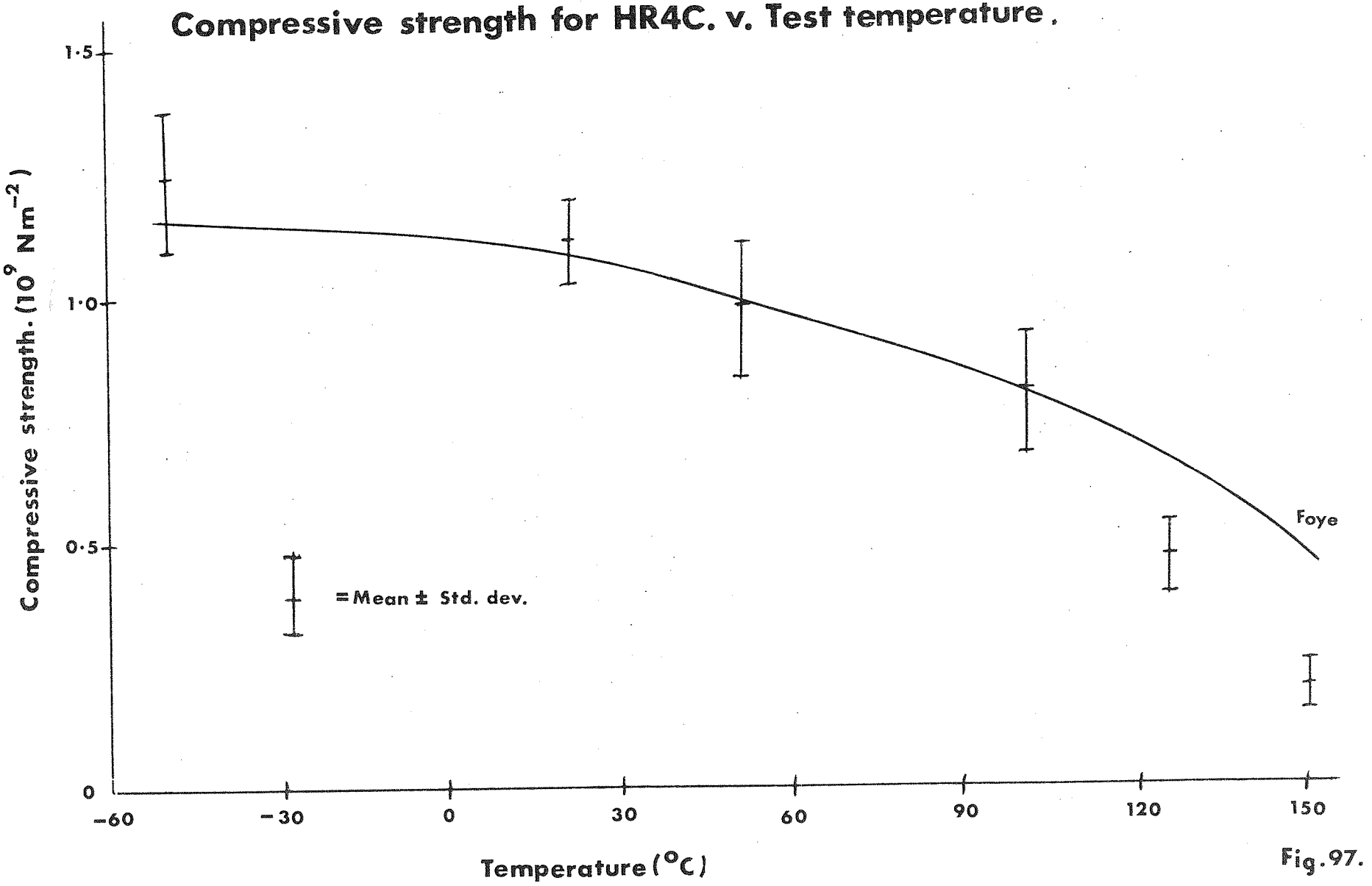
Compressive strength for HR4C. v. Test temperature.
Compressive strength. (10^9 Nm^{-2})
1·5
1·0
0·5
0
= Mean ± Std. dev.
Foye
−60
−30
0
30
60
90
120
150
Temperature (°C)

Fig. 97.

The mean breaking strength at failure at room temperature was 1.41 GNm^{-2} and as the test temperature was reduced to $-55^{o}C$ the mean tensile strength increased, slightly, to 1.45 GNm^{-2}. There is no statistical significant difference between these two means, however a slight increase in strength would be expected from 'Rosens' theory (4) which predicts more efficient load transference for increased matrix shear modulus. As the test temperature was increased to $100^{o}C$ there was a very slight reduction in the mean breaking strength and at a temperature of $125^{o}C$, which is the softening point of the matrix, there was a sudden reduction in tensile strength. At this temperature the matrix can no longer transfer the load from fibre to fibre and the composite is behaving as a bundle of fibres. Coleman (3) predicts, for fibres with the coefficient of variation determined in Chapter 3 and a fibre volume fraction of 0.65, a bundle strength of 0.97 GNm^{-2} which is in good agreement with the mean tensile breaking strength of the composite tested at $150^{o}C$. (Fig. 98).

The failure region of the composite became more fibrous as the test temperature was increased from $-55^{o}C$ to $150^{o}C$, indicating a decrease in load bearing efficiency.

6.2.5 Interlaminar shear

Two series of specimens, with HR4C and LY558 matrices and fibre volume fraction of 0.65 have been tested in interlaminar shear at Rolls Royce (79). The test was a short beam test similar to that described in Appendix II and it was conducted over a range of temperatures.

The shape of the curve of interlaminar shear strength plotted against the test temperature for the HR4C composites (Fig. 99) is similar to the plot of the transverse torsional modulus against temperature (Fig. 95).

Tensile Strength For HR4C v. Test Temperature

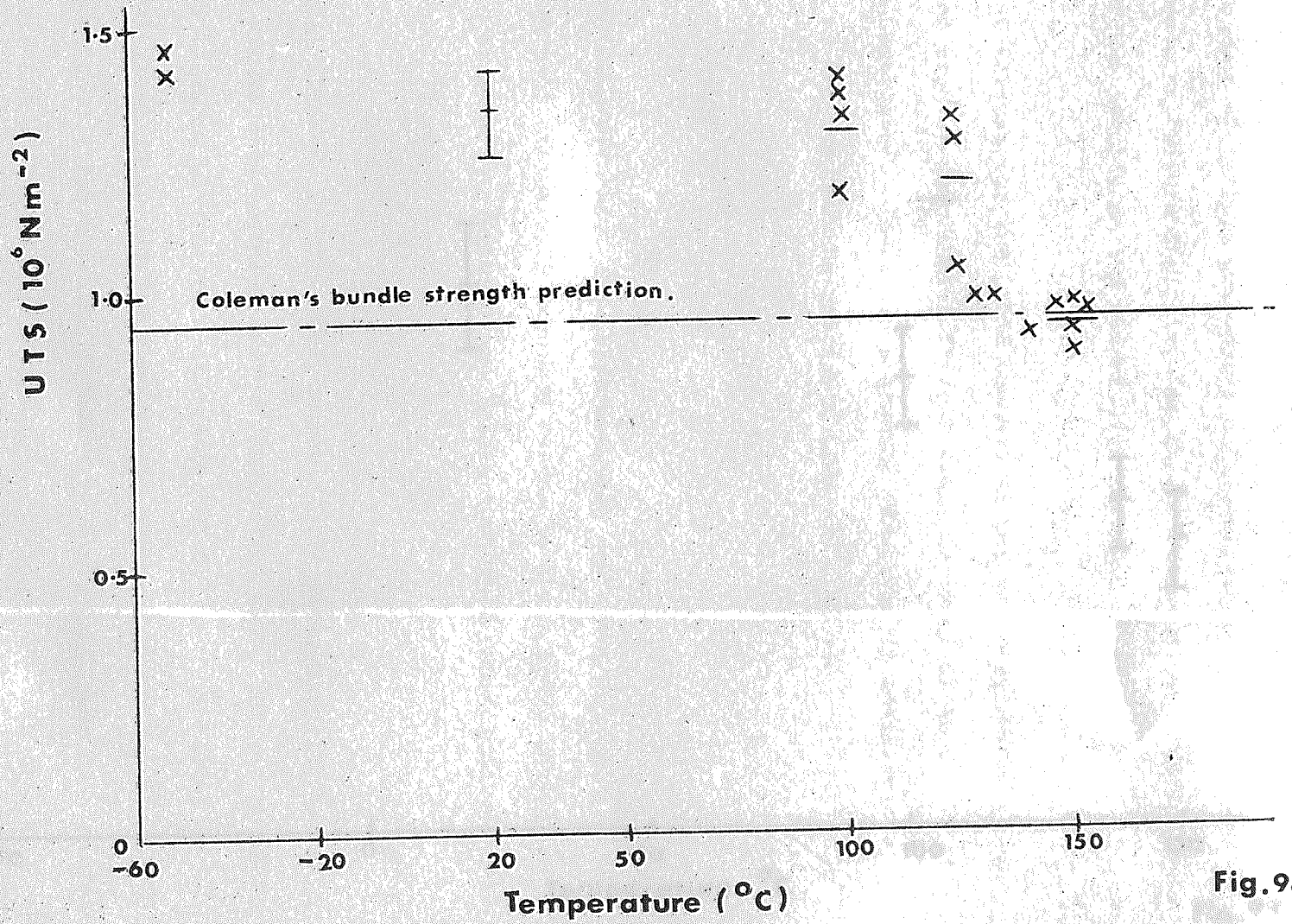

Fig. 98 .

Interlaminar shear strength (HR4C) v. Test temperature.

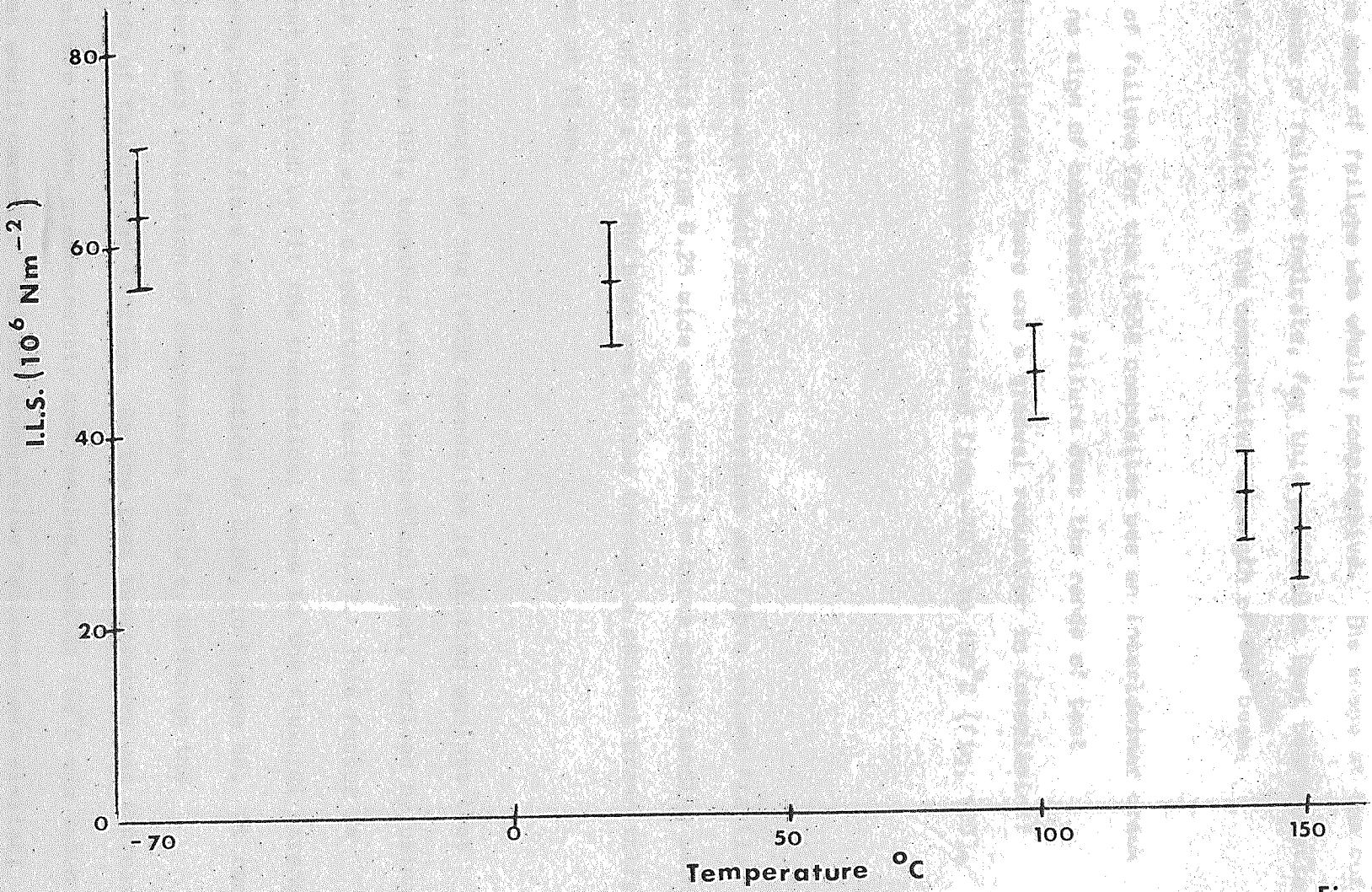

Fig. 99.

At room temperature, although the final failure was an interlaminar crack, there were signs of compressive failure under the central roller. As the temperature increased, the compressive failure became more pronounced and above 125°C the mode of failure was wholly compressive. The shape of the curve (Fig. 99) and mode of failure indicate, for this particular test configuration, a dependence of the results on the compressive strength of the beam.

The mode of failure for the LY558 composites was an interlaminar crack and there was no sign of compressive failure over the range of test temperatures investigated. There was a gradual reduction in interlaminar shear strength as the temperature increased from -70°C to 150°C (Fig. 100).

6.2.6 Flexural strength

Composite plates with HR4C and LY558 matrices and fibre volume fraction of 0.65 were cut into strips 0.25 wide and tested in three point bending with an aspect ratio of 40 : 1. The beam was loaded through a central brass roller with a diameter of 13 mm.

The flexural strength of the LY558 composites is plotted against test temperature in Figure 101, together with a theoretical plot, derived by using Foye's analysis together with a reduction factor of 0.27. This factor is the same as that required to fit the theoretical curve to the flexural strength of the specimens, with a fibre volume fraction of 0.65, in Figure 88. At room temperature there was indication of compressive failure, although the predominant mode of failure was tensile. As the test temperature was increased, the mode of failure became predominantly compressive, and at 100°C and above the failure was wholly compressive. All the compressive failures were similar; they failed by a crack propagating in the compressive region, under the roller, up to the neutral axis. At a test temperature of 200°C the resin was very soft

Interlaminar shear strength (LY 558) v. Test temperature.

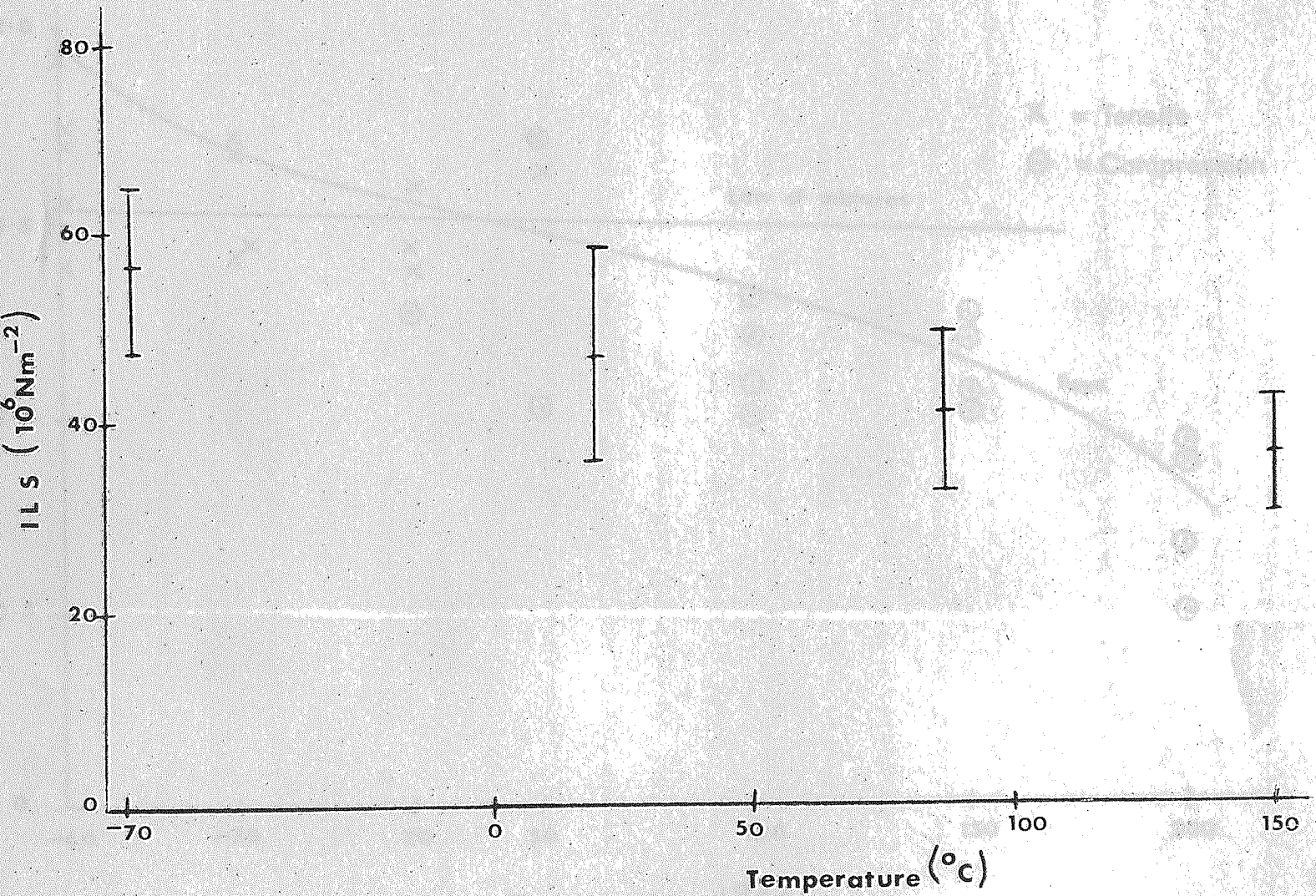

Fig. 100.

Flexural stress at failure for LY558 v. Test Temperature.

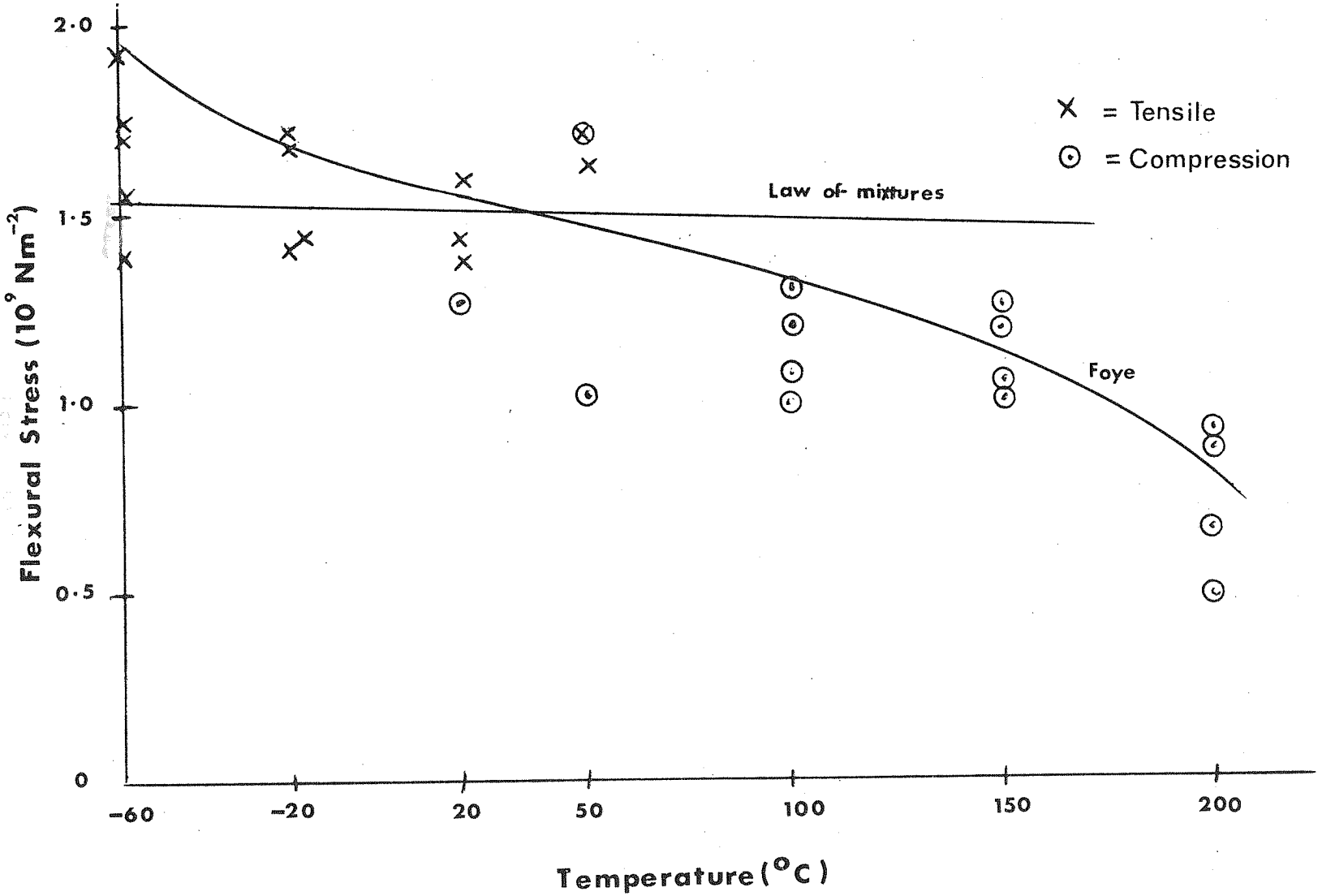

Fig. 101.

and the composite 'yielded' as soon as the load was applied. The corrected theoretical curve predicts very closely the flexural strength of the composites, which failed in compression.

As the test temperature was reduced from the room temperature, the matrix became more rigid and consequently the compressive strength increased and at a temperature of $+20^{o}C$ and below, the compressive strength of the beams was higher than the tensile strength, and the beams failed in tension.

The flexural strength of the HR4C composites is plotted in Figure 102 against the temperature at which the test was conducted. Also plotted is a theoretical compressive curve derived as in figure 101 using a correction factor of 0.27 and a tensile curve obtained using the law of mixtures. At room temperature, all the specimens tested failed in compression, with the crack propagating into the tensile region, causing a brittle tensile failure. At $50^{o}C$ half of the specimens failed in the same way and although the remainder failed in compression, the crack was stopped near to the neutral axis by delamination. As the test temperature was increased above $100^{o}C$ the resin became very soft and the specimens 'yielded' at very low loads, as the fibres were allowed to buckle by the soft resin. The theoretical curve tends to underestimate the flexural strength of the specimens tested at room temperature and $50^{o}C$. HR4C has a relatively short gel time, at the curing temperature used in the manufacturing process, which makes it easier to remove the voids, from the mouldings, than with the LY558 composites. Hence the HR4C specimens contain fewer flaws than the LY558 specimens which means, if a flaw criteria is assumed for compressive strength, a higher correction factor is required for the compressive strength of the HR4C composites.

As the test temperature was reduced from room temperature, the compressive strength increased with increasing matrix shear modulus and at $-20^{o}C$ and below the compressive strength of the beams was higher than the

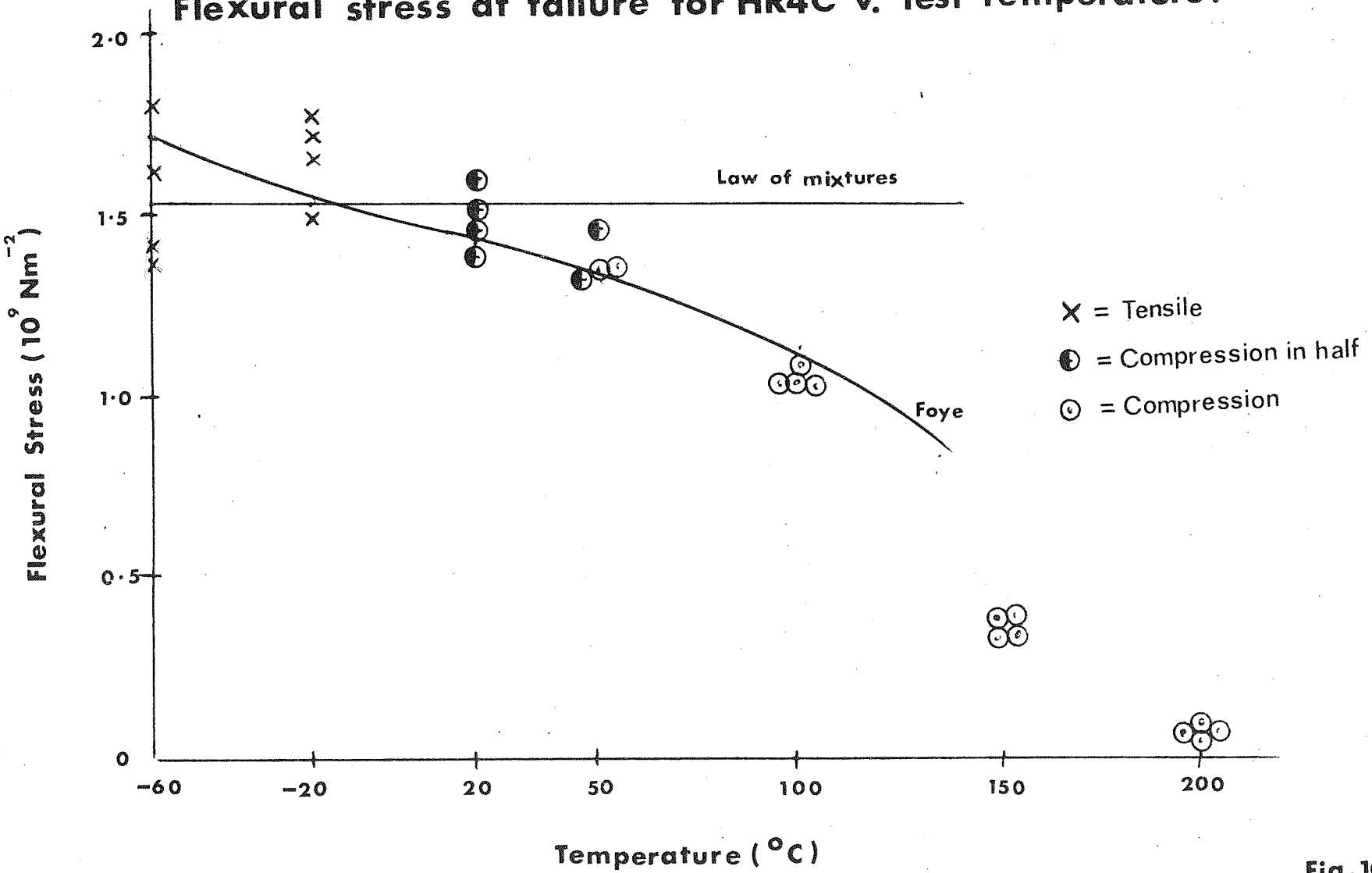
Flexural stress at failure for HR4C v. Test Temperature.
Flexural Stress (10^9 Nm^{-2})
2·0
1·5
1·0
0·5
0
Law of mixtures
Foye
× = Tensile
◐ = Compression in half
⊙ = Compression
−60
−20
20
50
100
150
200
Temperature (°C)

Fig.102.

tensile strength and the beams failed in tension.

6.3 Volume effects in composite materials

To be able to predict the behaviour of larger components such as a fan blade it is necessary to understand how carbon fibre composites behave when the volume of material under test is varied.

6.3.1 Tensile strength

The breaking strengths of specimens of shape 3, (see Chapter 5) in which tensile failure was observed to take place over the whole length of the specimen between the grips, are lower than those for specimens of shape 4 which fail over a shorter length and are narrower. Assuming that the grips do not effect the strength of the composite, there appears to be a gauge length effect. To check this, specimens 108 mm long were machined to shapes 3 and 4 and tested.

The mode of failure of short specimens of shape 3 was similar to that of the longer specimens, but because the aluminium grips were closer, 62 mm instead of 150 mm, it was confined to a similar length. The mean breaking strength of the shorter composites was 1.49 GNm^{-2}, this compares to a mean strength of 1.35 GNm^{-2} for the 216 mm long specimen (Fig. 57).

When the shorter specimens of shape 4 were tested, although the mode of failure was similar to that of the long specimens, there was fibrous failure at the grips. This was because the distance between the grips for the shorter specimens was approximately the same length as the extent of failure of the longer specimens. The mean strength of 1.43 GNm^{-2} is similar to that of 1.40 GNm^{-2} for the longer specimens, which is not surprising as the extent

of fibre failure was similar for both sizes of specimen. This suggests that the effects of the grips are not significant.

Although only a limited number of tests have been carried out, there does appear to be a size effect as predicted by Rosen and Zweben (5).

6.3.2 Effect of Increasing volume on the flexural strength

LY558 specimens were tested in four point bending. The test configuration used had an inside span of 30 mm and an outside span of 100 mm. The specimens were the same size as those recommended in Chapter 5. The load was applied at a cross head speed of 100 mm/min.

The mode of failure of specimens tested in four point bending was predominantly tensile and the stress at failure is plotted in figure 103 together with the failure stress of the specimens, from the same mouldings, tested in 3 point bending. The mean strength of the 4 point bend specimens is 1.46 GNm^{-2} which is significantly lower than the 3 point bend results (1.65 GNm^{-2}).

In a four point bend test the whole of the beam, between the two internal supports, is subjected to a maximum stress, but in a three point bend test only a small volume of specimen, just above the central roller, is loaded to a maximum stress. Hence the fact that the flexural strength of the four point bend test is lower than that of the three point bend test implies that there is a gauge length effect.

Nine out of eleven specimens, tested in four point bending, failed in tension, one failed in shear, and the other in compression. The compressive failure was a sharp crack under one of the inside rollers which propagated to

Comparison between three & four point bend tests.

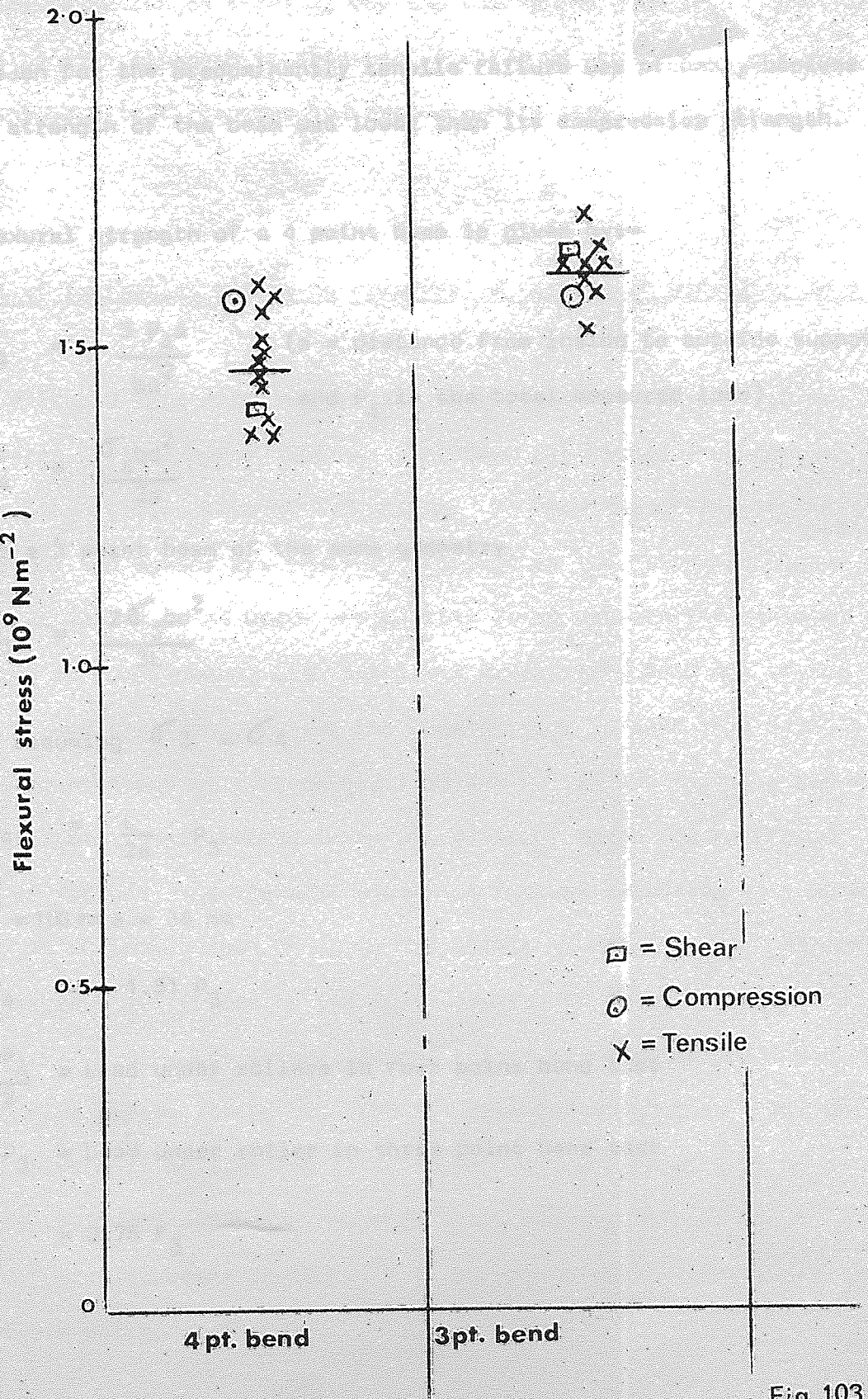

Fig. 103.

the neutral axis where it was stopped by localised delamination. The whole of the beam, between the central rollers, was subjected to a maximum compressive stress, and the reason why it failed at the rollers was probably because of stress concentrations round the roller.

The reason for the predominantly tensile failure was probably because the tensile strength of the beam was lower than its compressive strength.

The flexural strength of a 4 point beam is given by:-

$$\sigma_4 = \frac{3 P_4 a}{bd^2}$$ (a = distance from inside to outside support and P_4 is the total measured load)

$$\therefore P_4 = \frac{\sigma_4 bd^2}{3a}$$

Now for a 3 point beam of the same geometry

$$\therefore P_3 = \frac{2 \sigma_3 bd^2}{3L}$$

assuming $\sigma_3 = \sigma_4$

$$P_4 = \frac{L}{2a} \cdot P_3$$

when L = 100 mm a = 34 mm

$$P_4 = 1.51 P_3$$

Let $F_4 = \frac{P_4}{2}$ = Load under rollers in four point bend test

$F_3 = P_3$ = Load under roller in three point bend test

$$F_4 = 0.75 F_3$$

The load at each of the rollers in the four point bend test is only 75% of the load at the central roller in the three point bend test, hence the stress concentration effects at the rollers in the compressive region will be less by a similar amount. The tensile strength is slightly lower, because of the gauge length effects, for the four point bend test. However the ratio of tensile strength to compressive strength should be lower for the four point bend test, causing the predominantly tensile failure of the specimens.

6.3.3 Effect of increasing volume on compressive failure of specimens in bending

Beams, produced from HR4C composites, were cut 6 mm wide and 2.5 mm thick and tested in four point bending. The beam was loaded through two 13 mm rollers at a strain rate of 100 mm/sec. To keep the effect of the rollers constant the moment arm remained constant as the distance between the rollers was varied. The beams tested with 25 mm between the central rollers failed in compression, with the crack propagating from one of the rollers up through the beam, causing the beam to fail in half in a brittle manner. The mean stress at failure was 1.55 GNm^{-2}. As the distance between the central rollers was increased to 44 mm, although there was no change in the mode of failure, the flexural stress at failure decreased to 1.48 GNm^{-2} (Fig. 104). At an inside span of 63 mm the stress at failure was 1.45 GNm^{-2}. A students 't' test was fitted to the test results, to judge the significance of the reduction of flexural stress, as the volume of material subjected to a maximum bending stress increased. The 't' test indicated that there was no significant difference between the beams tested with an inside span of 44 mm and the other test configurations, however there was 95% probability of a difference between the beams tested with 25 mm between the inside rollers and the beams with a mid-span of 63 mm.

Effect of increasing volume on compressive failure .

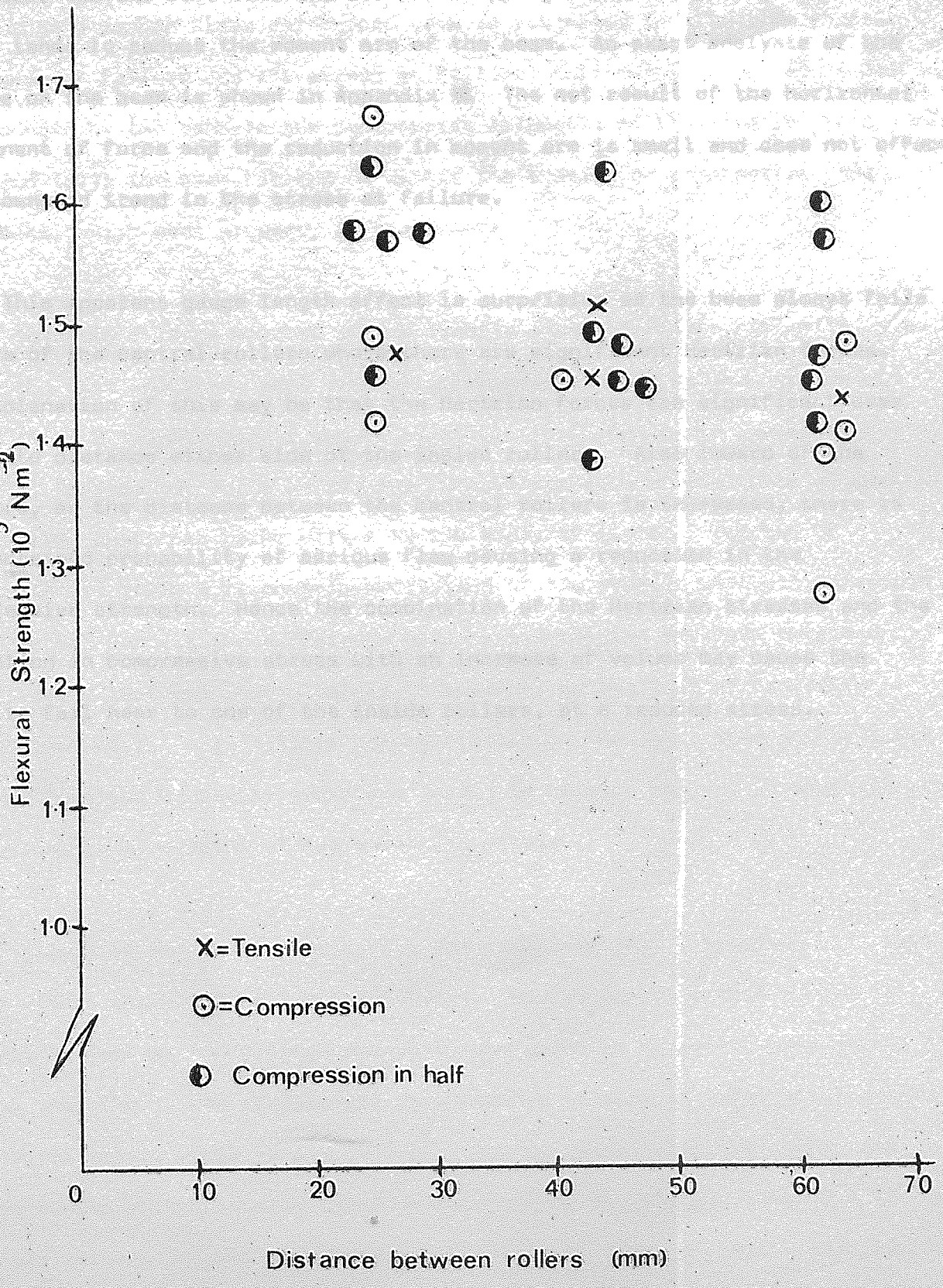

Fig.104.

As the distance between the supports is increased, the deflection increases, and the beam wraps round the support. As the beam wraps further round the support the horizontal component of the load becomes significant and the measured load, the vertical component, does not represent the true force on the beam. At the same time the beam is wrapping round the outside roller which tends to reduce the moment arm of the beam. An exact analysis of the forces on the beam is shown in Appendix VI. The net result of the horizontal component of force and the reduction in moment arm is small and does not effect the downward trend in the stress at failure.

This apparent gauge length effect is surprising as the beam always fails at one of the central rollers where there are significant Hertzian forces. An explanation of this may be that the Hertzian forces are significant over a finite distance either side of the inside rollers. Also inward of the rollers, as the distance between the central rollers is increased, there is an increased probability of serious flaw causing a reduction in the compressive strength. Hence the combination of the Hertzian stresses and the reduction in compressive stress with an increase of volume may cause the beam to fail near to one of the inside rollers, at a reduced stress.

Chapter 7

Discussion

When a carbon fibre reinforced beam is subjected to a bending stress, the mode of failure and the stress at failure, fall within an envelope which is bounded by the tensile and compressive strengths of the material (Figs. 88, 101 and 102); the beam failing on either the tensile or compressive side of the beam, which ever property is the weaker.

There is a large scatter on the tensile strength of the composite, even when the test specimens were carefully prepared and the optimum test shape used (Fig. 72). Although a number of statistical models are available (5 - 8) they do not fully define the tensile strength of the three dimensional composite, described here, with a random array of fibres. The law of mixtures (1) gives a reasonable prediction of the tensile strength, although it does not predict the difference between the tensile strength obtained by the tensile test and that obtained in bending, or the loss of composite efficiency at the higher fibre volume fractions. However, when higher fibre volume fraction composite beams are tested in bending the law of mixtures gives a reasonable prediction of their bending stress.

Figure 54 shows that there is a 95% certainty that a specimen will fail at a stress above 84% of the mean stress. Hence, assuming that a beam is likely to fail within a wedge shaped volume which is subjected to a stress above 84%, the volume of material under such a stress, in three point bending, is approximately equal to 6×10^{-6} m^3. The volume of material within the gauge length of the tensile specimen (Chapter 5) is approximately 12×10^{-6} m^3. Weibull's shape parameter (m) was found, using the results of the tensile tests of 0.5 fibre volume composites, shown in Figure 73, to be 8.3. Hudson's

analysis (59) predicts, for the above parameter and tensile stress, that the stress in bending, as a result of the reduced volume, will be 1.33 GNm^{-2}. This compares favourably to a mean of 1.34 GNm^{-2} obtained in three point bending (Fig. 88). Hence it appears that the difference in the tensile strength obtained by tests shape 4 and three point bending is mainly due to volume effects. This confirms the dependence of volume on the tensile strength as indicated in Figure 57.

As the fibre volume fraction decreased from 0.7 the appearance of the fracture face became less fibrous, and below 0.5 the specimens failed in a brittle manner (Fig. 73). When the specimens with fibre volume fractions less than 0.7 were tested in tension there was no appreciable difference in the failure stress and that predicted by the law of mixtures. This would imply that as the fibre volume fraction decreases any increase in composite efficiency, because of improved fibre-resin bonding, is off-set by the specimen becoming more brittle, with an increased possibility of a crack propagating through fibres and matrix alike (8). At 0.7 fibre volume fraction the fibre-matrix bond was weakened by increased fibre-fibre contact, which reduced the matrix's ability to transmit load from fibre to fibre, and the failure stress was lower than expected.

The dependence of the tensile strength upon the properties of the matrix is clearly shown in Figure 98 where the tensile strength is plotted against test temperature. The law of mixtures would predict that the tensile strength would be constant over the whole range of temperatures. However, when the shear modulus is significantly reduced, at the higher temperatures, the failure stress falls away to that value predicted by Coleman's bundle strength analysis (3). At the temperatures below room temperature, there appears to be a slight increase in the failure stress, although there are a few test results, this would suggest that as the matrix becomes more rigid it is able to transfer

the load more efficiently.

From the preliminary investigation to determine the optimum shape of the compressive test specimen, there was an indication of a volume effect, the compressive strength increasing as the volume decreased. For very small volumes the test specimens were very fragile and were subject to premature failure as they were being loaded in the compression fixture. This trend appears to be reinforced by the results of the tests where the flexural strength is plotted as a function of the specimen width (Fig. 69) and the distance between the rollers when tested in four point bending (Fig. 104). However, extreme caution should be taken with the four point bending tests as the fracture originated from near one of the central rollers where high Hertzian forces exist, irrespective of the distance between the central rollers.

Hudson's analysis was applied, as with the tensile results, using parameters obtained on the three point bending tests with the 13 mm nose diameter. A stress of 1.54 GNm^{-2} was predicted for the compressive test, which compares with a value of 1.12 GNm^{-2} obtained in Figure 97. Obviously, assuming Hudson's analysis to be applicable the differences in the two forms of tests cannot be explained on the basis of volume effects. There is evidence that the central roller is constraining the fibres as they buckle (Fig. 86) which will produce a higher compressive strength. (17 - 19). However, there does appear to be a volume effect, within a particular test configuration, which is possibly a result of the increased possibility of a larger volume of material containing flaws.

Hand (23) has shown that there is a relationship between voids and compressive strength; again caution should be taken when interpreting these results because, as shown in Figure 22, the interlaminar shear strength is also

dependent upon the presence of voids in the specimen, which will influence the compressive strength. A weak bond between the fibre and the matrix will allow the fibre to buckle more readily. In Figure 23 where the void content is plotted against the flexural stress at failure the mode of failure changes from tensile to compressive as the void content increases. Although little conclusive evidence has been found, because it is difficult to determine whether the compressive strength is affected directly by voidage or a reduced interlaminar shear strength, there is a strong indication that the compressive strength is dependent upon flaws as predicted by Foye (20).

Both the micro and the macro stability analysis (12 & 20) state that the compressive strength is directly proportional to the composite shear modulus. The theoretical shear modulus of the composite given by Adams and Doner (21) predicts accurately the change in torsional modulus with matrix shear modulus for the specimens tested with their fibres at 90^{o} to the axis (Fig. 95). However, because the fibres, in the longitudinal specimen, appeared to be constraining the twisting movement the theoretical plot underestimates the torsional modulus (Fig. 94).

The composite shear modulus, found by Adams and Doner's analysis, was used in Foye's equation to determine the compressive strength. This predicted a theoretical value of the compressive strength approximately four times higher than the experimental results obtained (Fig. 72). When the shear modulus is varied, the compressive strength changes as predicted by Foye but at the reduced level. This suggests that the basic theory is correct but a further factor must be considered which causes a serious reduction in the compressive strength.

Griffith's criterion (80) states when the elastic energy of a body containing a flaw is greater than the surface energy required to form two new

surfaces of a crack, the crack will propagate and the material will fail. For an isotropic material in tension Griffith showed that:-

$$\sigma \approx \sqrt{\left(\frac{\gamma E}{C}\right)}$$

where γ = surface energy

C = crack length

However, the growth of cracks is opposed in brittle, isotropic materials, which are subjected to an applied compressive stress.

For an unidirectional composite material, stressed in compression, it is possible that the propagation of 'cracks' may be explained using a modified Griffith criterion. Difficulty arises, however, in calculating the surface energy of a crack as it propagates through the fibre, matrix and their interface, and also the energy that is required in the buckling and crushing of the fibres and matrix.

From the available information, a suggested mode of failure in compression would be as follows; assuming that a flaw or void is present within the material, and as Figure 21 shows, it is almost impossible to achieve a completely void free composite. The void will act as a stress concentration and the material near to the flaw will be subjected to a stress greater than the applied stress. Lekhnitskii (46) has shown that the stress concentration factor for a circular hole, in a composite material with typical values for the elastic properties, is within the range 4 to 5. Therefore, a stress of 0.8 GNm^{-2}, which is the breaking stress of a composite with a fibre volume fraction of 0.5, would be magnified to over 3.0 GNm^{-2} at the void, which is in excess of the theoretical value for the compressive strength. This high stress would cause localised buckling around the flaw.

The second requirement for the propagation of the crack is that there is sufficient volume for the fibre and crushed matrix to buckle into. This allows the damaged material to be removed from the failure zone and provides a further volume for damaged material to occupy. If the energy absorbed in the buckling and breaking of the fibres is greater than the elastic compressive energy stored, then the failure zone will not propagate. However, if the stored elastic compressive energy is greater than the energy required to crush and buckle the composite material into the void, then further buckling will occur at the edges of the failure zone and the damaged material will buckle into the crushed region, thus producing another flaw. This process will be repeated, through the specimen, causing a rapid compressive failure.

A similar mechanism could occur at an outside surface where it would be possible for a bundle of misaligned fibres to fail in shear and buckle outwards, thus producing a failure zone which would act as a stress concentration, this, if the energy conditions were suitable, would cause compressive failure as above.

A larger reduction factor is required to fit the compressive strength of a composite with a fibre volume fraction of 0.7 to Foye's theoretical value. As before at these high fibre volume fractions the fibre-fibre contact causes a reduction in the fibre-matrix bond. Hence the fibres will be more prone to buckle under a compressive stress.

The compressive strength of the composite was derived using the values of shear modulus for the matrix shown in Figure 92. There was very good agreement between the theoretical values and the experimental results obtained, as the test temperature was increased up to 100^{o}C (Fig. 97). Above this temperature the matrix began to yield before failure, causing a reduction in the

compressive strength. Hence at these higher temperatures a yielding model of failure is required to define the mode of failure (24). However, up to a temperature of 100°C the compressive strength is directly proportional to the shear modulus of the matrix; therefore by increasing the shear modulus of the matrix, an improvement will be made in the compressive strength.

When the beam fails in compression, there is a sudden fall-off in the load as the compression crack propagates in a brittle manner. This mode of failure is undesireable as very little energy is absorbed by the crack as it moves through the beam. When a beam fails in tension, small groups of fibres begin to fracture on the outer surfaces of the beam. When the outer layer has failed, more and more bundles of fibres, near to the centre of the beam begin to fracture. Finally, when the net cross sectional area of the beam can no longer support the load, the beam will fail. This gradual failure gives a saw tooth appearance to the stress-strain curve as the load is slowly being shed as bundles of fibres fail. Hence there is a greater area under the stress strain curve for the beam which fails in tension rather than in compression, indicating a greater amount of energy is being dissipated as individual bundles of fibres fail in tension. Although the nature of tensile failure for this particular composite system is brittle, because of the gradual load shedding, which absorbs energy, the tensile failure can be considered to be a pseudo-ductile mechanism.

The tensile failure of a beam in bending is therefore desirable for two reasons. The first is that because under impact conditions, for example bird ingestion into a jet engine with composite fan blades, the material will be able to absorb more energy as it is failing. Secondly because the compressive failure is heavily dependent upon a number of variables, such as interlaminar shear strength, voidage, matrix and fibre moduli, it is very difficult to control, whereas the strength of the beam failing in tension is mainly

dependent upon the strength and the position of the fibres which are more controllable. Hence it is necessary to identify the variables which affect the compressive failure with the aim of improving the compressive strength of a composite beam to a value above its tensile strength.

The role of the interface between the fibres and the matrix is of great importance. Consider Figure 68, a plot of the flexural strength against the aspect ratio. At the low aspect ratios, where the interlaminar shear stresses are high, the composite material failed in shear. At an aspect ratio of 30 to 1 the specimens failed in the compressive region with the crack running up to near the neutral axis. At the same time an interlaminar shear crack was opening up in the region of high shear strength, centred on the neutral axis. When the compression crack ran into the interlaminar shear crack it was stopped. Therefore, a similar mechanism to the Cook Gorden appears to operate (32), with the compressive crack being stopped by the failed interface.

Higher aspect ratio beams fail in compression but, because the shear stresses imposed on the beam are much lower, the interlaminar cracks do not open up and hence the compression crack is able to propagate through the beam in a brittle manner.

The beams of different aspect ratios were produced from the same material moulded under similar conditions, therefore they should all contain similar flaw distributions. Hence the specimens tested with an aspect ratio of 30 : 1 should have the same theoretical compressive strength as the beams tested with an aspect ratio of 40 : 1. However the beams with the shorter span failed at a stress of 1.34 GNm^{-2} in compression, which was lower than the failure stress of the 40 : 1 aspect ratio beams (1.63 GNm^{-2}). The average load to failure, for the beams with an aspect ratio of 30 : 1 was 48 Kg compared

to 45 Kg for those with an aspect ratio of 40 : 1, a difference of approximately 6%. Whereas the difference in the failure stress was over 20%. Hence this would suggest that the difference in failure stress is not completely explained by increased Hertzian pressures, and that the high shear stresses, in the shorter beams, may also be a contributing factor in reducing the compressive strength of a composite material.

Unfortunately, because the interlaminar strength and the compressive strength are so directly linked, it is very difficult to separate the two variables. One way that this may be done would be to compare the compressive strength of two composite materials with matrices of different intrinsic interlaminar shear strengths with the same shear moduli thus ensuring the same theoretical compressive strength. However, at the time of this project no such polymers were available.

Chapter 8

Conclusion

8.1 Flexural strength and failure mechanisms

8.1.1 Failure mode

When a beam is subjected to a bending stress it will fail in either the tensile or compressive faces, which ever is the weaker of the two properties.

8.1.2 Tensile failure

When the tensile strength, of the beam, is lower than the compressive strength it will fail in a tensile manner. As a beam with a fibre volume fraction of 0.5 and above, begins to fail the load is slowly shed as individual and groups of fibres are failing within a layer. This produces a controlled failure with a large area under the stress strain curve as energy is being absorbed by the failure of individual groups of fibres.

8.1.3 Flexural strength of beams failing in tension

The "law of mixtures" prediction of the tensile strength underestimates the flexural strength of the specimens which fail in tension, except at the high fibre packing densities where there does appear to be a loss of composite efficiency due to a large amount of fibre-fibre contact. However, at the lower fibre volume fractions it has been shown that a volume effect may be responsible for the higher stress at failure, obtained in the bending tests.

8.1.4 Compressive failure

If the beam has a higher tensile strength than compressive strength, the beam fails in the compressive area of the beam. The crack is initiated in the regions of high stress, on the outer surface, near to the central roller, and propagates rapidly, in a brittle manner, up to the neutral axis. If the high interlaminar shear stress, near to the neutral axis, causes shear failure then the crack will be stopped by this region of delamination. However, if there is no shear failure then the crack propagates up through the former neutral axis, reducing the aspect ratio, until finally the beam can no longer carry the load and fails instantaneously in tension.

As failure takes place there is a sudden drop in the stress-strain curve and little energy, compared to the tensile failure, is absorbed by the beam as it fails.

8.1.5 Flexural strength of beams failing in compression

A factor of 0.37 is required to fit the theoretical prediction of Foye to the bending stress of failure, except at the higher fibre packing densities where a factor of 0.27 was required. This is a further indication of a loss of a composite efficiency with increased fibre-fibre contact. Again the stress at failure is higher than the stress at failure obtained from the normal compressive test; however the evidence suggests that this may only in part be explained by a size effect, the main reason being the different test configuration.

8.2 Tensile behaviour

8.2.1 Fibre properties

The tensile strength of a composite material, in the direction of the fibres, is heavily dependent upon the properties and the volume of the fibres.

8.2.2 Fibre volume effects

As the fibre volume fraction increases, the mode of failure changes from brittle at very low fibre densities to the 'controlled' fibrous failure at fibre volume fractions of 0.5 and above.

8.2.3 Tensile strength

The 'law of mixtures' accurately predicts the tensile strength except at the high fibre volumes where fibre-fibre contact weakens the matrix-fibre interface, reducing the load transferring efficiency of the composite.

8.2.4 Effects of the matrix stiffness

As the matrix stiffness is reduced by increasing test temperature there is a slight decrease in the tensile strength. When the test temperature is near to the softening point of the matrix the composite no longer is able to transfer load from fibre to fibre, and it behaves as a bundle of fibres.

8.3 Compressive behaviour

8.3.1 Failure mode

The stress-strain curve was linear up to failure, where there was a sudden drop in load. At failure the matrix is unable to support the fibres and they

all buckled in one direction failing at the extremities of the buckle.

8.3.2 Compressive strength

A factor of 0.25 is required to fit Foye's prediction, using a macrostability model, to the tests results. This factor of 1:4 is similar to the stress concentration factor at a circular flaw i.e. void, in the composite. Therefore it is probable that the compressive failure commences at a flaw in the composite, as fibres buckle into the void, producing a larger damaged area. This new area of damage in turn causes a stress concentration and a failure region propagates through the material.

8.3.3 Shear modulus of the matrix

Any change in the compressive strength is directly proportional to a change in the modulus of the matrix. As the test temperature increased from sub zero the shear modulus and compressive stress decreased. Near to the softening point of the resin, the matrix was unable to support the fibres, even at low loads, and a yielding model for failure is required to define the compressive failure.

8.3.4 Volume effects

Only slight evidence exists of a size effect with the compressive mode of failure. The difference in the bending and the compression test results are attributed to different test geometries, and in particular the effect of the central roller in the three point bending test. The central roller tends to support the matrix, in the highly stressed regions, which are also supported by layers of lower stress near to the neutral axis. Also Hertzian pressures, under the central roller, cause localised shear and compressive stresses which

may initiate a compressive crack.

8.3.5 Fibre volume effects

The macrostability model predicts that the higher the fibre packing density the higher the compressive strength. At the higher fibre volume fractions Foye's theoretical prediction, using a reduction factor of 0.25, overestimates the compressive strength. Again, this is because of increased fibre-fibre contact which is reducing the support of the fibres.

8.4 Application of Results

When a composite beam is subjected to bending stresses, as under impact, more energy will be absorbed, if it fails in tension, also failure is more controllable. To ensure this, the compressive strength must be improved so that it is higher than tensile strength. The compressive strength can be increased by removing all the flaws or by improving the shear modulus of the matrix. Any increase in shear modulus will also bring about a slight improvement in the tensile properties. The optimum fibre volume fraction is within the range 0.5 - 0.6. Below this the fibres are well bonded to the matrix and once a crack is initiated it will propagate rapidly through the matrix in a brittle manner. At high fibre packing densities, increased fibre-fibre contact reduces the bond between the fibre and matrix, consequently the matrix is less efficient at transferring the load from fibre to fibre or supporting the fibres under a compressive load.

Care must be exercised when operating composite structures at elevated temperatures, because near to the softening point of the matrix, the load is not transferred from fibre to fibre and the composite behaves as a bundle of fibres.

Chapter 9

Suggestions for further work

9.1 Theoretical

For both the tensile and compressive modes of failure very little theoretical work has been completed to predict the mode of failure and strength of three-dimensional composite materials with a random array of fibres. At the time of this project the major studies of the theoretical aspects of strength were limited to two dimensional planer composites with a uniform array of fibres. To be able to understand completely the failure mechanisms of composites, when they fail in tension and compression, and how they combine in the complex bending failure mechanism, it is necessary to have a rigorous theoretical basis for any future work.

9.2 Experimental

Difficulty was experienced in separating the effects of voidage. Whether they affect the compressive strength directly or reduce the interlaminar shear strength and thus weaken the support of the fibres as they buckle is not clear. To separate these two variables it is necessary to conduct extensive tests on materials of widely different interlaminar shear strengths of constant voidage and specimens keeping the interlaminar shear strength constant and varying the voidage. Voidage measurement requires careful consideration, as the disadvantage to the method described in Chapter 3 is that the area measured is some distance away from the gauge length under load.

The compressive strength of a composite material can be improved by increasing the shear modulus of the matrix. Limited variations in modulus were obtained by varying the test temperature, and significant improvement of compressive strength may be obtained by including fillers in the matrix to support it as the fibres tend to buckle. Foyle (20) considered this possibility and it may be extended by including, in the matrix, larger diameter fibres of either carbon or any other material, which are more stable under compressive loading and are able to support the matrix as it constrains the fibres from buckling.

Work is required to be completed to determine the energy required to crush the fibres and matrix so as to give the suggested mode of failure (Chapter 7) a mathematical basis. Previous work has considered the energies required for the three standard fracture modes, opening mode, forward shearing mode and parallel shearing mode. The work of the project appears to suggest that a compression buckling mode should also be considered for composite materials.

Before the bending failures can be related to the impact failure, it will be necessary to determine the effects of the central roller on the stress at failure and the failure mode. The analysis, for isotropic materials, used in this project, to determine the Hertzian pressures, can only give an indication of the type of stress situation present at the roller. Stress analysis techniques on this type of material may prove to be complex, and useful information can be obtained by using photoelastic methods. A photoelastic coating could be bonded onto the surface of the beam under a stress, and the stress distributions around the central roller may be observed under polarised light.

Finally the conclusions of this report should be related to the impact loading condition, the mode of failure being observed as the compressive strength of the specimen is improved by improving the matrix shear moduli either by different resin systems or by reinforcing the matrix with fillers or fibres of larger diameters.

APPENDIX I

The Generalised Hooke's Law

The stresses σ_{ii} are normal components ard the stresses τ_{ij} are shear components.

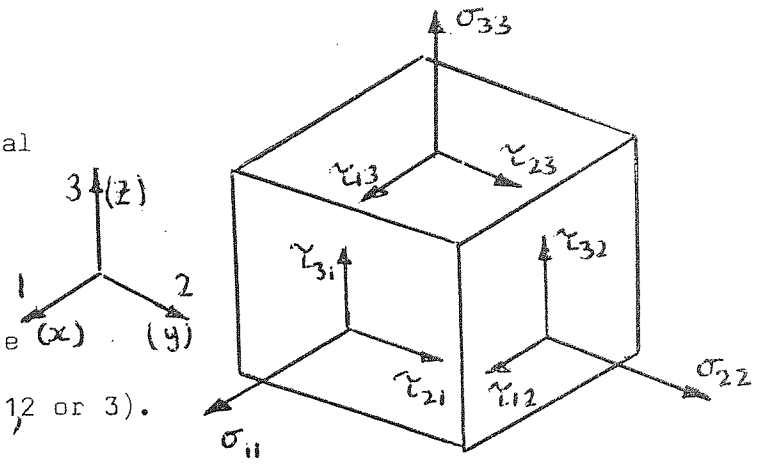

These stress components will cause strain at a point ϵ_{ij} (ij = 1, 2 or 3).

Hooke's law can be expressed:-

Each stress component is directly proportional to each strain component or in symbols

$$\tau_{ij} = C_{ijkl}\,\epsilon_{kl} \quad - (1) \quad \text{ijkl} = 1, 2, 3$$

and

$$\epsilon_{ij} = S_{ijkl}\,\tau_{kl} \quad - (2)$$

As these equations stand there are 81 stiffnesses and compliences but because $\tau_{ij} = \tau_{ji}$ + $\epsilon_{ij} = \epsilon_{ji}$ this number is reduced to 36 also it can be shown that $C_{ijkl} = C_{klij}$ and $S_{ijkl} = S_{klij}$ which reduce the number of independent stiffnesses to 21 in the most general case.

Expand (2)

$$\epsilon_{11} = S_{1111}\sigma_{11} + S_{1122}\sigma_{22} + S_{1133}\sigma_{33} + 2S_{1112}\tau_{12} + 2S_{1113}\tau_{13} 2S_{1123}\tau_{23}$$

$$\epsilon_{22} = S_{2211}\sigma_{11} + S_{2222}\sigma_{22} \quad - - - - - - - - - - - -$$

$$\epsilon_{12} = S_{1211}\sigma_{11} \quad - - - - - - - - - - - - - -$$

This is a very long winded notation which can be simplified by letting:-

$$\sigma_{11} = \sigma_1 (\sigma_x) \quad , \quad \sigma_{22} = \sigma_2 (\sigma_y) \quad , \quad \sigma_{33} = \sigma_3 (\sigma_z)$$

$$\tau_{23} = \tau_4 (\tau_{yz}) \quad , \quad \tau_{13} = \tau_5 (\tau_{xz}) \quad , \quad \tau_{12} = \tau_6 (\tau_{xy})$$

and

$$\epsilon_{11} = \epsilon_1 (\epsilon_x) \quad , \quad \epsilon_{22} = \epsilon_2 (\epsilon_y) \quad , \quad \epsilon_{33} = \epsilon_3 (\epsilon_z)$$

$$2\epsilon_{23} = \epsilon_4 (\gamma_{yz}) \quad , \quad 2\epsilon_{13} = \epsilon_5 (\gamma_{xz}) \quad , \quad 2\epsilon_{12} = \epsilon_6 (\gamma_{xy})$$

NOTE These are tensor shear strains not engineering strain. Hence the generalised Hooke's law becomes:-

$$\tau_q = C_{qr} \epsilon_r$$

$$\epsilon_q = S_{qr} \tau_r \qquad (q, r = 1, 2, 3, 4, 5 \text{ or } 6)$$

which we can now expand.

$$\epsilon_1 = S_{11}\sigma_1 + S_{12}\sigma_2 + S_{13}\sigma_3 + S_{14}\tau_4 + S_{15}\tau_5 + S_{16}\tau_6$$

$$\epsilon_6 = S_{61}\sigma_1 + S_{62}\sigma_2 + S_{63}\sigma_3 + S_{64}\tau_4 + S_{65}\tau_5 + S_{66}\tau_6$$

Therefore the above can be summarised as follows:-

(1) Sqq (q = 1, 2 or 3) relates an extensional strain to an extensional stress both in the same plane.

(2) Sqr (q r, q r = 1, 2 or 3) relates an extensional strain to a perpendicular extensional stress.

(3) Sqr (q = 1, 2 or 3, r = 4, 5 or 6) relates an extensional strain to a shear stress in the same plane or it can relate an extensional strain to a shear stress in a perpendicular plane.

(4) Sqq (q = 4, 5 or 6) relates a shear strain to a shear stress in the same plane.

(5) Sqr (q ≠ r, q,r = 4, 5 or 6) relates a shear strain to a shear stress in a perpendicular plane.

Transverse isotropy (Hexagonal)

An unidirectional composite is assumed to be transversely isotropic. By letting the fibres be in the (3) direction we have

$$\epsilon_1 = S_{11}\sigma_1 + S_{12}\sigma_2 + S_{13}\sigma_3$$

$$\epsilon_2 = S_{21}\sigma_1 + S_{22}\sigma_2 + S_{23}\sigma_3$$

$$\epsilon_3 = S_{31}\sigma_1 + S_{32}\sigma_2 + S_{33}\sigma_3$$

$$\gamma_4 = S_{44}\tau_4$$

$$\gamma_5 = S_{55}\tau_5$$

$$\gamma_6 = S_{66}\tau_6$$

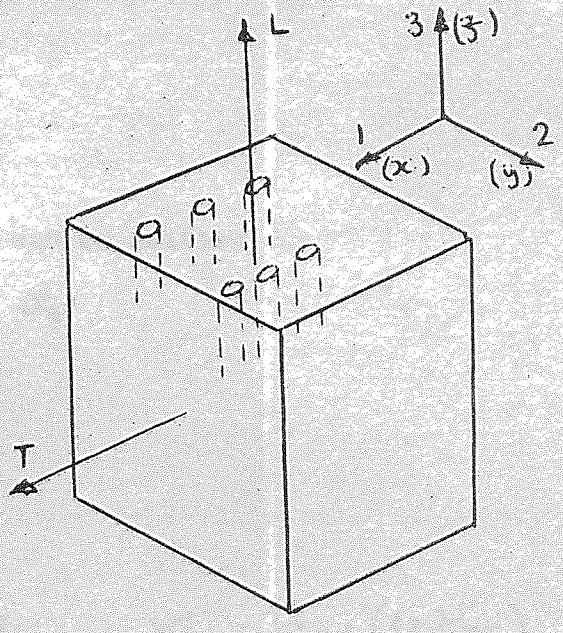

Hence we have 12 elastic constants which reduces to 5 independent elastic constants because:-

(1) Symmetry $S_{12} = S_{21}$ $S_{13} = S_{31}$ $S_{23} = S_{32}$

(2) Assuming the properties to be the same in the 1(X) and 2(Y) planes

$$S_{13} = S_{32} \qquad S_{22} = S_{11} \qquad S_{44} = S_{55}$$

(3) Because of isotropy in the 1, 2 planes $S_{66} = 2(S_{11} - S_{12})$.

Rewriting above in the X-Y- notation we have:-

$$\epsilon_x = S_{11}\sigma_x + S_{12}\sigma_y + S_{13}\sigma_z$$

$$\epsilon_y = S_{12}\sigma_x + S_{11}\sigma_y + S_{13}\sigma_z$$

$$\epsilon_z = S_{13}\sigma_x + S_{13}\sigma_y + S_{33}\sigma_z$$

$$\gamma_{yz} = S_{44}\tau_{yz}$$

$$\gamma_{xz} = S_{44}\tau_{xz}$$

$$\gamma_{xy} = 2(S_{11} - S_{12})\tau_{xy}$$

By introducing engineering constants this can be written

$$\epsilon_x = \frac{1}{E_T}(\sigma_x - \nu_{TT}\sigma_y) - \frac{\nu_{TL}}{E_L}\sigma_z$$

$$\epsilon_y = \frac{1}{E_T}(\sigma_y - \nu_{TT}\sigma_x) - \frac{\nu_{TL}}{E_L}\sigma_z$$

$$\epsilon_z = -\frac{\nu_{LT}}{E_T}(\sigma_x + \sigma_y) + \frac{\sigma_z}{E_L}$$

$$\gamma_{yz} = \frac{\tau_{yz}}{G_{LT}}, \qquad \gamma_{xz} = \frac{\tau_{xz}}{G_{LT}}, \qquad \gamma_{xy} = 2\frac{\tau_{xy}}{E_T}(1+\nu_{TT})$$

where $S_{11} = S_{22} = 1/E_T$, $S_{33} = 1/E_L$

$$S_{13} = \frac{-\nu_{LT}}{E_T} = -\frac{\nu_{TL}}{E_L}, \qquad S_{12} = -\frac{\nu_{TT}}{E_T}$$

$$S_{44} = S_{55} = 1/G_{LT}, \qquad S_{66} = 1/G_{TT} = \frac{2(1+\nu_{TT})}{E_T}.$$

APPENDIX II

1. Chemistry

The resin system used in the earlier part of this work was an epoxylated novalac resin, Araldite LY558, produced by C.I.B.A., LY558 was used with a Boron triflouride monethylamine curing agent, Sheet Epicure $BF_3$400.

1.1 Epoxylated Novalac

Novalac resins are produced by the reaction of phenol and formaldehyde in acid solution. Such resins have the following idealised structure:-

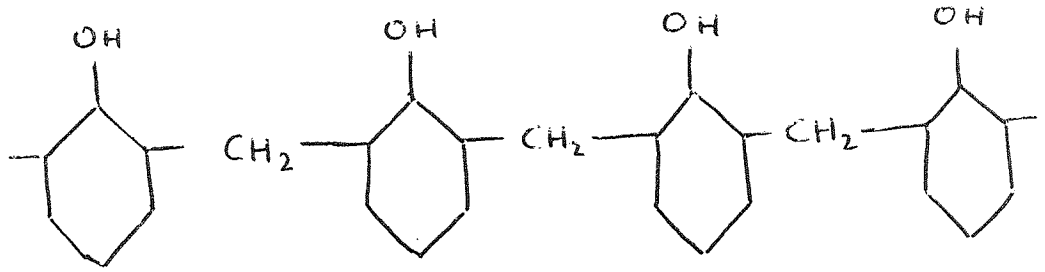

The novalac-based epoxy resins are synthesised by reaction with epichlorohydrin

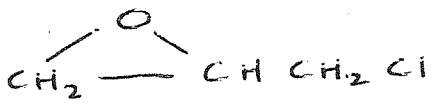

to form epoxylated phenol-formaldehyde novalac resin.

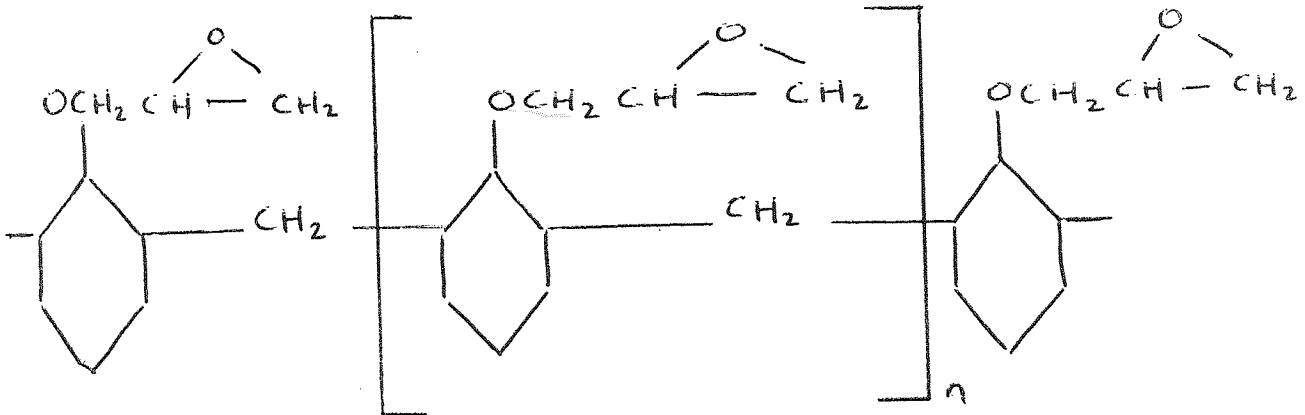

LY558 has been shown, by comparing the I.R. spectra obtained from a sample of LY558 to the I.R. spectra quoted in the 'Handbook of Epoxy Resins' by Lee and Nevill (40), to have a similar structure to the one above, with n = 1.6.

Theoretically all the phenolic hydroxyls may be reacted, but in practice selective expoxidation offers an advantage, and its importance will be demonstrated later.

Commercially preferred epoxidised novalacs have epoxy functionalities from 3 to 5. (Functionality is defined as the number of reactive sites within the molecule which will participate in the cross-linking of the polymer chain). The LY558 system has a functionality of 3.6.

With epoxy resins high functionalities will give improved thermal resistance and solvent resistance. However there is an upper limit in the functionality, where any increase beyond this limit does not necessarily mean increased thermal properties (40).

Epoxidised novalacs having higher functionalities than three are extremely viscous liquids, virtually immobile at room temperature. On heating, however, the viscosity reduces sharply and solventless systems may be formulated.

<u>BF_3 MEA (Boron trifluoride monethylamine)</u>

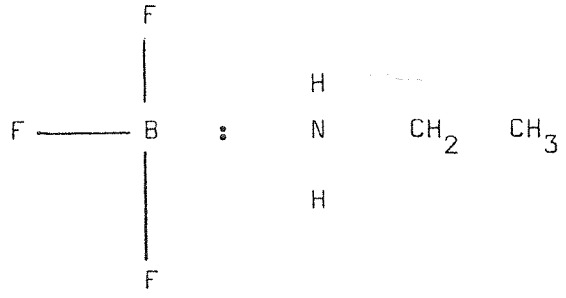

BF_3 MEA is an association of Boron trifluoride and monoethylamine on a one to one molecular basis. At room temperature it is a yellowish-white cyrstalline solid which melts close to its dissociation temperature (approximately 90°C). Upon exposure to moist air it hydrolyses to a viscous liquid, unsuitable as a curing agent.

Preparation of the LY558 - BF_3 400 system

(a) The LY558 was heated to 80°C to reduce its viscosity to a level where it could be readily handled. An amount was weighed.

(b) The LY558 was allowed to cool, as it was cooling it was mixed with acetone, to reduce the viscosity.

(c) Four parts per hundred (by weight) of the BF_3 400 were mixed with acetone.

(d) When the LY558 acetone system was at room temperature it was thoroughly mixed with the $BF_3$400 acetone system.

(e) The LY558 - BF_3 400 system was further diluted with acetone to a density of 0.873 g/ml.

The resin was diluted with acetone to reduce its viscosity at room temperature to such a level that during the impregnation process the fibres were completely wetted with resin.

There was no evidence to suggest that the acetone reacts with the resin to degrade its properties, however the acetone may contain impurities which will react with the resin.

Curing Mechanisms

The most valuable single property of the epoxy resins is their ability to

transform readily from the liquid (or thermoplastic) state to tough, hard thermoset solids. The conversion normally occurs without the evolution of by products.

The conversion is accomplished by the addition of a chemically active compound known as a curing agent (hardener, activator or catalyst). Some curing agents (including BF_3 MEA) promote curing by catalytic action, others participate directly in the reaction and are chemically bound into a resin chain. Depending on the particular agent, curing may be carried out at room temperature, with heat produced by exothermic reaction, or it may require application of external heat.

The epoxy ring 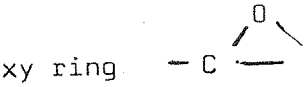 will differ in reactivity, depending on whether it is terminal, internal, or ring-situated. Suitably located and under proper conditions it has been found to be highly reactive.

Basically the cured structure may be a homopolymer (one composed essentially of epoxy resin molecules linked together through their own reactive sites) or heteropolymer (one composed essentially of epoxy resin molecules linked together through the reactive sites of the curing agents) or a mixture of both types. The LY558 - BF_3 400 cured system is essentially a homopolymer.

In epoxy resin technology, the degree of cure has, by custom, come to refer to the extent to which the epoxy groups have been consumed, and when present, the extent of consumption of the reactive groups in the curing agent. For practical purposes a thoroughly cured system is considered one in which the degree of crosslinking is sufficient to provide optimum physical properties for a particular application. During the cure two phenomena are involved, conversion, (the disappearance of the reactive groups) and more

important production of networks through reactive sites to form the desired thermoset resins.

The Lewis acids which are capable of catalising the polymerisation of epoxy resins are those with unfilled orbitals in their outer shells. They are attracted to areas of increased electron density. The reaction may proceed in the simplified form as follows:-

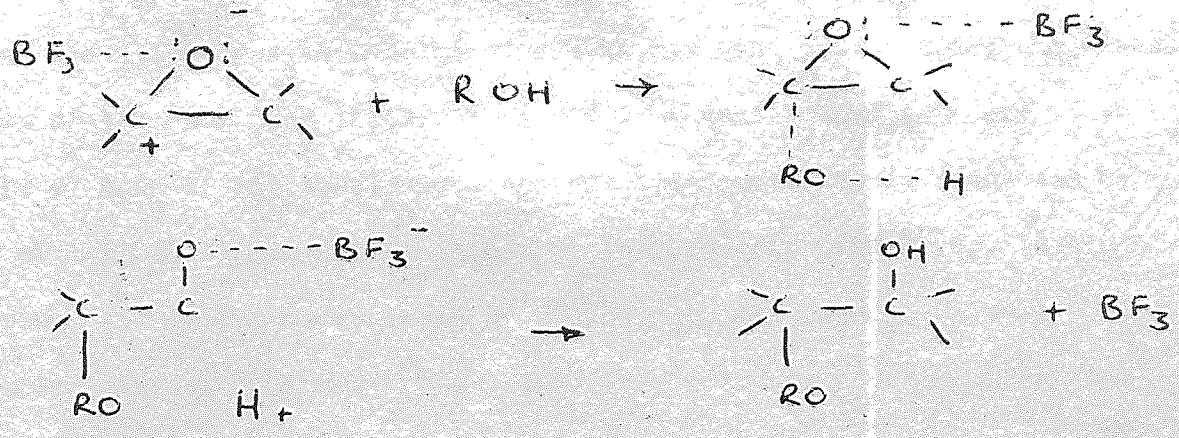

The group then becomes R in the hydroxyl at the beginning of the reaction and thus proceeds through the reaction forming a cross link.

The initial hydroxyls are probably phenolic hydroxyls from the starting novalac which forms the LY558 in which case

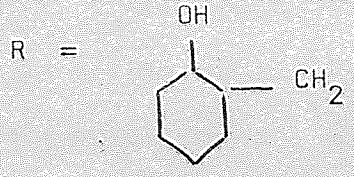

Another possibility is that the hydroxyls are from trace moisture in the system then R would be H_2O.

At temperature above the dissociation temperature of BF_3 and MEA the BF_3 is released to commence the curing reaction. The monoethylamine can

initiate cure, but because of the small proportion present in the system, the amount of epoxy rings it reacts with are insignificant. From the reaction therefore it can be seen that the only by-product of the curing reaction is BF_3, which comes off in the form of a gas.

The exact chemical analysis of HR4C is not known, except that it has an epoxy base an incorporates polysulphanes. Cure is initiated by a BF_3 amine complex.

APPENDIX III

Test Procedures

1. Dynamic Modulus

The analysis of a vibrating beam has been used to determine the dynamic modulus of anisotropic materials by various workers (82-84). In this work a Bruel and Kjaer complex modulus apparatus was used to determine the flexural modulus of the specimens (Figs. 105 & 106). A small metal shim was stuck to one end of each of the specimens. The specimens were freely suspended by two loops of thread with the metal shim over the magnetic transducer. A signal generator, with a frequency range of 20 Hz to 20 KHz powered by an acoustic horn which excited the beam. The signal frequency was adjusted until the beam was vibrating at one of its resonant frequencies, indicated by a signal peak on the level indicator of the receiving amplifier. To check which mode the beam was resonating in, fine sand was sprinkled on to the beam. The sand vibrated towards the mode points and after a short time the mode of vibration could be clearly seen (Fig. 107). The position of the thread did not appear to affect the resonant frequency.

Accurate measurements were taken of the beams. An average of 30 measurements of the depth, and 10 of the breadth of each beam was measured with a 0-1 inch micrometer, and the beam lengths were measured by means of 0-12 inch vernier calliper. The need for extreme accuracy, particularly with depth measurements, will be demonstrated later.

The flexural modulus of the beams were calculated from the formula:-

$$E_D = C_n \frac{Ws}{b} \left(\frac{L}{d}\right)^3 f_n^2 \quad - - - \quad 1 \qquad (82)$$

Fig.105. Bruël and Kjaer complex modulus apparatus.

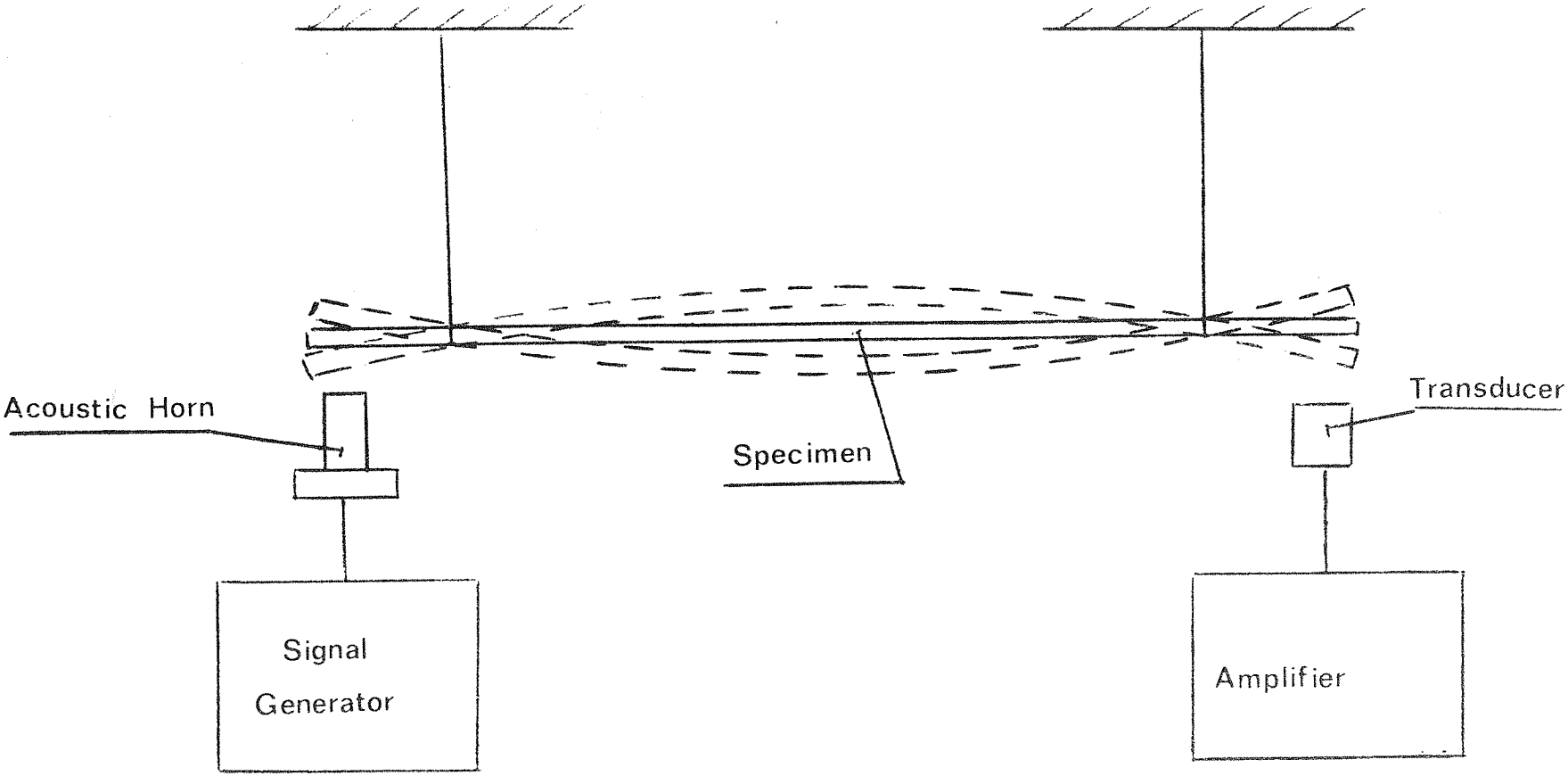

Fig.106. Dynamic modulus apparatus.

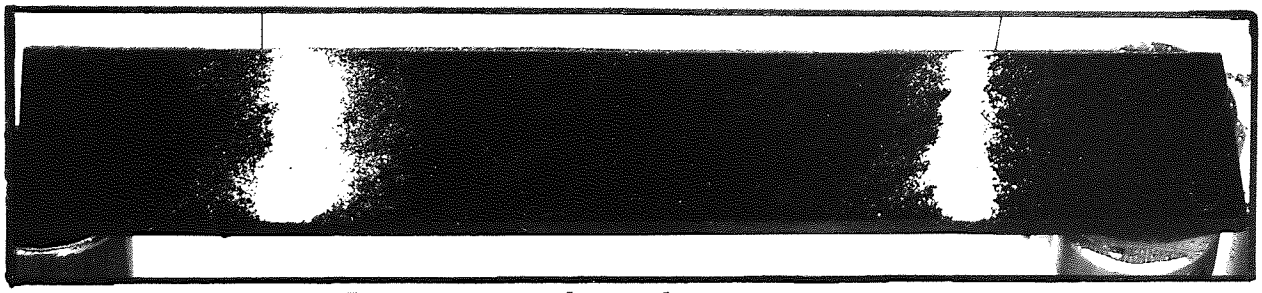

1st Flexural mode.

1st Torsional mode.

Fig.107. NODAL PATTERNS FOR RESONANT BEAMS.

where E_D = Dynamic Young's modulus of the beam

L = Specimen length

b = Specimen width

d = Specimen depth

W_s = Specimen weight (including the weight of the shims)

f_n = Frequency

C_n = Constant

The experimental errors have been calculated to be:-

$$\frac{E_D}{E_D} = \pm \left[\frac{\Delta W_s}{W_s} + \frac{3\Delta L}{L} + \frac{2\Delta f}{f} + \frac{\Delta b}{b} + \frac{3\Delta d}{d} \right.$$

$$= \pm \quad 0.005 + 0.086 + 0.25 + 0.1 + 3.0$$

$$= \pm \ 3.4$$

As can be seen the main cause of experimental inaccuracy ($\pm$ 3%) is in the measurement of the depth of the beam.

1.1 The effect of aspect ratio on measured dynamic Young's modulus

The basic theory of a vibrating beam (83) demands that the beam is long and slender. To study the effect of aspect ratio on the measured dynamic modulus, three specimens with a fibre volume fraction of 0.7 and measuring 180 mm x 13 mm x 3 mm were tested and the dynamic Young's modulus measured as above. Each of the beams was reduced in length, down to 50 mm in intervals of 13 mm. At each length the modulus was determined from the beam's fundamental flexural resonant frequency using equation (1). The modulus is plotted against aspect ratio in Figure 108. At aspect ratios below approximately 40 : 1 there was a fall off in the measured value of modulus. This suggests that for carbon fibre-resin composites, equation (1) was only true for beams with aspect ratios greater than 40 : 1.

Dynamic Young's modulus v. aspect ratio.

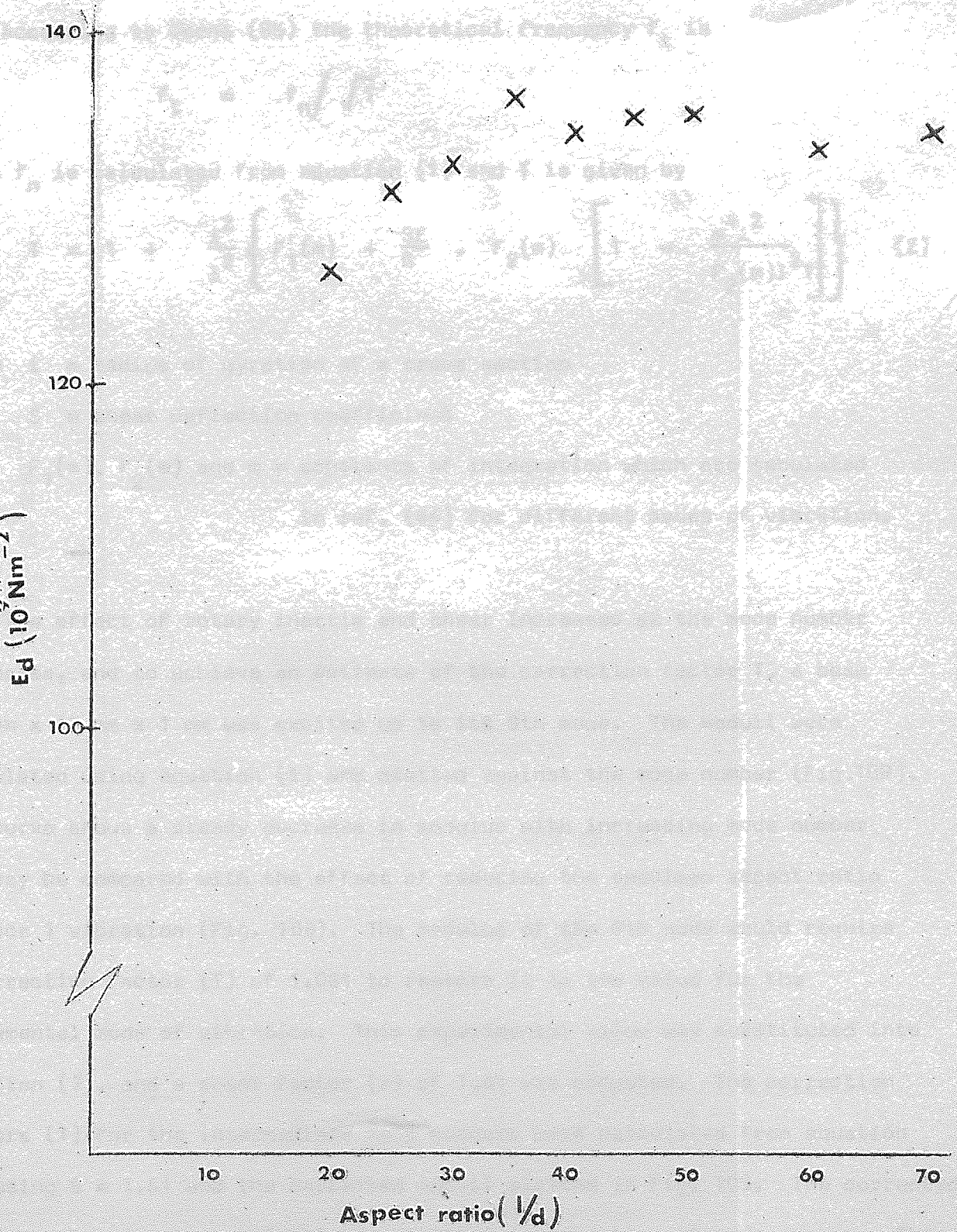

Fig. 108.

1.2 The effect of shear and rotary inertia on the flexural vibration of a beam

The existence of shear and rotary inertia leads to a reduction in the frequency of flexural vibration of wooden beams (84).

According to Goens (85) the theoretical frequency f_t is

$$f_t = f_n / \sqrt{T}$$

where f_n is calculated from equation (1) and T is given by

$$T = 1 + \frac{i^2}{l^2}\left\{F_1(m) + \frac{SE}{G} \cdot F_2(m)\left[1 - \frac{m^4 i^2}{F_2(m) l^2 T}\right]\right\} \quad (2)$$

where i = radius of gyration of a cross section

S = shear deflection coefficient

$F_1(m)$, $F_2(m)$ and m = constants of integration which are tabulated in ref. (84) for different modes of vibration.

The effect of rotary inertia and shear increases as the mode number increases, and to achieve an estimate of the correction factor T, a beam 150 mm x 13 mm x 1 mm was excited up to its 8th mode. The moduli were calculated using equation (1) and plotted against the mode number (Fig.109). The curve shows a steady decrease in modulus with increasing mode number and may be compared with the effect of reducing the specimen aspect ratio on mode 1 vibration (Fig. 108). The modulus of the 8th mode would require a correction factor (T) of 1.081 to restore it to the value for the fundamental mode of vibration. This experimental value was substituted into equation (2), and a shear factor (s) of 1.61 was computed. The correction factors (T) for the intermediate mode numbers were calculated from equation (2) using S = 1.61 and the corrected moduli plotted in Fig. 109. The corrected modulus value is now substantially constant irrespective of mode number. This

Dynamic Young's modulus v. Mode number.

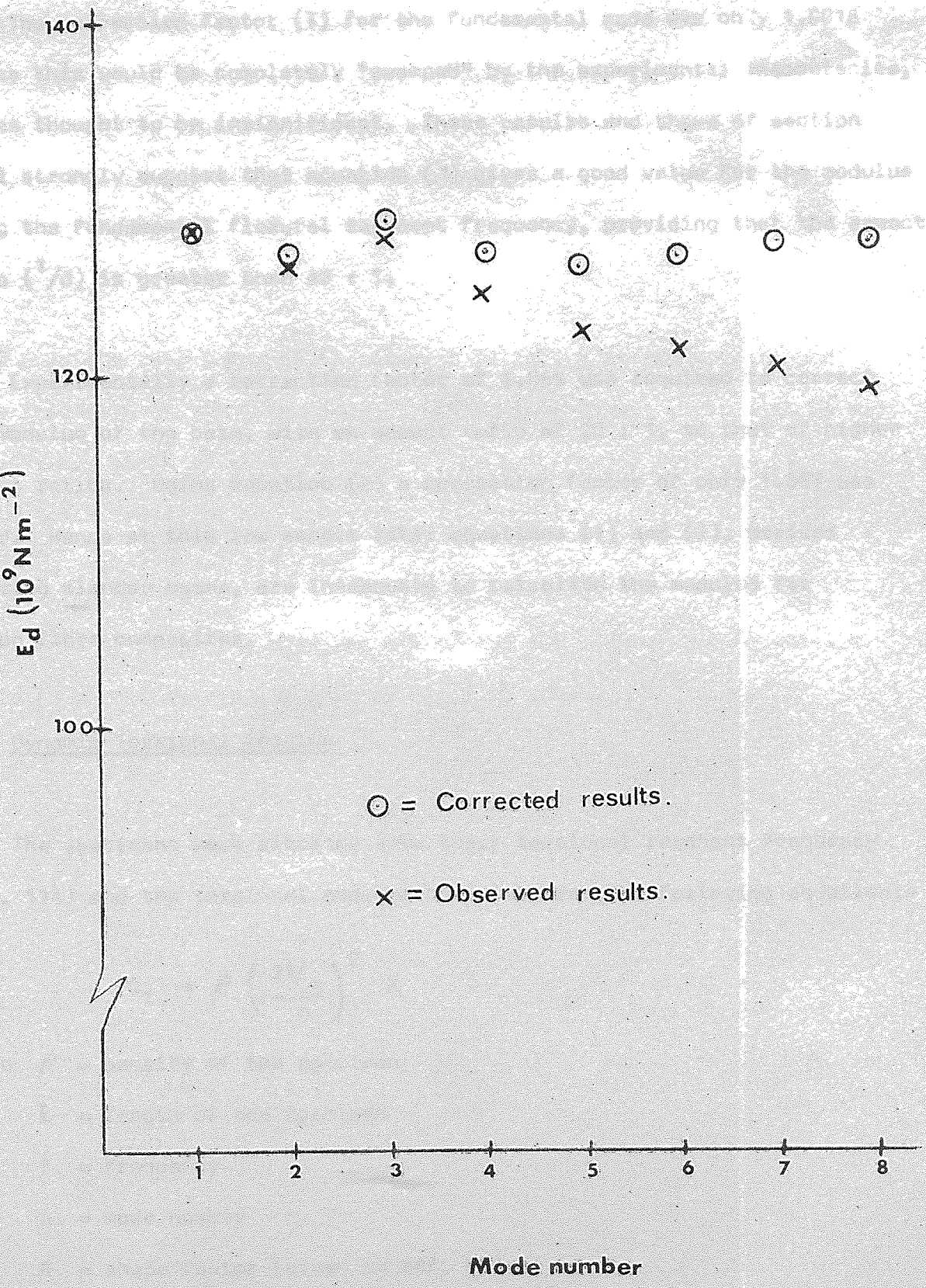

Fig. 109.

experiment was repeated with the two other specimens and the moduli determined using a shear factor of 1.61 and again there was a good agreement between the moduli computed for different mode numbers.

The correction factor (T) for the fundamental mode was only 1.0016 and as this would be completely "swamped" by the experimental inaccuracies, it was thought to be insignificant. These results and those of section 6.1.1 strongly suggest that equation (1) gives a good value for the modulus using the fundamental flexural resonant frequency, providing that the aspect ratio ($^{l}/_{d}$) is greater than 40 : 1.

Experimentally a correction factor of 1.065 was required to correct the modulus of the beam, with an aspect ratio of 20 : 1, to that of higher aspect ratios. Using equation (2) a correction factor of only 1.007 was found. Hence at this low aspect ratio equations (1) and (2), derived assuming slender beams, are inadequate to calculate the modulus for carbon fibre composites.

2. Dynamic Torsional modulus

The specimens were vibrated into their torsional resonant frequency (Fig. 114) and the torsional modulus computed from the following equation:-

$$G_T = \rho \left(\frac{2lf_n}{n} \right)^2 R$$

where ρ = density of the specimen

l = length of the specimen

f = frequency

n = mode number

R = shape factor (given in Ref. 82).

3. Interlaminar shear strength

The short beam test is a convenient means of measuring composite shear strength, being simple to execute and requiring only a small amount of material for each test piece. It is subject to an ASTM standard (86) and consists of a short beam with a typical aspect ratio (span/thickness) of between 4 and 10, tested in 3 point bending. The classical expression for the maximum shearing stress along the neutral surface of a bent beam.

$$\tau = 3F/4bd$$

Where F is the load borne by the central roller, b is the breadth and d the thickness of the test piece. The specimen aspect ratio must be kept sufficiently small so that the compressive and tensile stresses in the top and bottom surfaces of the specimen,

$$\sigma = 3F\ell/2bd^2$$

where ℓ is the specimen span, do not exceed the compressive or tensile strengths of the material before it fails in shear.

APPENDIX IV

Precuring and moulding in a vacuum

If voidage is caused by pockets of gas, whether air or volatiles, trapped between the laminates, then it can be argued that this would be removed more effectively if the precure operation was conducted at low pressures.

A series of mouldings were produced using the following precure cycle.

(a) The specimens were placed in a vacuum oven at the required temperature.
(b) Over a period of two minutes air was pumped out of the oven by a rotary pump.
(c) One minute from the end of the precure cycle the oven was slowly brought back to atmospheric pressure.
(d) The precure time was the total time the specimen was in the oven.

Early investigators showed that the gel time was much reduced when specimens were precured under low pressures at 125^{o}C than when precured at atmospheric pressure at the same temperature. N. Judd (81) has shown that the effect of moisture present in an unsaturated polyester resin is to retard the gelation. The effect of water on the Epoxy-BF_3 system has yet to be documented. A possible effect may be that the water attacks the BF_3 reducing the amount of BF_3 available for the catalytical curing operation, thus increasing the time before the resin gels. Precuring in a vacuum would remove any moisture from the system more efficiently than precuring in air, hence leaving the BF_3 to cure the epoxy more efficiently. However so that a reasonable gel time would be obtained, the precure temperature of the vacuum oven was reduced to 100^{o}C.

The length of precure was varied from 5 to 30 minutes. Micrographs (Fig. 110) showed that those specimens which were precured for 25 minutes or longer were free of voids, while the remaining specimens had increasing void content for decreasing lengths of precure.

Precuring in a vacuum was only partially successful in reducing voidage and it appeared that when the prepreg was taken out of the vacuum, air could return back into the prepreg. Figure 111 is a micrograph of a specimen which was precured in a vacuum and cured without the application of a pressure. The paths through which the air travelled on leaving the specimen during precure are clearly visible. These paths also enable air to return back into the specimen when it is removed from the vacuum. Therefore to get the best out of curing in a vacuum, a moulding pressure must be applied to the specimen while it is still under a vacuum.

A rig was designed to mould specimens in a vacuum (Fig. 112) using concertina bellows fitted to the base of the rig to apply the moulding pressure. A tube ran from the bellows to the outlet of the oven, in which the rig was placed, and allowed the pressure within the bellows to be reduced independently of the oven. The mould was placed under the bellows. To ease the removal of air from the specimen the mould had open ends.

The rig and the mould were placed in the oven for a period of time which was sufficient for the mould to reach the precure temperature of 100^{o}C. The specimen was then placed in the mould and the pressure in the bellows reduced by a vacuum pump, this caused the slide to move up. Specimens were then moulded in a vacuum using the following cycle:-

(a) Over a period of two minutes the air was pumped out of the oven.

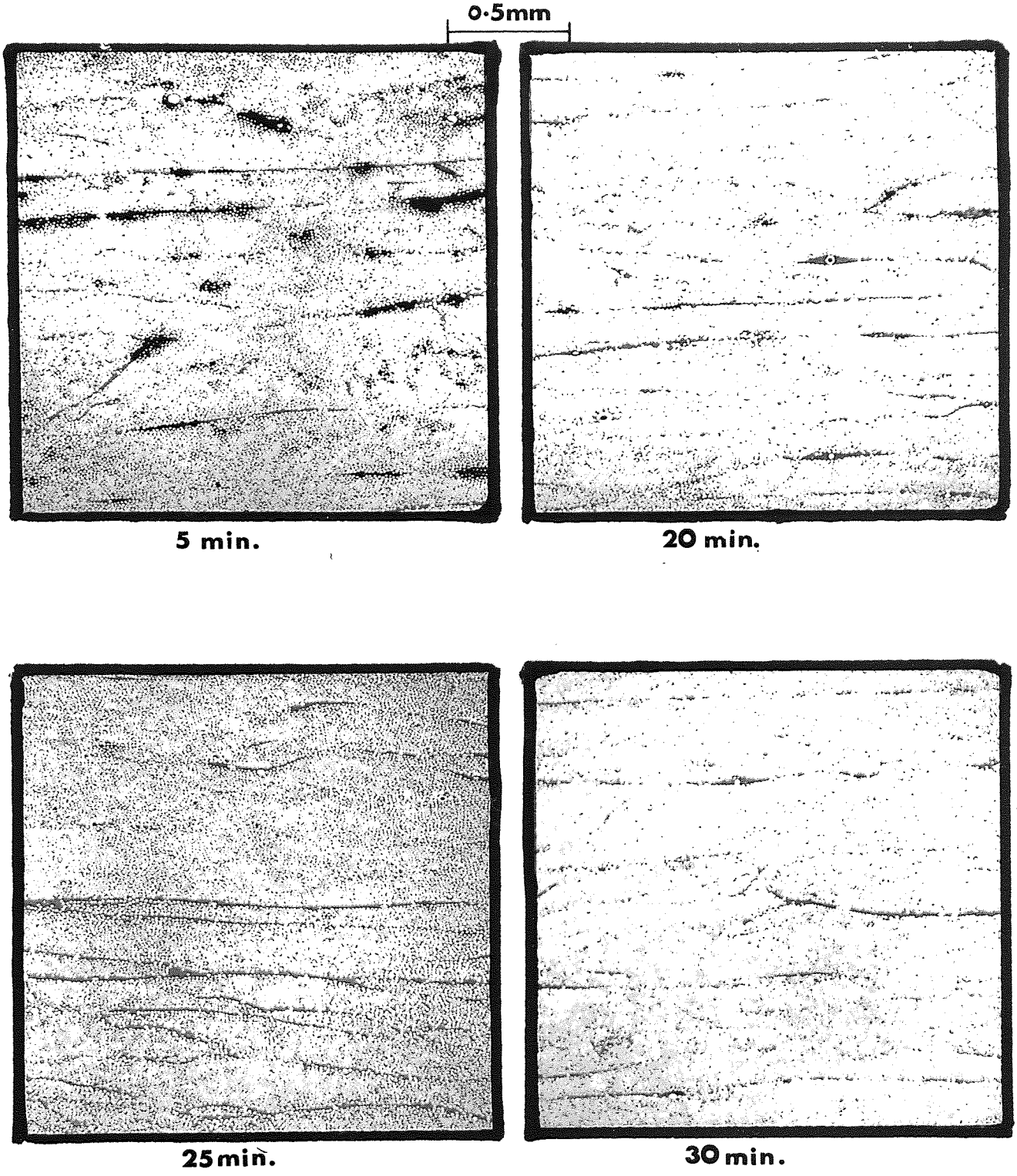

Fig.110. SPECIMENS PRECURED IN A VACUUM FOR VARYING LENGTHS OF PRECURE.

Fig. 111. SPECIMEN PRECURED IN A VACUUM.

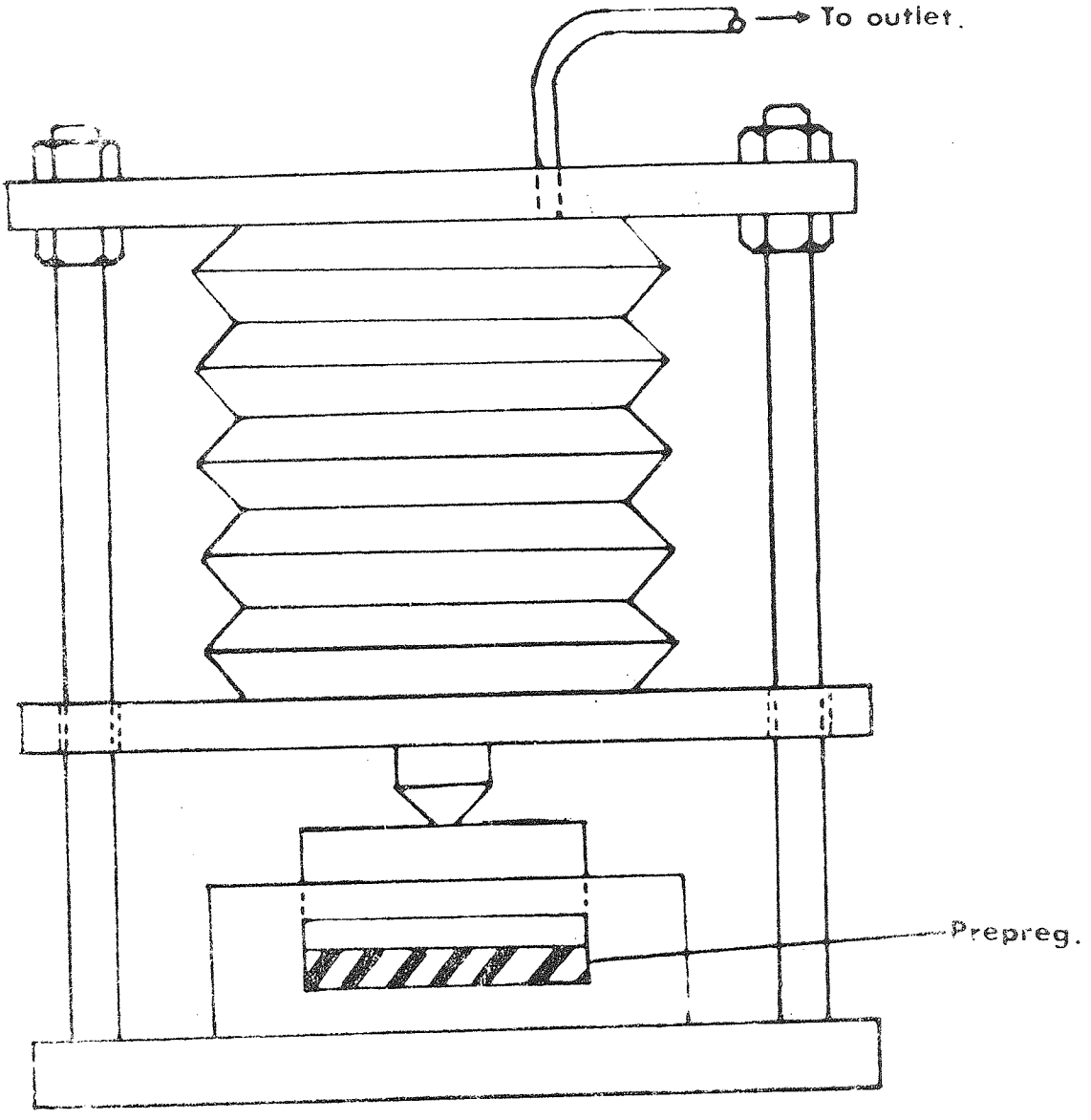

Fig. 112. VACUUM MOULDING RIG.

(b) At the end of the precure stage the oven was set at the moulding temperature of 150°C and the vacuum pump removed from the concertina bellows. Air was slowly allowed to enter the bellows thus forcing the slide down on to the plunger of the mould. It was found that by having the inside of the concertina at atmospheric pressure with the remainder of the rig under a vacuum, a pressure could be applied to the mould which was sufficient to mould the specimens down to a fixed volume of 203 mm x 25.4 mm x 2.5 mm. (The moulding pressure was 0.11 MNm^{-2} on the specimen obtained by atmospheric pressure acting on an 82.5 mm diameter bellows.)

(c) The specimens took approximately an hour to reach 150°C from 100°C. When the moulding temperature was finally reached the specimens were allowed to 'soak' at this temperature for 30 minutes.

(d) At the end of the moulding cycle the specimens were removed from the mould and post cured in the standard way for 4 hours at 180°C and 2 hours at 200°C.

The length of the precure was varied from 20 to 60 minutes. One of the two specimens precured 55 minutes did not quite mould down to fixed volume, and the specimen precured for 60 minutes was well oversize, in fact there was no resin flow.

Micrographs (Fig. 113) of the specimens showed that all the specimens moulded which had precures less than 55 minutes, were substantially free of voids.

The interlaminar shear strength of a void free specimen is usually in the range 41-48 MNm^{-2} for this particular resin system. Figure 114 shows that the specimens precured from 20 to 55 minutes are all within this range.

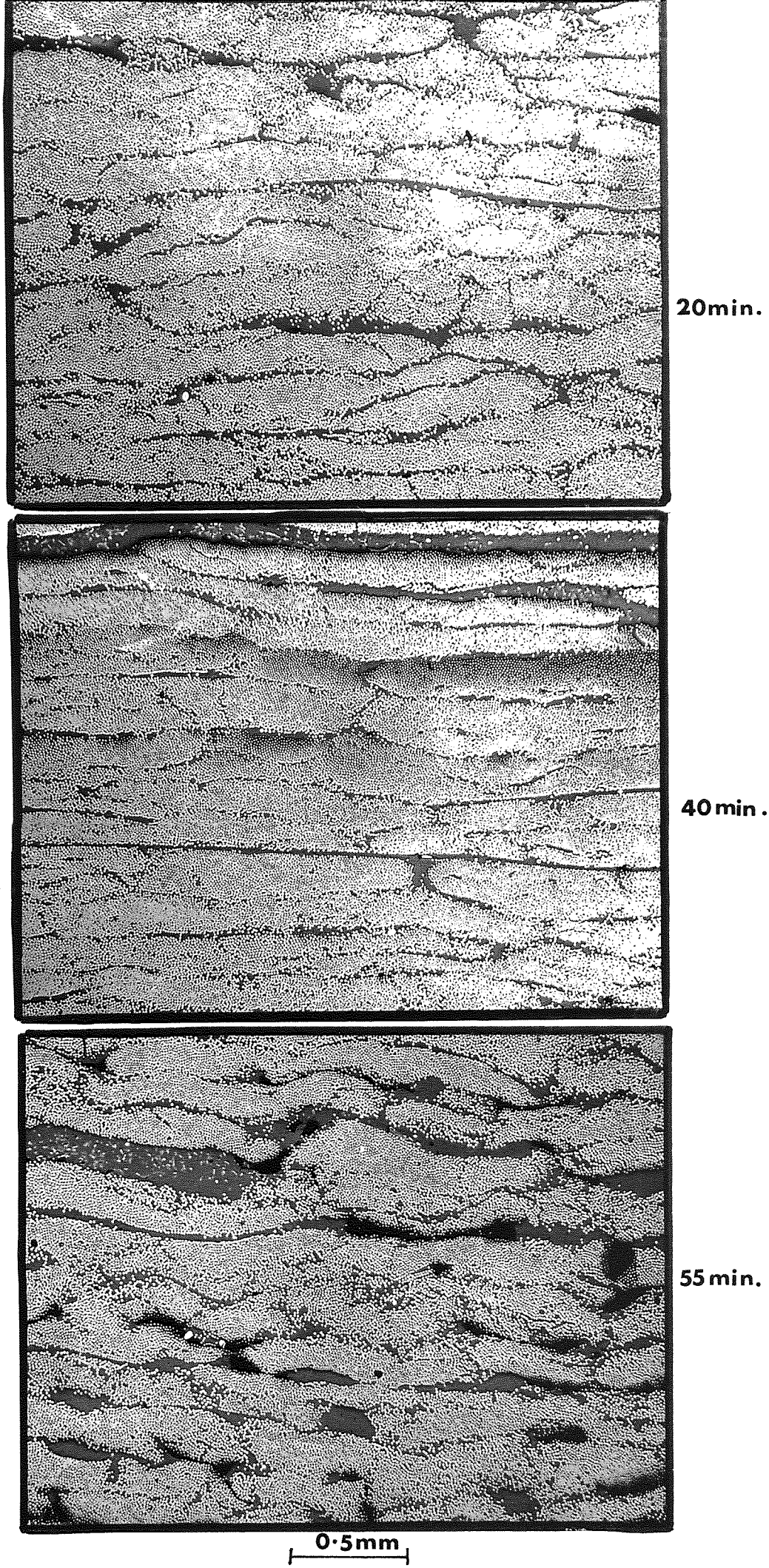

Fig113. SPECIMENS PRECURED AND MOULDED IN A VACUUM FOR VARYING LENGTHS OF PRECURE

Precuring and moulding in a vacuum enables void free specimens to be manufactured without the need for careful control over the precure time. However void free specimens can be moulded reproducibly and more easily using the moulding procedure described in section 3.5, at atmospheric pressure, using carefully prepared laminates and controlling the precure so that the resin was gelling as the moulding pressure was being applied. The interlaminar shear strength obtained by the two methods being the same and because moulding in a vacuum takes a considerable length of time it was judged to be preferable to (a) mould in normal dies at atmospheric pressure and (b) control the specimen precure.

APPENDIX V

To determine the shear stresses on the radii of the tensile specimen shape 3

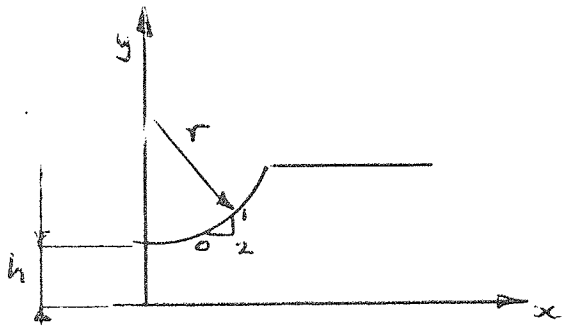

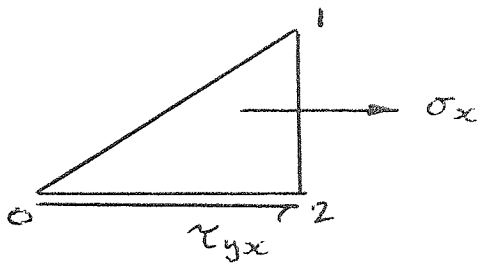

Equilibrium equation (Two dimensions)

$$\frac{\partial \sigma_x}{\partial x} + \frac{\partial \tau_{xy}}{\partial y} + A = 0$$

Assuming body forces = 0

Considering the rates of change of stresses over element.

$$\frac{\Delta(\sigma_x)}{\Delta x} + \frac{\Delta(\sigma_y)}{\Delta y} = 0$$

$$\frac{(\sigma_x)_{12} - (\sigma_y)_0}{\Delta x} = \frac{(\tau_{xy})_1 - (\tau_{xy})_2}{\Delta y}$$

Let all the stress on the surface of element = 0 i.e. $(\sigma_x)_0 = (\tau_{xy})_1 = 0$

$$\therefore \quad \frac{(\sigma_x)_{12}}{\Delta x} = \frac{(\tau_{xy})_2}{\Delta y}$$

$$\frac{\Delta y}{\Delta x} = \frac{\tau_{xy}}{\sigma_x}$$

$\therefore$ At the limit $\tau_{xy} = \sigma_x \frac{dy}{dx}$

From the equation of a circle $\tau_{xy}\, y = \frac{h}{y} \frac{(2yr + 2yh - y^2 - 2hr - h^2)^{\frac{1}{2}}}{r + h - y} \sigma_x$

APPENDIX VI

To determine the effect of large deformation in four point bending

A beam is stressed in four point bending (Fig. 115a) assuming simple bending theory $\frac{E}{R} = \frac{M}{I}$ - (1)

where E = Young's modulus of elasticity

R = Radius of curvature

I = Moment of inertia of beam

M = Bending moment

However from Figure 115a

$$\text{Sin}\,\theta \approx \frac{C}{2R}$$

$\therefore$ from 1. $\text{Sin}\,\theta = \frac{CM}{2EI}$

$\therefore$ $EI = \frac{bd^3}{12} E$ where $E = 130\ GNm^{-2}$

$$= \frac{6\ (2.5)^3}{12} \times 10^{-12} \times 120 \times 10^9 = 1.02\ Nm^2$$

from .2. $\text{Sin}\,\theta = 0.49\ cM$ - 3

when c = 25 mm, b = 38 mm, V = 300 N

$$M = 300 \times 38 \times 10^{-3} = 11.4\ Nm$$

from 3. $\text{Sin}\,\theta = 0.49 \times 25 \times 10^{-3} \times 11.4 = 0.14$

$\therefore$ $\theta = 8^o$

$\therefore$ $\sigma = \sigma_v \text{ Cos}\,\theta = 0.99\,\sigma_v$

(σ_v = the measured stress)

the actual stress is 1% higher than the measured stress, also it can be shown that:-

when C = 45 m $\theta = 12^o$ the actual stress is 2% higher than the measured stress.

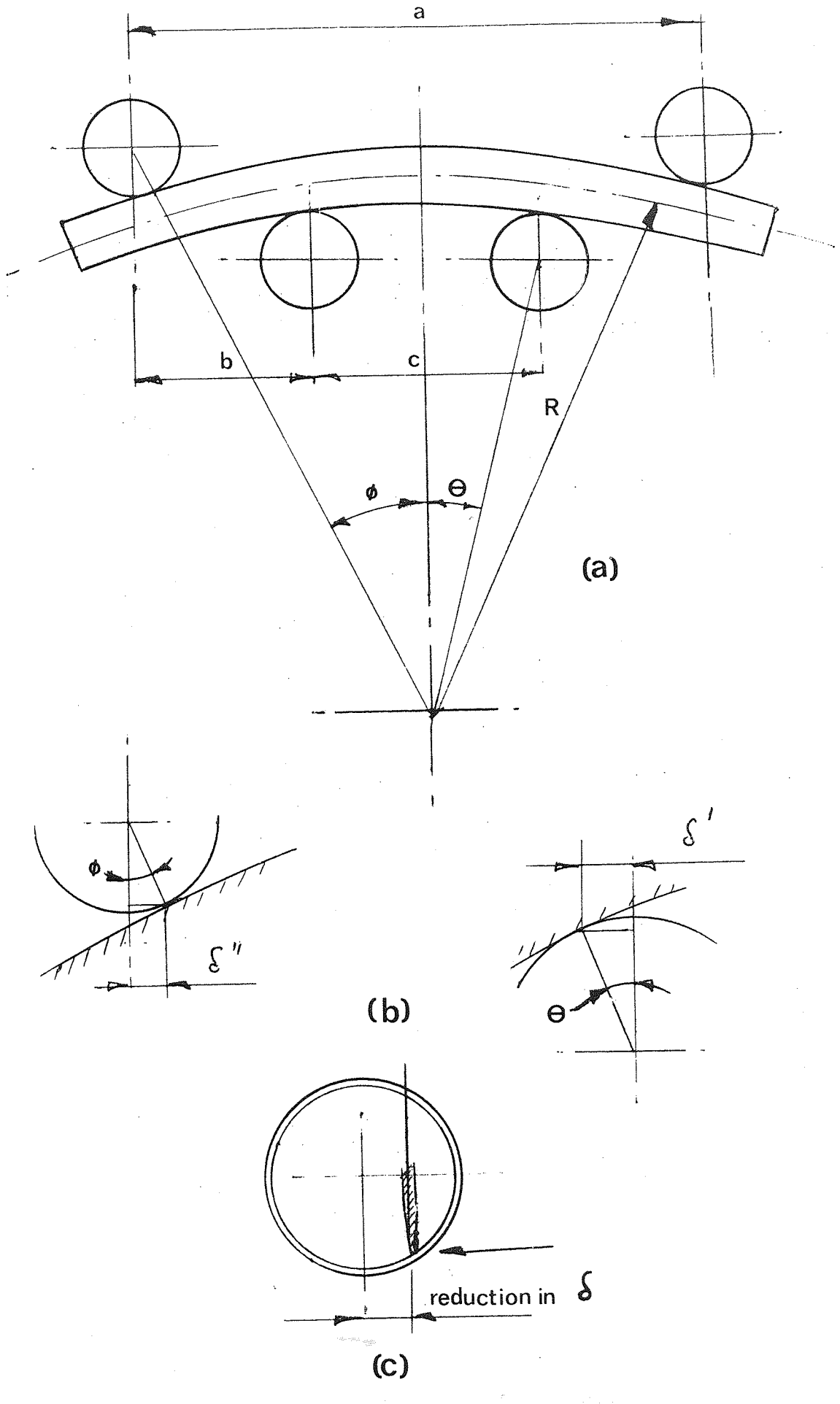

Fig.115 Change in moment arm due to large deflections in four-point bending.

When C = 60 mm $\theta = 17^{o}$ the actual stress is 4% higher than the measured stress.

When the beam deflects, it 'wraps' round the rollers this reducing the moment arm (Fig. 115). Hence the actual stress will be lower than the measured stress because equation 4 assumes a constant moment arm b.

Flexural stress in four point bending is given by:-

$$\sigma_4 = \frac{3P_4 a}{bd^2} \quad - 4$$

(a = distance from inside to outside support and P_4 is the total measured load).

The reduction in the moment arm = $\delta' + \delta''$ (Fig. 115b)

when C = 25 mm a = 100 mm

$$\therefore \sin\phi \approx \frac{a}{2R} = 0.49 \text{ am}$$

$$= 0.49 \times 100 \times 10^{-3} \times 11.4 = 0.56$$

$$\therefore \phi = 34^{o}$$

$$\delta' = r \sin\theta = 6 \times 0.14 = 0.84$$

$$\delta'' = r \sin\phi = 6 \times 0.56 = 3.36 \text{ mm}$$

the total reduction in moment arm = 4.2 mm.

Hence the actual stress will be 11% lower than the measured stress.

when C = 45 mm total reduction = 5.0 mm

Hence the actual stress will be 13% lower than the measured stress.

when C = 60 mm total reduction = 5.8 mm

Hence the actual stress will be 15% lower than the measured stress.

The above errors in the measured stress represent the maximum value that may occur. The loading rollers were made from cylinders which slipped over a knife edge. This allows a lateral movement of the roller when it is subjected to a horizontal stress, caused when the beam is bent into the large

deformation region, which will reduce the factor δ (Fig. 115c). Therefore the error will be less than that calculated above.

The errors caused by the reduction in the moment arm will completely off-set the errors caused by the horizontal component. The movement of the roller round the knife-edge will reduce the errors in the moment arm so they are similar to those caused by the horizontal component. Hence the net result will be that the errors are insignificant or if there are any errors then they will reinforce the trend in Figure 103.

References

1. Kelly A. & Davies, G.E., Metalurgical Reviews, 10, No. 37, 1965.

2. Gorden, J.E., The Science of Strong Materials, Published by Penguin Books Ltd., 1968.

3. Coleman, B.W., J. Mech. Phys. Solids, 7, 60, 1958.

4. Rosen, B.W., A.I.A.A., Jnl., 2, 1985, 1964.

5. Zweben C., A.I.A.A., Jnl., 6, 2325, 1968.

6. Zweben, C. & Rosen, B.W., A statistical theory of material strength with application to composite materials. A.I.A.A. paper no. 69.123 presented at the 7th A.I.A.A. Aerospace sciences meeting, 1966.

7. McKee, R.B. & Sines, G., Jnl. Elastoplastics, 1, 185, 1969.

8. Gatti A., et al., The role of the bond strength in the fracture of advanced filament reinforced composites', A.S.T.M., STP460, 1969.

9. Armenakas, A.E., et al., Experimental mechanics, Jan. 1972.

10. Hedgepath, Stress concentrations in filamentary structures, N.A.S.A. report TN D 882, 1961.

11. Corten, H.T., "Modern composite materials", Edited by Broutman, L.J. and Krock, R.H., published by Addison Wesley, 1967.

12. Rosen. B.W., "Mechanics of composite strengthening", Fibre composite materials, American Soc., for metals, 1964.

13. Ewins, P.D., "A compressive test specimen for unidirectional carbon fibre reinforced plastics", R.A.E. Tech. report 70007, 1970.

14. Lager, J.R. & June, R.R., Jnl.of Composite Materials 3, 48, 1969.

15. Moncurill, E. & Harris, B., Jnl. of Composite Materials, 4 24, 1970.

16. Friedq, N., "The compressive strength of parallel filament reinforced plastics - the role of the resin", Proc. of the 18th Annual Tech. and Management Conf., Reinforced plastics div. of the Soc., of Plastics Industry Inc., 1965.

17. Price, N., "Mechanical Properties of Non metallic materials", Editor - Walton, W.H., Published by Butterworths, 1964.

18. Price, N., "Fault and Joint development in brittle and semi-brittle rock", Published by Pergamon Press, 1966.

19. Bridgeman, P., "Studies in large plastic flow and fracture", Published by Havard University Press, 1952.

20. Foye, R.L., "Compressive strength of unidirectional composite materials", A.I.A.A. paper 66-143 presented at the 3rd A.I.A.A. Aerospace Sciences meeting, 1966.

21. Adams, D.F. & Dover, R.D., Jnl. Composite materials 1, 152, 1967.

22. Adams, R.D., et al., Jnl. Composite materials, 3, 594, 1969.

23. Hand, "Quality control of filament wound materials for deep submergence vessels, Proc. 20th Conf., SPI Reinforced plastics Div., Section 1-E, 1965.

24. Hayashi, T., Compressive strength of unidirectionally fibre reinforced composite materials, Paper No. 11 presented at the Seventh International Reinforced plastics conference - Brighton 1970.

25. Chambers S.R.E. & McGarry, F.J., ASTM Bulletin, TS 222, 1958.

26. Allen, H.G., Jnl. Composite materials 1 1 1967.

27. Hall, M., Private communication with M. Hall.

28. Ryder, G.H., "Strength of Materials", Published by Cleaver-Hume press, 1961.

29. Broutman, L.J., et al., "Investigation of mechanics of reinforced plastics", Technical Documentary Report WADD-TR-60-746 Part 2 - AD607828, 1962.

30. Bader, M.G., et al., "The fracture behaviour of carbon fibre reinforced materials" - reported in "Carbon fibre composite materials", editor - Gill, R.M., Published by The Plastics institute, 1972.

31. Booty, G.A., Rolls Royce Report RR(OH) 367, 1968.

32. Cook, J. & Gordon, J.E., Jnl. E. Roy. Soc., A282, 508, 1963.

33. Mallinder, P., To be published.

34. McCullough, Concepts of Fibre-Resin Composites, Published by Marcel Dekker, 1971.

35. Ashton, J.E. & Waddoups, M.E., Jnl. Composite Materials, 3, 148, 1969.

36. Cox, Brit. Jnl. of App. Phys. 3, 1952.

37. Gill, M.R., "Carbon fibres in composite materials", Published by the Plastics Ins. 1972.

38. Weil, J.D., "Advanced materials application", Symposium on mechanical reliability of Turbo-machinery blading, Derby, 1968.

39. A.S.T.M., Tentative nomenclature relating to plastics, A.S.T.M., D883, 65 a.T.

40. Lee, H. & Nevil, "Epoxy Resins", page 6-4.

41. Lee, H., & Nevil, "Epoxy Resins, page 11-5.

42. Jones, B.H., & Noyes, J.V., "Effect of voids on the transverse and inplane shear strength and elastic properties of fibrous composite materials". Douglas Aircraft, Paper No.4706, 1967.

43. Nordy, G.M., et al., "The effect of resin content and voids on the strength of fibre glass reinforced plastics for air frame use", Oklahoma Univ., Res. Inst. AD627362.

44. Ishai, O. & Cohen, L.J., Jnl. Composite materials, 2 302, 1968.

45. Hearmon, R.F.S., Proc. Royal Soc., 55 671, 1943.

46. Lekhnitskii, "Theory of Elasticity of an Anisotropic Elastic Body", Published by Holden-Day, 1963.

47. Hill, R., "The mathematical theory of plasticity", Published by Oxford University Press, 1950.

48. British Patent, Brit. Pat. 1, 128, 043.

49. Johnson, J., Applied Polymer Symposia, No. 9, 229 243.

50. Jones, W.R., & Johnson, J., To be published in Carbon.

51. Watt, W. & Johnson, W., The Engineer, 221 815, 1966.

52. Jones, W.R., Assessment of errors in the experimentally determined Young's modulus of elasticity of fine wires, Rolls-Royce report RR(OH) 348.

53. Thorne, D.J. & Gough, V.J., Rolls Royce report RR(OH) 365.

54. Love., A.E.H., "The mathematical theory of Elasticity" published by Cambridge University Press, 1934.

55. Sinclair, D., Jnl. Applied Physics, 21 380, 1950.

56. Weibull, W., Jn. Applied Mechanics, 18 293, 1951.

57. Johnson, J. & Thorne, D.J., Carbon 7 659, 1969.

58. Griffith, A.A., Phil. Trans. Roy. Soc. A221, 168, 1921.

59. Hudson, J.A. & Fairhurst, C., "Tensile strength, Weibull's Theory and a general statistical approach to rock failure".

60. A.S.T.M., A.S.T.M. Standards Pt. 27D, 638.

61. Timoshenko, S., Strength of materials Part II 2nd Ed. Published by Van Norstrand, 1941.

62. Spurgeon, J.B., Notes on preferred specimens for testing carbon fibre reinforced plastics, RAE report LSP/302101/JBS.

63. A.S.T.M., A.S.T.M. Test methods, D695-61 T 1961.

64. Ewins, P.D., R.A.E. Tech. Report 70007, 1970.

65. Fried, N. & Winnas, R.L., "The compressive strength of parallel filament reinforced plastics - proposals on standards for filament reinforced plastics" A.S.T.M., STP 327, 1965.

66. A.S.T.M., A.S.T.M. Test Method, D695-61T, 1969.

67. Elkins, R.A., et al., "Characterisation of Graphite Fibre/Resin matrix composites, A.S.T.M. STP460, 1969.

68. Park, I.K., "Tensile and compressive test methods for high modulus graphite fibre-reinforced composites". International conf. on carbon fibres, their composites and applications, 1971.

69. Freeman, J.G., Phil. mag., 37 855 (1946).

70. Booty, G.A., et al., Rolls Royce report R.R.(OH) 367, 1968.

71. Kellog, D.H. & Satter, S.A., "The effect of geometry on the mode of failure of composites in short-beam shear tests" A.S.T.M. S.T.P. 460, 1969.

72. Whitney, T.M., "Analysis of beam bending experiments of fibre reinforced composites". Air force materials, Lab., Tech. report No. AFMLTR 69-19, 1969.

73. Timoshenko, S. & Goodier, J.N., "Theory of Elasticity", Published by McGraw-Hill, 1951.

74. Duckworth, W.H., Jnl. Am. Ceramic Soc. 34 1, 1951.

75. Heap, R.D. & Norman R.H., "Flexural testing of plastics", published by the Plastics Institute, 1969.

76. Hertz, H., 'Gesommelt Werke', Vo. Leipzig 1895.

77. Mallinder, F.P. & Procter, B.A., Rolls-Royce report RR(OH)200.

78. Goggin, P.R., "Comparison of data obtained on carbon fibres by different laboratories," RAE report HCFWP68/P.2.

79. Hall, M., Private communication with M. Hall.

80. Griffiths, A.A., Phil. Trans. Roy. Soc. A221, 168, 1921.

81. Judd, N.C.W., Plastics and Polymers, Feb. 1968.

82. Spinner, S. & Teft, W.E., "A method for determining mechanical resonance frequencies and for calculating elastic moduli from these frequencies", Nat. Bur. Standards, 1960.

83. Timoshenko, S., Vibration problems in Engineering, Published by Van Nostad, 1955.

84. Hearman, R.F.S., Brit. Jnl. of Applied Physics 9, 381, 1958.

85. Goens, E., Ann. Physic, Ser 5 11 649, 1931.

86. A.S.T.M., A.S.T.M. standard test No. D2344 - 65T.

Acknowledgement

The work described in this thesis was undertaken at the "Plastics" Laboratory of Rolls-Royce Ltd., Derby and was carried out under the supervision of Dr. H.D. Williams (Aston University) and Mr. F.P. Mallinder (Rolls Royce Ltd) to whom I wish to express my sincere thanks for their helpful guidance and encouragement.

I would also wish to thank Mr. C.H. Hannah of Rolls Royce Ltd., and Mr. B.A. Proctor of Pilkinton Bros. Ltd., for their co-operation in enabling me to carry out this work. Also Mr. J. Pidduck of the Department of Mechanical and Production Engineering at the Leeds Polytechnic for his assistance in the completion of this work.

Finally I would express my gratitude to Mr. A. Deakin and Mr. N. Letts of Rolls Royce Ltd., for their invaluable assistance rendered during the experimental work, and to Mrs. J. Kemp for typing the report.